Numerical modeling of two-phase flashing propellant flow inside the twin-orifice system of pressurized metered dose inhalers

Loughborough University

Thesis Access Form

Copy No.....**Location**.....

Author ABDUL QAIYUM SHAIK

Title NUMERICAL MODELING OF TWO-PHASE FLASHING PROPELLANT FLOW INSIDE THE TWIN-ORIFICE SYSTEM OF PRESSURIZED METERED DOSE INHALERS (PMDIs)

Status of access OPEN / ~~RESTRICTED / CONFIDENTIAL~~

Moratorium Period:.....years, ending...../.....200.....

Conditions of access approved by (CAPITALS) MR. HENK VERSTEEG

Supervisor (Signature).....

Department of WOLFSON SCHOOL OF MECHANICAL AND MANUFACTURING ENGINEERING

Author's Declaration: *I agree the following conditions:*

Open access work shall be made available (in the University and externally) and reproduced as necessary at the discretion of the University Librarian or Head of Department. It may also be digitised by the British Library and made freely available on the Internet to registered users of the EThOS service subject to the EThOS supply agreements.

*The statement itself shall apply to **ALL** copies including electronic copies:*

This copy has been supplied on the understanding that it is copyright material and that no quotation from the thesis may be published without proper acknowledgement.

Restricted/confidential work: All access and any photocopying shall be strictly subject to written permission from the University Head of Department and any external sponsor, if any.

Author's signature.....A.Qaiyum.....Date.....26/03/2010.....

users declaration: for signature during any Moratorium period (Not Open work): ***I undertake to uphold the above conditions:***			
Date	Name (CAPITALS)	Signature	Address

NUMERICAL MODELING OF TWO-PHASE FLASHING PROPELLANT FLOW INSIDE THE TWIN-ORIFICE SYSTEM OF PRESSURIZED METERED DOSE INHALERS (pMDIs)

BY

ABDUL QAIYUM SHAIK

A DOCTORAL THESIS

SUBMITTED IN PARTIAL FULFILLMENT OF THE REQUIREMENTS FOR THE AWORD OF DOCTOR OF PHILOSOPHY OF LOUGHBOROUGH UNIVERSITY

WOLFSON SCHOOL OF MECHANICAL & MANUFACTURING ENGINEERING

NOVEMBER 2009

Loughborough University

Certificate of Originality

This is to certify that I am responsible for the work submitted in this thesis, that the original work is my own except as specified in acknowledgments or in footnotes, and that neither the thesis nor the original work contained therein has been submitted to this or any other institution for a higher degree.

Author's signature .....Afaiyum.....

Date ..26/03/2010.....

DEDICATED TO MY FAMILY MEMBERS WHOSE

CONSTANT PRAYERS, SACRIFICE AND INSPIRATION

LED TO THIS WONDERFUL ACCOMPLISHMENT

ABSTRACT

Pressurized metered-dose inhalers (pMDIs) are the most widely-prescribed inhaler devices for therapeutic aerosol delivery in the treatment of lung diseases. In spite of its undoubted therapeutic and commercial success, the propellant flow mechanics and aerosol formation by the pMDIs is poorly understood. The process involves a complex transient cavitating turbulent fluid that flashes into rapidly evaporating droplets, but details remain elusive, partly due to the difficulty of performing experiments at the small length scales and short time scales.

The objective of the current work is the development of a numerical model to predict the internal flow conditions (pressure, temperature, velocity, void fraction, quality, etc.) and provide deeper insight into the atomization process and fluid mechanics involved in the twin-orifice of pMDIs. The main focus is propellant metastability, which has been identified by several past authors as a key element that is missing in accounts of pMDI performance. First the flashing propellant flow through single orifice systems (both long and short capillary tubes) was investigated using three different models : homogeneous equilibrium model (HEM), delayed equilibrium model (DEM) and improved delayed equilibrium model (IDEM). Both, the pure propellants and the propellant mixtures were used as working fluid. The numerical results were compared with the experimental data. For long capillary tubes the three models gave reasonable predictions, but the present results showed that DEM predicts the mass flow rate well for pure propellants and IDEM predicts the mass flow rate well for propellant mixtures. For short capillary tubes, the present results showed that DEM predicts the mass flow rate and pressure distribution along the short tube better compared to HEM and IDEM.

The geometry of the twin-orifice system of a pMDI is complex and involves several singularities (sudden enlargements and sudden contractions). Various assumptions were made to evaluate their effect on the vaporisation process and to evaluate the flow variables after the shock at the exit of the spray orifice when the flow is choked. Also, three different propellant flow regimes were explored at the inlet of the valve orifice.

A specific combination of assumptions, which offers good agreement with the experimental data was selected for further computations. Numerical investigations were carried out using delayed equilibrium model (DEM) with these new assumptions to validate the two-phase metastable flow through twin-orifice systems with continuous flows of various propellants studied previously by Fletcher (1975) and Clark (1991). A new correlation was developed for the coefficient in the relaxation equation. Along with this correlation a constant coefficient was used in the relaxation equation to model the metastability. Both the coefficients showed good agreement against the Fletcher's experimental data. The comparison with the Clark's experimental data showed that the new correlation coefficient predicted the mass flow rate well in compare to that of the constant coefficient, but over predicted the expansion chamber pressure.

The DEM with both the coefficients for continuous discharge flows were applied to investigate the quasi-steady flashing flow inside the metered discharge flows at various time instants. The DEM results were compared with the Clark's metered discharge experimental data and the well established homogeneous equilibrium model (HEM). The comparison between the HEM and DEM with Clark's (1991) experimental data showed that the DEM predicted the mass flow well in compare to that of HEM. Moreover, both the models underpredicted the expansion chamber pressure and temperature.

The findings of the present thesis have given a better understanding of the role played by the propellant metastability inside the twin-orifice system of pMDIs. Also, these have provided detailed knowledge of thermodynamic state, void fraction and critical velocity of the propellant at the spray orifice exit, which are essential step towards the development of improved atomization models. Improved understanding of the fluid mechanics of pMDIs will contribute to the development of next-generation pMDI devices with higher treatment efficacy, capable of delivering a wider range of therapeutic agents including novel therapies based around.

ACKNOWLEDGEMENTS

All praise and thanks are due to Almighty **Allah,** *subhana-wa-taala,* the most Merciful; the most Benevolent, for bestowing me with the health, knowledge, opportunity, courage and patience to complete this work.

I wish to express my heartfelt thanks to my research supervisor, Mr. Henk Versteeg, for providing me the opportunity to pursue Ph.D degree. Throughout the course of this research work, he has been immensely helpful, supportive and has made every effort to carefully consider my ideas and interests and keep me on track. The freedom and encouragement he rendered to explore varied areas of research in computational multiphase flow helped me gain the necessary skills and self belief. His advice, support, guidance and enthusiasm toward this project have been of invaluable benefit and its been an honour working with him.

I am grateful to a number of people who have helped me meeting the challenges I encountered during the course of this research. Dr. J.M. Seynhaeve from Universite Catholique de Louvain, Belgium for his quick response to my emails on metastability. Professor W. Malalasekera, for giving me access to one of his computer. Mr Chris Blatchford of 3M Health Care Limited for reviewing the work and giving useful feedback and Dr. M. Maslehuddin of Research Institute, King Fahd University of Petroleum and Minerals, Saudi Arabia for his encouragement and support.

Special thanks are due to my colleagues at the Wolfson School, Dr. Rahul Swarankar and Rupesh for answering my queries in C++ programming. I would also like to thank my fellow researcher Mr. Suranga, Dr. Murthy, Dr. M. Deiveegan, Mr. Suresh and Dr. M.A. Kamran for their time spent with me for thoughtful discussions. I would also like to thank my friends Hari, Ayub, Mazher, Riyaz, Yoga, Deepak, Soma and Farhat aunty family for their moral support.

Family support plays a vital role in the success of an individual. My deepest gratitude goes to my family for their love, support and prayers throughout my life especially my

wife for her immense support and encouragement through out this study. I am indebted to my mother and father who devoted their lives in the endeavor of getting me a quality education. I am grateful to my sister and brothers for their emotional and moral support throughout my academic career.

Finally, this work was funded with a research studentship from Loughborough University and is gratefully acknowledged.

TABLE OF CONTENTS

LIST OF FIGURES

LIST OF TABLES

NOMENCLATURE

Roman Letters

A	area (m^2)
C	orifice constant
C_c	single phase contraction coefficient
c_p	specific heat at constant pressure (J/kg K)
c_v	specific heat at constant volume (J/kg K)
D	diameter (m)
f	frictional factor
G	mass flux (kg/m^2s)
h	enthalpy (J/kg)
k	concentration factor
k_y	coefficient of relaxation equation
$\dot{m}$	mass flow rate (kg/s)
L	length (m)
N	total number of CVs
p	pressure (Pa)
P	perimeter (m)
p_{bc}	back pressure (Pa)
p_c	critical pressure (Pa)
p_s	saturation pressure (Pa)
p_v	vaporisation pressure (Pa)
q	wall heat flux (W/m^2)
Re	Reynolds number

s entropy (J/kg K)

T temperature (°C)

U velocity (m/s)

x quality (-)

z axial distance (m)

ΔT_s degree of subcooling (K)

Δz_i size of the i^{th} CV

Greek Letters

ρ density (kg/ m^3)

τ wall shear stress [$\tau = (f/4)(G^2/2\rho)$] (Pa)

ε roughness of the tube

μ viscosity (Pas)

v specific volume (m^3/kg)

α void fraction

γ ratio of specific heats (c_p/c_v)

δ increment decrement in $\dot{m}$ for next iteration

θ spray cone angle (°)

Subscripts and superscripts

c critical

dis discharge

down downstream

ec expansion chamber

exp experimental

equil thermodynamic equilibrium

f	evaporation / flashing
in	inlet
l	liquid
lm	metastable liquid
out	outlet
s	saturated
so	spray orifice
sp	single phase
tp	two-phase
up	upstream
v	vapour
vo	valve orifice
poss	possible
imp	impossible

Acronyms

HEM	Homogeneous Equilibrium Model
DEM	Delayed Equilibrium Model
IDEM	Improved Delayed Equilibrium Model
LOF	Liquid Only Flow
MOF	Metastable Only Flow
TPF	Two-phaseFlow
MMD	Mass Median Diameter
pMDI	Pressurized Metered Dose Inhaler
CFCs	Chlorofluorocarbons
HFA	Hydrofluoroalkane

VO	Valve Orifice
EC	Expansion Chamber
SO	Spray Orifice

CHAPTER 1

INTRODUCTION

1.1. Background

The story of the pressurized metered dose inhalers (pMDI) began in 1955, when a 13 year old asthamatic girl told her father that asthma medications should be as convenient to use as her mother's hair spray, and she complained that the bulb atomizer leaked in her school bag. Susie was the daughter of Dr. George Maison, the president of the Riker company. A three person development team, consisting of Maison, Charles Thiel, and Irving Porush, started with an old ice cream freezer, a case of empty perfume vials, a bottle copper, and some propellants from Dupont to produce the first pMDI prototype (Thiel, 1996). The pMDI evolved to include a 50 μL metering device developed for the perfume industry, a 10-mL amber vial, and a plastic mouthpiece with molded nozzle to administer slats of isoproterenol and epinephrine. The first clinical trials began that same year at the Veterans Administration Hospital in Long Beach, California. In January of 1956, a new drug application was filed with the Food and Drug Administration and approved two months later. The next year, a surfactant and micronized powder were added to propellant, creating the first commercially available formulation. Today the pMDI (Figure 1.1) is a compact pressurized metal canister containing a mixture of propellants, surfactants, preservatives, and drug. The drug represents about 1% of the contents, while the propellants are greater than 80% of the contents by weight (Rubin and Fink, 2005).

Pressurized metered-dose inhalers (pMDIs) are the most common devices, around the world, for therapeutic aerosol delivery to the lungs in the treatment of asthma, bronchitis, cystic fibrosis and other pulmonary diseases. However, the mechanics of flow of propellant through the twin-orifice of the pMDIs is complex and poorly understood, involving a transient cavitating turbulent fluid that flashes into rapidly evaporating droplets (Finlay, 2001). The detailed mechanics of the flow through the twin-orifice of pMDI remains elusive due to the difficulty of performing experiments

at the small length scales and short time scales. As the conventional chloro-fluoro carbon propellants are being phased out because of the Montreal Protocol (1987), it has put pressure on the pharmaceutical industry to redesign the current pMDIs with the non-chlorinated propellants such as R134A and R227. The cost and time involved for the optimization of design by experimental methods are very high.

1.1.1. Respiratory Illness

Respiratory illness is the term for diseases of the respiratory system. These include diseases of the lung, bronchial tubes, trachea, upper respiratory tract and of the nerves and muscles of breathing. Respiratory diseases range from mild and self-limiting such

Figure 1.1 Commercial pressurized Metered Dose Inhaler (pMDI)

as the common cold to life-threatening such as bacterial pneumonia or pulmonary embolism. The most common respiratory diseases are Asthma and Chronic obstructive pulmonary disease (COPD). Some facts about these diseases are:

- Asthma and COPD cause 8% of deaths in the developed world

- 130 million known asthma sufferers worldwide
- Diagnosed incidence in children rapidly rising
- UK - 8 million patients (1 in 7 incidence), cost to NHS £0.85 billion/year
- US - 31 million sufferers; 12 million had attack in 2003
- Direct treatment costs US$9.4 billion/year
- 50% of costs to treat 20% of patients suffering attacks

1.2. pMDI Operation

Pressurized metered-dose inhalers (pMDIs) are the most common devices, around the world, for therapeutic aerosol delivery to the lungs in the treatment of asthma and

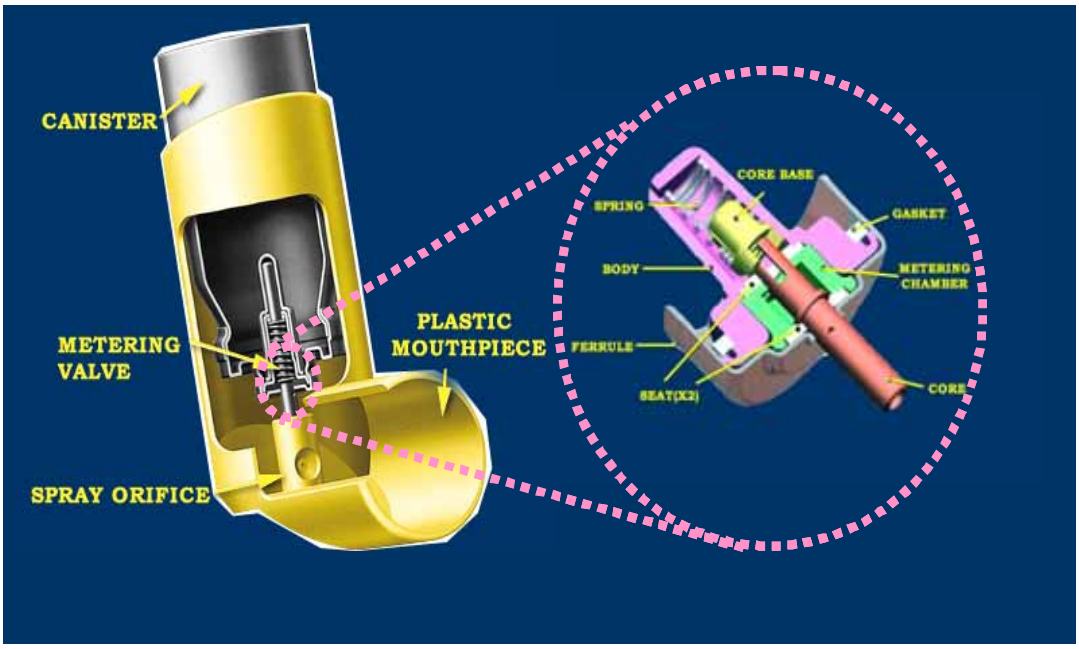

Figure 1.2 Schematic of a pressurized metered dose inhaler

COPD. Approximately 250 million units/year are prescribed. Figure 1.2 shows a schematic view of a typical pMDI, which consists of a canister and actuator. The canister is equipped with a metering valve comprising a metering chamber and a spring-loaded valve. The canister is a storage reservoir for drug in suspension or solution in propellant.

Before the 1990's the propellants would be mixtures of R12 and R114 (CFCs); more recently the industry has converted to more the environment friendly HFCs R134A or R227. The mixture may also contain co-solvents and small amounts of other excipients. The metering valve interfaces the canister contents with an actuator. In storage, openings in the valve stem connect the canister contents with a metering chamber, which is filled with a precisely known volume of drug/propellant mixture. The device is actuated by depressing the actuator, which moves the valve stem to isolate the metering chamber from the bulk liquid in the canister. Next, the metering chamber contents flow through the valve orifice into the so-called expansion chamber, which comprises the valve stem and actuator sump. The pressure drop across the valve orifice causes partial flashing of the propellant and a two-phase mixture enters the spray orifice where further propellant expansion takes place. The drug leaves the actuator through the spray orifice exit inside the droplets of a fine propellant spray. Typical drop sizes range between 1 and 5 μm, which can be readily inhaled through the mouthpiece of the pMDI, whence drug particles are deposited in the patient's lungs.

1.2.1. pMDI Technology

The advantages of pMDIs are their portability, ease of use (in a properly instructed and adequately co-ordinated patient), low cost of production, multidose, ability to store in orientation without a leak and high patient prescriber. The challenges of pMDI are high oropharynageal deposition: the inhaled particles deposits in the oropharynx (oral cavity and throat) if the size is greater than 5 μm, inhalation/actuation coordination, which includes the impact of press-breath asynchrony and nose breathing and cold-Freon effect: when a patient inhales the aerosol, the cold aerosol plume reaches back of the throat and stops the patient to inhale.

To understand these performance limitations of current pMDIs and indicate routes for possible improvements it would clearly be essential to be able to predict the thermodynamic state and flow regime of the fluid. Previous work by Fletcher (1975) and Clark (1991) has done much to reveal the general nature of pMDI propellant

flows. They developed semi-empirical models of flashing propellant flows through a pMDI based on assumptions of thermodynamic equilibrium in the metering and expansion chambers and homogeneous frozen flow in the valve and spray orifices. The results of the models were in good overall agreement with their experimental results, but a number of detailed issues remained unresolved. One of these was the experimental observation that propellant temperatures in the metering and expansion chambers were consistently higher than the saturation temperature at the prevailing pressures. This conflicted with the assumed modeling conditions of thermodynamic equilibrium within these spaces and the above authors suggested metastability in the expansion chamber as a potential cause of these discrepancies. Also, the prediction of aerosol formation requires knowledge of the thermodynamic state, void fraction and velocity of the fluid at the spray orifice exit, so metastability could play a significant role in determining aerosol droplet size and plume velocity. Thus, the main aim of this work is to develop a numerical model to predict the internal flow conditions and the mass flow rate along the twin-orifice system of pMDIs with an accurate account of propellant metastability.

1.3. Thesis Outline

In this chapter the background, the operation of pMDI and the objective of the current work have been discussed. The remainder of the thesis has been organized as follows:

Chapter 2: Literature in the area of flashing propellant flow through short tubes, long adiabatic capillary tubes and propellant flow through twin-orifice system of pMDIs have been reviewed. Different models used for the two-phase flow have been presented. Finally, the chapter is conclude with the problem justification.

Chapter 3: The governing equations for the propellant flow through short tubes, long tubes and propellant flow through twin-orifice system of pMDIs is presented. The semi-empirical model, homogeneous equilibrium model (HEM), delayed equilibrium model (DEM) and improved delayed equilibrium model (IDEM) are discussed in detail.

Chapter 4: The numerical schemes employed to solve the governing equations for different models mentioned in chapter 4 is presented along with flow charts. The numerical parameters and analysis of grid independence test for propellant flow through capillary tube and propellant flow through twin-orifice system of pMDIs is discussed.

Chapter 5: Propellant flow through adiabatic short tubes and long capillary tubes is evaluated to understand the metastability in single orifices. The validation of semi-empirical model, HEM, DEM and IDEM against the available experimental results have been discussed. Both the pure propellant and propellant mixtures are used as working fluids with various inlet conditions (subcooled, saturated and two-phase).

Chapter 6: Analysis of various assumptions and possible flow scenarios to evaluate for a range of different quasi-steady inlet conditions are discussed.

Chapter 7: Validation of propellant flow through the twin-orifice system of pMDI for continuous discharge flows using DEM are presented. A new correlation coefficient to model the metastability has been proposed and validated with continuous discharge flows of Fletcher (1975) and Clark (1991). Later, results pertaining to the DEM and HEM for metered discharge flows through twin-orifice system of pMDI are presented and the relative strengths and limitations of these models are discussed.

Chapter 8: Conclusions from the present study, directions for future work and key contributions from the current research work have been presented.

1.4. Closure

A concise introduction to background of pMDIs and their operations has been presented in this chapter. The general outline of thesis has been highlighted.

CHAPTER 2

LITERATURE REVIEW

2.1. Introduction

From the concise description of the metering process described in Chapter 1, it is clear that the most important parameter in determining the effectiveness of pMDI is the size of the inhaled aerosol particles. For an efficient therapy, the droplet size of the inhaled aerosol must be between 1μm – 5 μm. These droplet sizes are achieved by a flash evaporation of propellant inside the twin-orifice atomizer. Spray formation by flash evaporation provides the opportunity to generate the desired spray at low injection pressures. Before 1990's mixtures of CFC propellants R12 and R114 were used as propellant for pMDI application. As a consequence of the Montreal Protocol (1987) these propellants are being phased out as they were causing depletion in the ozone layer. More recently, they have been replaced by R134A or R227, which are more environmental friendly.

Twin-orifice nozzle consist of two short tubes (valve orifice and spray orifice) separated by an expansion chamber. Figure 2.1 show how the twin-orifice nozzle is different from the other tubes (short tube and capillary tube). The pressure drop across the first orifice causes the propellant to vaporize within the expansion chamber. A two-phase mixture of propellant liquid and vapour flows through the spray orifice. The process of atomization in these systems is considered to be a two-stage process: (i) initial break-up takes place in the expansion chamber (ii) further break-up takes place through the spray orifice (Fletcher, 1975). In short tube/capillary tube the atomization takes place within the tube or at the end of the tube.

Flash evaporation is a thermodynamic instability of a liquid that occurs under superheated conditions. As the pressure accelerating of liquid goes below its saturation value, a metastable state is reached and then the rapid boiling of the liquid might occur. As, flashing is one of the major primary atomization mechanisms in

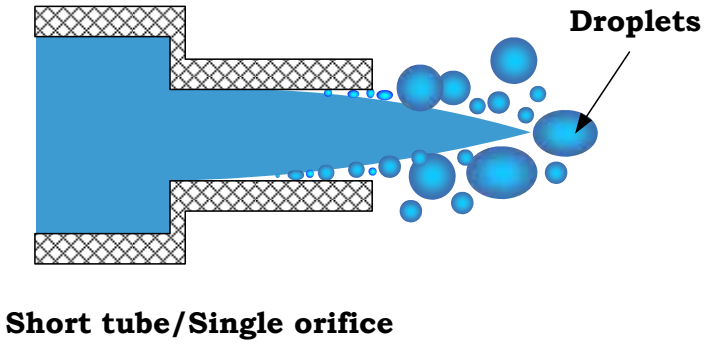

(a) short tube /single orifice

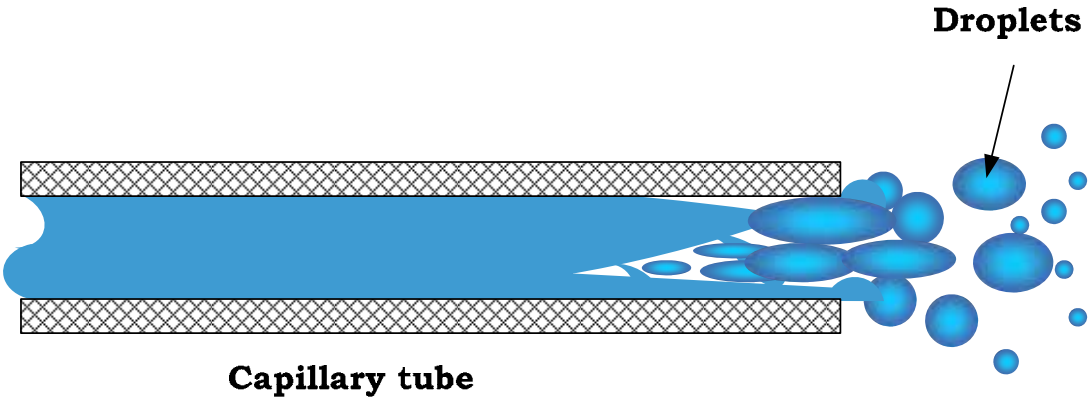

(b) capillary tube

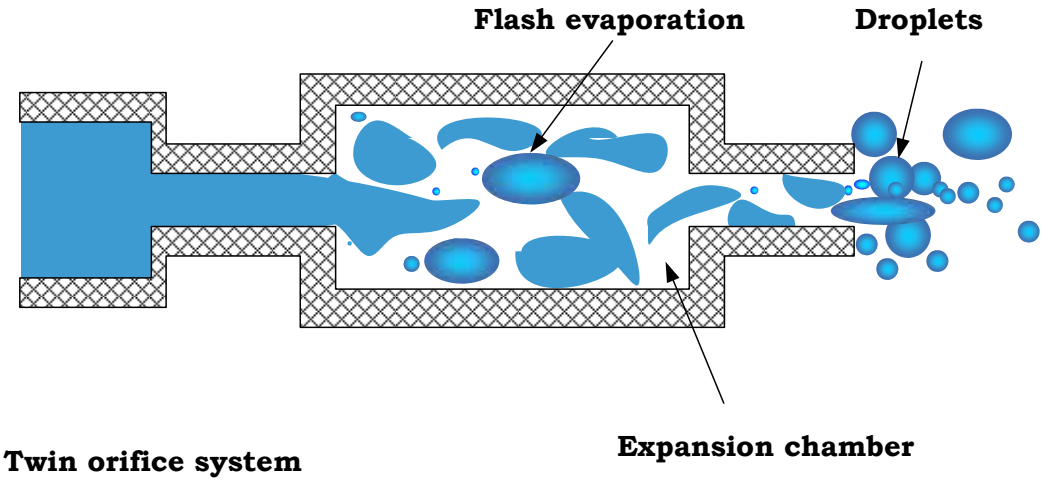

(c) twin-orifice nozzle

Figure 2.1 Atomization in different types of orifices

twin-orifice systems, first the literature on flash evaporation is considered. Thereafter the literature on different two-phase critical flow through tubes with water/steam as working fluid is reviewed. Because of its application in nuclear engineering, refrigeration and air conditioning system, an extensive amount of literature is available for two-phase flow. Only the literature which has direct relevance to the present study will be discussed. Then the previous work done on two-phase propellant flow through short tube and capillary tube considering the propellant metastability is presented. First, experimental investigations are discussed, thereafter various theoretical models to model two-phase propellant flow though short tube/capillary tube are considered. Finally, the literature available for two-orifices systems with particular relevance to pMDI will be discussed.

2.2. Flash Evaporation

Thermodynamically, flashing evaporation occurs when a liquid is exposed to a sudden pressure drop below the saturated vapour pressure corresponding to the liquid temperature. Under adiabatic conditions, part of the liquid vaporizes to regain equilibrium. The latent heat of vaporisation is drawn from the remaining liquid, whose temperature reduces to the saturation temperature corresponding to the lowered pressure. Flashing of cylindrical liquid jets, using water and Freon-11, were investigated experimentally by Brown and York (1962). Significant flashing was observed only when the temperature is substantially above the saturation temperature corresponding to the pressure (i.e. when the liquid is metastable). The temperature below which no effect is shown on the jet and above which the jet is shattered by flashing was observed to be in a narrow range of 5 degrees.

Lienhard (1966) studied the behaviour of flashing jets using short pulse flash photography. Two regimes were identified, a spray and a column jet broken by a vapour bubble explosions which were defined based on the ratio between the velocity generated by evaporative explosion and jet velocity. It was shown that the spray angle of the flashing jet depends on the degree of superheat. Subsequently Lienhard and Day (1970) studied the break up length and break up time of the vapour bubble in the

jet column using superheated water and superheated nitrogen. The expressions for the break-up time and maximum break-up length were developed.

A mathematical model to describe the size of the droplets produced by flash evaporation was developed by Sher and Elata (1977). Experiments were conducted to validate the theory using a mixture of toluene and R22 discharged through an expansion chamber and orifice. The flash evaporation process was described as the generation of vapour nuclei by cavitation within the expansion chamber, the vapour nuclei then being filled by evaporating propellant and the inception of flashing occurring when a close packed array of growing bubbles touched, causing the bubbles to explode. Experimental results showed that the proposed droplet size model correlated reasonably well with observation, but deviations from thermodynamic equilibrium (i.e. metastability) had to be accounted for using an empirical correction factor. Suzuki et al (1978) carried out the photographic studies of the atomization of superheated water and developed a similar expression for break-up length to that of Lienhard. They reported the growth rates of vapour bubbles as a function of degree of the superheat.

Miyatake et al. (1981a, 1981b, 1985) experimentally studied the spray flash evaporation in superheated water injected through a circular jet tube nozzle into a low-pressure vapour zone. The effects of the degree of superheating, the spray flow rate and nozzle diameter on the spray formation were discussed. The initial liquid temperature ranged from 40°C to 80°C. The glass nozzles used had internal diameters of 0.346 cm, 0.502 cm and 0.815 cm, with lengths of 12 cm, 25 cm and 25 cm, respectively. With the increase of superheat, the flashing became more violet and the liquid column at the nozzle exit became shorter. A Correlation for temperature variation at the centerline of the jet with residence time was developed over the experimental range.

Solomon et al. (1985) studied the effect of including an expansion chamber in the nozzle configuration using two different fluids: a dissolved gas/liquid mixture (Jet A/air) and a flashing propellant R11. Front illumination photography and a laser diffraction particle sizer were used for the experimental work. Both locally

homogeneous and separated flow models were developed based on the single-phase orifice equation to describe the mass flow rate from the upstream orifice and injector orifice in the expansion chamber. Both the models showed reasonably good agreement with some discrepancies in the mass flow rate for two-phase inlet conditions. The prefilming type airblast droplet size correlation was found to compare reasonably with the experimental data. They also presented the spray angle measurements for flashing superheated R11. It was observed that superheating yields a relatively large spray angle and enhanced atomization.

Chaves et al. (1988) experimentally studied the behaviour of the initially saturated or subcooled liquid jets discharging through a nozzle using perfluoro-n-hexane (PP1), perfluoro-1, 3 dimethylcyclohexane (PP3), ethanol and water. The jet phenomena were distinguished into four regimes depending on the normalized temperature (θ). The normalized temperature is defined as:

$$\theta = \frac{T_0 - T_s(p_{dis})}{T_s - T_s(p_{dis})} \qquad 2.1$$

where

T_0 = initial temperature (K)

T_s = saturation temperature (K) corresponding to prescribed pressure

p_0 = initial pressure (Pa)

p_{dis} discharge pressure (Pa)

In the first regime, at high sub-cooling of the liquid in the nozzle, θ<0 (negative normalized temperature), the jet angle was small and evaporation was not present. In the second regime, jet instability was observed at small positive normalized temperatures. The jet consists of a liquid-vapour mixture which created “bell” structure with relatively well defined boundaries. In the third regime, at high superheat values (θ ≈ 0.7) the differences between PP1/PP3 and ethanol/water becomes apparent in the volumes of vapour in the jet due to difference in molar specific heats. In the case of PP1/PP3 jet evaporation has an explosive character, which completely disturbs the typical “bell shape” structure of the jet. At normalized temperatures close to unity the fluid starts to evaporate within the nozzle. At the values of normalized temperature greater than 1 or (θ > 1) a supersonic gas (vapour)

jet is observed. This is the fourth regime of jet phenomena. They also reported measurements of flashing jet spray angle and determined that the initial angles depend on initial superheat, but increased superheating and interaction with vapour gas and atmosphere results in higher than expected angles for the degree of superheat.

Domnick and Durst (1995) experimentally analyzed flashing flows of propellant R12 through a constriction using spatially resolved laser-Doppler anemometry, phase-Doppler particle analysis (PDPA) and laser-sheet visualization. Bubble nucleation and growth occurred in the small recirculation zone immediately after the constriction, with small bubbles collapsing downstream of the constriction due to the increase in static pressure and larger bubbles continuing to grow. The recirculation zone increased in volume due to continued bubble growth until a given threshold size was attained. At this point, the whole recirculation zone collapsed and was transported downstream by the mean flow. The recirculation zone was re-established cyclically, creating a periodic bubble cloud. The bubble cloud then expanded downstream due to turbulent motion until the bubbles reached the channel centre line, with flashing occurring preferentially on the walls. The observations of Domnick and Durst may be applicable equally to the pMDI, since flow constrictions occur between the metering chamber and valve orifice and expansion chamber and the actuator nozzle.

Gemci et al. (2001) experimentally studied cavitation and flash boiling atomization of water-acetone mixtures through a sharp edge orifice using nitrogen as propellant gas. Three operating variables were varied: the relative concentration of the propellant gas and the liquid, the injection temperature and the pressure. Mean droplet diameters were measured as a function of operating conditions. It was shown that acetone, as a propellant liquid, significantly enhances the atomization of water. Further enhancement was observed by adding a propellant gas (nitrogen). It was found that, for a given mean drop size, the presence of the flashing liquid (acetone), markedly reduced the propellant gas-to-liquid ratio. Gemci et al. (2004) further extended these studies with solutions of different concentrations of binary mixtures of n-hexadecane and n-butane. It was observed that the atomization of n-hexadecane was significantly enhanced by using butane as a propellant liquid. Also, the presence of butane

markedly reduced the propellant gas to liquid ratio. Both, pressure and temperature enhanced the atomization reducing the droplet size.

El-Fiqi et al. (2007) experimentally studied the flash evaporation process through a superheat liquid jet using tap water at low pressures. The experimental study was carried out with a degree of superheat ranging between 2 and 18 K, inlet feed temperatures from 40°C to 70°C, and at different feed flow rates by measuring the inlet and outlet temperatures through the flash chamber in vacuum. The flash efficiency (η) is defined as the ratio of the amount of actual evaporation to that of theoretical evaporation. i.e.

$$\eta = (T_{in} - T_{dis})/(T_{in} - T_s)$$

where

T_{in} = inlet temperature (K)

T_s = saturation temperature (K)

T_{dis} = discharge (outlet) temperature (K)

The results showed that with the increase of the degree of superheat both the flashing efficiency and the flashed vapour increases. The relation between the amount of flashed vapour is proportional to degree of superheat, and the factor of proportionality was obtained from energy balance through the flash chamber.

Recently, Mutair and Ikegami (2009) experimentally investigated the factors influencing the flash evaporation from superheated water jets. Flow velocity, initial water temperature, degree of superheat, and nozzle diameter were varied individually while the other factors were maintained constant. The degree of superheat was found to be the driving force for flash evaporation. Its increase results in faster and more violent evaporation and the level of jet shattering is strongly related to this factor.

From the above literature review on flash atomization it can be seen that superheat and, hence, metastability plays a significant role in flash evaporation. The degree of superheat effect the drop size, drop velocities, spray angle and the void fraction at the exit of the orifice. It also effects the intensity of evaporation, flashing efficiency and

the level of the shattering jet. This demonstrates that the effects of superheat and metastability has to be considered in this type of flow.

2.3. Two-phase flow through Tubes using water as working fluid

Critical flow occurs when the rate of generation of kinetic energy within the fluid cannot exceed the rate of supply of energy from the fluid at the expense of its decrease in pressure and expansion (Hewitt and Hall-Taylor, 1970). Critical flow is a limiting condition which occurs when the mass flow rate will not increase with a further decrease in the downstream pressure environment while upstream pressure is fixed. The flow is choked when the velocity reaches the sonic velocity and the Mach number becomes unity. At this point the mass flow rate reaches its upper limit.

Many experimental and numerical investigations have been carried out to study the two-phase critical flow in tubes because of its importance in the safety analyses of pressurized water, boiling water, liquid-metal-cooled nuclear reactors, fossil-fuel fired power plants, steam-water boilers and railway transportation of saturated and subcooled liquids. Wallis (1980) and Elias and Lellouche (1994) presented a comprehensive review and discussion of the key experimental results and analytical models of two-phase single component flow. Since then date many further papers have been published. It is not the purpose of this section to review the entire two-phase flow literature, rather it is to review the key papers which have direct bearing upon the theoretical development and understanding of the metastability in continuous discharge flows of pMDIs.

2.3.1. Experimental Investigations

Sozzi and Sutherland (1975) experimentally studied the critical flow of saturated and subcooled water at high pressures. Three different test facilities and seven different nozzles were used for the experimental work. The critical mass flow rate through both short and long nozzles was decreased with increase in throat diameter. It increased with increase in inlet subcooling and decreased with increase in inlet quality. It

showed strong dependency for low inlet quality (x<0.002) and subcooled liquid. Incontrast, for x>0.002, the critical mass flow rate was not too sensitive to the inlet quality. The mass flow rate decreased with increases in the length (L) of the nozzle. It showed, sharp decrease for nozzle lengths from 0 to 127 mm and a gradual decrease with longer length for L>127 mm. This demonstrated the influence of metastable, thermodynamic states for short flow lengths as the fluid passing through the short length will not have sufficient time to completely nucleate before leaving the pipe.

Ardron and Ackerman (1978) experimentally investigated the critical flow of subcooled water in a pipe. Mass velocities and axial variation of pressure, void fraction, and bubble number were measured. The bubble number densities were evaluated from flash photographs. Results showed that the strong influence of non-equilibrium effects on flow-rate, pressure drop and vapour production rates in the critical flow of initially subcooled water. The effects of the location of flashing inception on maximum and minimum critical two-phase flow rates was investigated experimentally by Fraser and Abdelmessih (2002 a). In their investigation a new method of controlling the location of flashing inception during critical two-phase flow was developed. The method involves the use of a cavitating ring that could be easily positioned axially along the test section length thus allowing for a systematic study of the effect of flashing inception on critical two-phase flow. The maximum critical mass flow rate was obtained with flashing inception located near the exit of the pipe and the degree of superheat was maximum at this point. For fixed inlet conditions, decreasing the length of the tube resulted an increase in the critical mass flow rate and moving the location of flashing inception upstream resulted in a decreased superheat at the onset of flashing, that caused a corresponding reduction in the mass flow rate.

2.3.2. Theoretical Models

Mathematical model were developed based on equilibrium and non-equilibrium theories. Starkman et al. (1964) introduced a homogeneous equilibrium model (HEM), which is based on the assumptions of no slip i.e. vapour and liquid velocities are equal (S=U_v/U_l=1), thermal equilibrium between phases and isentropic expansion.

The critical mass flow rate from these assumptions is evaluated from the following expression

$$G_c = \frac{\left[2\{h_0 - (1-x_E)h_{lE} - x_E h_{vE}\}\right]^{1/2}}{\frac{1-x_E}{\rho_l} + \frac{1}{\rho_v}} \qquad 2.2$$

where

G_c = critical mass flux (kg/sm^2)

h_0 = stagnation enthalpy (J/kg)

x_E = equilibrium quality

h_{lE} = liquid equilibrium enthalpy (J/kg)

h_{vE} = vapour equilibrium enthalpy (J/kg)

ρ_l = liquid density (kg/m^3)

ρ_v = vapour density (kg/m^3)

The choking mass flux for this model can be reached by decreasing the downstream pressure until the flow rate reaches the maximum value. Beyond this, any further reduction in downstream pressure does not change flow rate as the flow is choked. The homogeneous equilibrium model under estimates the choking flow rate in short pipe.

The early model of non –homogeneous equilibrium model (NEM) derived by Moody (1965) is an extension of the HEM, by allowing different vapour and liquid velocities. A slip ratio, 'S' defined as the velocity ratio between the vapour and liquid, is treated as a variable which is determined by the condition of maximum kinetic energy flux at the exit. This category of models is called 'slip flow model'. The slip between the two-phases allows the gas phase to be discharged with higher velocity than liquid phase and this is more realistic approach than the homogeneous flow assumption. In Moody's model it is assumed that both the phases are in thermal equilibrium, gas and liquid are at different velocities, the two-phase flow pattern at the exit is annular flow without entrainment. The exit slip ratio is an independent variable given by correlation S = $U_v/U_l = (\rho_l/\rho_v)^{1/3}$ to get a maximum two-phase kinetic energy flow, whereas Fauske (1963) obtains the slip ratio as S = $U_v/U_l = (\rho_l/\rho_v)^{1/2}$ by minimizing

the momentum flow rate. According to him, the slip is generated due to density ratio between two-phases and therefore, light phase is easily accelerated by means of pressure difference between the phases and droplet caused by the liquid entrainment reduces the relative velocity between two-phases.

Henry (1968) model was derived from considering the one-dimensional, steady –flow of an adiabatic, one-component two-phase system in a constant area duct. The model was based on considering the mixture mass, momentum and total energy balance equations. It was assumed that, in the vicinity of the exit plane, the momentum pressure drop was considerably larger than the sum of the frictional and elevational head losses. It was further assumed that the flow was homogeneous with incompressible liquid phase. The comparison of the model against the experimental data showed good agreement. Henry (1970) defined a non-equilibrium coefficient, N (=x/x_E, where x_E is the equilibrium quality), to evaluate the mass transfer term (dx/dp), that allowed for only a fraction of the equilibrium vapour generation to occur. The parameter 'N' was determined experimentally. N = $20x_E$ for x_E<0.05 and N = 1.0 for x_E>0.05. It was assumed that the flashing would occur at length to diameter ratio, L/D = 12 and the two-phase mixture quality was relaxed in an exponential manner towards the tube exit. Comparisons between the prediction of Henry's model and available experimental data for nozzles and short pipes showed good agreement with the mass flow rate for subcooled and saturated inlet conditions. However, the critical pressure ratios were over predicted. The model did not account for the frictional losses or for possible variations in location of flashing inception (Fraser and Abdelmessih, 2002b).

Henry and Fauske (1971) developed a model to describe the two-phase critical flow of one-component, liquid-vapour mixtures through convergent nozzles requiring only a knowledge of the stagnation conditions. The model was formulated by examining pertinent high-velocity, two-phase flow data making reasonable approximations for the rates of interphase heat, mass and momentum transfer. The model assumes neither completely frozen not complete equilibrium heat and mass transfer process. Instead, it uses the best available data to determine reasonable approximations for the heat transfer process and the best available correlation for the rate of interphase mass transfer at the throat. The theoretical predictions showed good agreement with the

available experimental results of mass flow rates and critical pressure ratio for water, nitrogen, potassium and carbon dioxide as working fluids.

It was recognized that slip between the phases and metastability were the factors which have to be considered to bring theoretical estimations closer to experimental data. It was observed that slip flow models based on thermodynamic equilibrium gave a better agreement between theory and experiment but measured velocity ratios appeared to be much lower than those predicted by analytical or empirical models (Lackme, 1979), which indicates that the metastability has to be taken into account. Lackme (1979) developed a model for the flashing of a supersaturated liquid considering the metastable states between the saturation pressure (p_s) and onset of boiling pressure (p_v). The following empirical correlation was established from a numerous experimental data to calculate p_v :

$$p_v = k_{\text{meta}} p_s \qquad 2.3$$

where k_{meta} varies from 0.91-0.95.

The metastability was taken into account by introducing a vaporisation index (y), defined as the mass fraction of the metastable liquid which has evolved to give a mass 'x' of steam in equilibrium at the local pressure p with the mass (y-x) of liquid and the remaining fraction (1-y) consists of metastable liquid at superheated temperature (T_{lm}). When the flow was choked, the vaporisation products were expelled at the local sonic velocity. The model was applied to the flashing of hot water at low pressure($p \leq 2$ bar). There was a good agreement between the measured and calculated void fraction. A simple form of a relationship between the mass flux, the pressure at the onset of boiling and the effective critical quality was verified. This model neglected the length of two-phase flow compared with the total length of the tu be, as the length of the flashing zone was short in compare to length of the tube. Hardy and Mali (1983) enhanced the Lackme's model including the two-phase flow length into it. The two-phase length was estimated in two ways: the first way was based on Lackme's description of the vaporisation index whereas the second method was purely based on empirical correlation. Both the models predicted the mass velocity well against the experimental data. Comparing their results with the experimental data, it was suggested that the pressure at onset of boiling plays a major role in evaluating the

critical flow which emphasizes the necessity of a better knowledge of nucleation mechanism and of the triggering of boiling.

Feburie et al. (1993) developed a new model for two-phase choked flow of water through cracks incorporating some of the ideas expressed by Lackme. The model takes into account the persistence of some metastable liquid in the crack and the special flow pattern which appears in such particular geometry. The flow through crack involves two parts : a single phase liquid flow takes place near the crack inlet and extends to a cross section where nucleation starts. The onset of nucleation occurs at location with some water superheat and below the saturation pressure. Then steam bubbles grow and eventually coalesce into flat steam pockets. The fluid was modeled as a three-phase mixture consisting of metastable liquid, saturated liquid and saturated vapour. Slip between phases was neglected. A relaxation equation was used to evaluate the vaporisation index (y) along the crack which is expressed as follows:

$$\frac{dy}{dz} = k_y \frac{P}{A}(1-y)\left[\frac{p_s - p}{p_c - p_s}\right]^{0.25} \qquad 2.4$$

where

p_c = critical pressure (Pa)

p_s = saturation pressure (Pa)

P = perimeter (m)

A = area (m^2)

k_y = is an empirical constant, which is evaluated based on a cylindrical pipe and is 0.02.

According to the above expression, the fraction dy of liquid which is transformed from the metastable phase to the saturated liquid phase per unit length is proportional to the remaining quantity of metastable liquid (1-y) and to some function of metastability expressed by means of a pressure difference. The results showed very good agreement against the experimental data. The model was developed only for the subcooled inlet conditions and could not handle saturated/two-phase inlet conditions.

Giot et. al (1994**)** improved and extended the model developed by Feburie et. al., by making it applicable to all kinds of inlet conditions prevailing in the steam generator tubes: not only subcooled water, but also saturated water, steam-water mixtures, saturated dry stream or superheated steam. They proposed an appropriate methods to initialize the numerical integration of the flow after analyzing the flow at the crack inlet and assumed that the metastable liquid undergoes isentropic expansion. For the particular geometry studied considering the heat transfer between the wall and the fluid, they found that the results of mass flow rate were better predicted using a model with non-equilibrium assumption i.e. accounting for metastability compared to that of equilibrium assumption.

Attou and Seynhaeve (1999 a) studied the modeling of steady-state adiabatic flashing flow through a pipe line involving with an abrupt enlargement considering the metastable state. They considered two physical flow models: the Homogeneous Equilibrium Model (HEM) and the improved Delayed Equilibrium model (IDEM). For HEM the vaporisation is instantaneous and occurs as soon as the local pressure reaches the saturation pressure. HEM assumes that the two-phases are in thermodynamic equilibrium with equal velocities and temperatures. In common with Feburi's model described earlier, the IDEM assumes that during the vaporisation process, only a fraction y of fluid is transformed into saturated mixture, the other fraction (1-y) remains metastable liquid and is submitted to an isentropic evolution. The IDEM was improved by developing a new closure equation for the evolution of the fraction 'y' of the metastable liquid remaining valid for initial conditions of subcooled liquid near the saturation state as well as for initial conditions of two-phase mixture, which is given as:

$$\frac{dy}{dz} = k_y \frac{P}{A}(1-y)^2 \left(\frac{U_{in}}{U}\right)^{1/10} \left[\frac{p_s - p}{p_c - p_s}\right]^{1/4} \qquad 2.5$$

where

k_y = 0.001.

U_{in} = liquid velocity at the inlet (m/s)

The velocity factor in the above equation is always less than one and takes into account the delayed effect due to the important acceleration of the mixture which

occurs during vaporisation. Two algorithms were developed: possible and impossible flow algorithm (PIF) and iterative length algorithm (IL). The PIF algorithm was applied to predict the mass flow rate upstream from the enlargement. According to this algorithm, the critical flow rate corresponds to the maximum possible flow rate and to the minimum impossible flow rate which can be obtained under constant inlet conditions. The IL algorithm was applied to evaluate the flow variables downstream of the enlargement once the flow is choked at the abrupt enlargement. According to this algorithm, the base pressure at the step of the enlargement is evaluated iteratively knowing the critical mass flow rate. The methodology was applied to simple steam-water flow (choked at the exit of the pipe) and double-choked steam-water flow (choked both at the first abrupt enlargement and the exit of the pipe) through discharge line involving one abrupt enlargement (Attou and Seynhaeve, 1999b). A systematic comparison of experimental data of the mass flow rate and pressure profile with results of HEM and IDEM showed that the metastability of the liquid phase has to be taken into account. The predictions of the IDEM are compared favorably with the experimental data especially close to the saturated inlet conditions.

From the above literature review on two-phase critical flow of water through pipes it can be seen that the critical flow of single phase compressible fluids is well understood in a number of complex flow configurations involving abrupt changes of cross section. The liquid metastability observed in the experimental work can be accounted for by using the non-equilibrium models such as DEM and IDEM. Also, the PIF algorithm can be used to evaluate the mass flow rate along the twin orifice system of pMDI for a given inlet and outlet conditions. And, IL algorithm can be used to predict the downstream conditions after the abrupt expansion at the valve orifice exit, when the flow is choked in the vicinity of abrupt expansion at the valve orifice exit.

2.4. Two-phase propellant flow through capillary tubes

The literature review discussed in the previous section was focused on water as working fluid. As refrigerants such as R11, R12, R114, R134A, and R227 are used as propellants inside pMDI and the properties are quite different from those of water. It

is therefore important to review the literature on two-phase propellant flows through capillary tubes and short tubes.

A capillary tube is a common expansion device used in refrigerators, air-conditioners and heat pumps, the function of which is to reduce the high pressure in the condenser to low pressure in the evaporator. Beside the function of expansion, the other function of the capillary tube is to control the rate of flow of propellant in a refrigeration system by acting as a self-controlling flow restrictor. Capillary tubes can be short or long. Short tubes generally fall within a range of length to diameter (*L/D*) ratios 3 to 20 and are used in automotive air conditioners and residential-size air conditioners. Because of their low cost, easy installation and high reliability, several manufacturers prefer to use short tube orifices as expansion device. Although the geometry of capillary tubes is very simple, the two-phase flashing flow inside them is very complex. During the flashing process, the state of the propellant changes from subcooled liquid to two-phase vapour-liquid mixture. Thermal non-equilibrium i.e. metastable flow occurs in this process (Li et al., 1990a). Many experimental and numerical investigations have been carried out in order to characterize propellant flows in capillary tubes.

2.4.1. Experimental Investigations

2.4.1.1. Experimental Investigations on Short tubes:

Pasqua (1953) experimentally studied the flow of R12 through glass short tubes. For subcooled liquid entering the short tube, Pasqua's photographs showed that the fluid flashed inside the short tube when the downstream pressure was near or below the saturation pressure. A metastable inner core surrounded by a two-phase annular ring was observed inside the short tube and the diameter of this metastable liquid core decreased as the fluid proceed to the tube exit. Fauske and Min (1963) experimentally studied the flow of saturated and subcooled propellant, R11 through short tubes. Their results were in general agreement with Pasqua. Mei (1982) experimentally investigated the flow of initially subcooled propellant R22 through short tubes $7<L/D<12$. He reported that choking occurred at the degree of subcooling of 22.2°C and proposed a choked flow model for R22 flow with subcooling of more than 22.2°C

and a non-choked flow model for subcooling less than 22.2°C. Krakow and Lin (1988) experimentally investigated the flow of propellant R12 through capillary tubes and short tubes. They observed that flow through short tubes having $2<L/D<7$ was primarily dependent upon the upstream conditions and not on the downstream pressure; thus a choking phenomenon was indicated for short tube flow.

Aaron and Domanski (1990) experimentally investigated the flow of subcooled propellant R22 through short tube restrictors. The flow dependencies upon upstream subcooling, upstream pressure, downstream pressure, tube length, tube diameter, entrance chamfering and exit chamfering were examined. It was reported that for downstream pressures greater than the liquid saturation pressure, the flow was strongly dependent upon the downstream pressure and for downstream pressures below the saturation pressure, the flow demonstrated very week dependence upon the downstream pressure. Kim and O'Neal (1994) performed an experimental study to investigate the critical flow of propellant R134A through short tube orifices with *L/D* ratios ranging from 5 to 20. Both two-phase and subcooled liquid flow conditions entering the short tube were examined. Choked flow conditions were established when the downstream pressures were reduced below the saturation pressure corresponding to the inlet temperature. The propellant flow rate increased as the inlet sub-cooling increased and decreased as the inlet quality increased. In a subsequent study, Kim and O'Neal (1995) investigated the critical flow of propellants R22 and R134A and measured the mass flow rates and pressure profiles along the short tube orifice. Three specially designed short tubes were used for the present study. Five to six pressure taps were located inside the short tube. They observed that the flashing point moved toward the inlet section of the tube when the degree of sub-cooling decreased.

Singh et al. (2001) experimentally investigated the flow of propellant R134A through short tube orifices of different diameters and lengths, with and without inlet and outlet screens, over a wide range of operating conditions. The inlet conditions were varied from highly subcooled (40°C) to pure vapour (quality 0 to 1). The purpose of the inlet screen was to serve as strainer while the exit screen substantially reduced noise generated by the expansion. It was found that the mass flow rate was sensitive to inlet

pressure, inlet sub-cooling and diameter. The inlet and outlet screens had no significant effect on mass flow rate. Liu et al. (2004) experimentally studied the characteristics of propellant R744 through short tube orifices. The short tubes tested had diameters ranging from 0.83 to 1.53 mm and lengths ranging from 8.02 mm and 25.42 mm. The results showed that choked conditions were established for all the cases studied. The location of flashing inception moved to the exit of the tube when the upstream pressure was increased. The results showed that the inlet and outlet chamfer depths had no significant effects on the mass flow rate.

Tu et al. (2006) presented the experimental results of R134A flowing through micro-orifices with diameters of 31 and 52 μm, and length-to-diameter ratio of 2.5 and 4.2 respectively. The experimental result indicated that flow was not choked, even when the downstream pressure was reduced to more than 400 kPa below the saturation pressure for liquid-upstream/two-phase-downstream flow. This suggested that choked flow was much more difficult to increased metastability in smaller tubes. Recently, Nilpueng and Wongwises (2009) published most complete work on short tube orifices with propellant R134A as working fluid. They experimentally investigated the two-phase flow characteristics of R134A, including flow patterns, mass flow rate, pressure distribution and temperature distribution. Two groups of short tube orifices were used in the experiment. The first one (specially designed glass short tube orifices) used to visualize the flow pattern and the second used to measure temperature and pressure distributions along the tube. The short tube orifices used in this study had diameters of 0.605, 0.961 and 1.2 mm and length (L) to diameter (D) ratio, L/D, of 8.3-33. High speed digital camera and video camera were used to record the images of the flow pattern. The experimental results showed that metastable flow and choking occurred inside the short tube orifice. The observed flow patterns inside could be divided into two main types: the metastable liquid flow at the tube central core surrounded by a two-phase flow of bubbles mixed in the liquid; and the flow of vapour bubbles mixed in the liquid inside the tube. The results showed that the increase in the degree of sub-cooling and upstream pressure increases the length of the metastable liquid region and the mass flow rate is directly proportional to upstream pressure and degree of subcooling.

2.4.1.2. Experimental Investigations on Long Capillary Tubes:

As mentioned earlier, the capillary tubes are used as expansion devices in refrigeration and air conditioning systems. Long tubes generally fall within a range of length to diameter (L/D) ratios greater than 20. They are widely used in household refrigerators and small refrigerating systems, due to its high reliability and low cost. The process of propellant flow through a capillary tube is a flash process, in which the state of the propellant changes from liquid to vapour-liquid mixture. In such a process the inception of vaporisation does not take place at the location of thermodynamic saturated state with pressure p_s, but takes place at a location with a pressure, p_v (Figure 2.2) downstream from the thermodynamic saturated point. This is due to the fact that a finite amount of superheat is required for the formation of first vapour bubble. The pressure difference, (p_s-p_v), is a characteristic quantity for the metastable

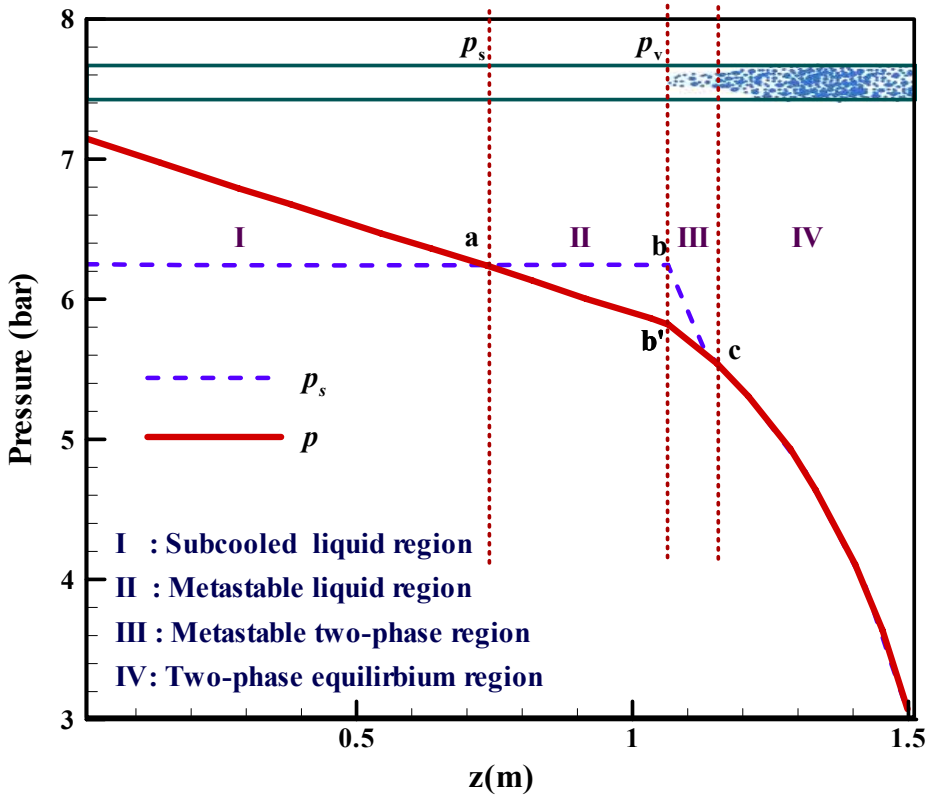

Figure 2.2 Typical pressure distribution along an adiabatic capillary tube (Li et al., 1990a)

flow and is know as underpressure of vaporisation. According to Li et al. (1990a), the metastable flow of propellant through adiabatic capillary tube consists of four different regions: subcooled liquid region, metastable liquid region, two-phase metastable region and two-phase equilibrium region (Figure 2.2). The existence of a metastable region results in a higher flow rate than would otherwise exist under thermodynamic equilibrium conditions.

Cooper et al. (1957) experimentally observed the metastable flow in a glass capillary tube and found that the calculated length of the liquid region was less than the measured length which indicated there was delay in vaporisation. The capillary tubes used in this study had diameters of 2.54 and 9.4 mm and *L/D* varying from 30- 360. Their results showed that the length of metastable flow increased with decrease in diameter, increase in length of the capillary tube and increase in upstream pressure. Thereafter, the existence of metastable flow was confirmed by Mikol (1963) and Mikol and Dudley (1964). They reported a detail experimental work on single-phase and two-phase flow in adiabatic capillary tubes. Mikol (1963) obtained pressure and temperature distributions along the capillary tube having a diameter of 1.4 mm and length of 1.83 m, which included the region of metastable flow. From these graphs, the regions of subcooled liquid flow, metastable flow and two-phase flow were determined. Mikol and Dudley (1964) used photographic approach to improve upon the observations of Cooper et al. They showed that the maximum distance for the delay of vaporisation was 70cm. Their major findings on metastable flow are:

- Metastable flow must be included in the design of the capillary tube as it was observed in all of their visual and data runs in adiabatic capillary tube.
- The flow in the capillary tube could be described as a subcooled liquid flow, metastable liquid flow, an inception of vaporisation that started with bubbles appearing at the tube wall and merging into a vapour core surrounded by liquid.

Rezk and Awn (1979) experimentally obtained the distributions of pressure and temperature along capillary tubes in which metastable flow was evident and the observed behavior similar to Mikol's work. The length of the metastable flow and the degree of superheat were determined. Metastable flow was also observed by Koizumi and Yokoyama (1980), who performed visual experiments using glass capillary tube

and instrumented copper and stainless steel capillary tubes under adiabatic conditions for diameters ranging from 1.0-1.5 mm and lengths varying from 0.38 -1.5 m. Some of their results are summarized as follows:

- The average length of metastable flow was 39 cm; the maximum length was 60cm
- The measured flow rate in capillary tube was higher by 14% than the calculated flow rate based on thermodynamic equilibrium flow, indicating that metastability plays an important role.
- The length of the metastable flow decreased with increase of velocity, while under pressure of vaporisation increased with increase of velocity.
- Under a constant mass flow rate, the length of metastable flow increased with decrease of tube diameter.

Li et al. (1990a) and Chen et al (1990) published the most complete work on metastable flow of propellant in adiabatic capillary tubes. Li et al. (1990a) experimentally investigated the metastable flow phenomenon of R12 through capillary tubes with length 1.5 m and diameters ranging from 0.66 – 1.17 mm. The pressure and temperature along the capillary tube were measured precisely. The inlet temperature was varied from 17-53 °C, pressure was varied from 6.3-13.2 bar, inlet subcooling was varied from 0-17 °C. The effects of the diameter of the capillary tube, the back pressure, the mass flow-rate and the inlet sub-cooling of the propellant on the delay of vaporisation of the propellant inside the capillary tube are discussed. The following conclusions were drawn from their experimental study:

- The larger the diameter of the capillary tube, the lower the under pressure of vaporisation, and the shorter the length of the metastable flow.
- The under pressure of vaporisation increases with an increase in the propellant mass flow rate at fixed inlet subcooling conditions.
- An increase of the inlet sub-cooling decreased the under pressure of vaporisation.
- The effect of change of back pressure on the under pressure of vaporisation was small.

Chen et al (1990) established a correlation for the evaluation of under pressure of vaporisation using the experimental data and classic nucleation theory for the heterogeneous nucleation of propellant flowing through capillary tube, which is expressed as:

$$\frac{(p_S - p_V)\sqrt{KT_S}}{\sigma^{3/2}} = 0.679\left(\frac{\nu_V}{\nu_V - \nu_l}\right)\mathrm{Re}^{0.914}\left(\frac{\Delta T_{sub}}{T_c}\right)^{-0.208}\left(\frac{D}{D'}\right)^{-3.18} \qquad 2.6$$

where

p_s = saturation pressure (Pa)

p_v = pressure of vaporisation (Pa)

T_s = saturation temperature (K)

K = Boltzman constant (1.380662 x 10^{-23} J/K)

σ = liquid propellant surface tension (N/m)

ν specific volume (m^3/kg)

T_c = propellant critical temperature (K)

ΔT_{sub} = subcooled temperature (K)

D` = reference length $\left(D' = \sqrt{KT_S/\sigma} \times 10^4\right)$

The empirical constants in this correlation were determined based on experimental data with adiabatic capillary tubes working with R12 for the parameter ranges shown in Table 2.1.

Table 2.1 Limitations of the Chen et al. (1990) correlation

0.464 x 10^4 <	Re	< 3.74 x 10^4
0 <	ΔT_{sub}	< 17°K
0.66 x 10^{-3}m <	D	< 1.17 x 10^{-3}m

Dirik et al (1994) experimentally studied the flow through adiabatic and non-adiabatic capillary tubes using propellant R134A. The parameters measure in the tests were inlet and outlet conditions of the test section and propellant flow rate. Two capillary tubes with 0.66 mm and 0.8 mm diameters with three different lengths (3.5, 4.5 and

5.5m) were used for the experimental work. The parameters measured during the test were inlet and outlet conditions and the propellant mass flow rate. Temperatures were also measured along the tube at various positions, which showed considerable delay in flashing.

Meyer and Dunn (1998) experimentally investigated the behaviour of propellant R22 and R134A in an adiabatic capillary tube, with an emphasis on the nature of metastable region. They presented the hysteresis curves for decreasing and increasing sub-cooling. It was found that different mass flow rates existed for the same specific set of conditions each with a unique metastable region, dependent on how that specific set of conditions was achieved. Also each different metastable region resulted in a different mass flow. Melo et al. (1999) experimentally investigated the flow of propellants R12, R134A and HC-600a through adiabatic capillary tubes. The experiments were performed with different condensing pressures and levels of subcooling under choked flow conditions. Eight capillaries with different combinations of lengths, ranging from 1.93-3.02 m, diameters, ranging from 0.77-1.05 mm, were used. The effect of capillary length, capillary diameter, propellant subcooling, condensing pressure and type of propellant on mass flow rate was investigated. However, no attempt was made to measure the pressure and temperature profiles along the capillary tube to investigate the effect of metastability. The results showed that the diameter affects the mass flow rate more significantly than the other variables.

Sami and Maltais (2001) experimentally studied the behaviour of new alternative propellants such as R410B, R407C and R410A under various inlet conditions, saturated, subcooled and two-phase. The experimental results showed that R 410-B has the highest pressure drop and temperature drop along the capillary tubes and R407-C has similar capillary behaviour to R22. The data also showed that the component concentration of the propellant mixture significantly affects the capillary tube behaviour and particularly the pressure drop along the capillary tube length. The pressure and temperature distribution was measured along the capillary tube. However, no comment was made on the propellants metastability. Bittle et al. (2001) experimentally investigated the metastable flow of propellant R134A through an

adiabatic capillary tube. The experimental parameters were : steady-state inlet subcool level (three levels), the direction of approach to the steady state inlet temperature (increasing or decreasing temperature), and the forced inlet temperature response rate (i.e. increasing or decreasing the subcooling fast/slow) used in attaining the steady state flow condition. From the results it was concluded that at inlet subcool levels less than 5.6 °C, there can be significant variation in measured mass flow rate, which was due to variation in the flash point location and thereby the metastable liquid region. It was shown that the variation in the flash point could be controlled and the length of the metastable liquid could be accurately predicted.

Sanzovo et. al.(2002) experimentally studied the flow of propellant mixtures R410A and R407C through a capillary tube with subcooled and two-phase inlet conditions. The results showed that R407C flow presents a larger liquid region than R410A. Sanzovo and Mattos (2003) experimentally investigated the flow of propellant mixtures R410A and R407C, monitoring the mixture composition (in mass percentage) with subcooled, saturated and two-phase inlet conditions for a wide range of inlet conditions. The capillary tubes tested had diameters ranging from 1.067 - 1.626 mm and length ranging from 1.0 -1.5 m. The relative roughness was evaluated by measuring the pressure losses of all liquid R410A propellant flow. The pressure and temperature distributions were measured along the capillary tube. The experimental results showed delay of vaporisation.

Silva et al. (2007) experimentally investigated the metastable flow through capillary tubes with pure propellants R134A and R600 and propellant-oil mixtures. A large number of experiments were carried out to verify the influence of inlet subcooling, internal diameter, mass flow rate and inlet pressure on the underpressure of vaporisation. The results showed that the mass flow rate and subcooling degree are the two most important parameters affecting the underpressure of vaporisation. Oil presence increases the metastable liquid region retarding flashing flow inception of mixture compared with pure propellant R134A.

From the above experimental investigations on propellant flow through short tubes and capillary tubes, it can be seen that metastable flow exists in these tubes, which

shows significant effect on the mass flow rate, quality and void fraction distribution. The experimental work of Mikol (1963) with R12 and R22, Li et al (1990a) with R12, Dirik et al (1994) with R134A and Sanzovo and Mattos (2003) with R410A and R407C are the benchmark experiments and are sufficiently high in quality to be used for validation.

2.4.2. Theoretical Models

Many theoretical studies have been conducted to model the two-phase critical flow through short tubes and capillary tubes. Some models of these are semi-empirical derived from the experimental data. Other models are derived from the solution of equations, describing the conservation of mass, momentum and energy, for each phase separately or for homogeneous mixtures. These can be classified into the following groups: (i) Homogeneous Equilibrium Model (HEM) (ii) Homogeneous Frozen Model (HFM) (iii) Non-Homogeneous Equilibrium Model (iv) Separated Flow Model (SFM) (v) Drift Flux Model (DFM) and (vi) Two-Fluid Model (TFM). Each of these model is reviewed below.

2.4.2.1. Semi-empirical Models

Most empirical correlation for predicting propellant mass flow rate through short tube orifices have been developed by applying the modified single-phase orifice equation. Mostly the orifice constant and downstream pressure were corrected empirically in the single phase orifice equation. Pasqua (1953) developed a model for propellant R12 with saturated inlet conditions and included the effects of vaporisation at the surface of the liquid core. Mei (1982) proposed a choked flow model for R22 flow with sub-cooling greater than 22.2 °C and non-choked flow model for sub-cooling less than 22.2 °C. He empirically corrected the orifice constant as a function of upstream subcooling and pressure difference between upstream and downstream. Krakow and Lin (1988) developed a one-dimensional model of the flow of R12 through short tube orifices for $2<L/D<7$ integrating the momentum equation. It was assumed that the flow upstream of the orifice was subcooled and sonic velocity was obtained at the exit. Aaron and Domanski (1990) proposed a semi-empirical choked flow model for R22 modifying the single-phase orifice equation. The saturation pressure was

empirically corrected as function of *L/D* ratio and a non-dimensional form of the sub-cooling temperature and downstream pressure. Based on their model flow charts were provided to predict the mass flow rate of R12 through short tubes which were easy to use. All these above models did not cover two-phase inlet conditions.

A semi-empirical model of two-phase flow was developed by Kim and O'Neal (1994) to predict the mass flow of R134A in a short tube orifices. A short tube orifice is a simple expansion device with *L/D=3-20.* The model was designed to cover both single phase and two-phase flow at the inlet of short tube orifices. As this model covers both subcooled and two-phase inlet conditions and gives the empirical coefficients for R134A, which is used as a propellant in pMDIs, this model is used to predicts the mass flow rate across the valve orifice of pMDI in chapter 5 and hence it is discussed in detail here. A single phase flow model was developed by empirically correcting the modified orifice equation as a function of normalized form of upstream pressure, upstream subcooling, downstream pressure, and short tube geometry. Figure 2.3 shows the control volume (CV) around the short tube orifice used for the model. The two-phase flow model was derived by including the effects of upstream quality

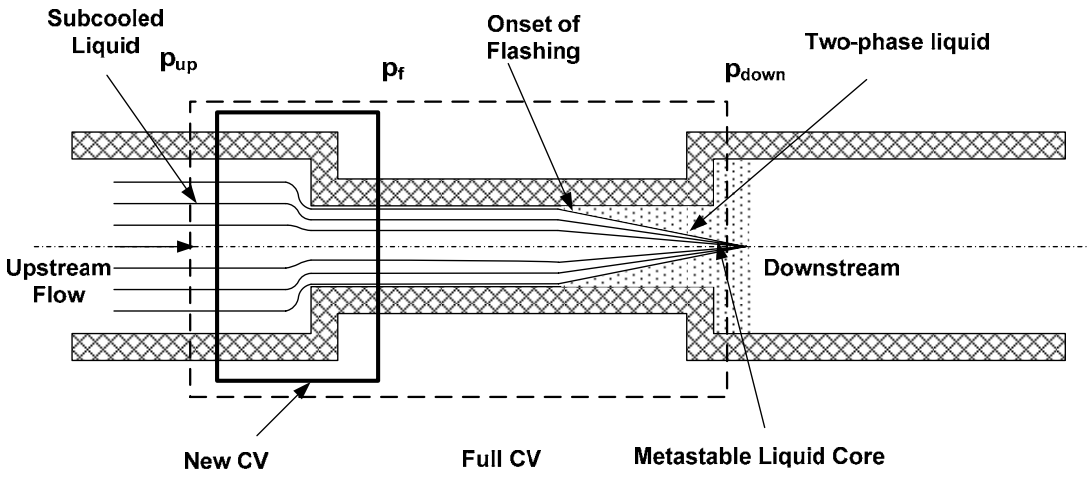

Figure 2.3 Control volume of the mass flow model (Kim and O'Neal, 1994)

and two-phase factor in the single-phase model. The final form of the semi-empirical mass flow model is given by

$$\dot{m} = C_{tp} A \sqrt{2\rho_f (p_{up} - p_f)} \tag{2.7}$$

where

$\dot{m}$ = mass flow rate (kg/s)

A = cross section area of the orifice (m^2)

ρ_f = fluid density (kg/m^3)

p_{up} = upstream pressure (kPa)

p_f = adjusted flashing pressure (kPa)

C_{tp} = correction factor for two-phase quality

The variables p_f and C_{tp} were correlated with respect to normalized form of each of the operating parameters and short tube geometries, which are given as:

$$p_f = p_s \left[\begin{matrix} b_1 + b_2 (p_{up} / p_c)^{b3} (L/D)^{b4} SUBC^{b5} + b_6 \exp(b_7 (D/D_{ref}) \times (L/D)^{b8} + \\ b_9 EVAP \end{matrix} \right] \tag{2.8}$$

$$C_{tp} = \frac{1}{(1 + a_1 x_{up}) \times (1 + a_2 (L/D)^{a3} Y^{a4 \ln(L/D)})} \tag{2.9}$$

where

$SUBC$ = $(T_s - T_{up})/T_c$ (T is in K)

$EVAP$ = $(p_c - p_{down})/p_c$ (p is absolute pressure)

$$Y = \frac{x_{up}}{(1 - x_{up})} \times \left(\frac{\rho_l}{\rho_v} \right)^{0.5}$$

D = diameter of the orifice (m)

L = length of the orifice (m)

D_{ref} = reference short tube diameter (1.35×10^{-3} m)

T_s = saturation temperature (K)

T_{up} = upstream temperature (K)

T_c = propellant critical temperature (K)

p_{down} = downstream pressure (kPa)

p_c = propellant critical pressure (kPa)

ρ_l = liquid density (kg/m^3)

ρ_v = vapour density (kg/m^3)

x_{up} = upstream quality (-)

The limitations of the above model are shown in Table 2.2. The model predicted approximately 95% of the measured data with ±5% error.

Singh et al. (2001) developed a semi-empirical model for R134A based on the orifice equation to describe the mass flow rate over a wide range of inlet and outlet conditions which included liquid, two-phase flow and vapour. The model was based on principles similar to those of Aaron and Domanski (1990) and Kim and O'Neal (1994). This model improved Kim and O'Neal's model, covering a wide range of

Table 2.Empirical constants in Flow Model equations (2.8) and (2.9)

Coefficients			
b_1	1.0156	b_8	2.9596
b_2	10.0612	b_9	-0.0745
b_3	-0.3296	a_1	-2.6519
b_4	-0.1758	a_2	5.7705
b_5	1.0831	a_3	-0.4474
b_6	-0.1802	a_4	0.3820
b_7	-0.00214		
Constants	p_c		T_c
	4056 kPa		374.205 K

Table 2.2 Limitations on the application of Flow Model equations (2.8) and (2.9)

Parameters	Minimum	Maximum
L	9.53mm	25.40mm
D	1.09 mm	1.72 mm
p_{up}	896KPa	1448 KPa
p_{down}	138 KPa	p_s
Subcooling	0 °C	13.9 °C
Quality (x_{up})	0%	8%

operating parameters, inlet qualities 0 to 1 and subcooling up to 40°C. Their experimental data was used to determine the new constants empirically.

Liu et al. (2004) correlated a short tube flow model for R744 with short tube geometric parameters and operating conditions based on their experimental data. The model was similar to that of Kim and O'Neal (1994) model, except that a new expression was given for the adjusted flashing pressure. The empirical coefficients were obtained from their experimental data. The prediction of mass rate compared favourably with experimental data for a wide range of automobile air conditioning operating conditions and a range of short tube geometries. However, two-phase inlet conditions were not considered in their study. A generalized correlation to predict the propellant flow rate through short tubes at subcooled and two-phase inlet conditions was developed by Choi et. al (2004) from a power law form of dimensionless Pi groups using pure (R12, R22 and R134A) and alternative (R407C, R410A and R502) propellants. The available experimental data in the literature was used to develop this correlation The dimensionless parameters are generated by applying the Buckingham Pi theorem to the variables for operating conditions, fluid properties and short tube geometry. For subcooled inlet conditions, the correlation yields an average deviation of 0.3% and a standard deviation of 6.1%, while for two-phase inlet conditions, it gave an average deviation of 0.2% and a standard deviation of 5%. The present correlation yields a good agreement with the database at subcooled inlet conditions and at two-phase inlet conditions. Tu et al. (2006) proposed a semi-empirical

correlation based on correction of discharge coefficient in orifice equation using downstream quality from their experimental data. This correlation was capable of predicting 90% of their experimental data within ±5% deviation.

From the above literature review on short tube orifices, it can be observed that various semi-empirical model exists to predict the mass flow rate along the short tube orifice for various propellants. These models are modified version of the basic orifice equation. All these models do not take frictional losses into account. The main drawback of these models is the presence of semi-empirical coefficients that require case-by-case adjustment for different fluids and geometries.

2.4.2.2. Homogeneous Equilibrium Model (HEM)

This model of two-phase flow has known for many years. In the HEM, the two-phase mixture is simulated as a pseudo-fluid that obeys the usual equations of single-component flow, possessing mean fluid properties. Hence, the mixture is homogeneous in phase composition, vapour and liquid velocities are equal, and two-phase mixture is in thermodynamic equilibrium i.e. vapour and liquid are at the same pressure and temperature. HEM is likely to be successful in long tubes, where there is a sufficient time for equilibrium to be achieved.

Bolstad and Jordon (1949) presented an analytical solution for adiabatic capillary tubes based on the homogeneous flow and constant friction factor. The governing momentum equation through the two-phase region was solved using a graphical integration method and assuming an isenthalpic process. Later Marcy (1949) did a similar study correlated the friction factor as a function of a two-phase Reynolds number. Although the predicted flow rates were with in 5% of the measured data, the measured flow rates were much lower than those seen in actual industrial applications. Goldstein (1981) presented a mathematical general iterative approach to model the flashing flow assuming adiabatic and homogeneous flow condition in capillary tubes with single and two-phase inlet conditions. System analysis of commercial and residential propellant units showed good correlation with manufactures data.

The effects of the various two-phase viscosity correlations on friction factor and prediction of the homogeneous model was studied by Wong and Ooi (1995). The results showed that the single phase Moody's friction factor expressed by Colebrook equation with Dukler mixture viscosity expression gives the best prediction in applying with the homogeneous model with an average error of 1%. Wong and Ooi (1996a) presented a numerical model for propellant flow through an adiabatic capillary tube using a homogeneous two-phase model to study the effects of the various design parameters on capillary tube performance with R12 and R134A. The governing equations were solved using the standard fourth order Runge-Kutta technique with a 1 mm length increment. The computations were terminated at the critical flow condition. The two-phase friction factor was evaluated using Colebrook's equation model along with Dukler viscosity model. The model predicted the length and pressure, temperature and quality distribution along the capillary tube for given mass flow rate and inlet conditions. The comparison of the flow characteristics of R134A and R12 revealed that R134A yields higher pressure drops than R12 for both subcooled liquid region and two-phase region. For the same operating conditions R134A always settled with a shorter tube length and an approximation of about 15 to 20% reduction in tube length is expected. The results also confirmed that for the same tube dimensions and conditions, R12 can accommodate a higher mass flow rate before the flow reaches the choked conditions.

Escanes et al. (1995) developed a numerical method to simulate the thermal and fluid-dynamic behaviour of capillary tubes, in transient and steady state assuming the homogeneous equilibrium model. The governing equations of the flow (continuity, momentum and energy) were solved using an implicit step-by step numerical technique. Due to high pressure gradients at the exit of the capillary tube, a non-uniform grid, concentrated at the exit of the capillary tube was used. The numerical model allows calculation of the mass flow rate through capillary tubes and the local values of the flow variables (pressure, temperature, velocity, etc.). The calculation of the mass flow rate in both critical and non-critical flow was performed iteratively by means of a Newton-Raphson algorithm. In case of critical flow, discharge shock wave is solved at the exit of the capillary tube. Good agreement was observed between numerical and experimental data.

Sami and Tribes (1998) developed a numerical model to predict the performance of adiabatic capillary tube for zeotropic and azeotropic binary mixtures as well as pure HFC propellants using HEM under saturated, subcooled and two-phase inlet conditions. The friction pressure drop was calculated using the correlation reported by Beattie (1973). The governing equations were solved using fifth-order Runge-Kutta-Fehlberg method, which was more stable than the earlier existing methods. The numerical results fairly predicted the experimental data for alternative propellant mixtures. However slight discrepancies were observed for pure propellants R22 and R134A, which was due to use of the Beattie correlation.

Bansal and Rupasinghe (1998) developed a homogeneous two-phase model, CAPIL, to study the performance of adiabatic capillary tubes in small vapour compression refrigeration systems. The numerical model was based on the fundamental equations of conservation of mass, energy and momentum that are solved simultaneously through iterative procedure. REFPROP data base was used to calculate the propellant properties. The frictional factor was evaluated using Churchill's correlation. The flow was divided into two regions: single phase liquid region and two-phase region. First, the single phase length was calculated using the momentum equation. Then, the two-phase region was divided into a number of small elements and the governing equations are solved for the flow variables at the exit of each element. The model was validated with earlier experimental data and simulation models and was found to agree within ±10%.

Wongwises et al (2000b) studied a two-phase homogeneous flow model to determine propellant flow characteristics in adiabatic capillary tubes. Colebrook correlation was used to determine the two-phase friction factor. Both, the conventional propellants R12 and R22 and alternative propellants R134A, R401A, R401B, R401C, R407C, R410A were considered. REFPROP was used to evaluate the propellant properties. Three different viscosity models were used and they were varied depending on the propellant based on previous research. The numerical calculation was divided into two parts: subcooled single-phase region and two-phase region. First, the single-phase length was calculated using the friction factor and saturation pressure of propellant. In the two-phase region, governing equations were solved using the fourth-order Runge-

Kutta method. Initial conditions required in the calculation are pressure and temperature of propellant at the capillary tube inlet, mass flow rate of propellant, roughness and diameter of pipe. Their results showed that the traditional propellants consistently gave lower pressure drops for both single-phase and two-phase flow than the environmentally acceptable alternative propellants which resulted in longer capillary tube lengths for traditional propellants. In a subsequent study Wongwises and Pirompak (2001) used five viscosity models and developed a 'capillary tube selection chart' which is helpful in selecting the capillary tube size from the flow rate and flow condition.

Bhupesh Chandra and Prabhu (2004) developed a numerical model to study the two-phase flow of propellants (R22 and R134A) through adiabatic capillary tubes using the homogeneous model. They considered three single friction factors and six two-phase viscosity models and three two-phase friction factor from single phase friction factors. It was observed that the Haaland friction factor correlation along with Dukler two-phase viscosity correlation for R22 propellant and Colebrook friction factor correlation with Mc Adams viscosity model for R134A were the best choices. It should be noted that in all of the above mentioned models, the slip effect between the two-phases was not taken into consideration.

From the above literature review on propellant flow through long capillary tubes, it can be seen that HEM is used to model both pure propellants and propellant mixtures. Many of the models discussed above use numerical techniques which can predict pressure-flow characteristics (as empirical models) but also detailed distributions of thermodynamic and flow variables. The predictions of HEM are fairly good because HEM is applicable for the long pipe as there is a sufficient time for equilibrium to be achieved.

2.4.2.3. Non-Homogeneous Equilibrium Model

This model is an extension of the HEM model that permits different vapour and liquid velocities. The model assumes adiabatic flow and the phases are in thermodynamic equilibrium. A velocity ratio, S, defined as the ratio between the vapour and liquid

velocities, is considered and treated as a variable which is determined by the conditions of the maximum mass flux at the exit. The velocity ratio, $S = (\rho_l/\rho_v)^{1/3}$. This model is well documented in Elias and Lellouche (1994).

Kim and O'Neal (1995) studied eight critical flow models: four homogeneous equilibrium models, two homogeneous frozen models (HFM) and two non-homogeneous equilibrium models (NEM). The results were compared with their experimental data. Based on the comparison, they found that the NEM was fairly consistent with the experimental data for qualities above 0.15. However, no verification was made for exit qualities above 0.2. Only the HFMs showed the best agreement with the measured data for a wide exit pressure range except for the low quality region (quality <0.06).

2.4.2.4. Separated flow Model (SFM)

In a two-phase flow, owing to differences in the physical properties (e.g. density and viscosity) of the phases the vapour phase tend to flow at a higher in situ velocity than the liquid phase, hence slip exists between the phases. Separated flow models take account of the fact that the two-phases can have differing properties and different velocities. This may be developed with various degrees of complexity. In the most sophisticated version, separate equations of continuity, momentum and energy are written for each phase and these six equations are solved simultaneously together with equations which describe how the phases interact with each other and with the walls of the duct. In the simplest version, only one parameter, relating to the difference of velocity of the two-phases is evaluated along with conservation equations for the mixture. When the number of variables to be determined exceeds the available number of equations, correlations or simplifying assumptions are introduced (Wallis, 1969).

Wong and Ooi (1996b) compared the HEM and a SFM, considering the slip between the phases, for simulating the flow in adiabatic capillary tubes. The slip between the phases was accounted using Miropolskiy's (1970) slip ratio The comparison between theoretical prediction with the Li et al (1990a) and Mikol (1963) experimental results

showed that in a single phase flow region, Moody's friction factor is applicable in predicting the pressure drop, while for two-phase flow region, both the HEM and SFM with slip between the phases may be used adequately to predict the flow of propellants in capillary tubes. They concluded that the separated flow model with Miropolskiy slip ratio combined with Lin et al. (1991) frictional pressure gradient showed a better agreement with the experimental results, particularly closed to exit of the tube where the flow is choked.

A two-phase separated flow model was developed by Wongwises et al. (2000a) to compare the various two-phase friction pressure gradient correlations and slip ratio correlations. Four different pressure gradient correlations and slip ratios were used. The results were compared against the experimental results of Mikol (1963), Li et al. (1990a) and Koizumi and Yokoyama (1980). The agreement between the experimental and numerical results obtained using R12, R22 and R134A through capillary tubes has indicated that the separated flow model with appropriate correlations of the frictional pressure gradient and slip ratio can be used to predict the two-phase flow of propellant in capillary tubes.

Sanzovo and Mattos (2003, 2004) compared the homogeneous equilibrium model and a separated flow model to investigate the flow through propellant mixtures along a capillary tube. The slip ratio was evaluated using Premoli et al. 's (1971) correlation and two-phase frictional pressure gradient was evaluated using Lin et al. (1991) correlation. The friction factor was evaluated using Serghides correlation and the two-phase viscosity was calculated using Dukler's correlation. The simulation results showed that both the models predicted the same error level (±8%) when compared to measured values of mass flow rate, temperature and pressure profiles. Garcia-Valladares (2006) developed a numerical method to analyze the fluid-dynamic behaviour of adiabatic short tube orifices working with trans-critical carbon dioxide (CO_2 or R744). A separated two-phase flow model, using Premoli et al. (1971) correlation for the slip ratio, was used to model the two-phase flow. The two-phase frictional pressure gradient was evaluated using Yoon et al. (2003) correlation. The discretized governing equations were coupled using an implicit step-by-step method.

The numerical results predicted the mass flow rate with an average error of 3.55% with the experimental data.

The Drift Flux model is essentially a separated flow model in which attention is focused on the relative motion rather than on the motion of the individual phase. The separated flow model requires information for the void fraction and friction effects The drift flux model uses conservation equations for the entire mixture. The formulation is expressed in terms of four field equations three for the mixture (continuity, momentum and energy) plus the drift velocity.

Liang and Wong (2001) numerically studied the modeling of two-phase propellant flow through adiabatic capillary tubes using drift flux model. They considered the slip effect between the two-phases. The model was validated against the experimental results of Li et al. (1990a) and Mikol (1963) for subcooled inlet conditions. The predicted pressure profiles showed good agreement against the experimental data. The detailed flow characteristics of R134A within a capillary tube, such as distribution of pressure, void fraction, dryness fraction, phase's velocities and their drift velocity relative to the centre of the mass of the mixture were presented.

2.4.2.5. Two-Fluid Model (TFM)

In TFM, hydrodynamic as well as thermal non-equilibrium effects are considered. Separate conservation equations are written for each phase (or for one phase and the combined phases separately) and interaction terms are included to represent the interphase heat, mass and momentum transfer. Upstream conditions, including a description of the nucleation centers, are supplied as one boundary condition and the solution is developed numerically in the downstream direction (Wallis, 1980). TFM showed good agreement against the experimental results for water flow in long/short tubes (Richter, 1983)

Seixlack et al. (1996) and Seixlack and Barbazelli (2009) presented a TFM to simulate the steady state propellant flow through an adiabatic and non-adiabatic capillary tube. The TFM was employed for the two-phase region considering the

hydrodynamic and thermodynamic non-equilibrium between the liquid and vapour phases. The governing equations were solved using the fifth order predictor-corrector method. The numerical results were compared against the experimental results of Dirik et al. (1994) and Melo et al. (1999). The numerical results showed that thermal non-equilibrium between the phases is very small in the two-phase flow region of the capillary tube. It was observed that the flow in capillary tubes closely resembles a homogeneous situation, as the relative velocity between the phases is quite small. Their results indicated that the relative mean error in prediction of the choked mass flow rate by the two-fluid model and the homogeneous model was 3.6% and 5% respectively.

The application of TFM to propellant flow through short tubes was studied by Yang and Zhang (2005). They developed a non-equilibrium two-fluid model (TFM) for propellant two-phase critical flow inside the short tube orifice. Both inter-phase velocity slip and inter-phase temperature differences were taken into account in the model. The interfacial frictional force and interfacial heat transfer were evaluated using the empirical correlations from the literature. The mass flow rate, the two-phase velocity and temperature distributions were calculated with both subcooled and two-phase inlet conditions. The comparison between the TFM and HEM results showed that the TFM gives good predictions while the HEM underestimates the flow rate by 20%.

2.4.2.6. Metastable Flow Models

The experimental work on propellant flow through capillary tubes reviewed earlier in section 2.4.1.2 (Cooper et al., 1957; Mikol, 1963; Rezk and Awn, 1979; Koizumi and Yokoyama, 1980) clearly demonstrates that the metastable phenomenon exist in these flows. After the pioneering work done by Li et al. (1990a) and Chen et al (1990) on metastable flows, many researchers have accounted to metastability in their models.

Li et. al (1990b) developed a numerical model to study the steady-state, two-phase flow in capillary tubes, considering thermodynamic non-equilibrium phenomenon during vaporisation and relative velocity between the liquid and vapour. The under

pressure of vaporisation was evaluated using the Chen et al (1990) correlation. The five differential equations of the drift flux model were solved by using Runge-Kutta method. The numerical results showed a good agreement with their experimental data of R12.

Dirik et al (1994) numerically studied the flow through adiabatic and non-adiabatic capillary tubes using propellant R134A. The friction factor was evaluated using Colebrook's correlation along with McAdams viscosity model. Again, the under pressure of vaporisation was calculated using Chen et al. (1990) empirical correlation. The flow rates predicted by the numerical model showed good agreement with their measurements over a wide range of operating conditions and geometric parameters.

Bittle and Pate (1996) presented a numerical model to predict the adiabatic capillary tube performance with alternative propellants R134A, R22, R152a and R410a. The two-phase friction factor was presented as a function of Reynolds number. Three different viscosity models were evaluated by comparing predicted results to high quality inlet test data for the three pure propellants R134A, R22 and R152a. The metastable region was modeled using Chen et al. (1990) correlation. The comparison of the numerical results against the experimental data showed good agreement with discrepancies of 6% for subcooled liquid inlet and 10% for two-phase inlet conditions.

Garcia-Valladares (2002a, 2002b) developed a detailed one-dimensional steady and transient numerical model to study the thermal and fluid dynamic behaviour of capillary tube expansion devices working with pure and mixed propellants considering the metastable region. In the two-phase metastable region, the model of Feburie et al. (1993) was used to evaluate the vaporisation index along the capillary tube. The under pressure of vaporisation was evaluated using Chen et al. (1990) and Lackme's (1979) correlation. REFPROP was used to calculate the propellant properties. The discretised governing equations are coupled using an implicit step-by-step method. The numerical model allows analysis of aspects such as geometry, type of fluid (pure substances and mixtures), critical or non-critical flow conditions, metastable regions, adiabatic or non-adiabatic capillary tubes and transient aspects. Both pure propellants (R12, R22) and propellant mixtures (R407C and R410A) were

used as working fluids. In general, it was found that Chen et al (1990) correlation predicted the delay of vaporisation better compared to Lackme's correlation. Comparison of the numerical simulation with experimental data of presented in the technical literature (Li et al.,1990a; Mikol,1963; etc.) shows the importance of considering the metastable region in the mathematical model giving more accurate mass flow rate predictions.

Wongwises and Suchatawutt (2003) developed a numerical model for a two-phase propellant flow through adiabatic capillary tube taking into account the metastable region assuming annular flow assumption. The fourth-order Runge Kutta method was used to solve the governing equations. The under pressure of vaporisation was predicted from the correlation of Chen et al.(1990) and Lackme (1979). Their results showed that the annular flow model with Chen et al. correlation predicts the metastable length close to the experimental data.

Bansal and Wang (2004) numerically studied the metastable choking flow through an adiabatic capillary tube using propellants R134A and R600A. The underpressure of vaporisation was evaluated using Chen et al (1990) correlation. A new diagram called 'full range simulation diagram' were developed which helped to understand the choked flow phenomenon graphically and could help in design of capillary tubes.

From the above literature review, it can be seen that the metastability of propellant flow through capillary tube is modeled well by evaluating the delay of vaporisation using Chen et al. (1990) correlation and using Feburie et al (1993) DEM (Garcia-Valladares, 2002 a-b). As the propellant flow inside the twin orifice system of pMDI is in metastable state and the regime inside the twin orifice system is in two-phase metastable region, the DEM proposed by Feburie et al (1993) can be applicable to model inside the twin orifice system of pMDI.

2.5. Flow through twin-orifice nozzles

Previous work on atomization through twin-orifice nozzles has results in empirical relationships, correlating the aerosol size with the nozzle geometry and propellant properties. In this section this work will be discussed.

Fulton et al. (1950) experimentally studied the atomization of a mixture of propellant R11/R12 /Insecticide (43%/43%/14%) through capillary tubes and two-orifice nozzles. The performance of the capillary tube was investigated using size analysis of the residual aerosol for different capillary diameters. The capillary tube diameters ranging from 0.34 mm to 0.74 mm found to produce the minimum mass median diameter (MMD) of approximately 16 μm. Where as for twin-orifice systems an expansion chamber volume of 0.13 cm^3 and upstream upstream and downstream orifice diameters of 0.38 mm and 0.53 mm respectively, were found to produce the optimum spray. The killing rate of the house fly (Musca domestica) was used to define the optimum spray production.

York (1956) reviewed the literature on liquefied gas aerosol generators and divided the atomization process into four stages:

(i) Primary atomization due to flashing

(ii) Secondary atomization of droplets from stage 1 due to aerodynamic forces during impact with the atmosphere.

(iii) Evaporation of the propellant droplets.

(iv) Entrainment and deceleration of the spray.

It was concluded that existing literature covered stages 2 to 4 but that no experimental work of a fundamental nature had been reported on primary atomization due to flashing.

The factors affecting the size distribution of kerosene propellant mixtures (propellant R11/R12, 50%/50% by weight) atomized by a twin-orifice nozzle were investigated by Lefebvre and Tregan (1964). The particle size of the aerosol was measured by sedimentation on to a glass slide coated with magnesium oxide. Flash photography

was used to give a qualitative assessment of the spray. process. Four variables were studied

- the temperature of the kerosene mixture (15^{o}C to 35 ^{o}C)
- the ratio of propellant to kerosene ratio (60% to 80%)
- percentage of propellant 12 in the propellant mixture (30% to 70%)
- different nozzle designs (four)

The standard conditions used for the study were temperature was 20°C and propellant/kerosene mixture was 85%/15% by weight. From their results it was observed that the spray becomes finer with increase in temperature, increase in percentage of propellant and increase in the fraction of propellant, R12 in the propellant mixture. All these variations increase the vapour pressure of the mixture which provides additional energy for the atomization process. The design of the nozzle also found to alter the size distribution considerably. The influence of propellant, composition, concentration and temperature upon the drop size produced from aerosols containing kerosene and Freon propellants were tested. The results showed that the spray becomes finer as propellant temperature is increased, as the percentage of propellant is increased and as a fraction of propellant R12 in the propellant mixture is increased.

The size distribution of kerosene and oil aerosols generated by a continuous spray from a twin-orifice nozzle was measured by Teslin (1969). A sedimentation chamber was used to collect the residual droplets on glass slides coated with dimethylchloride and MMD's were determined by optical microscopy. It was found that increasing solution vapour pressure by increasing the percentage of propellant, or increasing solution temperature, produced a finer cloud, which was general agreement with the result of Lefebvre and Tregan. Teslin used calculations based upon ideal gases to relate spray properties to 'specific work of expansion'. He concluded that 'specific work of vapour expansion' was a quantitative characteristic that causes dispersion by a superheated liquid to be different from that of other spray process.

Fletcher (1975) experimentally studied the flashing flow of propellant mixture along the twin-orifice system for continuous discharge. A mixture of propellant 11 (39.6%),

propellant 12 (59.4%) and surfactant (sorbitan trioleate) was used as working fluid. Double flash photographic technique was used to measure the aerosols. The valve and spray orifice diameters ranging from 0.25 mm to 0.7 mm were investigated. The length and diameter of the expansion chamber were 12.7 mm and 3.2 mm respectively. The MMD of the residual surfactant droplets for the cases where diameters of valve and spray orifice were equal, was found to be proportional to the spray orifice diameter. Fletcher concluded that the mass flow rate was proportional to the product of valve orifice and spray orifice diameters and showed that the quality of the propellant could be predicted from geometric and thermodynamic variables. It was observed that the propellant in the expansion chamber was not in thermodynamic equilibrium but in a metastable condition. An expression for the degree of metastability was developed as the difference between the saturation vapour pressure of propellant at expansion chamber temperature and the expansion chamber pressure.

The most comprehensive study of propellant flow through twin-orifice nozzle and pMDI atomization has been conducted by Clark (1991). Both continuous and metered flow were considered. The qualitative description of the process inside the two-orifice system of pMDI for continuous discharge flow (Clark, 1991) and metered discharge flow (Clark,1991; Versteeg and Hargrave, 2002) is summarized as follows :

Qualitative Description of flow process in Continuous Discharge Flow

The continuous discharge of saturated propellant through twin-orifice system consists of four process:

- The saturated liquid propellant initially flows from the metering chamber through the valve orifice.
- Due to pressure drop across the valve orifice, flash boiling of the liquid takes place and a two-phase mixture fills the expansion chamber
- The two-phase mixture inside the expansion chamber, still at a pressure above ambient, expands and discharges through the spray orifice.
- The secondary atomization of this two-phase mixture takes place downstream of the spray orifice. Steady state conditions are reached when the mass flow rate through the valve orifice is equal to the mass flow rate through the spray orifice.

Qualitative Description of flow process in Metered Discharge Flow

The metered discharge of saturated propellant through twin-orifice system consists of five process

- Prior to actuation, the metering chamber consists of know amount of propellant at ambient temperature and saturated vapour pressure; the expansion chamber is filled with atmospheric air at ambient temperature and pressure. As the valve is depressed liquid propellant starts to flow through the valve orifice into the expansion chamber, where flashing takes place.
- As the liquid flows out through the valve orifice, liquid evaporates and vapour is generated to fill the voidage in the metering chamber. Evaporation of the liquid decreases the temperature and pressure inside the metering chamber, so the mass flow rate through the valve orifice decreases throughout the discharge event.
- The resulting two-phase mixture expands into the expansion chamber, pushing the air ahead of it and out through spray orifice. The pressure in the expansion chamber is lower than the metering chamber but higher than atmospheric, so two-phase mixture is expelled through spray orifice.
- The final spray is produced at the actuator orifice exit, before it enters the ambient atmosphere. Liquid ligaments embedded in the propellant vapour are torn apart by flow forces and small droplets are formed.
- The droplets entrain surrounding air moving away from the actuator orifice. Further evaporation of droplet occurs due to heat supplied by the entrained air.
- Discharge continues until the pressure in the metering chamber and valve stem is equal to atmospheric.

Experiments were conducted using pressure transducers and thermocouples within the liquid supply reservoir and expansion chamber, with a force transducer used to calculate the thrust from the emergent spray. The thrust was related to the exit velocity of the spray. The expansion chamber pressures, temperatures and exit velocities for different propellants (R12, R134A, R12/R114 (60%/40%) and R227 with surfactant Sorbitan trileate) and various geometries valve orifice diameter (D_{vo}) ranging from 0.259 mm to 1.005 mm and spray orifice diameters (D_{so}) ranging from

0.294 mm to 1.147 mm were reported. Theoretical models were then developed from the study of a continuous spray and extended to the metered spray process. The theoretical model was based on homogeneous equilibrium (HEM) inside the expansion chamber and frozen flow (HFM) across the valve and spray orifice. For continuous discharge, the comparison between the theoretical predictions and the measured values of the expansion chamber and mass flow rate showed good agreement with spray to valve orifice diameter ratio less than 1.5. However, at diameter ratios greater than 1.5 the model showed following discrepancies:

(i) The measured expansion chamber temperature showed reasonable agreement with the theoretical values for low orifice diameter ratio (D_{so}/D_{vo}.). However, the theoretical models overpredicted the expansion chamber temperatures for high orifice diameter ratios (D_{so}/D_{vo}.)

(ii) The measured expansion chamber pressures were lower than the predicted values using the theoretical model.

(iii) The measured exit velocities showed large scatter with the theoretical predictions.

The discrepancies (i) and (ii) were attributed to metastability of the propellant. And the discrepancy (iii) was attributed to the method used to determine the exit velocity. Empirical correlations were developed to predict the expansion chamber pressure and temperature expressing the metastability as a exponential function of residence time inside the expansion chamber, but these predicted corrections based on these expressions showed poor agreement with measurements.

The atomization process was also investigated by measuring the residual droplets size using an aerodynamic particle sizer (APS) and applying simple vaporisation theory to extrapolate information on the initial droplet diameter. The following correlation was developed for initial droplet diameter, *D :*

$$D = \frac{8.02}{x^{0.56}\left(\frac{p_{ec} - p_{dis}}{p_{dis}}\right)^{0.46}} \qquad 2.10$$

where x is the quality of the flow in the expansion chamber and p_{ec} and p_{dis} are the expansion chamber and ambient pressures respectively.

Hickey and Evans (1996) developed a simple analytical model to describe droplet formation and evolution from pMDI. The model predictions were compared with droplet size data obtained using laser diffraction. The analytical model included considerations for the droplet formation and diffusional evaporation during secondary atomization. The predicted results were within an order of magnitude of the measured droplet sizes. The presence of solid particles and surfactant was neglected. It was recognized that droplet composition would be of great significance, affecting droplet formation, heat and mass transfer and contributing to complex thermodynamic phenomenon.

Dunbar et al. (1997a and b) developed a model of the primary atomization process and resultant spray characteristics for a pure HFC propellant (R134A), which involved the separated analysis of the multiphase fluid flow in the three compartments that are active during an actuation (i.e. metering chamber, expansion chamber and actuator nozzle). The discrete droplet model (DDM) was used in conjuction with a computational fluid dynamics model to predict the development of aerosol plume in stationary ambient air. Internal flash evaporation was considered to be a dominant mechanism for primary atomization. This assumption was based on experimental observations using flow visualization of the near-orifice flow field in which the spray was observed to be pre-atomized and discharged periodically (Dunbar 1996). Pre-atomization suggested that the spray was atomized upstream of the actuator nozzle.

Brambilla et al. (1999) experimentally studied the effect of non-volatile components such as glycerol or polyethylene glycol, dimensions of actuator and propellant on the particle size of the aerosol. The results showed that the absence of non-volatile additives generated very fine clouds. Decreasing the actuator aperture diameter increased the fine particle dose and a higher pressure propellant enhanced the atomization and gave finer sprays.

Versteeg and Hargrave (2001, 2002) studied the fundamentals of pMDI spray development experimentally. They visualized the transient flow and primary atomization in near-orifice region of a commercial pMDI actuator and in the

expansion chamber and near-orifice region of a rectangular transparent model of a pMDI actuator package using laser-based high speed imaging and image analysis. Visualizations of sprays in the near orifice region of pMDI revealed the following spray characteristics: (i) start-up transient, (ii) fully developed spray with slow spray density variations with a characteristic time scale around 100ms related to changes of pressure and vapour mass fraction of the two-phase mixture inside the actuator valve and expansion chamber and (iii) rapid spray density pulsation with large droplet production and considerable spray cone angle variation with characteristic time scale around 2ms.

Wigley et al. (2002) experimentally studied the spray characteristics in the near-orifice region of a pharmaceutical pMDI using PDA. Results showed that a highly pre-atomized spray with typical mean drop size between 2 and 5 microns emerges from the actuator orifice. The spray was found to exhibits a complex temporal behaviour including significant transient movement normal to the main spray direction. The measured velocities and drop sizes showed good agreement with the predicted trends of a phenomenological propellant flow model in conjuction with drop size equation (2.10) during the first 70 milliseconds of the actuation event confirming validity of its thermodynamic assumptions and associated pre-atomization mechanism.

Smyth (2003) presented a comprehensive review on the factors influencing the performance of alternative propellant driven metered dose inhalers. In his review, he concluded that the several methods exist to understand the design of pMDIs but they are empirical in nature. A general and systematic approach which can help in designing new-propellant pMDIs does not exist. Kakade et al. (2006) presented a systematic design optimization process to improve the actuator performance of a vortex nozzle actuator (VNA). The optimization effort mainly relied on laser-based optical diagnostics to provide an improved understanding of the fundamentals of aerosol formation and interplay of various geometrical factors. The performance of the optimized VNA design was characterized using phase Doppler anemometry and cascade impaction. The aerosol velocities for both standard and optimized VNA designs were found to be comparable and both notably less than conventional twin-

orifice actuators. The optimized VNA design also significantly reduces drug deposition in the actuator as well as USP throat adapter, which in turn, leads to a significantly higher fine particle fraction than the standard design. Recently, Smyth et al (2006) experimentally investigated the effect of actuator design on spray pattern of metered dose inhalers. Three actuator design features were selected for investigation : orifice diameter, sump depth and orifice length. Spray pattern and particle size profiles were measured. Their results showed that, in addition to orifice size, spray patterns are significantly influenced by the actuator orifice length and sump depth. Volume median diameter was minimized decreasing orifice size, orifice length, sump depth.

2.6. Closure

A detailed literature survey on flashing flow of propellant/propellant flow through short tubes, capillary tubes and twin-orifice systems has been presented covering experimental and theoretical work by a large number of researchers over a period of 60 years. The experimental investigations reveal that the flashing liquid flow through these orifices is in metastable nature. The liquid metastability plays a major role in atomization process and has significant effect on the mass flow rate and flow variables at the exit, particularly in tubes L/D <20. The prediction of these flow variables at the exit of the spray orifice of pMDI is of primary importance in determining the shape and penetration of the resulting spray as well as its detailed characteristics of number density, drop velocity, and drop size distributions.

The metastable flow through short tubes and capillary tubes is now better understood and a number of theoretical models such as a semi-empirical model proposed by Kim and O'Neal (1994), Delayed Equilibrium Model proposed by Feburie et al (1993) and Improved Delayed Equilibrium Model (IDEM) proposed by Attou and Seynhaeve (1999a) has been developed to model this metastable phenomena inside these devices. However, the models of twin-orifice system by Fletcher (1975) and Clark (1991) assumed frozen flow (i.e. complete metastability) in the orifices, but thermodynamic equilibrium (i.e. no metastability) in the metering chamber and expansion chamber.

In addition to this Clark (1991) made an attempt to account for metastability in the expansion chamber, but this was ultimately unsuccessful. The discrepancies between experiments and theoretical models developed by these authors suggests that there is a scope for the improvement. The metastability models available in the literature are DEM (Feburie et al, 1993)and IDEM (Attou and Seynhaeve, 1999a) which were very successful for steam-water flows. As the DEM was successful for the propellant flow through capillary tubes (Garcia-Valladares, 2002a-2002b), it would be the best model to consider to model the flow through twin orifice systems.

The purpose of this present work is to develop a general and systematic approach to model the metastability through twin orifice of pMDI accounting to propellant metastability which provides details of the variations of pressure, temperature, velocity and void fraction in the direction of propellant flow. The next chapter discus the objectives, method of attack along with the mathematical modeling.

CHAPTER 3

CONCEPTUAL AND MATHEMATICAL MODELS

3.1. Introduction

Previous work by Fletcher (1975) and Clark (1991) has done much to reveal the general nature of pMDI propellant flows. They developed semi-empirical models of flashing propellant flows through a pMDI based on assumptions of thermodynamic equilibrium in the metering and expansion chambers and homogeneous frozen flow in the valve and spray orifices. The results of the models were in good overall agreement with their experimental results, but highlighted number of problems with the model:

- The pressure drop and the temperature drop across the valve orifices are underestimated.
- Measured temperatures in the expansion chamber did not match with the saturation temperature at the measured pressure. This suggests that the mixture is metastable and the liquid is superheated.
- The expansion chamber quality is underestimated.
- The exit spray velocity is underestimated.

Fletcher (1975) and Clark (1991) models have good track record in directing pMDI design and have provided an adequate starting point for numerical work. Known problems with the model, however, suggest that there may be scope for improvements.

The key issues for the pharmaceutical community to know are as follows:

(i) total drug dose emitted and temporal profile of drug emission $\dot{m} = \dot{m}(t)$

(ii) spatial and temporal distributions of droplets carrying the drug produced at spray orifice

(iii) velocity of droplets/spray at spray orifice.

Work by Clark (1991) suggests that these are related to pressure ratio across the spray orifice and quality or void fraction in the final spray orifice. The atomization process

is strongly influenced by the liquid properties of density, viscosity and surface tension (Lefebvre, 1989). These properties depend on their local pressure and temperature. Hence, the detailed state of the fluid inside orifices, in particular in the vicinity of the spray orifice exit is needed to predict the atomization and spray formation. To enable modeling of pMDI atomization from first principles it is therefore essential that the thermodynamic state and two-phase flow conditions in the spray orifice can be accurately predicted.

Metastability is known to play a role in orifices and nozzles and has been extensively studied. A substantial number of theoretical models each with its own simplifying assumption, have been developed. From the literature it becomes apparent that liquid metastability can be modeled well in capillary tubes in steam-water flows and refrigeration and air-conditioning flows (e.g. Feburie et al.,1993; Attou and Seynhaeve, 1999a; Garcia-Valladares, et al. 2002a; Wongwises and Suchatawutt, 2003). However, no successful attempt has been made this far to model metastability in twin-orifice systems relevant to the pMDI.

3.1.1. Objectives

The main objective of the present work is to develop a new numerical model which would predict the internal flow conditions (pressure, temperature, velocity, void fraction, quality, etc.) and provides deeper insight into the atomization process and fluid mechanics involved in the twin-orifice of pMDIs accounting to the propellant metastability.

3.1.1.1. Method of Attack

In order to achieve the main objective of this research, the thesis is directed towards achieving the following sub-tasks:

(i) An assessment of the performance of existing theoretical, semi-empirical models to understand the two-phase flashing flow inside the short tubes with experimental results review in Chapter 2.

(ii) The development of a 1D code to predict the mass flow rate of the flashing propellant for the above models (Chapter 3 and Chapter 4).

(iii) An assessment of existing liquid metastability models inside the capillary tubes to understand the affect of liquid metastability by comparison with experimental results reviewed in Chapter 2.

(iv) The development of the 1D code to predict the mass flow rate along with the flow variables inside the capillary tube for metastability propellant flow (Chapter 3 and Chapter 4).

(v) Extend the above 1D liquid metastability model to include choked conditions at the exit of the capillary tube and validate against the existing experimental results (Chapter 3, Chapter 4 and Chapter 5).

(vi) Improved representation of thermodynamic and transport properties of pMDIs propellants and propellant mixtures using REFPROP v.7.0.

(vii) Extend the above 1D liquid metastability model to continuous flow through a twin-orifice assembly relevant to pMDIs (Chapter 3, Chapter 4 and Chapter 6).

(viii) Validate the above 1D model with the available experimental work (Chapter 7).

(ix) Develop the coefficient modifications for the relaxation equation used to account metastability to fit all twin-orifice assemblies relevant to pMDIs (Chapter 7).

(x) Test the capability of the above model for the quasi steady state flow of metered discharge flows (Chapter 7).

In this chapter, the governing equations and the boundary conditions for the two-phase propellant flow through short tube, long capillary tube and twin-orifice system of pMDIs are introduced.

When a propellant flows through a capillary tube in a refrigerating system, the drop in pressure in the flow direction changes the fluid from a subcooled liquid to a two-phase mixture. In such a process, the flow may be metastable. This means that the inception of vaporisation does not take place at a location of the thermodynamic saturated state (p_s in Figure 3.1 and Figure 3.2), but at a location further downstream

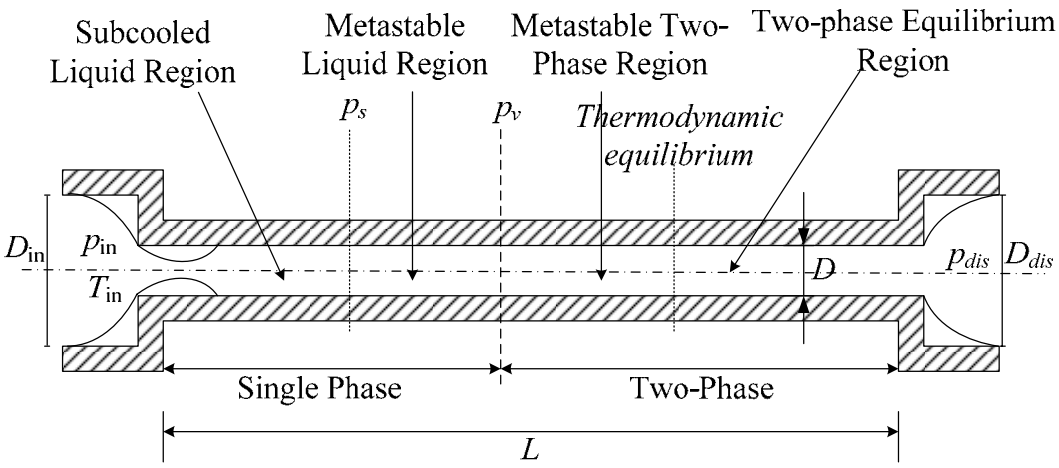

Figure 3.1 Schematic view of an adiabatic capillary tube with metastable regions

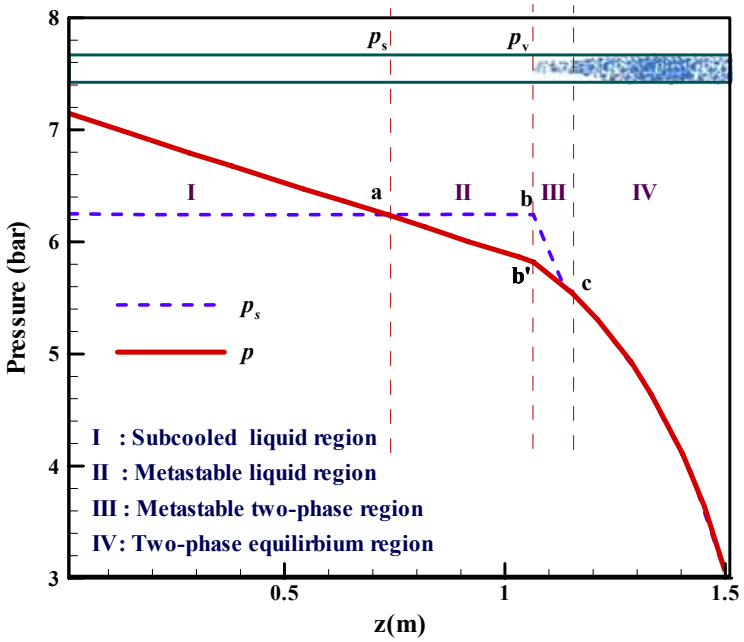

Figure 3.2 Typical pressure distribution along an adiabatic capillary tube (Li et al (1990a)

from the thermodynamic saturated point i.e. at point p_v (pressure of vaporisation) in Figure 3.1 and Figure 3.2

According to (Li et al., 1990a) the flow of propellant through an adiabatic capillary tube can be divided into four distinct regions (see Figure 3.1):

- subcooled liquid region (zone I: when $p \geq p_{s,} x = 0$)
- metastable liquid region (zone II: when $p_s > p \geq p_{v,} x=0$)
- metastable two-phase region (zone III: when $p_v > p_{,} 0< x \leq x_{equil,}$) and
- thermodynamic equilibrium two-phase region (zone IV:, $x_{equil} < x \leq 1$).

Figure 3.2 shows a typical pressure distribution (saturation pressure corresponding to the measured temperature to measured pressures) along an adiabatic capillary tube taken from Li et al. (1990a). At point 'a', the pressure is equal to the saturated pressure but vaporisation does not take place. A metastable liquid flow occurs for a short distance until the onset of vaporisation. In this region the pressure drop is due to friction and is almost linear as in a subcooled liquid. At point 'b', vapour bubbles appear and the pressure drops more rapidly due to the flow acceleration associated with the rapid reduction of the mixture density in the two-phase region. However, this is a metastable region because of the existence of superheated liquid together with saturated liquid and vapour fluid. After point 'c', the local thermodynamic equilibrium state is reached. Metastability can have strong effect on the mass flow rate, the exit pressure and the exit quality of the propellant as it alters the point of vaporisation and results in less two-phase flow (Chen et al., 1990).

A semi-empirical model developed by Kim and Neal (1994) described in section 2.4.2.2 (Chapter 2) is used to model the two-phase flow across the short-tube. For long tubes, three different models are used :

- Homogeneous Equilibrium Model (HEM) which assumes the fluid is every where in thermodynamic equilibrium
- Delayed Equilibrium Model (DEM) proposed by Feburie et al. (1993)

- Improved Delayed Equilibrium Model (IDEM) proposed by Attou and Seynhaeve (1999a)

Propellant metastability is accounted by means of the DEM and IDEM. Further, the DEM is enhanced to model the two-phase flashing propellant flow inside the two-orifice system of pMDIs.

3.2. Semi-Empirical Mass Flow Model For A Short Tube

Due to the complicated flow conditions and the possibility of choking at the exit plane of a short tube, many past investigators have chosen semi-empirical flow models to describe propellant flow in these cases. One approach is to start with the single-phase orifice equation and make corrections to it. This method has been used by several previous researchers (Pasqua, 1953, Mei, 1982 and Aaron & Domanski, 1990). Kim and O'Neal (1994) developed a semi-empirical flow model from the single-phase orifice equation with modifications to evaluate the flow characteristics through short tubes (equations 2.7 to 2.9). These equations are underpinned by a very substantial data base and were used in this work to solve the flow through short tube orifices with both subcooled and two-phase inlet conditions for R134A.

The above semi-empirical model successfully predicts the mass flow rate, but it has the following disadvantages:

- Semi-empirical coefficients a_1-a_4 and b_1-b_8 in equation 2.8 and 2.9 have been obtained only for propellant R134A. Fletcher (1975) and Clark (1991) also used other propellants (such as R12/R11 (60% 40%), R227, R12/R114 (60%40%)) to study the flow of propellant through twin-orifice systems of pMDIs. Insufficient data is available to find the coefficients of these propellants. So, this semi-empirical model cannot be employed as a general tool to predict the flows in pharmaceutical pMDIs.
- Orifice dimensions (diameter and length) used to develop the semi-empirical model are limited (Table 2.2), and the actual dimensions (D and L) of the orifices of twin-orifice in pMDI assemblies fall outside these limit, which challenges the accuracy of the semi-empirical model.

- Semi-empirical models such as that of Kim and O'Neal (1994) only evaluates the mass flow rate along an orifice as a function of the pressure drop, but does not predict other flow variables (such as quality, etc). Also, it would be useful to calculate the distribution of flow variables.

The above limitations make the semi-empirical model inadequate for our purpose and is more appropriate to develop a more general method based on the conservation of mass, momentum and energy.

3.3. Mathematical Modeling of Flow Through Capillary Tubes

In this section, the governing equations and boundary conditions for long capillary tubes are introduced. Three different models have been used to predict the two-phase flow through an adiabatic capillary tube: (i) Homogeneous Equilibrium Model (HEM) (ii) Delayed Equilibrium Model (DEM) and (iii) Improved Delayed Equilibrium Model (IDEM).The DEM and IDEM account for propellant metastability

3.3.1. Governing Equations

The governing equations used in this work are the one-dimensional conservation equations for mass, momentum and energy. The following assumptions are made in modeling the flow:

- One-dimensional, adiabatic flow: most of the previous investigators (Li et al. (1990a); Escanes et al.,1995; Bittle and Pate, 1996; Garcia-Valladares, 2002a; Wongwises and Suchatawut, 2003; Bansal and Wang, 2004 etc.) have assumed the flow through capillary tube is one-dimensional and adiabatic
- Straight, horizontal, constant inner diameter and uniform surface roughness.
- Kinematic equilibrium between the phases: both the liquid and vapour phases are thoroughly mixed and move with the same velocity.
- The effect of surface tension is neglected: pressure of liquid and vapour phase are locally equal.
- The effect of gravity is neglected.

- The fluid is pure propellant or propellant mixture. This is a valid assumption as the concentration of oil is very low in compare to that of the propellant.
- At locations where the pressure drops below the saturated vapour pressure the propellant is a mixture of saturated vapour and liquid and metastable liquid.
- In metastable flows evaporation only starts at a pressure 'p_v' (vaporisation pressure), which is lower than the saturated vapour pressure at the prevailing liquid temperature.

With the above assumptions in place, the equations governing the propellant flow through an adiabatic capillary tube are as follows:

Continuity:

$$\frac{d}{dz}(\dot{m}) = 0 \tag{3.1}$$

Momentum:

$$\frac{d}{dz}(\dot{m}U) + A\frac{dp}{dz} = -P\tau \tag{3.2}$$

Energy:

$$\frac{d}{dz}\left(\dot{m}\left(h_m + \frac{U^2}{2}\right)\right) = 0 \tag{3.3}$$

The mass flow rate is related to the fluid velocity by

$$\dot{m} = \frac{UA}{v_m} \tag{3.4}$$

where

$\dot{m}$ = mass flow rate (kg/s)

P = perimeter (m)

A = cross sectional area (m^2)

h_m = mixture enthalpy (J/kg)

z = axial distance (m)

τ = shear stress (Pa)

ν_m = mixture specific volume (m^3/kg)

3.3.2. Mixture Properties

Figure 3.3 shows the schematic view of an adiabatic capillary tube for HEM, where the capillary tube is divided in to two regions: (i) subcooled liquid region (ii) two-phase equilibrium region. For HEM, vaporisation is instantaneous and vaporisation occurs when $p=p_s$. The phases are in thermal equilibrium are intimately mixed. The propellant liquid and vapour are everywhere saturated.

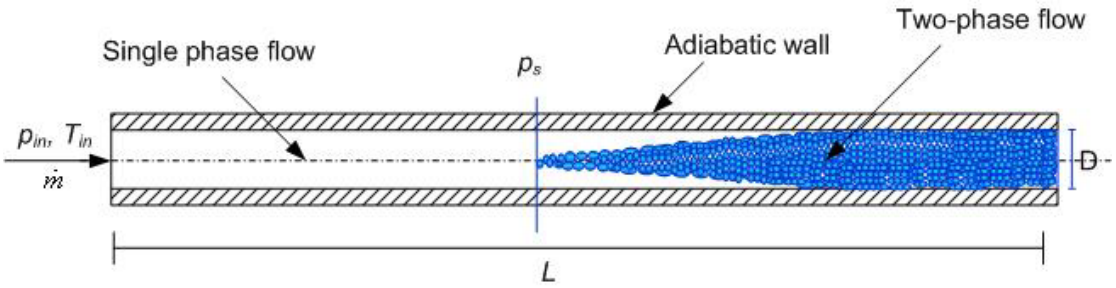

Figure 3.3 Schematic diagram of an adiabatic capillary tube

The mixture properties i.e. the mean specific volume and enthalpy of the mixture for HEM are given by the following constitutive relations:

HEM:

$$\nu_m = \frac{1}{\rho_m} = (1-x)\nu_l + x\nu_v \qquad 3.5$$

$$h_m = (1-x)h_l + xh_v \qquad 3.6$$

where the subscripts '*l*' and '*v*' correspond to saturated liquid and vapour respectively. According to DEM/IDEM, evaporation does not happen instantaneously, but only a fraction *y* (the so-called vaporisation index) of the propellant is transformed into saturated mixture, the other fraction *(1-y)* remains metastable liquid and is submitted

to an isentropic evolution. The constitutive relations for DEM and IDEM are as follows:

DEM/IDEM:

$$v_m = \frac{1}{\rho_m} = (1-y)v_{lm} + (y-x)v_l + x v_v \qquad 3.7$$

$$h_m = (1-y)h_{lm} + (y-x)h_l + xh_v \qquad 3.8$$

where the subscript '*lm*' correspond to metastable liquid.

The mean enthalpy equation (3.6 and 3.8) allows the evaluation of the vapour mass fraction (x) for HEM and DEM/IDEM respectively.

All the properties are evaluated using REFPROP v.7.0 (2002). The propellant properties for different regions are evaluated as follows:

Subcooled liquid region : fluid properties are estimated as a function of pressure and temperature

Metastable liquid region : fluid properties are estimated as a function of saturated pressure and entropy.

Metastable two-phase region: fluid properties are estimated as a function saturated pressure and metastable liquid properties are estimated as function of pressure and entropy

Two-phase equilibrium region: fluid properties are estimated as a function of saturated pressure.

3.3.3. Relaxation Equation

In the metastable two-phase region the DEM and IDEM proposed by Feburie et al (1993) and Attou and Seynhaeve (1999a and 1999b) are used respectively. As noted in the previous section, evaporation does not happen instantaneously. The vaporisation index 'y' is a measure of the departure from local saturated state. If y=1, the fluid is saturated mixture and if y=0, the fluid is metastable liquid. In the flow direction 'z' a conversion of metastable fluid into saturated fluid will take place, which is evaluated using the following relaxation equations:

3.3.3.1. DEM:

$$\frac{dy}{dz} = k_y \frac{P}{A}(1-y)\left[\frac{p_s - p}{p_c - p_s}\right]^{0.25} \qquad 3.9$$

where k_y is the coefficient of the relaxation equation and has a value of 0.02.

The constant determining the rate of return to saturated conditions is dependent on the difference between the local pressure p, saturation pressure p_s at the fluid temperature, on the critical pressure p_c of the propellant. The relevant length scale is P/A.

3.3.3.2. IDEM:

The DEM has been applied to both the steam-water (Feburie et al., 1993) and propellant flows (Garcia-Valladares et al, 2002a and 2002b) and gives good prediction of the mass flow rate when compared with experimental data. However, Attou and Seynhaeve (1999a) reported that the DEM underpredicts the mass flow rate for inlet conditions close to saturated and recommended an Improved Delayed Equilibrium Model (IDEM) for these cases. The correlation for the vaporisation index (equation 3.9) was modified to cover the whole range of inlet conditions, i.e. subcooled or saturated liquid and two-phase mixture. The IDEM closure equation proposed for the evaluation of the vaporisation index is written as follows:

$$\frac{dy}{dz} = k_y \frac{P}{A}(1-y)^2\left(\frac{U_{in}}{U}\right)^{1/10}\left[\frac{p_s - p}{p_c - p_s}\right]^{1/4} \qquad 3.10$$

where

k_y = 0.01.

U_{in} = liquid velocity at the inlet (m/s)

The velocity factor in the above equation is always less than one and takes into account the delayed effect due to the acceleration of the mixture during vaporisation. Thus far the IDEM has only been applied to steam-water flows and has not previously been tested on propellant flows.

3.3.4. Sub models

For the calculation of practical systems of pipes with abrupt changes of area, the above mathematical model requires the following collection of submodels.

- Models for the frictional shear stress 'τ' in equation (3.2) for single phase and two-phase conditions.
- Expression for vaporisation pressure 'p_v'.
- Correlations for inlet and exit losses.
- Conditions for choked flow.
- Discharge shock relations.

3.3.4.1. Single Phase Sub-Cooled Liquid Region (Zone I):

The wall shear stress is expressed as :

$$\tau = (f/4)\left(G^2/2\rho\right) \qquad 3.11$$

where

f = friction factor

G = mass flux (kg/m^{2}s)

ρ = liquid density (kg/m^3)

In the single-phase region, the friction factor is calculated from the expression proposed by Churchill (cited by Lin et al. (1991)), which is given as

$$f = 8\left[\left(\frac{8}{\mathrm{Re}}\right)^{12} + \frac{1}{(A+B)^{3/2}}\right]^{1/12} \qquad 3.12$$

where

$$A = \left\{2.457 \ln\left[\frac{1}{\left(\frac{7}{\mathrm{Re}}\right)^{0.9} + 0.27\frac{\varepsilon}{D}}\right]\right\}^{16}$$

$$B = \left(\frac{37530}{\mathrm{Re}}\right)^{16}$$

$$\mathrm{Re} = \text{Reynolds number} \left(= \frac{UD}{\nu_l \mu_l}\right)$$

μ_l = liquid viscosity (Pas)

ν_l = liquid specific volume (m^3/kg)

3.3.4.2. Metastable Liquid Region (Zone II)

The formation of the first vapour bubbles require a finite amount of superheat. Hence vaporisation is delayed and the actual point of inception of vaporisation does not coincide with the saturation point. The pressure of vaporisation (p_v) at the flashing point is evaluated by the correlation proposed by Lackme (1979) and Chen et al. (1990).

According to Lackme (1979), the pressure of vaporisation (p_v) a the point of flashing can be characterized as a fraction of the thermodynamic pressure of vaporisation, i.e.

$$p_v = k_{\mathrm{meta}} p_s \qquad 3.13$$

where k_{meta} varies from 0.91-0.95.

Chen et al. (1990) proposed following correlation to evaluate the p_v which is given as:

$$\frac{(p_s - p_v)\sqrt{KT_s}}{\sigma^{3/2}} = 0.679\left(\frac{\nu_v}{\nu_v - \nu_l}\right)\mathrm{Re}^{0.914}\left(\frac{\Delta T_{sub}}{T_c}\right)^{-0.208}\left(\frac{D}{D'}\right)^{-3.18} \qquad 3.14$$

where

p_s = saturation pressure (Pa)

p_v = pressure of vaporisation (Pa)

T_s = saturation temperature (K)

K = Boltzman constant (1.380662 x 10^{-23} J/K)

σ = liquid propellant surface tension (N/m)

ν specific volume (m^3/kg)

T_c = propellant critical temperature (K)

ΔT_{sub} = subcooled temperature (K)

D` = reference length $\left(D' = \sqrt{KT_S / \sigma} \times 10^4\right)$

The empirical constants in this correlation were determined based on experimental data with adiabatic capillary tubes working with R12 for the parameter ranges shown in Table 3.1.

Table 3.1 Limitations of the Chen et al. (1990) correlation

$0.464 \times 10^4 <$	Re	$< 3.74 \times 10^4$
$0 <$	ΔT_{sub}	$< 17°K$
0.66 mm<	D	< 1.17 mm

Previous researchers (Garcia-Valladares, 2002b; Wongwises and Suchatawut, 2003) reported that Chen et al. (1990) correlation is best to evaluate the underpressure of vaporisation for subcooled inlet conditions, but fails for saturated inlet conditions. For saturated inlet condition $\Delta T_{sub} = 0$, substituting this value in equation (3.14) yields infinity. Hence, Lackme's (1979) correlation is used to evaluate the underpressure of vaporisation for saturated and two-phase inlet conditions.

In the metastable liquid region, the propellant properties are estimated using the values corresponding to fluid pressure and entropy. So, the temperature is estimated as function of local pressure and entropy i.e. $T = T(p,s)$.

3.3.4.3. Metastable two-phase region (Zone III)

The friction factor in the two-phase metastable region is evaluated with the same form as used above (equation 3.12) except that Reynolds number is calculated by using mixture specific volume (equation 3.5 for HEM and equation 3.7 for DEM/IDEM) and metastable two-phase viscosity, which is evaluated using Dukler's correlation (recommended by Bittle and Pate, 1996):

The Dukler Model (Dukler et al. 1964):

In Dukler's viscosity model, the mixture viscosity must combine contributions of the vapour viscosity and the viscosity of the saturated liquid and metastable liquid. The two-phase viscosity is calculated as follows

$$\mu_{tp} = \frac{x\nu_v\mu_v + (1-x)\nu_{lm,l}\mu_{lm,l}}{(1-x)\nu_{lm,l} + x\nu_v} \tag{3.15}$$

where the specific volume of the saturated/metastable liquid mixture is evaluated using

$$\nu_{lm,l} = \frac{(1-y)}{(1-x)}\nu_{lm} + \frac{(y-x)}{(1-x)}\nu_l \tag{3.16}$$

and the viscosity of the saturated/metastable liquid mixture with

$$\mu_{lm,l} = \mu_{lm}^{\frac{(1-y)}{(1-x)}} + \mu_l^{\frac{(y-x)}{(1-x)}} \tag{3.17}$$

The subscripts *lm* = metastable liquid, *l*=saturated liquid, *lm,l*=mixture of metastable and saturated liquid, *v* = vapour and *tp* = two-phase.

In this region, the relaxation equation for DEM/IDEM (equation 3.9 and 3.10) recommended by Feburie et al. (1993) and Attou and Seynhaeve (1999a) are used. Two different fluid temperatures exists in this region, they should be distinguished : the superheated liquid temperature (T_{lm}) and the saturation liquid or gas temperature ($T_{equil}=T_s(p)$). For this reason, following Zhou and Zhang (2006), the following equation is used to evaluate average temperature distribution in this region.

$$T = (1-y)T_{lm} + yT_{equil} \tag{3.18}$$

where

T_{equil} = thermodynamic equilibrium temperature (K)

T_{lm} = metastable liquid temperature (K)

y = vaporisation index

Evaluation of void fraction

Void fraction (α)is evaluated from the following expression

$$\alpha = \frac{x/v_{lm,l}}{x/v_{lm,l} + (1-x)/v_v} \qquad 3.19$$

where $v_{lm,l}$ is given by (3.16).

3.3.4.4. Equilibrium Two-Phase Region (Zone IV):

In this region, homogeneous equilibrium model is assumed. When '*y*' approaches unity, the superheated liquid vanishes and the flow process enters into equilibrium two-phase flow (zone IV). The two-phase friction factor and void fraction are evaluated in the same way as discussed above by setting *y*=1 in equations (3.15)-(3.19).

3.3.4.5. Entrance Correction:

Single and Two-phase Inlet:

The sudden drop associate with the abrupt contraction for single and two-phase inlet is evaluated using the following assumptions:

- The velocities of the phases are equal
- There is no heat or mass transfer between the phases
- The gas or vapour is modeled as a perfect gas; there is no heat transfer between the phases, so vapour expansion is isentropic : pv^{γ} = constant.
- Incompressible liquid
- For two-phase inlet, the quality (x) assumed to be constant across the sudden contraction as the residence time is too short for the vaporisation to happen. For DEM/IDEM, it is assumed that the saturated liquid gets converted into metastable liquid as it passes through the abrupt contraction due to sudden pressure drop and, the vaporisation index '*y*' is evaluated from the energy equation. For HEM '*y=1*'.

The pressure drop across the sudden contraction for two-phase inlet condition is obtained using the expression proposed by Mendler (cited in ESDU 89012, 1989):

$$p = p_{in} - \Phi^2 \times \Delta p_{sp} \qquad 3.20$$

where the two-phase multiplier, Φ^2, is given by

$$\Phi^2 = 1 + \left[x\left(\frac{\nu_v}{\nu_l}\right) - 1 \right] \tag{3.21}$$

and the single-phase pressure loss, Δp_{sp}, is given by

$$\Delta p_{sp} = \frac{G^2}{2\rho_l}\left\{1 - \left(\frac{A}{A_{in}}\right)^2 + \left(\frac{1}{C_c} - 1\right)^2\right\} \tag{3.22}$$

where v_v - vapour specific volume at the exit of sudden contraction (m^3/kg), which is evaluated as

$$\nu_v = \nu_{v,in}\left(\frac{p_{in}}{p}\right)^{1/\gamma} \tag{3.23}$$

where

A_{in} = area of the upstream tube (see Figure 3.1)

Δp_{sp} = single phase pressure drop (Pa)

p_{in} = upstream pressure (Pa)

$\nu_{v,in}$ = upstream vapour specific volume (m^3/kg)

C_c = single phase contraction coefficient (=0.617)

γ = ratio of specific heats (c_p/c_v)

For two-phase inlet conditions, after calculating the pressure drop, the enthalpy is calculated using the energy equation (3.3). As the liquid passes through the sudden contraction some part of the saturated liquid gets converted into metastable liquid, which is evaluated using the mean enthalpy equation (3.8) keeping the quality constant across the sudden contraction. The vaporisation index at the exit of the sudden contraction can be obtained by rearranging equation (3.8):

$$y = \frac{(h_{lm} - h_m) + x_{in}(h_v - h_l)}{(h_{lm} - h_l)} \tag{3.24}$$

3.3.4.6. Exit correction

The exit of the capillary tube is characterized by a sudden expansion. The pressure recovery associated with a sudden expansion for a single-phase liquid and two-phase liquid is evaluated from the expression proposed by Mendler (cited in ESDU 89012, 1989)

$$p_{dis} = p + \Phi^2 \times \Delta p_{sp} \tag{3.25}$$

where the two-phase multiplier, Φ^2, is given by

$$\Phi^2 = [1 + x\{(\rho_l / \rho_v)^{1/6} - 1\}][1 + x\{(\rho_l / \rho_v)^{5/6} - 1\}] \tag{3.26}$$

and the single-phase pressure recovery, Δp_{sp}, is given by

$$\Delta p_{sp} = -\frac{G^2}{2\rho_l}\left(\left(\frac{A}{A_{dis}}\right)^2 - 1 + \left(1 - \frac{A}{A_{dis}}\right)^2\right) \tag{3.27}$$

where A_{dis} = downstream area of the abrupt expansion (see Figure 3.1)

3.3.4.7. Critical Flow

Critical flow occurs when the rate of generation of kinetic energy within the fluid cannot exceed the rate of supply of energy from the fluid at the expense of its decrease in pressure and expansion (Hewitt and Hall-Taylor, 1970). The critical mass, $\dot{m}_{crit}$ is reached when the velocity reaches the sonic velocity, U_c, and the Mach number approaches unity. At this point the flow is choked and the mass flow rate reaches its upper limit.

The sonic velocity was evaluated using the expression proposed by Attou and Seynhaeve (1999a), which is given as :

$$U_c = \sqrt{\left(\frac{\partial p}{\partial \rho}\right)_s} = \left[\frac{v_m^2 (h_v - h_l)}{(v_v - v_l)(\partial h_m - v_m) - \partial v_m (h_v - h_l)}\right]^{\frac{1}{2}} \tag{3.28}$$

For HEM

$$\partial v_m = x\left(\frac{\partial v_v}{\partial p}\right)_{sat} + (1-x)\left(\frac{\partial v_l}{\partial p}\right)_{sat} \quad 3.29$$

$$\partial h_m = x\left(\frac{\partial h_v}{\partial p}\right)_{sat} + (1-x)\left(\frac{\partial h_l}{\partial p}\right)_{sat} \quad 3.30$$

and v_m is given by relation (3.5). The subscript '*sat*' indicates that the derivatives are evaluated following saturation line

For DEM/IDEM

$$\partial v_m = x\left(\frac{\partial v_v}{\partial p}\right)_{sat} + (y-x)\left(\frac{\partial v_l}{\partial p}\right)_{sat} + (1-y)\left(\frac{\partial v_{lm}}{\partial p}\right)_{s_{lm}} \quad 3.31$$

$$\partial h_m = x\left(\frac{\partial h_v}{\partial p}\right)_{sat} + (y-x)\left(\frac{\partial h_l}{\partial p}\right)_{sat} + (1-y)\left(\frac{\partial h_{lm}}{\partial p}\right)_{s_{lm}} \quad 3.32$$

and v_m is given by the expression (3.7). The subscript 's_{lm}' indicates that the derivatives are evaluated following isentropic line.

Attou and Seynhaeve (1999a) reported that the velocity of sound at x=0 (saturated condition) predicted by HEM is considerably smaller than the actual single-phase liquid one, which is due to discontinuity of the first order derivative property $(\partial p/\partial \rho)_s$ at the saturation line along an isentropic evolution. Whereas with DEM severe increasing of sound velocity was observed when x and y tend towards zero. The intrinsic metastability character of the liquid phase in the DEM leads to satisfy the continuity of the sound velocity between the liquid and the two-phase mixture.

The critical mass flow rate is given by

$$\dot{m}_c = \frac{AU_c}{v_m} \quad 3.33$$

3.3.4.8. Discharge shock wave

In the case of critical flow, a discharge shock proposed by Escanes et al.(1995) is solved. A control volume of larger diameter than inlet diameter is defined at the

discharge. Assuming no heat transfer, the outlet vapour quality is calculated by means of the energy equation, the pressure at the outlet of the discharge control volume (CV) is equal to the discharge pressure, and the mass flow rate remains constant. i.e.

- $p_{exit} = p_{dis}$
- $U_{exit} = \dot{m}_c v_m / A_{dis}$
- Evaluate h_{exit} using the energy equation (3.3)
- Evaluate y_{exit} using the equation (3.9).
- Evaluate x_{exit} using the mean enthalpy equation (3.8)

3.4. Mathematical Modeling of Flow through Twin-Orifice System of pMDIs

In this section, the conceptual model of twin-orifice assembly relevant to pMDI, review of most common assumptions and the method of solving the flow through twin-orifice system of pMDI is described.

3.4.1. Conceptual Model of Twin-Orifice System

Fletcher (1975) and Clark (1991) give a clear conceptual image, which forms the basis of models of propellant flow in two-orifice systems. Figure 3.4 shows a cross-section diagram of pMDI, which consists of a canister and actuator. The schematic representation of twin-orifice system is shown in Figure 3.5, consisting of metering chamber, valve orifice, expansion chamber (valve stem and sump together) and spray orifice. Figure 3.6 shows the simplified version of schematic view neglecting the orientation of the valve and spray orifice which is being used as the conceptual model for twin-orifice system (Fletcher,1975 and Clark, 1991).

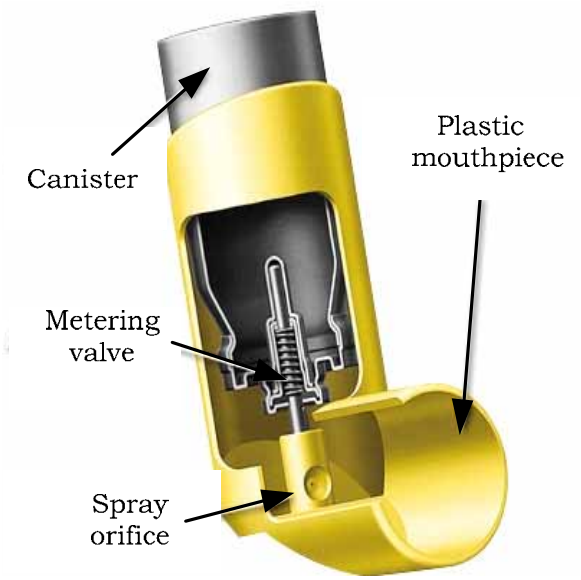

Figure 3.4 Cross section view of pressurized Metered Dose Inhaler (pMDI)

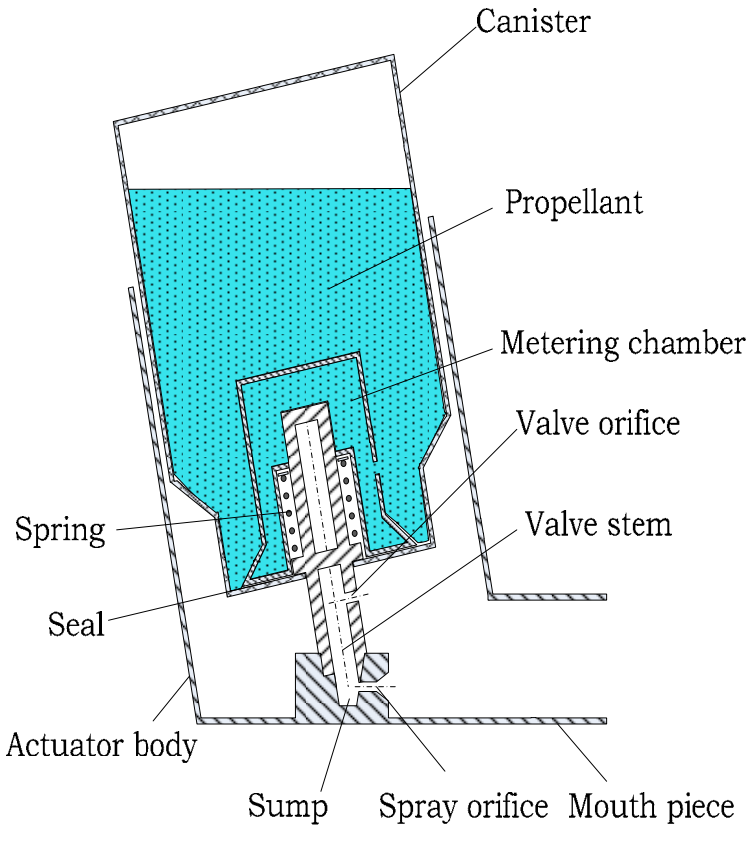

Figure 3.5 Schematic representation pressurized Metered Dose Inhaler (pMDI)

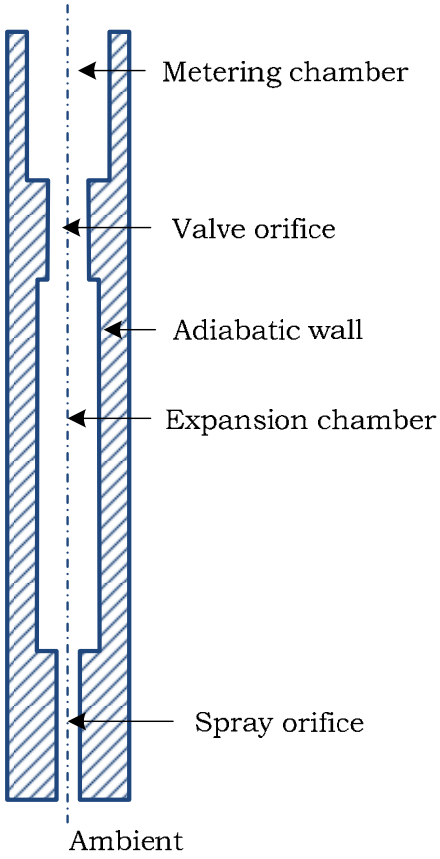

Figure 3.6 Conceptual diagram of twin-orifice system

3.4.2. Modeling Assumptions

The main purpose of the present work is to develop a numerical model for the continuous discharge propellant flow. The model is assumed based on the assumption that the steady conditions are prevailed for the propellant flow through twin-orifice assembly. This slightly limits the application of the model in cases of metered discharge to conditions where the mass flow rates through the valve orifice and spray orifice are in balance. However, Clark (1991) has shown that this condition is rapidly achieved after a short initial transient. Now, the most common modeling assumptions are reviewed

General:

- One-dimensional flow: the most significant changes governing the propellant flow are in the flow direction. Variations of thermodynamic and transport properties perpendicular to the flow direction are neglected.
- Adiabatic flow: no heat transfer between the fluid and its surroundings. The discharge of propellant through twin-orifice system is a rapid process and they are manufactured from polymer materials.
- Steady state: Steady state conditions are reached when the single-phase mass flow rate through the valve orifice is equal to the two-phase mass flow rate through the spray orifice.
- Fluid properties: The fluid properties are assumed to be equal to those of the propellant and are evaluated using REFPROP v7.0 (2002). This assumption is valid as the propellant represent more than 99% by weight of the pMDI's canister contents in many drug formulations.
- Effect of surface tension: the effect of surface tension is neglected: pressure of liquid and vapour phase are locally equal.
- Effect of gravity: the effect of gravity is neglected.

Two-phase flow regime:

- Homogeneous flow: the dispersed phase and the continuous phase are thoroughly mixed and interaction between the phases is distributed all over the mixture. Both

phases move with the same velocity. This assumptions has been made by previous researchers (e.g. Fletcher, 1975; Clark, 1991; Wong and Ooi,1994; Escanes et al. 1995; Bansal and Rupasinghe, 1998)

- Thermal non-equilibrium : The non equilibrium effects are considered by accounting to propellant metastability.

Orifice flow regimes

- The flow of propellant inside the twin-orifice system is assumed to be in two-phase metastable region, i.e. the propellant exists in three phases: metastable liquid, saturated liquid and vapour.
- Abrupt contraction: The inlet of the valve and spray orifice is formed by an abrupt contraction. The residence time of the fluid in this regions is assumed to be sufficiently short that it can be assumed that no evaporation exists across the abrupt contraction at the entrance of the valve and spray orifice, so the mixture quality remains constant or frozen composition. At typical velocities, the saturated liquid and the metastable liquid are combined together to form a new metastable liquid which undergoes isentropic expansion along with the vapour.

As the gravity effects have been neglected and the flow is one-dimensional, the conceptual sketch of twin-orifice system in Figure 3.6 can be represented horizontally as in Figure 3.7 as for the convenience to view the pressure and temperature profiles along the axial direction.

From the literature it becomes apparent that propellant metastability is modeled well with the vaporisation index (y) concept (Lackme, 1979; Mali & Hardy, 1982, Feburie et al., 1993, Attou and Seynhaeve, 1999a-b) for steam-water applications and refrigeration air conditioning systems (Garcia-Valladares, 2002a-b). For the flow along the twin-orifice system, the DEM proposed by Feburie et al. (1993) is used as it has been tested on both the steam-water flows and the propellant flows along the capillary tubes and showed good predictions with the experimental data.

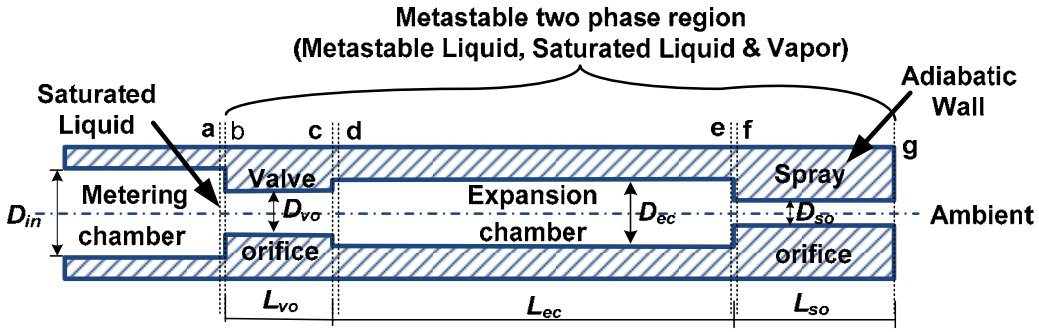

Figure 3.7 Schematic view of twin-orifice system of pMDI

a-b Sudden contraction at the entrance of the valve/upstream orifice

b-c Valve/upstream orifice

c-d Sudden Expansion at the entrance of the expansion chamber

d-e Expansion Chamber

e-f Sudden contraction at the entrance of the spray/downstream tube orifice

f-g Spray/downstream orifice

g Sudden expansion at the exit of the spray orifice

3.4.3. Delayed Equilibrium Model (DEM)

The geometry of the twin-orifice system of a pMDI has been simplified as a series of capillary tubes connected by abrupt contractions and expansions. The fundamental equations (3.1) – (3.3) are again solved in conjunction with an account of metastability as before. Metastability is modeled using the relaxation equation (3.9). The friction factor is evaluated in the same way as mentioned in section (3.3.4.3). And the mean temperature is calculated using the expression (3.18). Additional submodels are required for :

- Pressure drop and fluid state changes in abrupt contractions and expansions at the inlet and exit of each capillary tube.
- Condition for choked flow and expressions to compute flow velocity and mass flow rate.
- Relationships for discharge shock waves occurring at choked expansions.

3.4.4. Submodels

The geometry of the twin-orifice system related to pMDIs is complex and involves several abrupt changes in the geometry: sudden contraction at the entrance of the valve orifice (a-b in Figure 3.7); sudden expansion at the exit of the valve orifice (c-d in Figure 3.7); sudden contraction at the entrance of the spray orifice (e-f in Figure 3.7); sudden expansion at the exit of the spray orifice (g in Figure 3.7). The purpose of this section is to evaluate the flow variables across these sections.

3.4.4.1. Abrupt Contraction at Tube

The cross sectional areas of the tubes representing the metering chamber and expansion chamber are large compared with those of the valve orifice and spray orifice. Therefore entrance to these orifice is characterized as a sudden contraction and rapid changes in the fluid state and pressure occur.

Conceptual idea of the flow process

- At the inlet to the abrupt contraction the propellant is either in saturated condition or in two-phase metastable condition.
- As the propellant passes through the abrupt contraction, initially saturated liquid becomes metastable due to the sudden pressure change across the abrupt contraction.
- At the exit of the sudden contraction, the propellant is a mixture of saturated vapour and metastable liquid.
- A schematic diagram of a control volume for the analysis of the abrupt contraction is given in Figure 3.8.
- The flow of propellant inside the twin-orifice system is assumed to be in two-phase metastable region, i.e. the propellant exists in three phases: metastable liquid, saturated liquid and vapour.

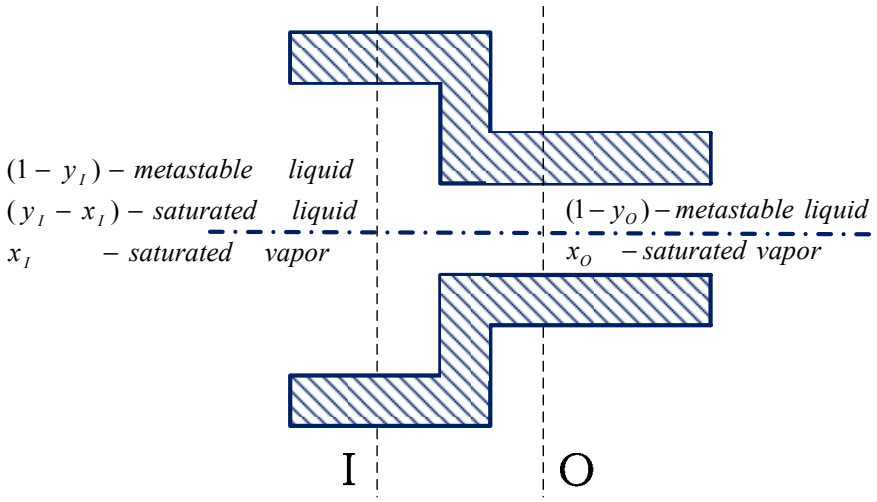

Figure 3.8 Control Volume for abrupt contraction across the valve and spray orifice inlet

Mixture properties

The following assumptions are made to evaluate the mixture properties at the exit of an abrupt contraction at the inlet of the valve orifice and spray orifice:

- Vapour : As mentioned before the quality across the sudden contraction is constant ($x_I = x_O$) and the vapour expands isentropically across the contraction (pv_v^{γ} = constant).
- Liquid: Metastable liquid with mass fraction $(1-y_I)$ and saturated liquid with mass fraction $(y_I - x_I)$ at the inlet of CV, are mixed together to form one new metastable liquid with mass fraction $(1- y_O)$. The subscripts 'I' and 'O' represent inlet and outlet of the abrupt contraction CV respectively.
- The mixed mean liquid enthalpy before the sudden contraction is evaluated as:

$$(1-x_I)h'_{lm,I} = (1-y_I)h_{lm,I} + (y_I - x_I)h_{l,I} \qquad 3.34$$

and the mixture enthalpy can therefore be evaluated as

$$h_m = (1-y_I)h_{lm,I} + (y_I - x_I)h_{l,I} + x_I h_{v,I} = (1-x_I)h'_{lm,I} + x_I h_{v,I} \qquad 3.35$$

As $x_I = x_O$, equation (3.41) can also be written as follows:

$$(1-x_O)h'_{lm,I} = (1-y_I)h_{lm,I} + (y_I - x_I)h_{l,I} \qquad 3.36$$

Hence

$$h'_{lm,I} = \frac{(1-y_I)h_{lm,I} + (y_I - x_I)h_{l,I}}{(1-x_O)} \quad 3.37$$

Similarly, the mean entropy and specific volume can be written as:

$$s'_{lm,I} = \frac{(1-y_I)s_{lm,I} + (y_I - x_I)s_{l,I}}{(1-x_O)} \quad 3.38$$

$$v'_{lm,I} = \frac{(1-y_I)v_{lm,I} + (y_I - x_I)v_{l,I}}{(1-x_O)} \quad 3.39$$

where

$h'_{lm,I}$ mean enthalpy of new metastable liquid (J/kg)

$s'_{lm,I}$ mean entropy of new metastable liquid (J/kg-K)

$v'_{lm,I}$ mean specific volume of new metastable liquid (m^3/kg)

The pressure drop associated across the abrupt contraction for a two-phase metastable liquid is evaluated from the equations (3.20)- (3.23).

- The mixture of liquid and vapour expands isentropically as it flows through the abrupt contraction forming a new mixture of metastable liquid and superheated vapour, whose mixture specific volume and enthalpy are given by the following equations

$$v_{m,O} = (1-y_O)v_{lm,O} + x_O v_{v,O} = (1-x_o)v_{lm,O} + x_O v_{v,O} \quad 3.40$$

$$h_{m,O} = (1-y_O)h_{lm,O} + x_O h_{v,O} = (1-x_o)h_{lm,O} + x_O h_{v,O} \quad 3.41$$

The liquid and vapour properties are calculated as function of saturated pressure and mixture properties are calculated:

$s_{lm,O} = s'_{lm,I}$ from equation (3.38)

$h_{lm,O} = f(p_O, s_{lm,O})$, $v_{lm,O} = f(p_O, s_{lm,O})$ from REFPROP

$$v_{v,O} = v_{v,I}\left(\frac{p_I}{p_O}\right)^{\frac{1}{\gamma}} \text{ and } h_{lm,O} = f\left(p_O, v_{v,O}\right) \text{ from REFPROP}$$

Pressure drop:

The pressure drop across the abrupt contraction for a two-phase metastable liquid is evaluated from equations (3.20)-(3.23) using fluid properties computed as above.

3.4.4.2. Abrupt expansion at Tube

The exit of the valve orifice is also characterized as abrupt expansion as the cross-section area of the expansion chamber is larger than area of the valve orifice. The equations described in section (3.3.4.6 and 3.3.4.8) may not be appropriate here for the following reasons:

- For subcritical flow, the propellant at the exit of the capillary tube is in two-phase equilibrium state (i.e. entire metastable liquid is vaporised into saturated mixture; only saturated liquid and vapour exist) and the equations used to evaluate the pressure recovery and the flow variables do not account for propellant metastability. However, the valve orifice is a short tube, so the flow at the entrance of the expansion chamber is in two-phase metastable state and propellant metastability has to be considered in evaluating the flow variables along the abrupt expansion.
- For the critical flow, the discharge shock wave (section 3.3.4.8) used for the capillary tubes is not appropriate to solve the shock at the exit of the valve orifice because the discharge shock wave requires the downstream pressure (p_{dis}) to evaluate the flow variables after the shock. This is a known value for the capillary tube applications, but the expansion chamber pressure emerges as part of the solution process, so it cannot be specified at the exit of the valve orifice. Hence, the discharge shock wave model needs to be modified to solve the critical flow at the exit of the valve orifice.

The first main concern in the calculation of the flow variables along the abrupt expansion is the treatment of metastable liquid across the abrupt expansion (i.e. the

evaluation of vaporisation index (y)). To model this metastable liquid across the abrupt expansion of the valve orifice, two different assumptions were considered:

1. Following Attou and Seynhaeve (1999a), the vaporisation index 'y' is kept constant across the abrupt expansion.

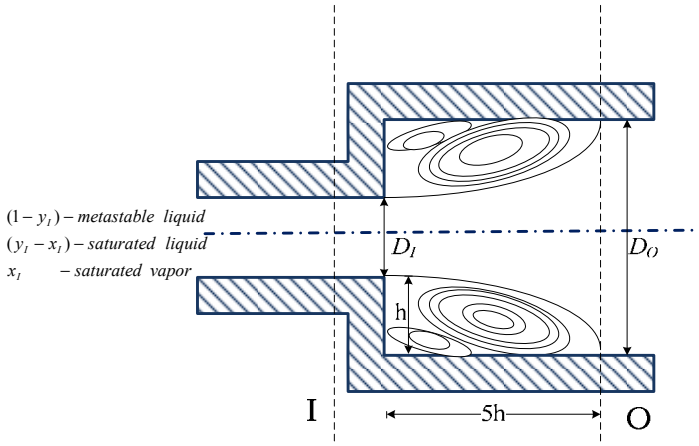

Figure 3.9 Reattachment plane for abrupt expansion across the valve orifice exit

2. The flow is assumed to expand as sketched in Figure 3.9. The DEM relaxation equation (3.9) is integrated over a length of 5h as the reattachment plane occurs at about 5h downstream of the enlargement, as indicated in Figure 3.9. The inlet diameter is taken equal to the valve orifice diameter and outlet diameter is equal to the expansion chamber diameter. DEM relaxation equation (3.9) is integrated using three different 'k_y' values to evaluate 'y' across the sudden expansion. The standard value of 'k_y = 0.02' in the relaxation equation (3.9) was considered along with a significant increase and decrease to reflect the expected differences between nucleation and vaporization delay in straight pipes and sudden expansion flows.

Governing Equations

The flow through an abrupt enlargement is modelled using the method proposed by Attou and Seynhaeve (1999a). For given values of the flow variables at the inlet to the abrupt expansion i.e. at the valve orifice cross-section (A_{vo}), the problem consists to predict the flow variables at the downstream cross section (A_{ec}). For this purpose, the global balance of mass, momentum and energy of the mixture are applied to the control volume of fluid sketched in Figure 3.10, which is bounded by the pipe walls.

By neglecting, the wall friction and gravity terms compared to inertia, in the momentum balance equation, the following algebraic model is obtained:

Mass conservation

$$\rho_{m,O} U_O = \frac{A_I}{A_O} \rho_{m,I} U_I \qquad 3.42$$

Momentum conservation

$$p_O + \rho_{m,O} U_O^2 = \frac{A_I}{A_O} p_I + \frac{A_I}{A_O} \rho_{m,I} U_I^2 + \left(1 - \frac{A_I}{A_O}\right) p_{bc} \qquad 3.43$$

Energy conservation

$$h_{m,O} + \frac{1}{2} U_O^2 = h_{m,I} + \frac{1}{2} U_I^2 \qquad 3.44$$

where p_{bc} is back pressure (Pa), $A_I = A_{vo}$ and $A_O = A_{ec}$.

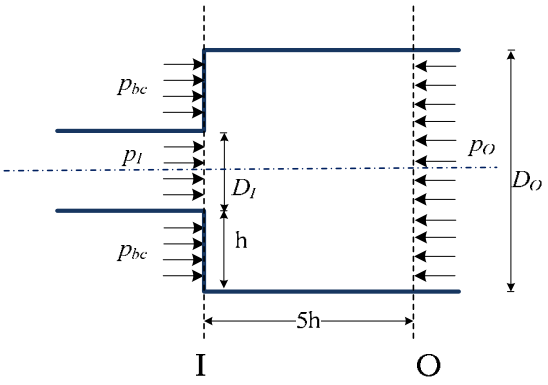

Figure 3.10 Control Volume for abrupt expansion across the valve orifice exit

Assumption 1: $y_I = y_O$ (Attou and Seynhaeve, 1999a)

Following Attou and Seynhaeve (1999a) the vaporisation index across the abrupt expansion has been assumed constant. i.e.

$$y_I = y_O. \qquad 3.45$$

Assumption 2: Integrating the DEM relaxation equation to evaluate 'y'

The vaporisation index at the outlet of abrupt expansion (y_O) is evaluated integrating the modified DEM relaxation equation over a distance of 5h (Figure 3.10).as the flow is fully recovered at this point. The DEM relaxation equation (3.9) has to be modified as it has been developed for a gradual expansion pipe. Here, we have

$$\frac{P}{A} = \frac{\pi D}{(\pi/4)D^2} = \frac{4}{D} \text{ with } D = D(z)$$

Where *D(z)* follows the profile of conical gradual between inlet diameter D_I and outlet diameter D_O

The modified DEM relaxation can be expressed as:

$$\frac{dy}{dz} = k_y \frac{4}{D(z)}(1-y)\left[\frac{p_s - p}{p_c - p_s}\right]^{0.25} \qquad 3.46$$

The value of k_y in equation (3.9) originates from experiments on steam water systems for a straight pipe and it may or may not be appropriate for the evaluation of '*y*' across the assumed expansion process with propellant as the fluid. To study its effect, three different values of k_y are considered.

Case 2(a) k_y = 0.002 (reduced by a factor 10)

Case 2(b) k_y = 0.02 (the basic case)

Case 2(c) k_y = 0.2 (increased by a factor of 10)

The quality at the outlet of CV (x_O) is evaluated from the mean enthalpy obtained from energy equation, which is give as

$$x_O = \frac{y_O\left(h_{lm,O} - h_{l,O}\right) - \left(h_{lm,O} - h_{m,O}\right)}{\left(h_{v,O} - h_{l,O}\right)} \qquad 3.47$$

Sub-critical Flow :

For sub-critical flow, the base pressure at the step of the enlargement can be assumed equal to the mean pressure in the jet. i.e. $p_{bc} = p_I$. The four unknowns of equations (3.42)-(3.44) (along with property equations 3.7-3.8) the problem are *U, p, x, y.* Using assumption 1 or assumption 2 to evaluate the vaporisation index across the abrupt

expansion, the system of equations (3.42)-(3.44) becomes closed and the model can be solved numerically by an iterative procedure (see section 4.4.1.4).

Critical Flow:

When the flow is choked in the vicinity of the valve orifice enlargement, the variables of the flow beyond the critical section can no longer be determined from upstream conditions and the base pressure cannot be supposed to be equal to the pressure in the jet and depend on the back pressure. The system of equations (3.42)-(3.44) with assumptions (1 or 2) is only closed if the base pressure (p_{bc}) is fixed. The model is solved numerically by an iterative procedure for evaluating the back pressure (p_{bc}) fixing the downstream mass flow rate.

3.4.4.3. Discharge Shock Wave (DSW) at the exit of spray orifice

For the critical flow at the exit of the spray orifice, the discharge shock wave (section 4.3.4.8) used for the capillary tubes cannot be used because a downstream tube diameter is required. The spray orifice of a pMDI discharges to the ambient atmosphere and the choked flow at the exit of the spray orifice accelerates into the atmosphere as $p_{choke.} > p_{dis.}$ The geometry of the emerging jet is undefined by the exit conditions. Here, two extreme scenarios are considered:

Case 1: Straight jet: see Figure 3.11

Case 2: Conical jet: see Figure 3.12

The mathematical formulation of these two jets are discussed below :

Case 1: Straight Jet:

Figure 3.11 shows the schematic view of the straight jet CV at the exit of the spray orifice The following assumptions are made for the flow across the straight jet expansion at the exit of the spray orifice:

- Flow is governed by one-dimensional conservation of mass, momentum and energy.
- There is no exchange of mass with surrounding air.
- The friction and gravity terms are neglected.

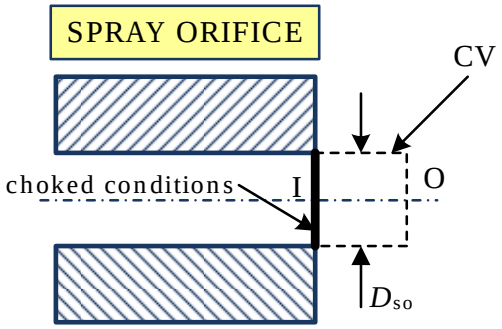

Case 1a

y_O & x_O are evaluated solving mixture equations. i.e. mean specific volume and enthalpy

Case 1b

$y_O = y_I$

x_O is evaluated using mean enthalpy equation

Figure 3.11 Control Volume for DSW at the exit of spray orifice for a straight jet

Governing Equations:

Under the given assumptions, $A_I = A_O = A_{so}$, the conservation equations are as follows:

Mass conservation

$$\frac{U_O}{v_{m,O}} = \frac{U_I}{v_{m,I}} \tag{3.48}$$

Momentum conservation

$$p_I A_{so} - p_O A_{so} = \dot{m}(Uo - U_I) \tag{3.49}$$

The above equation is rearranged to obtain the outlet velocity

$$U_O = U_I + \frac{p_I A_{so} - p_O A_{so}}{\dot{m}} \tag{3.50}$$

Energy conservation

$$h_{m,O} + \frac{1}{2}U_O^2 = h_{m,I} + \frac{1}{2}U_I^2 \tag{3.51}$$

where v_m and h_m are the mean specific volume and enthalpy evaluated using equations (3.7) and (3.8). As the CV outlet pressure (discharge ambient pressure) is known, the momentum equation (3.50) and the critical mass flow rate can be used to evaluate the exit velocity at the outlet of CV. Then the mean specific volume at the exit of the CV

is calculated with the help of mass conservation (equation 3.48). The mean specific enthalpy at the outlet of CV is obtained using energy equation (3.51).

As mentioned before in the previous section, it is unclear how the evaluation of vaporisation index (y) and quality (x) should be calculated at exit of CV. Now, the x and y at the exit 'O' of CV can be evaluated in two different ways:

Case 1a : By solving the mean specific volume and enthalpy equations simultaneously (equations 3.7 and 3.8). Solving of these two equations simultaneously, assumes that the propellant evaporates across the abrupt expansion. The mean specific volume and enthalpy obtained from the continuity (equation 3.48) and energy equation (3.51) respectively are used to evaluate the vaporisation index and quality at the exit of the CV. The following expressions are obtained solving the mixture equations :

$$y_O = \frac{(h_{m,O} - h_{lm})(v_v - v_l) - (v_{m,O} - v_{lm})(h_v - h_l)}{(h_v - h_l)(v_{lm} - v_l) - (v_v - v_l)(h_{lm} - h_l)} \qquad 3.52$$

$$x_O = \frac{(h_{m,O} - h_{lm})(v_{lm} - v_l) - (v_{m,O} - v_{lm})(h_{lm} - h_l)}{(h_v - h_l)(v_{lm} - v_l) - (v_v - v_l)(h_{lm} - h_l)} \qquad 3.53$$

Case 1b: Following Attou and Seynhaeve (1999a) y is assumed constant across the expansion (i.e. metastable liquid does not have time to evaporate across the expansion), so $y_O = y_I$ and the quality (x_O) is calculated using the mean enthalpy equation (3.8) which is given as

$$x_O = \frac{(1 - y_O)h_{lm,O} + y_O h_{l,O} - h_{m,O}}{h_{l,O} - h_{v,O}} \qquad 3.54$$

Case 2: Conical Jet

In this case, it is assumed that the spray at the exit of the spray orifice expands as a cone (Figure 3.12) and the fluid has completed adiabatic evaporation, so $y_O = 1$ at the outlet. The governing equations and derivation for the conical jet expansion are presented in Appnedix A which are taken from Versteeg (2009). The final expression to evaluate the velocity, quality at the exit of the CV are given as follows

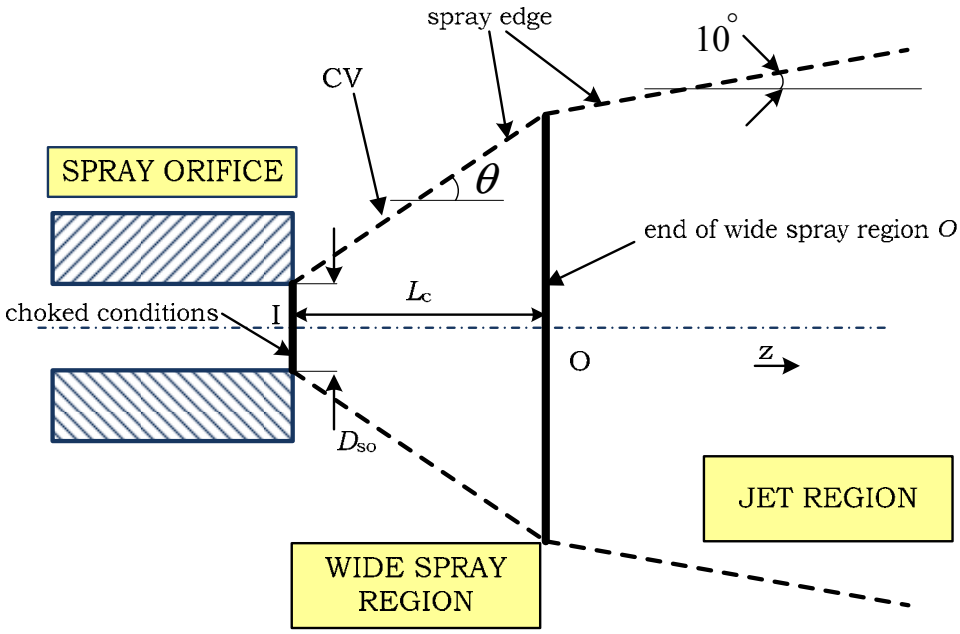

Figure 3.12 Control Volume for DSW for conical expansion at the spray orifice exit

$$U_O = \frac{U_I}{F(\theta)}\left[1+\frac{(p_I - p_O)A_{so}}{\dot{m}U_I}\right] \qquad 3.55$$

$$x_O = \frac{h_{m,O} - h_{l,O}}{h_{v,sat,O} - h_{l,O}} \qquad 3.56$$

where

$$F(\theta) = \frac{\ln(1/\cos\theta)}{(1/\cos\theta - 1)} \qquad 3.57$$

and θ is spray cone angle (see Appendix A).

When the flow is choked at the spray orifice exit, the maximum effective angle, θ=45° and when the flow ceases to be choked towards the end of metered spray event, θ = 0° (Versteeg, 2009). Therefore, these two extreme scenarios have been considered to study the effect of cone angle on the exit velocity.

Case 2a: θ=45°

Case 2b: θ = 0°

As the exit pressure (discharge ambient pressure) and critical mass flow rate at the CV outlet are known, the exit velocity at the outlet of CV is evaluated using the equation (3.55) and (3.57). Then the mean specific volume at outlet of the CV is evaluated with the help of mass conservation (equation 3.48). The mean specific enthalpy and quality at the outlet of CV are obtained using equations (3.51) and (3.56) respectively.

3.5. Closure

In this chapter the mathematical modeling of flow through short tube, capillary tube and two-orifice system of pMDIs was presented in detail. A semi-empirical model for short tube, HEM, DEM and IDEM for an adiabatic capillary tube was presented. The submodels to evaluate the flow variables in different regions of the capillary tube have been presented. The DEM was used to model the two-phase metastable flow through twin-orifice system of pMDI. The existing algorithms for metastable flow through adiabatic capillary tubes and through ducts with expansions were integrated into a computer code for the calculation of propellant flows through twin-orifice systems. This required the development of following submodels:

- Abrupt contraction at tube.
- Abrupt expansion at tube.
- Discharge shock wave at the exit of the spray orifice.

The equation set along with the associated submodels is numerically integrated. The numerical procedure is presented in the next chapter along with the flow charts describing the method in detail.

CHAPTER 4

NUMERICAL APPROACH

4.1. Introduction

In the previous chapter the mathematical modeling of propellant flow through short tubes, long capillary tubes and twin-orifice system was described. Apart from the semi-empirical models discussed at the start of the previous chapter, the governing equations are ordinary differential equations which require a numerical solution method. A grid is drawn to cover the whole domain. With a sufficiently fine grid distribution, the complete distribution of flow variables can be expressed in terms of their values at neighboring grid points. Thus, the task of the numerical method is to evaluate the flow variables at each grid point. In a numerical scheme, a set of algebraic equations are derived from the differential equations for the grid points. The accuracy of the obtained results depends mainly on the discretization technique and the proper selection of grid. But detail and accuracy somehow require computational effort (calculation time and computer memory). Hence, in developing a numerical scheme, the primary consideration is a trade-off between the model detail and reasonable computational effort.

The purpose of this chapter is to discuss the numerical algorithm to solve the governing equations and sub-models described in the previous chapter for the flow through the short tube, adiabatic capillary tube and twin-orifice systems. The working procedure, algorithm and boundary conditions for each of the models (discussed in the previous chapter), detailing the calculation and sequence of the numerical code is presented. For the flow through a capillary tube, both subcritical and critical flows are considered. For the flow through twin-orifice systems, the criteria for double choking (choking at the exit of the valve orifice and spray orifice) and the procedure to solve the double choking flows are discussed in detail. The computer programming language used to solve these flows is Microsoft Visual C v6.0.

4.2. Algorithm for Semi-empirical Model in Short Tubes:

In this section, the procedure to evaluate the mass flow rate using Kim and O'Neal semi-empirical model has been presented. The semi-empirical model predicts the mass flow rate along short tubes of a given geometry (D and L) and inlet and outlet pressure. It has been developed to cover both single phase and two-phase flow conditions at the entrance of the short tube. The model assumes saturated/equilibrium two-phase conditions. However, the model is limited to propellant R134A only and to the parameter range mentioned in Table 2.2. For subcooled inlet conditions, the inlet pressure (p_{in}), inlet temperature (T_{in}) are specified as inlet conditions. For two-phase inlet conditions, the inlet pressure and inlet quality (x_{in}) are specified at the entrance of the short tube. At the exit of the short tube, discharge pressure (p_{dis}) is given as outlet condition. Equations (2.7)-(2.10) along with the empirical coefficients in Table 2.2 are used to evaluate the mass flow rate of propellant R134A through short tubes. As these equations are not in differential form, they are solved directly with help of a code written in Microsoft Visual C.

4.2.1. Procedure

Step 1: Input parameters : diameter (D), length (L), p_{in}, p_{dis}, T_{in} or x_{in}

Step 2: Calculate saturation pressure, $p_s(T_{in})$, critical pressure (p_c), and saturation temperature, $T_s(p_{in})$ for R134A using REFPROP 7.0

Step 3: Evaluate p_{in}/p_c, L/D, $SUBC$, $EVAP$ and D/D_{ref}

Step 4: Evaluate p_f using equation (2.8)

Step 5: Calculate ρ_l and ρ_v at p_{in} from REFPROP 7.0

Step 6: Evaluate C_{tp} using equation (2.9)

Step 8: Evaluate mass flow rate, $\dot{m}$, using equation (2.7)

where

p_f = adjusted flashing pressure (kPa)

C_{tp} = correction factor for two-phase quality

$SUBC$ = normalized subcooling $(T_s - T_{in})/T_c$ (T is in K)

$EVAP$ = normalized downstream pressure $(p_c - p_{dis})/p_c$ (p is absolute pressure)

D_{ref} = reference short tube diameter (1.35×10^{-3} m)

4.3. Numerical Algorithm for Capillary Tubes

The governing equations described in previous chapter (chapter 4) for HEM, DEM and IDEM have been used to solve the flow through long adiabatic capillary tubes. In this section, the discretized form of these governing equations and numerical procedure to solve them are presented.

4.3.1. Delayed Equilibrium Model (DEM)

The numerical model for DEM allows the calculation of the mass flow rate of the propellant through the long adiabatic capillary tubes and the local values of the flow variables (pressure, temperature, velocity, void fraction, quality, etc). The model solution is iterative and a guessed mass flow rate for a given boundary condition (inlet and outlet pressure) and systematic variations of the mass flow rate until: (i) the calculated discharge pressure agrees with the actual exit pressure or (ii) the mass flow rate is found to be critical at the exit of the tube and all constraints on the final flow solution are satisfied. This method which is based on 1D approach to model the compressible choked flows, has been widely used by the previous authors in steam-water flows (Feburie et al., 1993; Attou and Seynhaeve, 1999a) and refrigeration air-conditioning system (Bittle and Pate.,1996; Escanes et al, 1995; Garcia-Valladares et al. 2002a).

4.3.1.1. Spatial Discretization

The entire domain is discretized into 'N' control volumes (CVs), with discretization nodes located at the inlet and outlet sections of the control volumes. Owing to the high gradients of flow variables at the end of a capillary tube, a non-uniform grid is used with CVs concentrated at the outlet section. Figure 4.1 shows grid generated for an adiabatic capillary tube according to the expression given by Escanes et al. (1995).

$$\Delta z_i = \frac{L}{\tanh(k)}\left[\tanh\left(k\frac{i}{N}\right) - \tanh\left(k\frac{(i-1)}{N}\right)\right] \quad 4.1$$

where k is concentration factor. k = 0 corresponds to uniform grid and $k \geq 0$ corresponds to non-uniform grid. Following Escanes et al. (1995) k = 3.5 has been used for the present study.

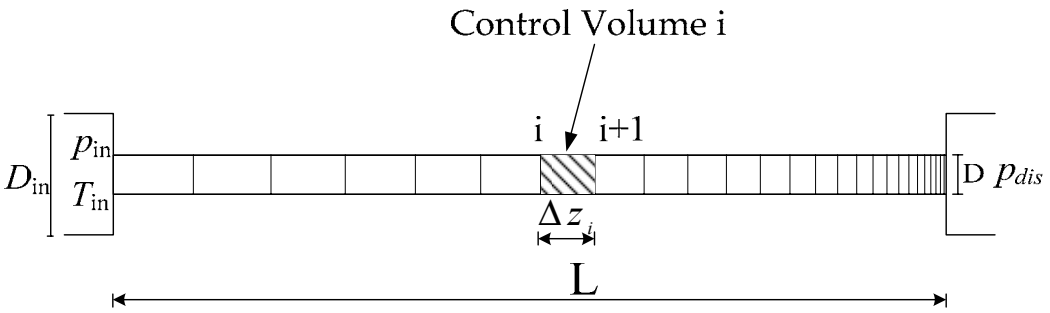

Figure 4.1 Grid system for DEM in adiabatic capillary tube

4.3.1.2. Discretization of Governing Equations

A set of algebraic equations is obtained by integration of the governing equations (3.1- 3.3) over each control volume (CV).

The discretized continuity equation solved for the CV outlet may be expressed as:

$$\dot{m}_{i+1} = \dot{m}_i = \dot{m} \quad 4.2$$

where 'i' is ith CV (see Figure 4.1Figure 3.1)

The discretized momentum equation solved for the control volume outlet pressure gives

$$p_{i+1}^{j} = p_i^{j} - \frac{\Delta z_i}{A}\left(\frac{f_{i+1}^{j}}{4}\frac{\dot{m}^2}{2\rho_{m,i+1}^{j-1}A^2}P + \frac{\dot{m}\left(U_{i+1}^{j} - U_i^{j}\right)}{\Delta z_i}\right) \quad 4.3$$

where 'j' is the current iteration step and is the previous iterated value

The discretized energy equation solved to obtain the enthalpy at the CV outlet is given as

$$h_{i+1}^{j} = h_{i}^{j} - \frac{\left(U_{i+1}^{j^2} - U_{i}^{j^2}\right)}{2} \qquad 4.4$$

The mixture entropy at the outlet of CV is obtained from

$$s_{i+1}^{j} = (1 - y_{i+1}^{j}) s_{lm,i+1}^{j} + (y_{i+1}^{j} - x_{i+1}^{j}) s_{l,i+1}^{j} + x_{i}^{j} s_{v,i+1}^{j} \qquad 4.5$$

Given the mass flow rate and the geometry of the capillary tube as well as velocity, pressure enthalpy and entropy at the inlet of each CV equations 4.2-4.5 are solved together to obtained the velocity, pressure, enthalpy and entropy at the outlet of each CV.

4.3.1.3. Boundary Conditions

Boundary conditions must be given at the inlet and outlet of the capillary tube

Inlet Conditions

- If the propellant is in a subcooled state at the inlet then the inlet pressure (p_{in}) and temperature (T_{in}) should be given.
- If the propellant is in two-phase state at the inlet then the inlet pressure (p_{in}) and vapour mass fraction (x_{in}) should be given.

Outlet Conditions

At the outlet section pressure (p_{dis}) is given

4.3.1.4. Propellant Properties

For different propellants, all the properties are obtained using the Reference Fluid Thermodynamic and Transport Properties (REFPROP) ver. 7.0 (2002). It is developed by the National Institute of Standard and Technology (NIST). It calculates fluid properties for many industrial propellants. The program uses the most accurate equation of state and models currently available. It has been widely used by the previous researchers (Sami and Tribes, 1998; Wongwises and Pirompak, 2001; Garcia-Valladares et al, 2002a; Sanzovo and Mattos, 2003) to calculate the properties of different propellants.

The fluid properties for different regions of the capillary tube are evaluated as follows:

- In the subcooled liquid region (zone I), the liquid density evaluated as a function of pressure and temperature *($\rho = \rho(p, T)$)* and viscosity and enthalpy as a function of temperature and density *($\mu = \mu(T, \rho)$* and *$h = h(T, \rho)$)*.
- Following Attou and Seynhaeve (1999a) the superheated liquid properties in metastable liquid region (zone II) are estimated as a function of pressure and entropy *f(p, s)*.
- According to Feburie et al (1993) the metastable two-phase region (zone III) consists of three states: superheated liquid (subindex, lm), saturated liquid, (subindex, l) and saturated vapour (subindex, v). In this region the saturated propellant properties are estimated using the values corresponding to saturated conditions at the prevailing fluid pressure and the superheated liquid properties are calculated as a function of pressure and entropy *f(p, s)*.
- The two-phase region is modeled using homogeneous equilibrium model and the properties are estimated using the values corresponding to saturated conditions at the fluid pressure.

4.3.1.5. Flow Solution Procedure

The execution of the capillary tube model begins by defining

- the propellant,
- the capillary tube geometry (*L & D*),
- inlet and outlet boundary conditions (p_{in}, T_{in} *or* x_{in}, p_{dis}),
- an initial assumed value for the mass flow rate.

The purpose of the model solution scheme is the calculation of the mass flow rate that ensures that the calculated pressure at the outlet of the capillary agrees with the discharge pressure (p_{dis}) and all constraints on the final flow solution are satisfied. The values of the flow variables at a control volume outlet section are obtained by solution of the set of algebraic equations (4.2)-(4.5), from the known values at the control volume inlet. The solution procedure is carried out in this manner, marching forward step-by-step in the flow direction from the capillary tube inlet to the outlet. The mass

flow rate is iteratively updated by using Possible and Impossible Flow (PIF) algorithm proposed by Attou and Seynhaeve (1999a) which is given as follows:

For a capillary tube there are two physically possible flow states:

(i) Subcritical flow: the correct mass flow rate is the value for which the exit pressure exactly matches the given discharge pressure.

(ii) Choked flow at the capillary tube exit: the flow is subcritical everywhere in the capillary tube except at its exit, where a discharge shock appears. The correct mass flow rate ensures that the sum of the pressure drop in the capillary tube due to acceleration and friction and the pressure drop across the discharge shock wave causes the outlet pressure to match the discharge pressure.

Other flows are impossible and the assumed mass flow rate is updated depending on the current flow rate.

PIF Algorithm:

Step 1: Initial guess of the mass flow rate.

Step 2 : From the initial conditions, the values of the flow variables at the control volume outlet section are obtained by means of the forward marching described above.

Step 3:If the flow is critical before the end of the pipe, the flow is impossible and the impossible mass flow rate is designated ($\dot{m}_{imp}$) . The mass flow rate $\dot{m}_{imp}$ has to be reduced and the new (hopefully) possible mass flow ($\dot{m}_{poss}$) rate for the next iteration is calculated using the following equation:

$$\dot{m}_{poss} = \frac{\dot{m}_{imp}}{(1+\delta)} \qquad 4.6$$

Step 4: If the flow is subcritical up to the end of the pipe and the calculated exit pressure is higher than the actual value the flow is a possible flow. However, since the exit pressure is too high the mass flow rate $\dot{m}_{pos}$ has to be increased and the new impossible mass flow rate for the next iteration is evaluated using the following equation:

$$\dot{m}_{imp} = \dot{m}_{poss}(1+\delta) \qquad 4.7$$

Step 5: The procedure is repeated until the mass flow rate is converged. The convergence criteria for the mass flow rate is $\left|\dot{m}_{imp} - \dot{m}_{poss}\right| / \dot{m}_{poss} \leq 10^{-6}$. Initially, the value of δ is taken as 100, there after it is reduced to half for every next iteration. i.e. $\delta_{new} = 0.5 \times \delta$.

Step 6: At the completion of a successful flow solution, $p_{out} \geq p_{dis}$. If $\left|p_{out} - p_{dis}\right| \leq 10^{-6} \times p_{dis}$, the flow solution is concluded. The flow chart for PIF algorithm is shown in Appendix B (Figure B-1).

As discussed in the previous chapter (section 3.1), the flow through an adiabatic capillary tube consists of four different zones. First, the calculation process for each zone is explained, next, the procedure to estimate the length in the z-direction is described. Purpose of each calculation is to produce, pressure, temperature, velocity, enthalpy and entropy at outlet of each CV from given inlet conditions.

4.3.1.6. Sub models

Sub-Cooled Liquid Region (Zone I)/ Metastable Liquid Region (Zone II):

Step 1: Using the discretized continuity equation (4.2), the mass flow rate for the outlet CV is obtained.

Step 2: Assume pressure and temperature at the outlet of CV, which is the same as the inlet of CV.

Step 3: Thermodynamic properties (density, viscosity, etc.) are evaluated at the outlet of CV using the REFPROP 7.0 (2002).

Step 4: Velocity is calculated using equation (3.4) after calculating the Reynolds number at the outlet of CV

Step 5: The single phase friction factor is calculated using the equation (3.12).

Step 6: The pressure, enthalpy and entropy at the outlet of CV are obtained iteratively using the discretized momentum, energy and entropy equation (4.3-4.5).

Step 7: For zone I, the temperature at the outlet of the CV is obtained by integrating the equation, $dh = c_p dT$, assuming constant value of c_p

$$T_{i+1}^{j} = T_{i}^{j} + \frac{1}{c_{p_{i+1}}}\left(h_{i+1}^{j} - h_{i}^{j}\right) \tag{4.8}$$

Step 8: For zone II, the temperature at the outlet of CV is obtained from REFPROP as a function of outlet pressure and entropy

$$T_{i+1}^{j} = f\left(p_{i+1}^{j}, s_{lm,i+1}^{j}\right) \tag{4.9}$$

Step 9: The outlet quality (x_{i+1}), void fraction (α_{i+1}) and the vaporisation index (y_{i+1}) are set to be equal to zero since the flow is single phase liquid.

Step 10: The flow chart to calculate the flow variables for zone I and zone II is shown in Appendix B (Figure B-2).

Metastable Two-Phase Region (Zone III):

In this region, the discretized vaporisation index for DEM at CV outlet is calculated by integration of the relaxation equation using trapezoidal rule

$$y_{i+1}^{j} = 1 - \frac{\left(1 - y_{i}^{j}\right)}{\exp\left(0.02 \frac{P}{A} \frac{\Delta z_i}{2} \left\{ \left(\frac{p_s - p_{i+1}^{j}}{p_c - p_s} \right)^{1/4} + \left(\frac{p_s - p_{i}^{j}}{p_c - p_s} \right)^{1/4} \right\} \right)} \tag{4.10}$$

Step 1: For saturated liquid and saturated vapour, the thermodynamic properties (density, viscosity, etc.) are evaluated as a function of pressure on saturation line, whereas the superheated liquid properties are calculated as function of pressure and entropy from REFPROP.

Step 2: Velocity is calculated using equation (3.4) after calculating the Reynolds number at the outlet of CV.

Step 3: The two-phase friction factor is calculated using equation (3.12) by considering the Reynolds number as $Re = mD/(\mu_{tp}A)$ where two-phase viscosity, $\mu_{tp,}$ is evaluated according to Duckler correlation (recommended by Brittle and Pate, 1996) (equations 3.15 - 3.17).

Step 4: Equations (4.3 - 4.5) give pressure, enthalpy and entropy at the outlet of CV respectively.

Step 5: The mean enthalpy (obtained from the above equations) is related to the individual enthalpies through their mass fractions to evaluate the quality at the outlet of CV.

$$x_{i+1}^{j} = \frac{(1-y_{i+1}^{j})h_{lm,i+1}^{j} + y_{i+1}^{j}h_{l,i+1}^{j} - h_{i}^{j}}{h_{l,i+1}^{j} - h_{v,i+1}^{j}} \qquad 4.11$$

Step 6: The temperature at the outlet of CV is calculated using equation (3.18) which is given as

$$T_{i+1}^{j} = \left(1-y_{i+1}^{j}\right)T_{lm,i+1}^{j} + y_{i+1}^{j}T_{l,i+1}^{j} \qquad 4.12$$

The flow chart for the above procedure is shown in Appendix B (Figure B-3).

Equilibrium Two-Phase Region (Zone IV):

The flow process enters into equilibrium two-phase flow when y approaches to unity i.e. the superheated liquid vanishes. The two-phase flow is modeled assuming the homogeneous equilibrium model. As mentioned before the properties of the propellant are evaluated using saturation line values at prevailing pressure using REFPROP. The velocity, pressure, enthalpy and quality at the exit of CV are calculated in the same manner as explained in the previous section (zone III).

Entrance and Exit Correction:

The pressure drop and pressure recovery associated with the sudden contraction and sudden expansion are evaluated using the equations (3.20 - 3.27).

Flash point location

The transition between zones I, II, III and IV is decided on the basis of the saturation pressure (p_s), pressure of vaporisation (p_v) and vaporisation index (y). If

$p \geq p_s$ zone I (subcooled region)

$p_v > p > p_s$ zone II (metastable liquid region)

$p < p_v$ zone III (metastable two-phase region)

$y = 1$ zone IV (two-phase region)

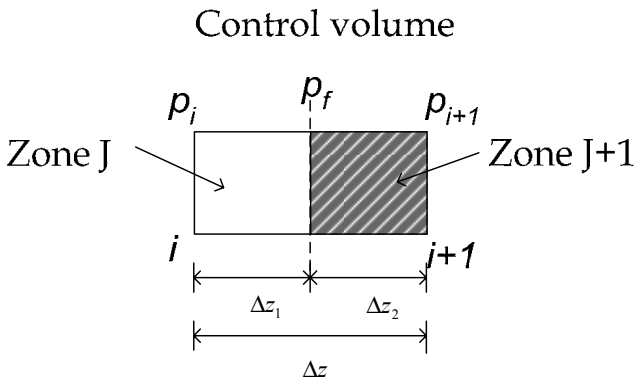

Figure 4.2 Transition Control Volume

In order to evaluate the position of the transition point accurately when it is located between the inlet 'i' and outlet 'i+1' of a CV, the relevant CV is split into two CVs (Garcia-Valladares et al., 2002a and 2002b) as shown in Figure 4.2.

The length of the first CV is calculated from the momentum equation, imposing pressure condition at the outlet section. i.e.

$$\Delta z_1 = \frac{2(p_i - p_f)D}{f\rho U_i^{\,2}} \qquad 4.13$$

where

p_f = p_s (if the transition occurs from Zone I to Zone II) or

p_f = p_v (if the transition occurs from Zone II to Zone III)

The length of the second CV is given by simple difference

$$\Delta z_2 = \Delta z - \Delta z_1 \qquad 4.14$$

When, the vaporisation index (y) reaches unity, the flow is in the two-phase equilibrium region (zone IV).

Critical Flow

The critical mass, $\dot{m}_c$ is reached when the velocity reaches the sonic velocity, U_c, which is evaluated using the equation proposed by Attou and Seynhaeve (1999a).

$$U_{c,i+1}^{j}=\left[\frac{\left(v_{m,i+1}^{\ j}\right)^2\left(h_{v,i+1}^{\ j}-h_{l,i+1}^{\ j}\right)}{\left(v_{v,i+1}^{\ j}-v_{l,i+1}^{\ j}\right)\left(\partial h_{m,i+1}^{\ j}-v_{m,i+1}^{\ j}\right)-\partial v_{m,i+1}^{\ j}\left(h_{v,i+1}^{\ j}-h_{l,i+1}^{\ j}\right)}\right]^{\frac{1}{2}} \tag{4.15}$$

where

$$\partial v_{m,i+1}^{\ j}=x_{i+1}^{j}\left(\frac{\partial v_v}{\partial p}\right)_{sat,i+1}^{j}+\left(y_{i+1}^{j}-x_{i+1}^{j}\right)\left(\frac{\partial v_l}{\partial p}\right)_{sat,i+1}^{j}+\left(1-y_{i+1}^{j}\right)\left(\frac{\partial v_{lm}}{\partial p}\right)_{s_{lm},i+1}^{j} \tag{4.16}$$

$$\partial h_{m,i+1}^{\ j}=x_{i+1}^{j}\left(\frac{\partial h_v}{\partial p}\right)_{sat,i+1}^{j}+\left(y_{i+1}^{j}-x_{i+1}^{j}\right)\left(\frac{\partial h_l}{\partial p}\right)_{sat,i+1}^{j}+\left(1-y_{i+1}^{j}\right)\left(\frac{\partial h_{lm}}{\partial p}\right)_{s_{lm},i+1}^{j} \tag{4.17}$$

and v_m is given by the expression (3.7). The subscript 'sat' indicate that the derivatives are evaluated following saturation line and 's_{lm}' indicates that the derivatives are evaluated following isentropic line. The derivatives are evaluated from the following expressions:

$$\left(\frac{\partial v_v}{\partial p}\right)_{sat,i+1}^{j}=\frac{v_v\left(p_{i+1}^{j}+\Delta p\right)-v_v\left(p_{i+1}^{j}-\Delta p\right)}{2\Delta p} \tag{4.18}$$

$$\left(\frac{\partial v_l}{\partial p}\right)_{sat,i+1}^{j}=\frac{v_l\left(p_{i+1}^{j}+\Delta p\right)-v_l\left(p_{i+1}^{j}-\Delta p\right)}{2\Delta p} \tag{4.19}$$

$$\left(\frac{\partial v_{lm}}{\partial p}\right)_{lm,i+1}^{j}=\frac{v_{lm}\left(p_{i+1}^{j}+\Delta p,s_{lm,i+1}^{j}\right)-v_{lm}\left(p_{i+1}^{j}-\Delta p,s_{lm,i+1}^{j}\right)}{2\Delta p} \tag{4.20}$$

In similar way the enthalpy derivative are evaluated

$$\left(\frac{\partial h_v}{\partial p}\right)_{sat,i+1}^{j}=\frac{h_v\left(p_{i+1}^{j}+\Delta p\right)-h_v\left(p_{i+1}^{j}-\Delta p\right)}{2\Delta p} \tag{4.21}$$

$$\left(\frac{\partial h_l}{\partial p}\right)^j_{sat,i+1} = \frac{h_l\left(p^j_{i+1}+\Delta p\right)-h_l\left(p^j_{i+1}-\Delta p\right)}{2\Delta p} \quad 4.22$$

$$\left(\frac{\partial h_{lm}}{\partial p}\right)^j_{lm,i+1} = \frac{h_{lm}\left(p^j_{i+1}+\Delta p, s^j_{lm,i+1}\right)-h_{lm}\left(p^j_{i+1}-\Delta p, s^j_{lm,i+1}\right)}{2\Delta p} \quad 4.23$$

Where Δp is a small pressure step which is taken as 500 Pa.

Discharge shock wave

In the case of critical flow at the exit of the capillary tube, the discharge shock wave described in previous chapter (section 3.4.4.3) is solved.

4.3.2. Improved Delayed Equilibrium Model (IDEM)

For the IDEM, the numerical discretization and the solution procedure is same as that of discussed in the previous section (section 4.3.1), only, instead of using equation (4.10) the vaporisation index, *y,* is evaluated using the following equation

$$y^j_{i+1} = 1 - \frac{1}{\frac{1}{\left(1-y^j_{i+1}\right)} + k_y \frac{P}{A} U_{in}^{1/10}\left[0.5\Delta z_{i+1}\left\{\left(\frac{1}{U^j_{i+1}}\right)^{1/10}\left(\frac{p_s - p^j_{i+1}}{p_c - p_s}\right)^{1/4} + \left(\frac{1}{U^j_i}\right)^{1/10}\left(\frac{p_s - p^j_i}{p_c - p_s}\right)^{1/4}\right\}\right]} \quad 4.24$$

4.3.3. Homogeneous Equilibrium Model (HEM)

Also for HEM, the numerical discretization and the solution procedure is same as that of DEM (section 4.3.1). As the vaporisation is instantaneous and happens at thermodynamic saturation pressure (i.e. p=p_s), the vaporisation index, y=1 in DEM corresponds to HEM.

4.4. Twin-orifice system

The numerical model discussed in the previous sections for DEM (sections 4.3.1) was used to solve the flow through twin-orifice system of pMDIs. The propellant inside

the twin-orifice system of pMDIs is generally in two-phase metastable region (zone III), so the subroutine for zone III is called to solve the flow variables throughout the valve orifice, expansion chamber and spray orifice.

4.4.1. Delayed Equilibrium Model

4.4.1.1. Spatial Discretization

The domain is discretized into N control volumes, with the discretization nodes located at the inlet and outlet sections of the control volumes (Figure 4.3). Owing to the high gradients produced at the exit of the valve and spray orifice, non-uniform grid concentrated at the exit section (Figure 4.3) are generated using the expression (equation 4.1) given by the Escanes *et. al* (1995). For the expansion chamber, a uniform grid is used, as there are no high gradients, which is generated using the following expression

$$\Delta z_i = \frac{L_{ec}}{\left(N_{ec} - N_{up}\right)} \qquad 4.25$$

Figure 4.3 shows the node distribution across the twin-orifice system with enlarged view of the valve and spay orifices.

where,

N_{vo} number of nodes at the end of valve/upstream orifice

N_{ec} number of nodes at the end of expansion chamber

N total number of nodes

4.4.1.2. Boundary Conditions

Boundary conditions must be given at the inlet of the valve orifice and the exit of the spray orifice

Inlet Conditions:

Continuous Discharge Flows:

For continuous discharge flow through twin-orifice system, the propellant is assumed in saturated state, so the temperature (T_{in}) at the inlet should be given.

Metered Discharge Flows:

For a quasi-steady metered discharge flows, inlet conditions are defined from the knowledge of the propellant state in the metering chamber. Experimental values of metering chamber pressure and temperature are available between 25 and 200 ms from Clarks (1991) experimental data. In order to completely specify the problem, quality (x) and the vaporisation index (y) of the mixture in the metering chamber are required. The vaporisation index, y is evaluated using the mean temperature equation (3.18) proposed by Zhou and Zhang (2006), considering the measured temperature (T_{exp}) as mean temperature and ambient temperature(T_0) as metastable temperature. The quality is evaluated from the mean enthalpy equation (3.8). The vaporisation index y and the quality x are evaluated using the following equations

$$y = \left(T_0 - T_{\exp}\right) / \left(T_0 - T_{s,l}(p)\right) \qquad 4.26$$

$$x = \left[h_{l,0} - (1-y)h_{lm} - yh_{l,s}(p)\right] / \left[h_{v,s}(p) - h_{l,s}(p)\right] \qquad 4.27$$

where $h_{l,0}$ is the liquid enthalpy at ambient temperature (T_0), T_{exp} is the experimental metering chamber temperature (Clark, 1991) and subscript 's' indicates saturated liquid at the prevailing local pressure.

Outlet Conditions

For both continuous discharge and metered discharge flows, ambient pressure (p_{dis}) is given at the outlet section.

4.4.1.3. Flow Solution Procedure

The solution of the flow through twin-orifice systems begins by defining

- the propellant or propellant mixture
- the dimensions of valve orifice (D_{vo}, L_{vo}), expansion chamber (D_{ec}, L_{ec}), and spray orifice (D_{so}, L_{so}).
- inlet and outlet boundary conditions (section 4.4.1.2),
- an initial assumed value for the mass flow rate.

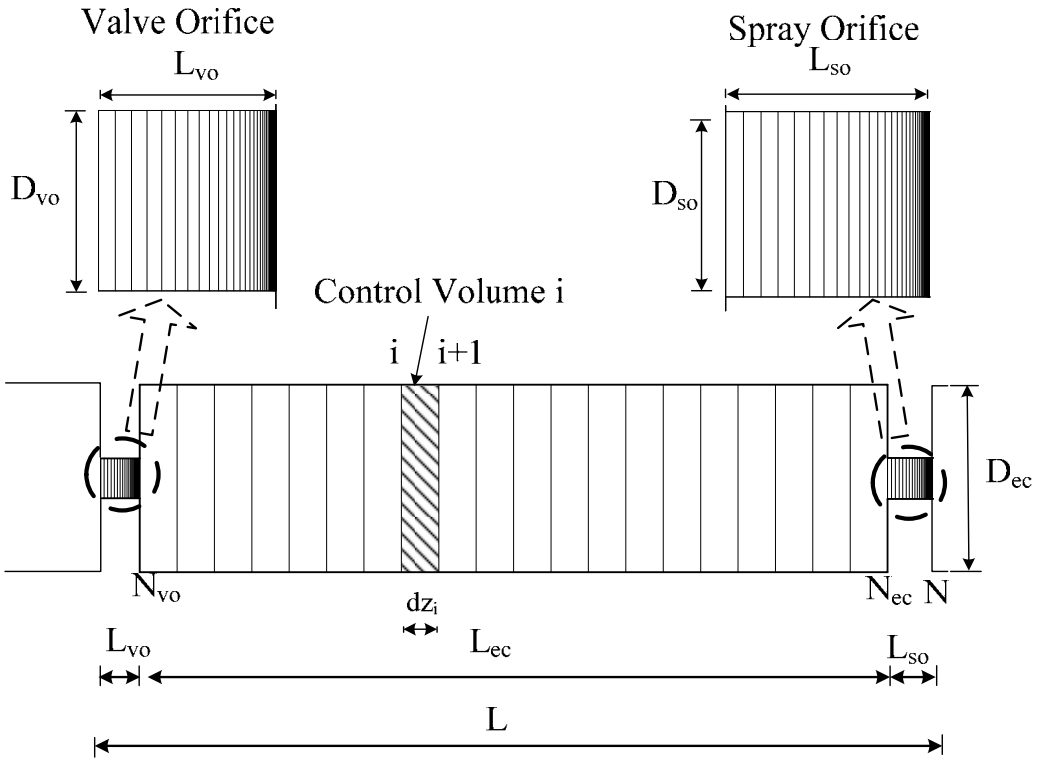

Figure 4.3 Node distribution along the twin-orifice system (valve orifice, expansion chamber and spray orifice)

The solution procedure is essentially same as that explained in previous section (4.3.1.5) for adiabatic capillary tube and is shown in schematic form in Figure B-4 (Appendix B). The flow chart shows the solution procedure for iterating the mass flow rate and solving the flow variables inside the valve orifice, expansion chamber and spray orifice. The subroutine for zone III (two-phase metastable region) is called to solve the flow variables inside the valve orifice, expansion chamber and spray orifice see (Figure B-3 in Appendix B).

4.4.1.4. Submodels

Abrupt Contraction at Tube

The procedure to solve the flow variables across the abrupt contraction of valve orifice and spray orifice are described in the previous chapter in (section 3.4.4.1). The pressure drop associated with a sudden contraction for a single phase or two-phase

inlet are evaluated using the equations described in (section 3.4.4.1). The main steps are summarized below:

Procedure:

Step 1: The pressure (p_{i+1}) at the outlet of the abrupt contraction CV is assumed.

Step 2: The mean enthalpy ($h'_{lm,i}$), mean entropy ($s'_{lm,i}$) and mean specific volume($v'_{lm,i}$) of new metastable liquid are evaluated at the inlet of the CV using equations (3.37 - 3.39) respectively.

Step 3: For saturated vapour, the thermodynamic properties (density, viscosity, etc.) are evaluated as a function of CV outlet pressure (p_{i+1}) on saturation line, whereas the superheated liquid properties are calculated as function of CV outlet pressure (p_{i+1}) and new entropy ($s'_{lm,i}$).

Step 4: Mixture specific volume is evaluated at the exit of the CV using equation (3.40)

Step 5: U_{i+1} at the exit of CV is evaluated using the mass conservation equation (3.4)

Step 6: Pressure drop at the outlet of CV is evaluated using the equations (3.20)-(3.23).

Step 7: Enthalpy, at the outlet of CV is evaluated from the energy equation (3.41)

Step 8: The CV outlet quality, $x_{i+1} = x_i$ and the vaporisation index, $y_{i+1} = x_i$

Abrupt Expansion at Tube

The twin-orifice system of pMDI has abrupt expansion at two different locations : (i) at the exit of the valve orifice (ii) at the exit of the spray orifice. The flow can be either critical or sub-critical at these locations. The purpose of this section is to define the criteria for choking at these two locations and discuss the procedure to solve the flow variables along these abrupt expansions for both subcritical and critical flows.

The pressure recovery associated at the valve orifice exit due to sudden expansion is evaluated using equations (3.42 -3.46).

Procedure for subcritical flow:

Step 1: The pressure at the exit of the abrupt expansion CV is assumed (p_{i+1}) and the base pressure $p_{bc} = p_i$.

Step 2: For saturated liquid and saturated vapour, the thermodynamic properties (density, viscosity, etc.) are evaluated as a function of pressure on saturation line, whereas the superheated liquid properties are calculated as function of pressure and entropy .

Step 3: After that, the mixture specific volume ($\nu_{m,i+1}$) at the outlet of CV is evaluated using equation (3.7)

Step 4: The velocity (U_{i+1}) at the outlet of CV is evaluated using equation (3.42)

Step 5: Equations (3.43 and 3.44) are used to evaluate the pressure and enthalpy at the outlet of CV.

Step 6: The vaporisation index at the outlet of CV (y_{i+1}) is evaluated using equation (3.45) or (3.46)

Step 7: The quality at the exit of CV (x_{i+1}) is evaluated using the equation (3.47)

Criteria for Double Choking

The criteria for the occurrence of double-choked flow is given by the following two conditions (Attou and Seynhaeve, 1999a). The two conditions are:

1. Mach Number Condition: the flow is choked at the **valve orifice** exit if

$$Mach = 1 \qquad 4.28$$

If the Mach number is less than one, the flow is not choked at this cross section.

2. Downstream pressure condition: one necessary condition to reach sound velocity at the **spray orifice** exit expresses that in this case the back-pressure must be lower or at least equal to the choking pressure, p_c.

$$p_{dis} \leq p_c \qquad 4.29$$

Considering these two criteria, four cases can be distinguished:

Case i: If both conditions 4.29 and 4.28 are satisfied then a double choked flow exists

Case ii: If the only condition 4.29 is satisfied and not 4.28, then the flow is choked at the exit of the spray orifice.

Case iii: If only the condition 4.28 is satisfied and not 4.29, then the flow is choked only at the exit of valve orifice.

Case iv : If the conditions 4.29 and 4.28 are not satisfied the flow remains subcritical throughout the pMDI.

In order to develop a general procedure which is valid for all cases discussed above, an iterative length algorithm proposed by Attou and Seynhaeve (1999 a) has been modified to calculate the flow downstream from the critical section and this algorithm is called Base Pressure Algorithm. The iterative algorithm of Attou and Seynhaeve (1999a) used a matrix method to solve the governing equations and the critical condition for their model was obtained from the condition of vanishing of the determinant of the flow model matrix. Whereas the current solution method involves solving the governing equations simultaneously along with the assigned submodels using the Mach number as choking criteria (as the current model do not have flow model matrix). Both the models give the same result. However, the current model is simpler then that of Attou and Seynhaeve's (1999a) model

Base pressure algorithm:

This base pressure algorithm solves the flow conditions for downstream of the valve orifice (i.e. expansion chamber and spray orifice), after the flow is choked at the exit of the valve orifice. Knowing the mass flow rate and the inlet conditions at the entrance of the valve orifice, the critical mass flow rate and the evaluation of flow variables along the valve orifice are calculated using PIF algorithm. Assuming that the two conditions 4.29 and 4.28 are satisfied for choking, the known mass flow rate is used in conjunction with the conditions of the fluid at the first critical section (i.e. exit of the valve orifice) to evaluate the flow variables along the expansion chamber and spray orifice by means of the following algorithm:

Step 1: Choice of the base pressure p_{bc} at the step of the enlargement. Initial guess is that the base pressure is equal to the pressure in the jet.

Step 2: Calculation of the variables of the flow at along the abrupt expansion using the equations (3.42-3.44). These values of the variables are initial conditions of the problem of the frictional flow through the expansion chamber and spray orifice.

Step 3: Taking into account the initial conditions, the values of the flow variables at all subsequent control volume outlet sections are obtained by solution of the set of algebraic equations (4.2-4.4) until the necessary condition of choking (equation 4.29) is satisfied or until the local pressure in the last CV 'N', designated by 'p_N' reaches the discharge pressure.

Step 4: New choice of the base pressure depending to the value of the calculated pressure in the last CV (p_N) at the exit of spray orifice :

(a) $p_N > p_{dis}$ and Mach=1 at the exit of the spray orifice, this corresponds to case (i) i.e. the flow is choked both in valve orifice and spray orifice. The flow is concluded at the exit of the spray orifice and the discharge shock wave is computed using the method described in next section.

(b) $p_N > p_{dis}$ and the Mach<1 at the exit of the spray orifice, this corresponds to case (iii) flow is choked at the exit of the valve orifice and remains subcritical at the exit of the spray orifice. The new choice of base pressure is calculated as

$$p_{b,c} = p_{b,c}\left(1-\frac{\delta}{100}\right)$$

(c) $p_N < p_{dis}$ or Mach = 1 within the spray orifice, the new choice of base pressure is calculated as

$$p_{b,c} = p_{b,c}\Big/\left(1-\frac{\delta}{100}\right)$$

where $\delta = 50$ initially and thereafter it is halved for at every iteration. i.e. $\delta_{new} = 0.5 \times \delta_{old}$.

Step 5: Return to step 1 until the Mach=1 at the exit of the spray orifice or $p_{dis} = p_N$.

Step 6: The flow is concluded if $p_{dis} = p_N$ or the flow is choked at the exit of the spray orifice.

The flow chart for the above algorithm is shown in Figure B-5 (Appendix B).

Discharge Shock Wave at the exit of spray orifice

When the flow is critical at the exit of the spray orifice, the discharge shock wave described in the section (3.4.4.3) is solved. Equations 3.48-3.57 are used to solve the discharge shock wave with various assumptions.

4.5. Closure

The discretization schemes of the governing equations to solve the flow through short tubes, long capillary tubes and twin-orifice system were presented in this chapter along with the algorithms procedure to solve these equations. Two main algorithms : (i) PIF algorithm (ii) Base Pressure Algorithm have been discussed in detail. The PIF algorithm is used to iterate the mass flow rate for the given inlet and outlet condition of a tube. The Base pressure algorithm is used for twin-orifice systems to solve the flow variables downstream of a choked valve orifice. The procedure is implemented in a computer program to obtain the flow variables along with the mass flow rate and in detailed in flow charts. The capability and robustness of these models will be tested in the following chapters by validation of these models against available experimental results in the literature. Validation of the semi-empirical model, DEM, IDEM and HEM for short and long capillary tubes with the available experimental data in the literature will be presented in the next chapter.

CHAPTER 5

PROPELLANT FLOW THROUGH ADIABATIC CAPILLARY TUBES

5.1. Introduction

The aim of the present research is to develop a numerical model to predict the mass flow rate and flow variables along the twin-orifice of pMDIs accounting to propellant metastability. In order to achieve this goal it is necessary to understand the metastable flow through single orifice as the orifice geometry controls the relationship between pressure drop and flow rate and hence flow velocity, void fraction, vapour mass fraction, etc. Inlet conditions for orifices in pMDI are almost entirely two-phase flow during the actuation event but the initial transient starts with slightly subcooled valve orifice conditions. Consequently, we need reliable prediction methods for the flow of propellant through a single orifice as an essential building block for a model of a twin-orifice system. Moreover, the literature review has shown that metastability phenomenon inside a single orifice systems has been understood and modeled well. The purpose of this chapter is to consider the existing metastability models through single orifice system before we proceed to the complex flow in twin-orifice systems of pMDIs.

In this chapter, the semi-empirical model proposed by Kim and O'Neal (1994) for the prediction of the relationship between the mass flow rate and pressure drop in short tubes is validated against their experimental results. After successful validation of the model, it is applied to predict the mass flow rate across the valve orifice of continuous discharge flow of pMDIs. For the prediction of additional details of two-phase propellant flows such as void fraction, quality and velocity at the orifice exit, as well as distributions of pressure, temperature etc. along the orifice, it is necessary to work with a numerical model. Thus, a comparison is presented of three models: Homogeneous Equilibrium Model (HEM), Delayed Equilibrium Model (DEM) (Feburie et al.,1993) and Improved Delayed Equilibrium Model (IDEM) (Attou and Seynhaeve 1999a) for a propellant flow through a capillary tube. Both pure propellant and propellant mixtures are considered. Initially, the numerical model to predict the

characteristics of flow inside the capillary tube was developed for pure propellants with subcooled inlet conditions, as most of the literature reviewed on pure propellants involves subcooled inlet conditions. Later, the range of test conditions was extended to saturated and two-phase inlet conditions with propellant mixtures. As a result of these developments, the numerical model is now capable of handling any propellant/propellant mixture available in REFPROP v.7.0 with saturated, subcooled and two-phase inlet conditions. Thereafter, these three models were used to study the propellant flow through short tubes. Finally, the chapter concludes with a summary of the findings of this work and recommendations for the computation of metastable propellant flows through short tubes and long capillary tubes.

5.2. Validation of Semi-Empirical Model

The semi-empirical model developed by Kim and O'Neal (1994) (section 2.4.2.1) covers flashing flow of R134A through short tubes for subcooling varying from 0 to 13.9°C and two-phase flows with inlet quality ranging from 0 to from 10% and *L/D* ranging from 5 to 20. The flow through a short tube represents the steady flow through a pMDI orifice, so this semi-empirical model is a useful tool to predict the pressure drop - mass flow rate relationships. The predictions of the model are first compared with Kim and O'Neal's experimental data. Subsequently, the model is compared with Clark's (1991) experimental data on pMDIs orifices, where the limitations of this model are identified.

5.2.1. Validation against Kim and Neal (1994) Experimental Data

The procedure explained in section 4.2 is used to evaluate the mass flow rate of propellant through short tubes for two different inlet conditions : subcooled and two-phase inlet conditions. Kim and O'Neal (1994) experimental data has been used as test cases for validating the semi-empirical model.

5.2.1.1. Test Cases

Kim and O'Neal (1994) carried out extensive work on short tube orifices using propellant R134A as working fluid. They choose testing conditions to cover a wide range of operating conditions for a short tube expansion device found in a typical residential heat pump or air conditioned. The inlet and outlet pressures for the present study are : p_{in} = 1172 kPa and p_{dis} = 379kPa. For a single-phase flow entering the short tube, the subcooling was varied between 0 and 13.9°C. For two-phase flow conditions at the inlet, quality ranged from 0 to 10%. The dimensions of the short tubes used are listed in Table 5.1.

Table 5.1 Dimensions of the test sections

Length (L) (mm)	Diameter (D) (mm)	L/D
12.69	1.72	7.38
9.50	1.34	7.09
12.70	1.34	9.48
25.40	1.35	18.81
9.50	1.09	8.72

5.2.1.2. Results and Discussion

For subcooled inlet conditions, one would expect the propellant to be in subcooled or metastable state inside the orifice as observed by Nilpueng and Wongwises (2009) in their experimental work and for two-phase inlet conditions the propellant to be in saturated liquid and vapour state. Hence the semi-empirical flow model described in the section (2.4.2.1) is used to predict the mass flow rate along the short tube.

Figure 5.1 shows the comparison of the semi-empirical model results with the experimental data of Kim and O'Neal (1994) for Propellant-134a with respect to upstream subcooling and short tube geometry. The sub-cooling is varied from 0 to

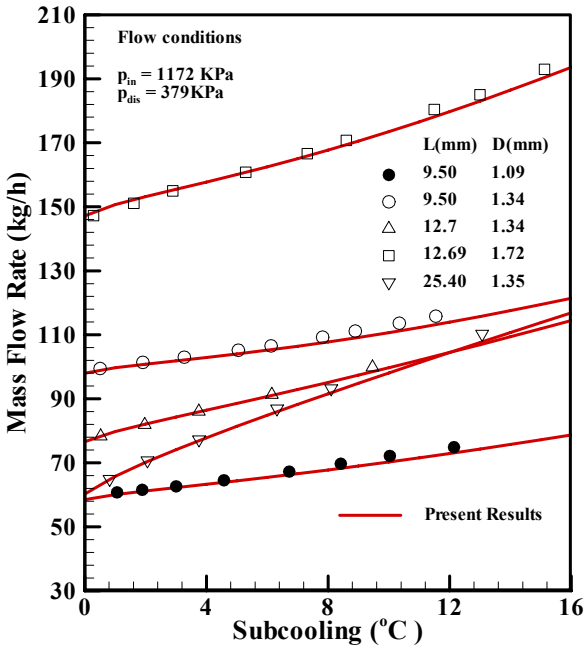

Figure 5.1 Comparison of the flow model with the Kim and O'Neal data for R134A as function of upstream sub-cooling

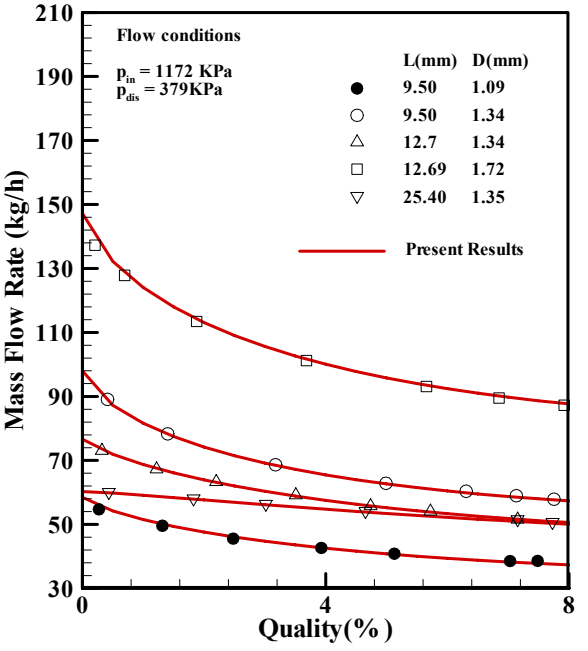

Figure 5.2 Comparison of the flow model with the Kim and O'Neal data for R134A as function of upstream quality

13.9°C. The mass flow rate increases as the subcooling increases. This is because with increase in subcooling, the density of the propellant increases, which causes the mass flow rate to increase. As expected, the results show excellent agreement against the experimental data because the coefficients of Kim and O'Neal semi-empirical model (see section 2.4.2.1) were calibrated using this data set. Figure 5.1 also shows the variation of the mass flow rate with sub-cooling for several different diameters. As the diameter increases, the slope of the sub-cooling line increases. Figure 5.2 shows the comparison of mass flow rate as a function of quality for several different diameters. The propellant mass flow rate decreases as the quality increases. From the figure it can be observed that the slope of the two-phase line appears to decrease slightly as the diameter increases. The comparison between the experimental data and Kim and O'Neal's semi-empirical model showed good agreement.

5.2.2. Validation of Semi-empirical model against Clark's (1991) experimental data.

After the successful validation of the semi-empirical model with the Kim and O'Neal (1994) experimental data, it has been applied to evaluate the mass flow rate along the valve orifice of the continuous discharge flow in pMDIs. Only the mass flow rate across the valve orifice is considered due to following reasons :

- the flow through valve orifice resembles that of a short tube as $L/D<20$
- the boundary conditions (i.e. upstream pressure, temperature and downstream pressure) are know accurately and are readily available from Clark's(1991) the experimental data for R134A.

5.2.2.1. Test Cases

The test cases and flow conditions used to validate the semi-empirical model are given below:

- The length of the valve orifice is kept constant: L_{vo} = 0.5425 mm.
- The diameters of valve orifice and discharge pressures are given in Table 5.2.

Table 5.2 Flow conditions of Clark's (1991) experimental data and predicted mass flow rate

Case	D_{vo} (mm)	p_{dis} (kPa)	L_{vo}/D_{vo}	$\dot{m}_{exp}$ (kg/h)	$\dot{m}_{num}$ (kg/h)
1	0.823	499.135	0.66	5.91	33.41
2	0.823	446.065	0.66	9.82	33.48
3	0.823	347.465	0.66	18.07	33.62
4	0.589	458.625	0.92	6.55	17.14
5	0.589	424.955	0.92	7.78	17.16
6	0.589	280.095	0.92	13.05	17.26
7	0.42	430.495	1.29	5.59	8.72
8	0.42	373.735	1.29	6.26	8.74
9	0.42	205.435	1.29	9.32	8.80
10	0.259	316.835	2.09	3.40	3.33
11	0.259	270.105	2.09	3.51	3.34

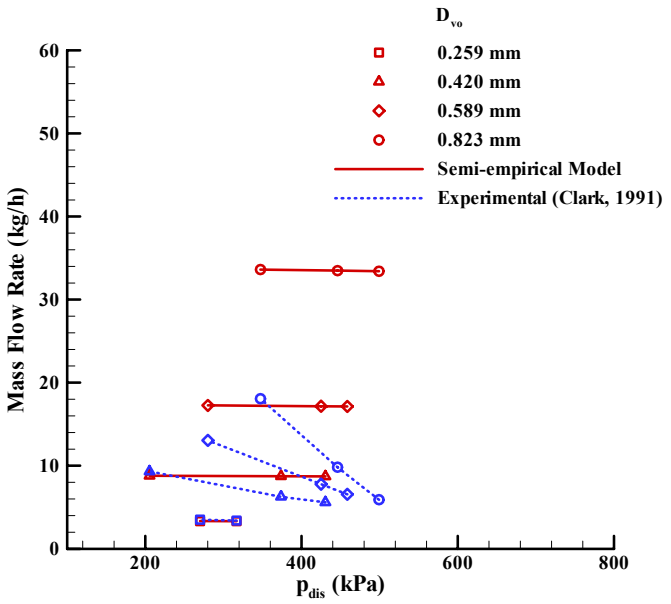

Figure 5.3 Comparison of the predicted mass flow rate against Clark's (1991) experimental mass flow rate across the valve orifice

- Propellant : R134A.
- The liquid at the inlet of valve orifice is assumed to be in saturated state. So, ambient temperature, *Tup*= 291 K and the corresponding upstream pressure, p_{up} = 537.18 kPa, defines the inlet conditions of the valve orifice.

5.2.2.2. Results and Discussion

Figure 5.3 shows the comparison of predicted mass flow rate with Clark's (1991) experimental mass flow rate across the valve orifice using the semi-empirical model. The ordinate represents the mass flow rate in kg/h, the abscissa gives the downstream pressure in kPa. From the figure it can be seen that for the low downstream pressures, the semi-empirical model predicts the mass flow rate well, whereas for the high downstream pressures, the semi-empirical model seriously overestimates the mass flow rate. It is likely that the predicted flashing pressure evaluated using equation (2.8) is too low. If the value is lower than the prescribed downstream pressure, large single-phase flow is predicted and the mass flow rate would be overpredicted. The reason for this is that the semi-empirical model was developed for length to diameter ratios 8.74< *L/D*<14.77, whereas the *L/D* ratio for the Clark's data ranges from 0.66 to 2.1 (Table 5.2), which is far outside the limitations of the semi-empirical model. Hence, the semi-empirical model predicts the large mass flow rate for high discharge pressures. The influence of *L/D* ratio on evaluation of flashing pressure can be analyzed from equation (2.8). For saturated inlet condition, the term with coefficient b_2 in equation (2.8) vanishes as SUBC = 0. So, the expression for the flashing pressure reduces to

$$p_f = p_s\left[b_1 + b_6 \exp(b_7 (D/D_{ref}) \times (L/D)^{b_8} + b_9 EVAP\right] \qquad 5.1$$

From the above expression, it can be seen that flashing pressure is an exponential function of *L/D*. As the value of coefficient b_8 = 2.9596, it has large effect on flashing pressure.

From the above analysis it can be seen that the semi-empirical model was successful in predicting the mass flow rate for Kim and O' Neal experimental results, but was unsuccessful in predicting the mass flow rate for Clark's experimental data. This suggest that there is a need for further model development beyond the accepted semi-

empirical correlation which is acceptable for the range of geometries and conditions in refrigerators but not for pMDIs.

5.3. Validation of HEM, DEM and IDEM for Capillary Tubes

In this section, the numerical method discussed in the previous chapter, namely HEM in section 4.3.3, DEM in section 4.3.1 and IDEM in section 4.3.2, are used to study the characteristics of flow through adiabatic capillary tubes. The main difference between DEM and IDEM is the relaxation equation, used to evaluate the vaporisation index along the tube. For DEM, equation (3.9) is used to evaluate the vaporisation index, whereas for IDEM equation (3.10) is used. Both pure propellants and propellant mixtures are considered for the validation purpose. First, the grid independence test was conducted to make sure that the results are independent of the grid. Thereafter, the results obtained using HEM, DEM and IDEM are compared against the experimental data available in the literature with pure propellants and propellant mixtures as working fluids.

5.3.1. Grid Details and Computation for capillary tube

The grid independence test was carried out to make sure that the gird size does not affect the computational results. As high gradients exists at the exit of the capillary tube, a non-uniform grid concentrated at the exit was generated as mentioned in section (4.3.1.1). Computations were carried out using four different grid sizes : grid 1 = 200 nodes, grid 2 = 300 nodes, grid 3 = 400 nodes and grid 4 = 500 nodes with concentration factor, k=3.5. Case 1 in Table 5.4 (Li et al., 1990a experimental data) is used for performing the grid independence test. As the geometry and the operating conditions for the capillary tubes considered are in similar range, it is expected that the grid independence test considered here will apply to other cases.

Figure 5.4 to Figure 5.7 shows the predicted pressure, temperature, quality and velocity distribution using four different grids. From the figure it can be seen that

.

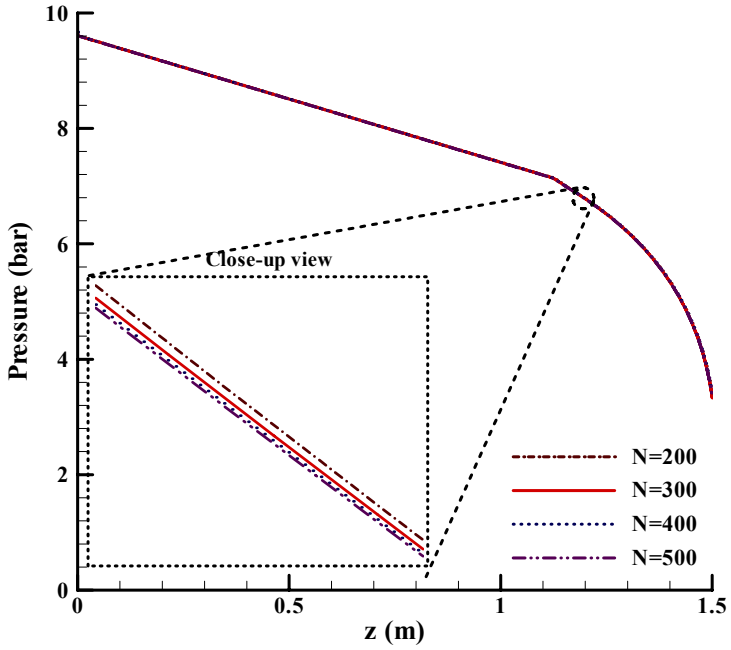

Figure 5.4 Predicted pressure distributions along the capillary tube with three different nodes : N=200, N=300, N=400 and N=500

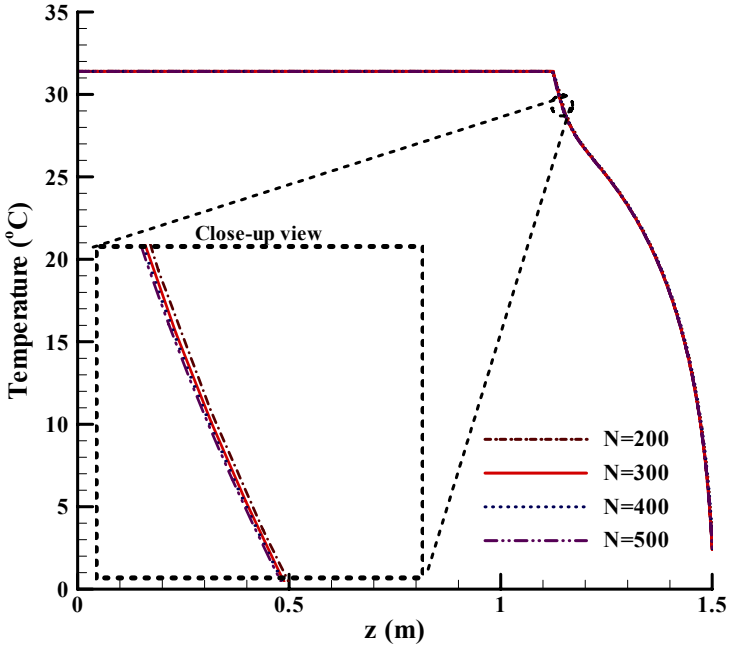

Figure 5.5 Predicted temperature distributions along the capillary tube with four different nodes : N=200; N=300, N=400 and N=500

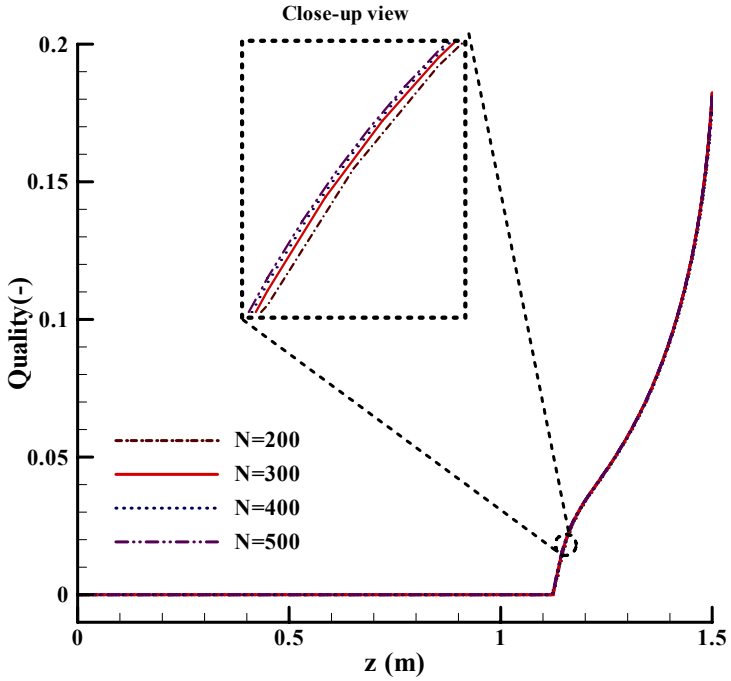

Figure 5.6 Predicted quality distributions along the capillary tube with four different nodes : N=200; N=300, N=400 and N=500

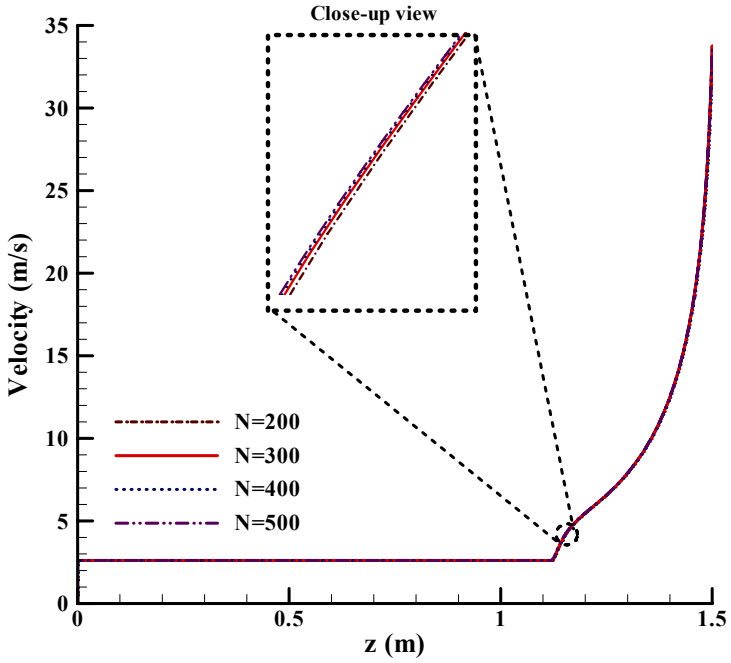

Figure 5.7 Predicted velocity distributions along the capillary tube with four different nodes : N=200; N=300, N=400 and N=500

Table 5.3 Evaluated mass flow rate for

N	$\dot{m}$ (kg/h)
200	4.1300
300	4.1324
400	4.1338
500	4.1346

these predicted profiles are almost identical on the normal scale. A close-up view (dotted box) in the two-phase region gives a better view and highlights minor differences between the results obtained using these grids. From these figures, it can be observed that there is no significant difference between the profiles obtained using grid 3, grid 4 and grid 5, whereas there is a slight difference in pressure profile (Figure 5.4) between grid 2 and grid 3. Table 5.3 shows the numerically calculated mass flow rates using different grids (grid 1, gird 2, grid 3, grid 4 and grid 5). From the table it can be observed that the relative discrepancy in the mass flow rate between the grid 1 and grid 2 is 0.06%, whereas the relative discrepancy between the grid 2 and grid 3 is 0.03%. Hence the grid 2, having N=300 with concentration factor, k = 3.5 was used in all subsequent work.

5.3.2. Pure Propellants

Both conventional propellants (R12 and R22) and alternative propellants (R134A) are used to validate the HEM, DEM and IDEM. As mentioned before in the introduction, only subcooled inlet conditions are considered for pure propellants. The following test cases are considered for the present study.

5.3.2.1. Test Cases

As data for conventional CFC propellants and alternative hydrofluoroalkane (HFA) propellants are available in the literature, the test cases are selected in such a way that they cover both type of propellants. The experimental data given by Li et al. (1990a) with propellant R12, Mikol (1963) with propellants R12 and R22 and Dirik et al. (1994) with propellant R134A are used as test cases because these experiments are

Table 5.4 Li et al. Cases (1990a)

Case	Fluid	L *(m)*	D *(mm)*	p_{in} (bar)	T_{in} (°C)	p_{dis} (bar)	ε/D
1	R12	1.5	0.66	9.67	31.4	3.33	3.0×10^{-3}
2				7.17	23.4	3.25	
3			1.17	8.85	30.0	2.45	1.69×10^{-3}
4				8.40	33.8	2.73	

Table 5.5 Mikol Cases (1963)

Case	Fluid	L *(m)*	D *(mm)*	p_{in} (bar)	T_{in} (°C)	p_{dis} (bar)	ε/D
5	R12	1.829	1.41	8.58	32.78	3.72	3.8×10^{-4}
6	R22			16.41	40.65	4.0	

Table 5.6 Dirik et al. Cases (1994)

Case	Fluid	L *(m)*	D *(mm)*	p_{in} (bar)	T_{in} (°C)	p_{dis} (bar)	ε/D
7	R134A	5.5	0.66	11.1	38.1	0.85	6.97×10^{-4}
8				11.1	34.6	0.88	
9				12.82	42.3	0.93	
10				12.82	40.1	0.96	
11				14.7	47.0	1.02	
12				14.7	39.7	1.14	
13	R134A	5.5	0.8	11.1	37.6	1.34	6.97×10^{-4}
14				11.1	33.7	1.50	
15				12.82	43.2	1.46	
16				12.82	39.3	1.58	
17				14.7	46.0	1.64	
18				14.7	43.6	1.69	

sufficiently high in quality and has been widely used by previous researchers (Wong and Ooi, 1996b; Bittle and Pate, 1996; Garcia-Valladares, 2002b; Wongwises and Suchatawut, 2003, etc.) for validation purposes. The dimensions of the insulated capillary tube and the flow conditions are given in Table 5.4-Table 5.6. Following Garcia-Valladares (2002 a, b) all problems are solved assuming an upstream connecting tube with internal diameter of 5 mm yielding an abrupt contraction and expansion associated at the inlet and outlet of the tube respectively.

5.3.2.2. Results and Discussion

For the cases under investigation, the pressure of vaporisation (p_v) for the metastable region is evaluated using the Chen et al. (1990) model (equation 3.14).

Comparison with experimental data Li et al. (1990a)

As the temperature distribution along the capillary tube is not reported by Li et al. (1990a), only the mass flow rate and pressure distribution are compared against their experimental data. Figure 5.8 graphically shows the comparison of predicted pressure profiles using HEM, DEM and IDEM against the Li et al. (1990a) experimental data with R12 as working fluid. The evaluated pressure profiles are in good agreement with the experimental pressure. The pressure profiles are almost identical for DEM and IDEM slight discrepancies are seen with HEM in the metastable region (zone-II and zone-III in Figure 5.8 a-d). DEM and IDEM predict the pressure profiles close to experimental data especially in metastable region in compare to that of HEM as these models account to propellant metastability. The discrepancies between the experimental data and all the three models are slightly large for case 4. This may be due to the limitation of our model which neglects the slip ratio between the phases. The inlet conditions for case 4 are closer to the saturated conditions, which results in more two-phase flow inside the capillary tube. Similar type of results were obtained by Bittle and Pate (1996) and Garcia-Valladares (2002b) using Chen et al. correlation for p_v. From the figures, it can also be observed that IDEM predicts longer metastable region and did not reach to equilibrium conditions till the end of the pipe. Whereas DEM predicts all the possible four regimes described in section (2.4.1.2).

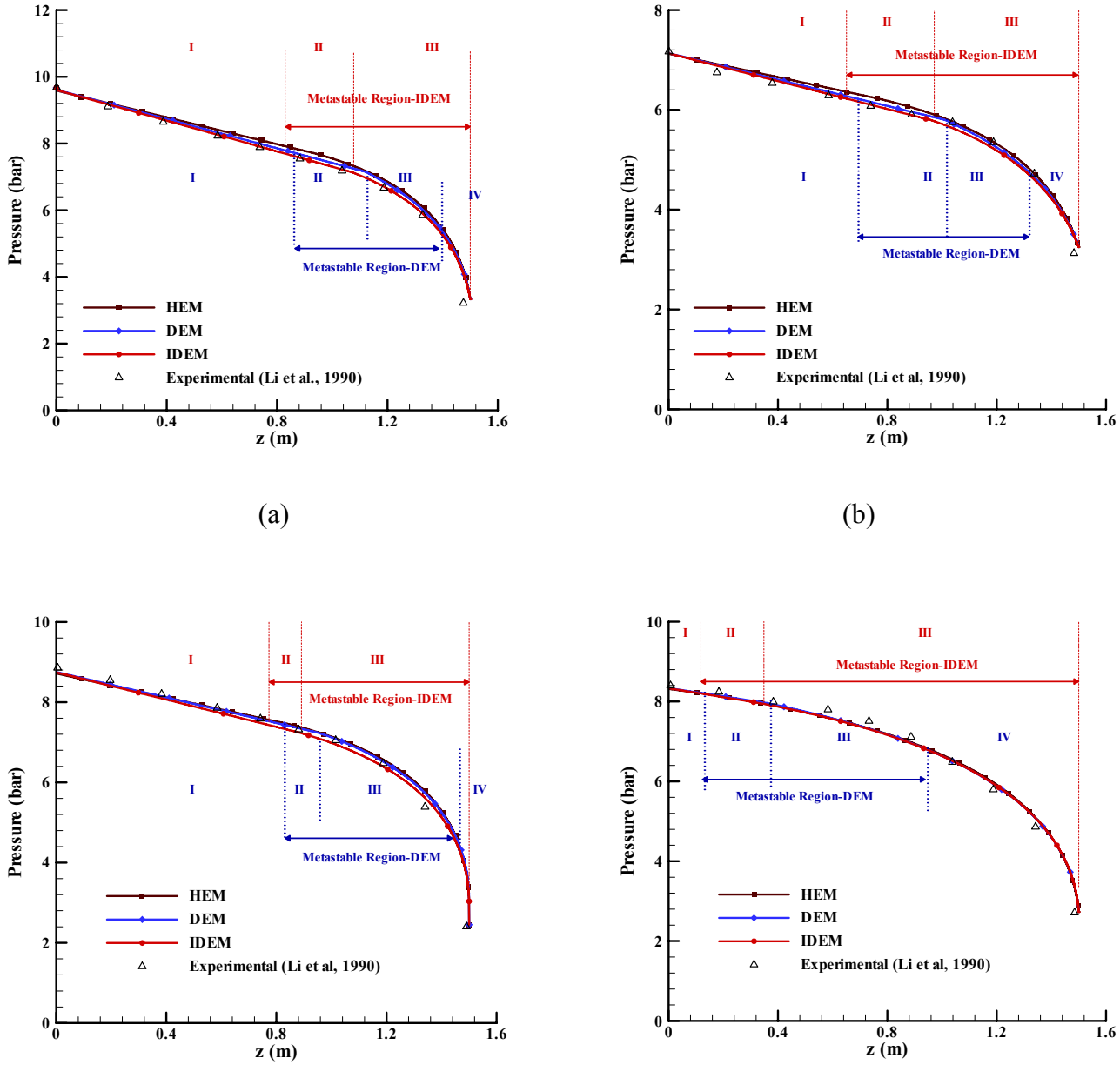

I: Subcooled liquid region

II : Metastable liquid region

III: Metastable two-phase region

IV: Two-phase equilibrium region

Figure 5.8 Comparison of predicted pressure profiles along the capillary tube against the experimental data (Li et al., 1990a) for (a) case 1 (b) case2 (c) case 3 and (d) case 4

Table 5.7 Comparison of mass flow rates against Li et al. (1990a) experimental data using HEM, DEM and IDEM

Case	$\dot{m}_{\exp}$ (kg/h)	HEM		DEM		IDEM	
		$\dot{m}_{HEM}$ kg/h	Error (%)	$\dot{m}_{DEM}$ (kg/h)	Error (%)	$\dot{m}_{IDEM}$ (kg/h)	Error (%)
1	4.072	3.869	-4.98	4.056	-0.39	4.166	2.32
2	3.040	2.884	-5.15	3.079	1.28	3.173	4.36
3	15.659	15.482	-1.13	16.002	2.19	16.604	6.03
4	12.246	11.966	-2.29	12.707	3.76	13.206	7.84
Mean deviation (%)			-3.39		1.71		5.14

Table 5.7 shows the comparison of mass flow rates using HEM, DEM and IDEM with experimental mass flow rate for R12. The negative sign indicates under prediction and the positive sign indicates over prediction. From the table it can be observed that DEM predicts the mass flow rate with a mean deviation of 1.71%, whereas HEM and IDEM predicts the mass flow rate with a mean deviation of -3.39% and 5.14% respectively. The differences in the mass flow rate between DEM and IDEM predictions is due to differences in the method of the evaluation of vaporisation index. The coefficient of relaxation equation dictates the rate of evaporation along the pipe. The constant coefficient of DEM relaxation equation and the factor (1-y) are greater than the corresponding constant and the factor $(1-y)^2$ in IDEM relaxation equation, hence DEM predicts a more rapid return to the equilibrium state than IDEM. As the length of the metastable region is longer in IDEM, it predicts high mass flow rates.

Comparison with experimental data by Mikol (1963)

Figure 5.9 shows the comparison of predicted pressure and temperature distribution along the capillary tube using HEM, DEM and IDEM against the Mikol (1963) experimental results for case 5 and case 6. The evaluated pressure and temperature profiles are in good agreement against the experimental pressure and temperature data for both the cases with R12 and R22. However, there are some discrepancies. From figures, it can be observed that, in the metastable region (zone II and zone III)), the predicted local temperature is lower than the measured temperature for R12 and R22

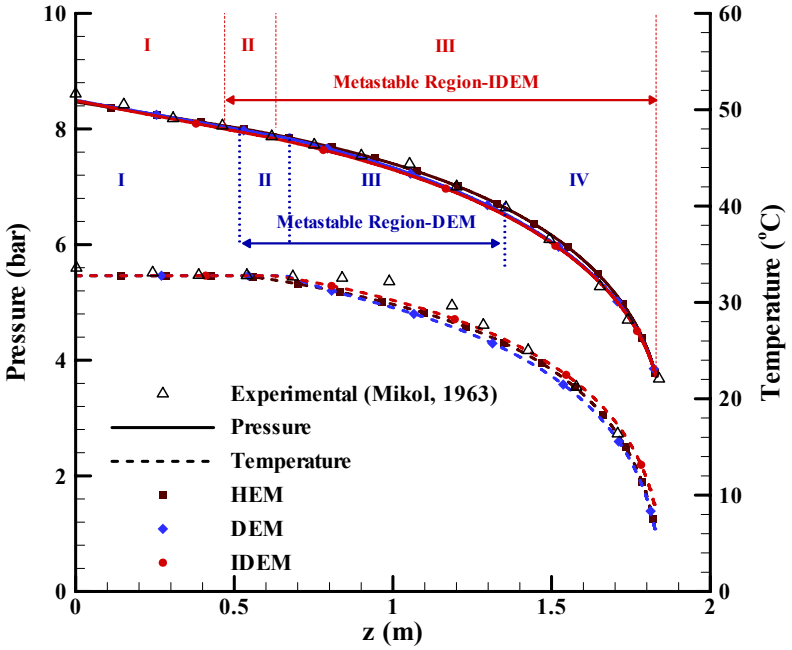

(a) Fluid : R12 with Chen et al. (1990b) correlation

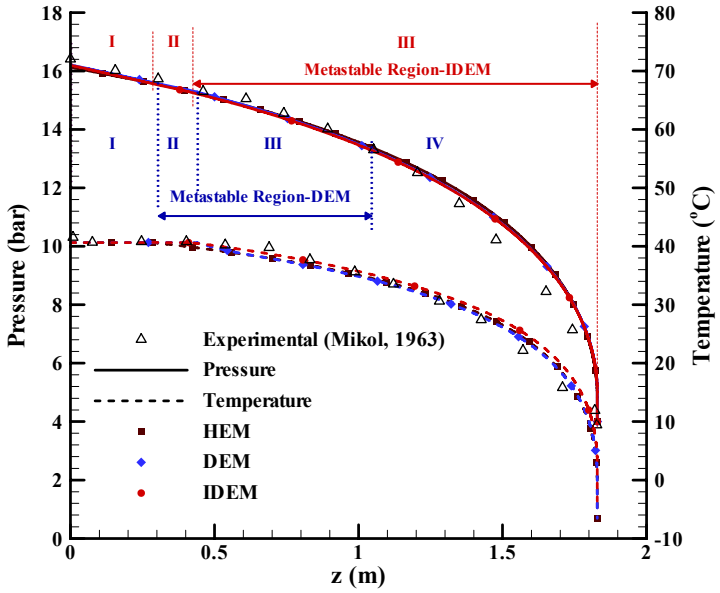

(b) Fluid : R22 with Chen et al. (1990b) correlation

Figure 5.9 Comparison of predicted pressure and temperature profiles along the capillary tube using Chen et al. (1990b) correlation against the Mikol (1963) experimental data for (a) case 5 and (b) case 6

Table 5.8 Comparison of mass flow rate against the Mikol (1963) experimental mass flow rate

Case	$\dot{m}_{exp}$ (kg/h)	HEM		p_v Chen's (1990)correlation				p_v Lackme's (1979)correlation			
				DEM		IDEM		DEM		IDEM	
		$\dot{m}_{HEM}$ kg/h	Error (%)	$\dot{m}_{DEM}$ (kg/h)	Error (%)	$\dot{m}_{IDEM}$ (kg/h)	Error (%)	$\dot{m}_{DEM}$ (kg/h)	Error (%)	$\dot{m}_{IDEM}$ (kg/h)	Error (%)
5	21.23	20.255	-4.59	21.477	1.16	22.228	4.70	22.054	3.88	22.904	7.88
6	30.7	29.652	-3.41	31.188	1.59	32.019	4.30	31.709	3.29	32.669	6.41
Mean deviation(%)			-4.00		1.38		4.50		3.58		7.15

and the predicted local pressure is higher than the measured pressure for R22 in two-phase equilibrium region (zone IV). Similar discrepancies have been observed by the previous researchers (Li et al., 1990b; Garcia-Valladares, 2002b; Wongwises and Suchatawut, 2003). The discrepancies in the metastable region have been attributed to calculation of vaporisation pressure (p_v) using Chen et al. (1990) correlation. Chen et al. (1990) correlation is developed from R12 experimental data for a limited range of capillary tube diameter ranging from 0.66 mm to 1.17 mm. So, using Chen's correlation with R22 may cause some errors. Another reason for these discrepancies might be that the capillary tube diameter used for the present simulations is beyond the range recommended by Chen et al. (1990). The discrepancies in two-phase equilibrium region may attributable to the limitations in the validity of the modeling assumptions (e.g. no slip between the phases) or to uncertainties in the experimental data.

Wongwises and Suchatawut (2003) simulated these results with Lackme's (1979) correlation using k_{meta} = 0.93 and observed that this correlation predicted a longer metastable region with R22 and showed reasonable agreement with R12. Figure 5.10 shows the results of the present numerical model with Lackme's (1979) correlation for the pressure of vaporisation using k_{meta} = 0.93 in equation (3.13). From the figure it can be observed that using Lackme's (1979) correlation the predicted temperature profiles are slightly in better agreement in the metastable region (zone II and zone III) for both R12 and R22.

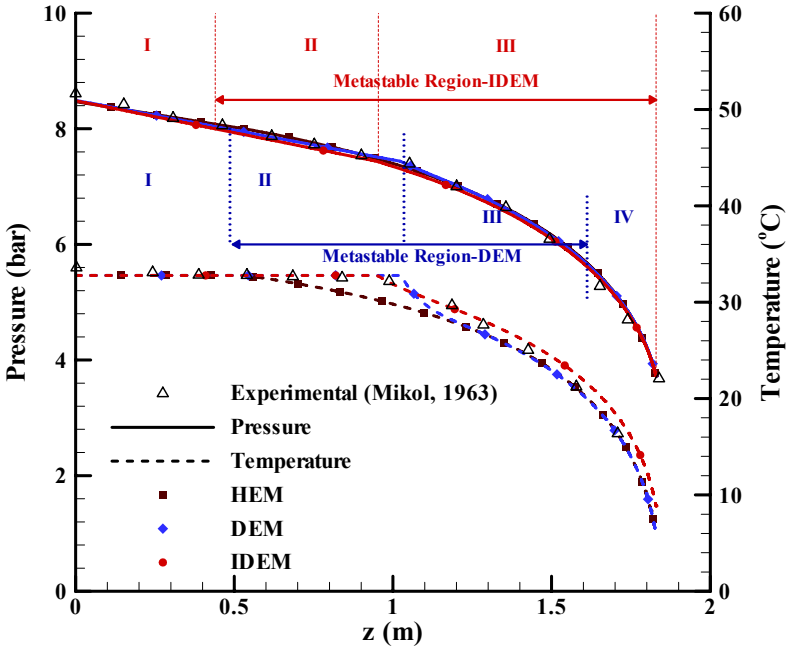

(a) Fluid : R12 with Lackme's (1979) correlation

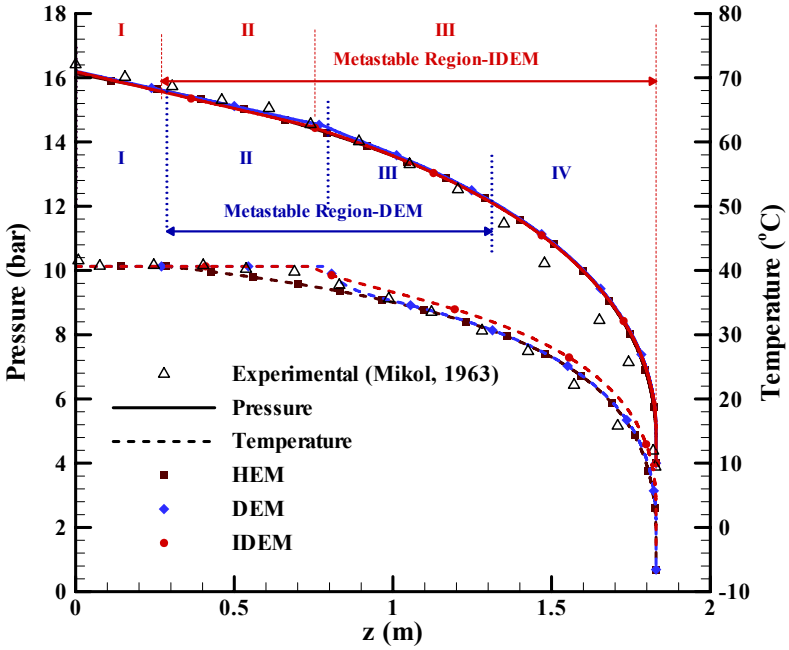

(b) Fluid : R22 with Lackme's (1979) correlation

Figure 5.10 Comparison of predicted pressure and temperature profiles along the capillary tube using Lackme's (1979) correlation against the Mikol (1963) experimental data for (a) case 5 and (b) case 6

Table 5.8 shows the comparison of mass flow rate using HEM, DEM and IDEM for cases 5 and 6. From the table it is clear that the DEM with Chen et al.(1990) correlation predicts the mass flow rate closer to the experimental data with a mean deviation of 1.38%, where as HEM under predicts the mass flow rate by -4.0% and IDEM overpredicts the mass flow rate by 4.5%. Using Lackme's (1979) correlation, the mass flow rate is overpredicted as it predicts longer metastable region then Chen's correlation.

Comparison with experimental data by Dirik et al. (1994)

As pressure and temperature profiles are not reported by Dirik et al. (1994) in their experimental work for R134A, only the mass flow rate has been compared against the experimental results. The mass flow rates evaluated using HEM, DEM and IDEM for cases 7 to 18 are compared against the Dirik et al. (1994) experimental mass flow rate. It can be seen that the numerical results are generally in good agreement against the experimental mass flow rate. Again the DEM predicts the mass flow rate well compared to HEM and IDEM with a mean deviation of 0.67%. HEM under predicts the mass flow rate, by -4.67% whereas IDEM over predicts the mass flow rate by 1.59%.

5.3.2.3. Summary

In the test cases presented above it can be seen that all the three models can be used to predict the flow along the capillary tube. The pressure and temperature profiles predicted by DEM and IDEM are almost identical and are close to the experimental data while HEM gave slightly higher predictions. DEM predicts the mass flow rate with a mean deviation of 1.71%, 1.38% and 0.67% for Li et al (1990a), Mikol (1963) and Dirik et al (1994) experimental data respectively. The HEM generally under predicts the mass flow rate with a mean deviation of -3.39%, -4.0% and -4.67%, whereas the IDEM was shown to overpredict the mass flow rate with a mean deviation of 5.14%, 4.50% and 1.59% for Li et al (1990a), Mikol (1963) and Dirik et al (1994) experimental data respectively. This study suggest that the DEM predicts

Table 5.9 Comparison of mass flow rate against the Dirik et al. (1994) experimental mass flow rate for cases 7 to 18

Case	$\dot{m}_{\exp}$ (kg/h)	HEM		DEM		IDEM	
		$\dot{m}_{HEM}$ kg/h	Error (%)	$\dot{m}_{DEM}$ (kg/h)	Error (%)	$\dot{m}_{IDEM}$ (kg/h)	Error (%)
7	2.070	1.910	-7.72	2.063	-0.34	2.082	0.58
8	2.240	2.125	-5.15	2.250	0.43	2.271	1.36
9	2.380	2.189	-8.02	2.338	-1.77	2.358	-0.93
10	2.430	2.324	-4.36	2.456	1.07	2.477	1.95
11	2.530	2.436	-3.71	2.586	2.20	2.606	3.02
12	3.070	2.849	-7.21	2.955	-3.75	2.980	-2.94
13	3.380	3.267	-3.35	3.482	3.01	3.517	4.05
14	3.950	3.655	-7.46	3.826	-3.14	3.865	-2.15
15	3.710	3.576	-3.60	3.802	2.49	3.838	3.44
16	4.150	3.977	-4.18	4.158	0.20	4.198	1.15
17	4.220	4.185	-0.83	4.389	4.00	4.428	4.92
18	4.440	4.422	-0.41	4.602	3.65	4.644	4.58
Mean deviation (%)			-4.67		0.67		1.59

propellant metastability accurately for the flow of pure propellants in capillary tubes. Whereas IDEM predicts a more metastable liquid development and consequently over predicts the mass flow rate. The HEM does not consider metastability and hence underpredicts the mass flow rate. Based on the above results it can be concluded that DEM predictions are better in compare to that of HEM and IDEM for pure propellants.

5.3.3. Propellant Mixtures

In this section, the above three models (HEM, DEM and IDEM) are used to study the behavior of the new propellant mixtures R410A (50% HFC 32 and 50% HFC 125 by mass) and R407C (23% HFC 32, 25% HFC 125 and 52% HFC 134A by mass) through an adiabatic capillary tube. Various inlet conditions (i.e. subcooled liquid, saturated liquid and two-phase liquid) have been considered to simulate the flow

through the capillary tube. Chen et al (1990) correlation (equation 3.14) and Lackme's (1979) correlation (equation 3.13) with k_{meta} = 0.93 are used to evaluate the pressure of vaporisation for subcooled and saturated inlet conditions, respectively.

5.3.3.1. Test Cases

The experimental data given by Sanzovo and Mattos (2003) with propellant 410A and 407C are used as test cases. The dimensions of the insulated capillary tube are : D (inner diameter) = 1.101 mm and L (length) = 1.5 m. The relative roughness (ε/D) = 2.354×10^{-4}. The internal diameter of the connecting tubes (to calculate the pressure drop in the inlet contraction and outlet expansion) is 10.0 mm. The test cases are selected in such a way that they could cover a wide range inlet conditions (i.e. subcooled/saturated/two-phase). Cases 1 in Table 5.10a-b (R410A) and Table 5.11a-b

Table 5.10 Boundary conditions for R410A (Sanzovo and Mattos, 2003)

(a) Subcooled Inlet conditions

Case	Propellant		p_{in} (bar)	T_{in} (°C)	ΔT_{sub} (°K)	p_{dis} (bar)
	R32 (%)	R125 (%)				
1	49.2	50.8	22.6	35.5	1.6	7.94
2a			24.33	34.6	5.6	7.96
2b	48.5	51.5	24.34	36.9	3.3	7.96
2c			24.31	38.8	1.4	7.97

(b) Saturated/two-phase inlet conditions

Case	Propellant		p_{in} (bar)	x_{in}	p_{dis} (bar)
	R32 (%)	R125 (%)			
1	48.3	51.7	24.31	0.044	7.96
2a			26.07	0	7.96
2b	48.5	51.5	26.06	0.02	7.96
2c			26.07	0.04	7.97

(R407C) were selected to compare the pressure and temperature profiles against the experimental results along the capillary tube for subcooled and two-phase inlet conditions. Cases 2a, 2b and 2c in these tables were selected to compare the mass flow rate with the experimental data as the inlet condition changes from subcooled to two-phase flow. Cases 1 Table 5.10a-b and Table 5.11a-b are considered for comparing the pressure and temperature profiles as these data sets are complete with all the required information.

Table 5.11 Boundary conditions for R407C (Sanzovo and Mattos, 2003)

(a) Subcooled Inlet conditions

Case	Propellant			p_{in} (bar)	T_{in} (°C)	ΔT_{sub} (°K)	p_{dis} (bar)
	R32 (%)	R125 (%)	R134A (%)				
1	21.3	23.7	55	16.00	33.8	3.6	5.59
2a				15.93	31.9	5.1	5.57
2b	21.7	23.9	54.4	16.01	33.9	3.3	5.56
2c				16.01	35.7	1.5	5.57

(b) Saturated/two-phase inlet conditions

Case	Propellant			p_{in} (bar)	x_{in}	p_{dis} (bar)
	R32 (%)	R125 (%)	R134A (%)			
1	21.6	24.1	54.3	14.934	0.00	5.62
2a				18.563	0.000	18.81
2b	21.9	24.3	53.8	18.557	0.025	17.71
2c				18.559	0.040	17.28

5.3.3.2. Results and Discussion

In this section results obtained using HEM, DEM and IDEM are compared against the experimental results with R410A and R407C. First, the results of R410A are presented. Thereafter, the results of R407C are discussed.

Propellant R410A

Table 5.12a shows the comparison of mass flow rates using HEM, DEM and IDEM with the experimental mass flow rates of Sanzovo and Mattos (2003) for R410A with subcooled inlet conditions. The mass flow rate increases with increase in the subcooling, as more single phase liquid flows through the capillary tube. From the table it can be observed that all the three models underpredict the mass flow rate. DEM predicts the mass flow rate with a mean deviation of -4.24%, whereas HEM and IDEM predicts the mass flow rate with a mean deviation of -6.11% and -1.77% respectively. These results obtained for case 1 are similar to those of Garcia-Valladares (2004) results obtained using DEM.

Figure 5.11 shows the comparison of pressure and temperature profiles for 410A with subcooled inlet conditions. The evaluated pressure and temperature profiles are in good agreement with the experimental pressure and temperature profiles. However, there are some small discrepancies in two-phase region. The pressure profiles predicted by all the models are almost identical and are slightly higher than the experimental data in the two-phase region (i.e. zone IV, $z > 0.78$ m). Similarly, the predicted temperature profiles are slightly higher then the experimental data in two-phase region. The temperatures predicted by HEM and DEM are almost identical in the two-phase region (i.e. zone IV, $z > 0.78$ m), whereas IDEM predicts slightly higher temperatures. The DEM predicts a more rapid return to the equilibrium state than IDEM because of its large coefficient in the relaxation equation which is responsible for the kink in the temperature profile. Hence, IDEM predicts long metastable region. From the figure it can be seen that the temperatures predicted by DEM is close to the experimental data especially in metastable region (zone II and zone III), which indicates that the DEM most accurately accounts for metastability.

Table 5.12 Comparison of mass flow rate for R410A with the experimental mass flow rate of Sanzovo and Mattos (2003)

(a) Subcooled inlet conditions

Case	$\dot{m}_{exp}$ (kg/h)	HEM		DEM		IDEM	
		$\dot{m}_{HEM}$ kg/h	Error (%)	$\dot{m}_{DEM}$ (kg/h)	Error (%)	$\dot{m}_{IDEM}$ (kg/h)	Error (%)
1	22.93	21.45	-6.45	21.89	-4.54	22.46	-2.04
2a	26.07	24.81	-4.82	25.27	-3.07	25.93	-0.53
2b	24.97	23.49	-5.92	23.95	-4.09	24.56	-1.65
2c	24.05	22.31	-7.23	22.79	-5.24	23.36	-2.85
Mean deviation (%)			-6.11		-4.24		-1.77

(b) Two-phase inlet conditions

Case	$\dot{m}_{exp}$ (kg/h)	HEM		DEM		IDEM	
		$\dot{m}_{HEM}$ kg/h	Error (%)	$\dot{m}_{DEM}$ (kg/h)	Error (%)	$\dot{m}_{IDEM}$ (kg/h)	Error (%)
1	21.78	19.94	-8.44	19.95	-8.41	20.27	-6.93
2a	23.94	22.37	-6.55	22.89	-4.38	23.38	-2.35
2b	23.21	21.97	-5.35	21.97	-5.35	22.35	-3.69
2c	22.85	21.16	-7.40	21.16	-7.38	21.50	-5.90
Mean deviation (%)			-6.93		-6.38		-4.72

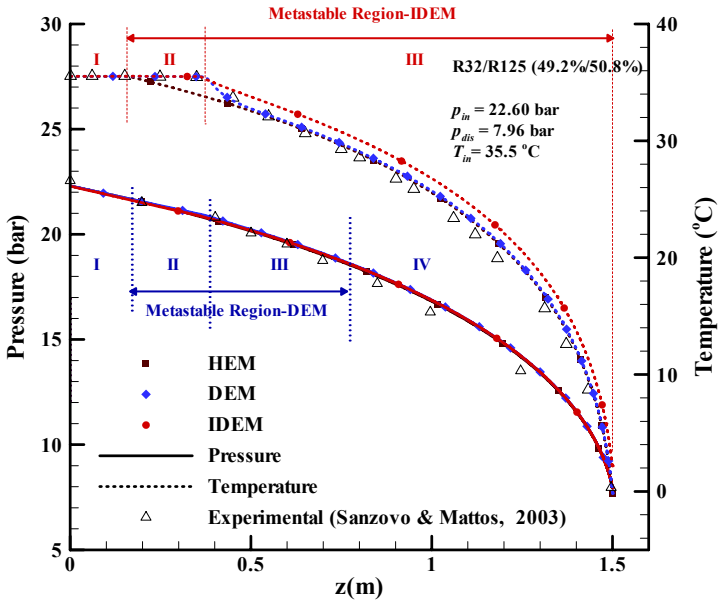

Figure 5.11 Comparison of predicted pressure and temperature distribution along a capillary tube with experimental data of Sanzovo & Mattos (2003) for R410A: subcooled inlet conditions

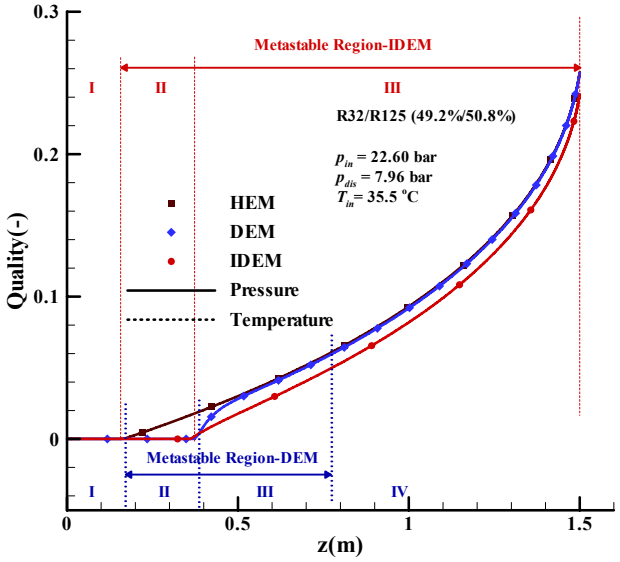

Figure 5.12 Comparison of predictions of quality distribution along the capillary tube using HEM, DEM and IDEM for R410A: subcooled inlet conditions

Figure 5.12, shows the predicted distribution of quality along the capillary tube for the three models. It can be noticed that, for HEM, vaporisation of propellant takes place when the pressure p is equal to the local saturated vapour pressure p_s. For the DEM and IDEM, on the otherhand, metastability causes a pressure undershoot; vaporisation is delayed until p is equal to a vaporisation pressure $p_v < p_s$. As one can see from the figure, once the vaporisation is started the DEM predictions rapidly approach those of the HEM, indicating that the metastable model is predicted to reach equilibrium within a short distance of 0.4 m. This causes a noticeable kink in the predicted temperature and quality profiles for DEM. The IDEM predictions tend to the HEM curve more slowly, indicating a more gradual return to equilibrium.

Table 5.12b shows the comparison of mass flow rate using the three different models for two-phase flow inlet conditions. For cases 2a, 2b and 2c, the mass flow rate decreases with increase in the inlet quality, as more vapour flow occurs inside the capillary tube. From the table, again it can be noticed that although all three models underpredict the mass flow rate, the IDEM predicts the mass flow rate better than HEM and DEM with a mean deviation of -4.72%.

Figure 5.13 shows the distribution of pressure and temperature profiles along the capillary tube using the three different models for R410A with two-phase inlet conditions. From the figure it can be observed that the predicted pressure and temperature profiles are almost identical for all the three models and yield higher values then experimental data. These discrepancies are larger than those observed with subcooled inlet conditions, which may be attributable to the limitations in the validity of the modeling assumptions (e.g. no slip between the phases) in two-phase region (zone IV) or to uncertainties in the experimental data.

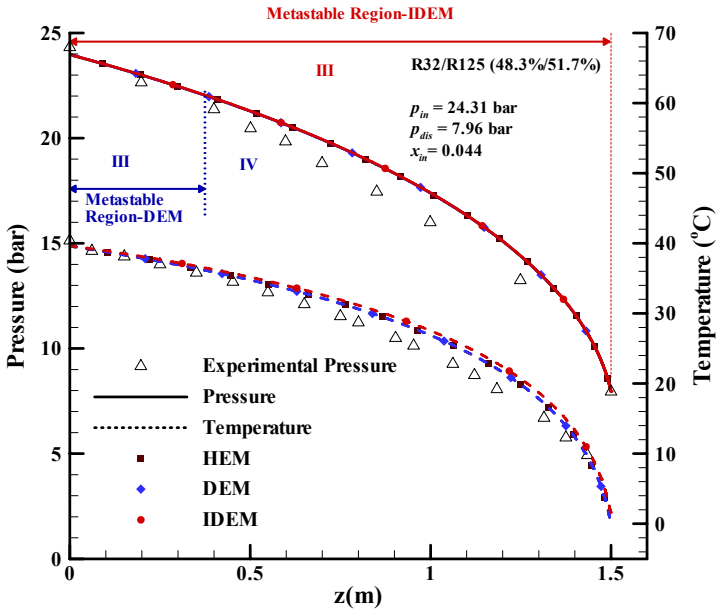

Figure 5.13 Comparison of predicted pressure and temperature distribution along the capillary tube for R410A with experimental data of Sanzovo and Mattos (2003): two-phase inlet conditions

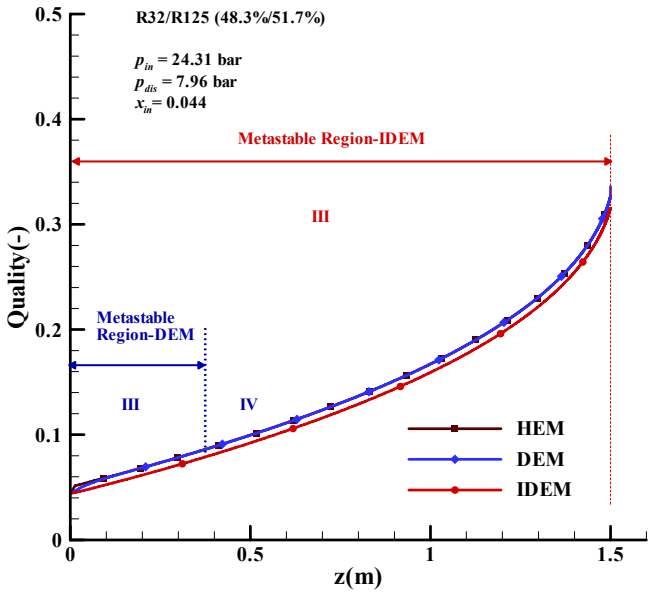

Figure 5.14 Comparison of predictions of quality distribution along the capillary tube using HEM, DEM and IDEM for R410A: two-phase inlet conditions

Figure 5.14 shows the predicted distribution of quality along the capillary tube using the three different models. From the figure, it can be seen that there is a slight difference between the HEM and DEM near the entrance of the capillary tube, which is due to differences in the modeling assumptions when evaluating the flow variables along the abrupt contraction at the entrance of the capillary tube (section 3.3.4.5). While evaluating the flow variables across the abrupt contraction, it was assumed that the quality remains constant across the contraction and the saturated liquid gets converted into metastable state due to sudden pressure drop across the contraction. From the figure a more pronounced difference between DEM and IDEM can be observed; the former returns to the equilibrium state rapidly, so the DEM curve meets the HEM. The IDEM on the otherhand does not return to equilibrium until the end of the tube and hence the propellant is in two-phase metastable state (i.e. zone III).

The discrepancies between the models and the experimental data in the two-phase region for both subcooled inlet and two-phase inlet conditions may be attributable to the limitations in the validity of the modeling assumptions (e.g. no slip between the phases) or to uncertainties in the experimental data.

The results also suggest that the real flow behaves as if it is 'more metastable' than the model predicts in term of mass flow rate, however as far as the pressure and temperature profiles are concerned the experimental data suggest more vapour evolution than any of the model predicts. Silva et al. (2007) noticed a challenging aspect of this type of near-azeotropic fluid mixture is its composition and high operating pressures and temperatures.

Propellant R407C

Table 5.13a shows the comparison of mass flow rates using HEM, DEM and IDEM with the experimental data for R407C with subcooled inlet conditions. The mass flow rate increases as the subcooling increases, similar to the results of R410A. From the table it can be observed that DEM predicts the mass flow rate with a mean deviation of -1.83%, whereas HEM and IDEM predicts the mass flow rate with a mean deviation of -7.23% and 1.32% respectively.

Table 5.13 Comparison of mass flow rate for R407C with the experimental mass flow rate of Sanzovo and Mattos (2003)

(a) Subcooled inlet conditions

Case	$\dot{m}_{\exp}$ (kg/h)	HEM		DEM		IDEM	
		$\dot{m}_{HEM}$ kg/h	Error (%)	$\dot{m}_{DEM}$ (kg/h)	Error (%)	$\dot{m}_{IDEM}$ (kg/h)	Error (%)
1	19.100	17.639	-7.65	18.631	-2.46	19.227	0.67
2a	19.640	18.443	-6.10	19.352	-1.47	19.981	1.73
2b	18.790	17.473	-7.01	18.484	-1.63	19.075	1.52
2c	17.830	16.376	-8.16	17.516	-1.76	18.074	1.37
Mean deviation (%)			-7.23		-1.83		1.32

(b) Saturated /two-phase inlet conditions

Case	$\dot{m}_{\exp}$ (kg/h)	HEM		DEM		IDEM	
		$\dot{m}_{HEM}$ kg/h	Error (%)	$\dot{m}_{DEM}$ (kg/h)	Error (%)	$\dot{m}_{IDEM}$ (kg/h)	Error (%)
1	15.320	14.950	-2.41	16.148	5.41	16.835	9.89
2a	18.810	17.101	-9.08	18.642	-0.89	19.227	2.22
2b	17.710	16.143	-8.85	17.197	-2.90	17.517	-1.09
2c	17.280	15.487	-10.37	16.597	-3.96	16.880	-2.31
Mean deviation (%)			-7.68		-0.58		2.18

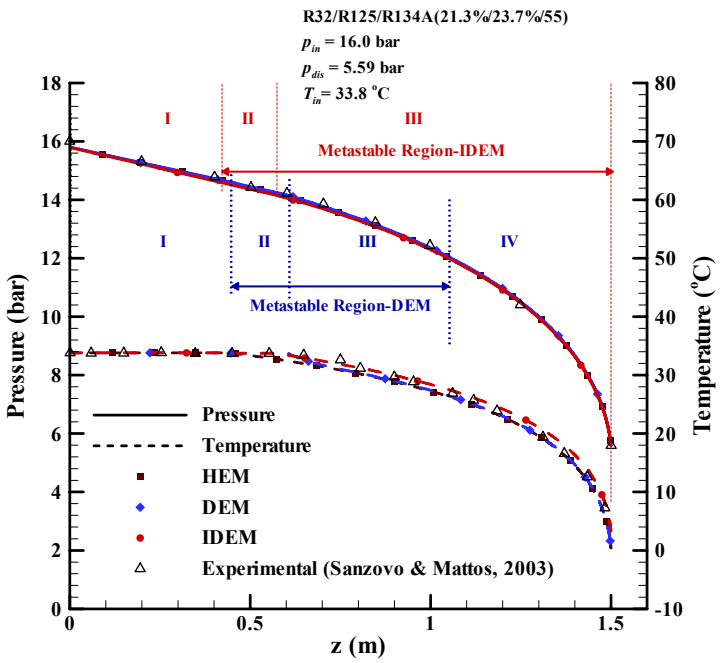

Figure 5.15 Comparison of predicted pressure and temperature distribution along the capillary tube for R407C with experimental data of Sanzovo and Mattos (2003): subcooled inlet conditions

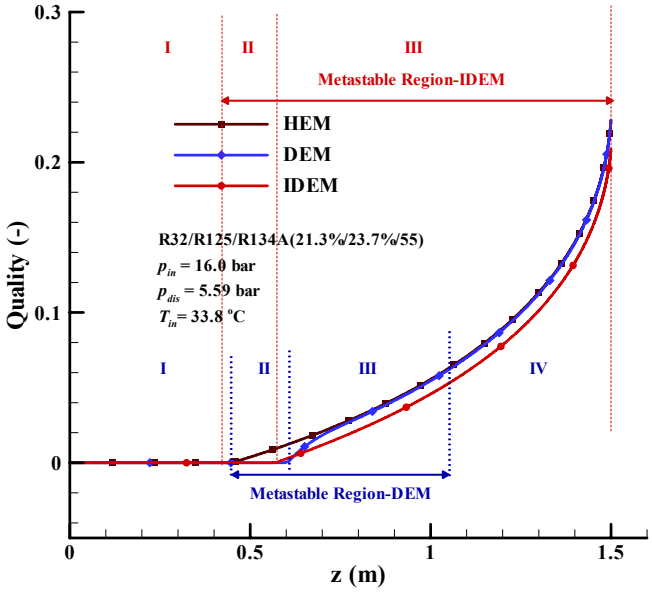

Figure 5.16 Comparison of predictions quality distribution along the capillary tube using HEM, DEM and IDEM for R407C: subcooled inlet conditions

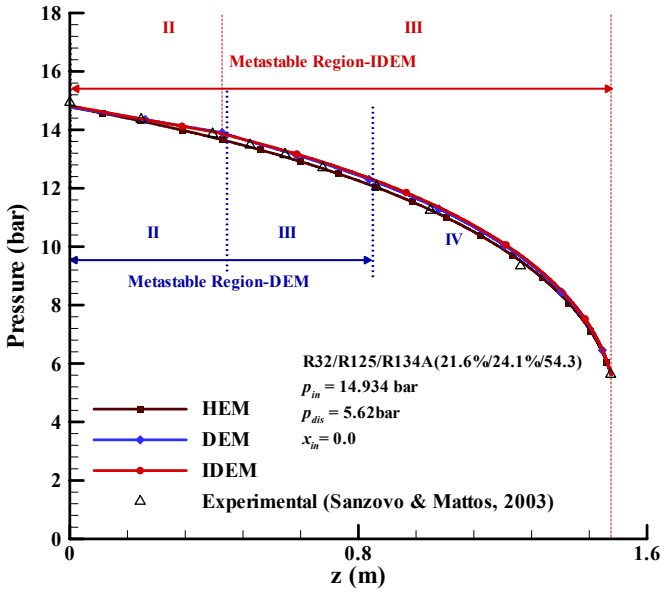

Figure 5.17 Comparison of predicted pressure distribution along the capillary tube with experimental data of Sanzovo and Mattos (2003) for R407C: saturated inlet conditions

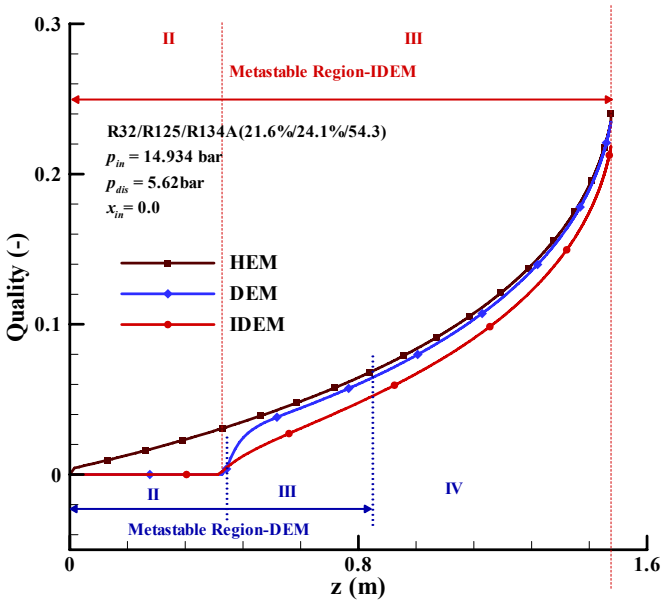

Figure 5.18 Comparison of predictions of quality distribution along the capillary tube using HEM, DEM and IDEM for R407C: saturated inlet conditions

Figure 5.15 shows the comparison of predicted pressure and temperature distribution along the capillary tube using HEM, DEM and IDEM with the experimental pressure and temperature profiles for propellant R407C with subcooled inlet conditions. The evaluated pressure and temperature profiles show very good agreement against the experimental results. The predicted pressure and temperature profiles are almost identical for all the three models. Figure 5.16 shows the distribution of quality for all the models. These profiles are similar to that of propellant R410A.

Table 5.13b shows the comparison of predicted mass flow rate with the experimental data for all the models with two-phase inlet conditions. From the table it can be seen that HEM underpredicts the mass flow with a mean deviation of -7.68%.Wheras DEM and IDEM predicts the mass flow rate with a mean deviation of -0.58% and 2.18% respectively.

For saturated inlet conditions with R407C, the temperature distribution was not reported by Sanzovo and Mattos (2003), hence only predicted pressure profiles for HEM, DEM and IDEM are compared with the experimental data in Figure 5.17. The evaluated pressure profiles show good agreement against the experimental values. Again, the predicted pressure profiles are slightly higher and almost identical for all the models. Figure 5.18 shows the distribution of quality along the capillary tube for the three models which are similar to that of R410A.

From the set of test cases investigated here, for propellant mixtures (R410A and R407C), it can be observed that the discrepancies in the numerical model and the experimental data are large for R410A in compare to that of R407C. This may be due to the reason that for subcooled inlet condition (case 1 in Table 5.10a and Table 5.11a), R410A has low subcooled inlet temperature then that of R407C and for two-phase inlet condition (case 1 in Table 5.10b and Table 5.11b) R410A has a higher inlet quality than R407C. In both the cases, R410A has more two-phase region in compared to that of R407C. As the present model do not consider the slip ratio between the phases, due to which the discrepancies are large for 410A as more liquid is in two-phase state. This argument further can be supported by findings of Sanzovo and Mottos (2003). Their numerical results evaluated using HEM and Separated flow

model (SFM) underpredicted the mass flow rate for these cases, but SFM showed a good agreement between the predicted pressure and temperature profiles with the experimental data in two-phase region. However, the discrepancies were large in metastable region as their model do not account for propellant metastability. Considering slip between the phases for the present models may give better agreement with the experimental data.

5.3.3.3. Summary

In this set of test cases for propellant mixtures (R410A and R407C) with subcooled and two-phase inlet conditions, it can be observed that all the three models: HEM, DEM and IDEM can be used to model the flow through adiabatic capillary tube. All the three models underpredicted the mass flow rate. HEM has been widely used by previous researchers to model the flow through adiabatic capillary tubes but it gives less accurate prediction of temperature distribution along the capillary tube especially in metastable region as it does not take metastability into consideration. DEM predicted the pressure and temperature distribution along the capillary tube close to the experimental data, indicating metastability effects are accounted accurately. However, the slight underprediction of the mass flow rate with DEM may be attributable to our modeling assumptions (e.g. no slip ratio between the phases) as mentioned earlier. The relaxation equation used for DEM to trace metastability has a strong track record of applications is steam-water flows (Feburie et al.,1993) and has been well validated for the flow of propellants through capillary tubes (Garcia-Valladares et al., 2002a, 2002b and 2004) for the application of refrigeration and air conditioning system.

Though the IDEM predicts the mass flow rate close to the experimental data, for these propellant mixtures, it predicts slightly higher pressure and temperature distribution along the capillary tube. The reason for IDEM to predict the mass flow rate well is that it returns to equilibrium conditions much slower then that of DEM, which makes more metastable liquid to flow through the capillary tube and results in high mass flow rate. It looks like IDEM predicts ‘more metastable’ flow than the real flow, which is evident from the pressure and temperature profiles. IDEM has been successfully validated in steam-water flows applications by Attou and Seynhaeve

(1999a, b), no attempt has been made to apply this to refrigeration/air-conditioning application system.

5.4. Validation of HEM, DEM and IDEM for Short Tubes

After successful validation of the HEM, DEM and IDEM with the available experimental data for the propellant flow through long capillary tubes, these models have been used to predict the flow variables and mass flow rate along the short tubes. As Kim and O'Neal (1994) did not report the flow variables distribution along the short tube, the experimental data of Aaron and Domanski (1990) with propellant R22 is used as test cases, as both the mass flow rate and the pressure distribution along the short tube are reported in their experimental work and the dataset is complete and sufficiently high in quality for the validation purposes.

5.4.1. Test Case

The dimensions of the short tube and the flow conditions are given in Table 5.14a-b. The outlet pressure was varied from 13-4.8 bars, keeping the constant inlet conditions for cases 1-3 in Table 5.14a. For cases 4-6, the subcooling was varied from 5.6 – 13.9°C, keeping the inlet and outlet pressures constant.

Table 5.14 Flow conditions for Aaron and Domanski (1990) cases

(a) at constant subcooling ΔT_{sub} = 13.9 °C

Case	Fluid	L *(mm)*	D *(mm)*	p_{in} (bar)	T_{in} (°C)	p_{dis} (bar)	ε/D
1	R22	12.7	1.35	17.23	30.95	13.0	3.8×10^{-4}
2				17.23	30.95	11.67	
3				17.23	30.95	4.80	

(b) at constant inlet and outlet pressure with different subcoolings

Case	Fluid	L *(mm)*	D *(mm)*	p_{in} (bar)	ΔT_{sub} (°C)	p_{dis} (bar)	ε/D
4	R22	12.7	1.35	17.23	5.6	4.80	3.8×10^{-4}
5				17.23	9.7	4.80	
6				17.23	13.9	4.80	

Table 5.15 Comparison of mass flow rate for R22 with the Aaron and Domanski's (1990) experimental mass flow rate

(a) at constant subcooling ΔT_{sub} = 13.9 °C

Case	$\dot{m}_{exp}$ (kg/h)	HEM		DEM		IDEM	
		$\dot{m}_{HEM}$ kg/h	Error (%)	$\dot{m}_{DEM}$ (kg/h)	Error (%)	$\dot{m}_{IDEM}$ (kg/h)	Error (%)
1	134	126.1	-5.89	126.2	-5.84	126.2	-5.84
2	152	137.5	-9.53	144.8	-4.74	144.8	-4.74
3	163	137.5	-15.63	152.0	-6.73	155.9	-4.38
Mean deviation (%)			-10.35		-5.77		-4.99

(b) at constant inlet and outlet pressure with different subcoolings

Case	$\dot{m}_{exp}$ (kg/h)	HEM		DEM		IDEM	
		$\dot{m}_{HEM}$ kg/h	Error (%)	$\dot{m}_{DEM}$ (kg/h)	Error (%)	$\dot{m}_{IDEM}$ (kg/h)	Error (%)
4	134	89.0	-33.58	114.8	-14.35	135.3	0.95
5	149	116.1	-22.09	133.9	-10.12	144.8	-2.84
6	166	137.5	-17.16	152.0	-8.42	155.9	-6.11
Mean deviation (%)			-24.28		-10.96		-2.67

5.4.2. Results and Discussion

Table 5.15a shows the comparison of predicted mass flow rate with Aaron and Domanski experimental mass flow rate for R22 with different discharge pressures. The mass flow rate increases with decrease in discharge pressure as more single-phase liquid flows through the short tube. All the three models under predict the mass flow rate. IDEM predicts the mass flow rate with a mean deviation of -4.99%, whereas HEM and DEM predicts the mass flow rate with a mean deviation of -10.35% and -5.77% respectively. For case 1, all the three models predict the same mass flow rate as the discharge pressure (p_{dis} = 13 bar) is greater than then saturation pressure (p_s = 12.22 bar) and the liquid is in single-phase inside the short tube. For cases 2 and 3, HEM predicts identical mass flow rate, which indicates that HEM predicts early choking then DEM and IDEM.

Table 5.15b show the comparison of predicted mass flow rate with the experimental mass flow rate of Aaron and Domanski (1990) for R22 with varying subcooling. From the table it can be observed that the mass flow rate increases with increase in subcooling as more single-phase liquid flows through the short tube. IDEM predicts the mass flow rate with an mean deviation of -2.67%, where as HEM and DEM predicts the mass flow rate with a mean deviation of -24.28% and -10.96% respectively.

Figure 5.19a-c show the comparison of predicted pressure profiles using HEM, DEM and IDEM against Aaron and Domanski's (1990) experimental data, along the short tube for R22 at three different discharge pressures. The sudden pressure drop in Figure 5.19 a-c at the inlet (z=0) is due to rapid fluid acceleration at the abrupt entry to the short tube. Thereafter, the pressure decreases inside the short tube due to acceleration and frictional effects. For case 1 with p_{dis} = 13.0 bar (Figure 5.19a), all the three models predict identical pressure profiles as the discharge pressure is greater than the saturated pressure (p_s = 12.22 bar) and the liquid inside the short tube is in single-phase. The evaluated pressure profiles and the measure pressure profiles show reasonably good agreement with some slight discrepancies, which may be attributable

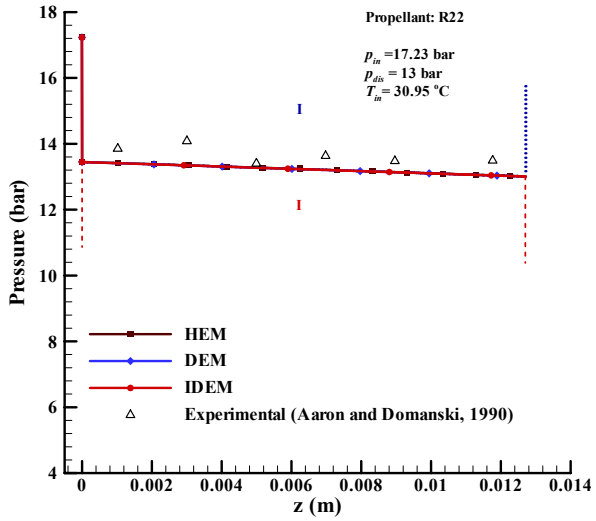

(a) Case 1: p_{dis} = 13.0 bar

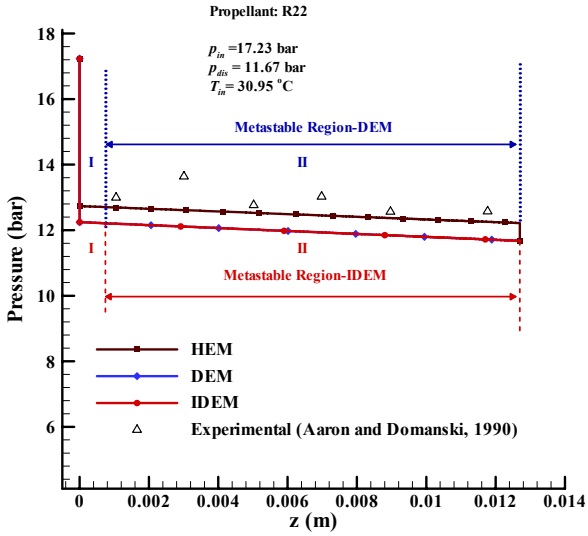

(b) Case 2: p_{dis} = 11.67 bar

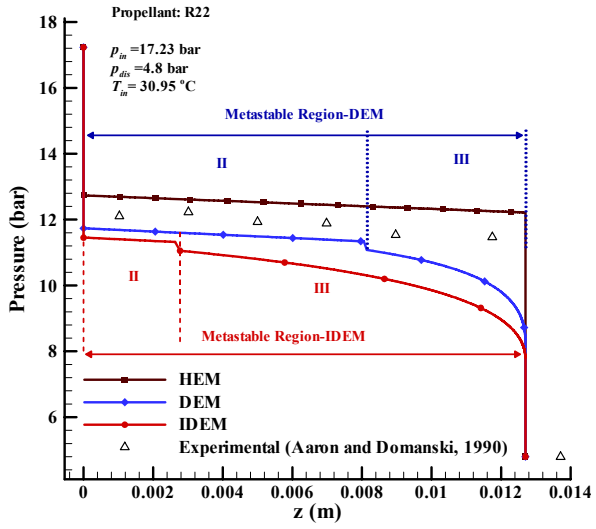

(c) Case 3: p_{dis} = 4.80 bar

I: Subcooled liquid region

II : Metastable liquid region

III: Metastable two-phase region

Figure 5.19 Comparison of predicted pressure profiles along the short tube against the Aaron and Domanski experimental data for (a) case 1 (b) case 2 and (c) case 3 using HEM, DEM and IDEM at a subcooling of 13.9°C

to experimental uncertainties. As the discharge pressure decreases, the liquid inside the short tube enters in metastable state. For case 2 with p_{dis} = 11.67 bar (Figure 5.19b) DEM and IDEM predict identical pressure profiles as both the models predict same metastable liquid region (zone II) as the discharge pressure is higher then the vaporisation pressure (p_v = 11.37 bar). HEM predicts slightly higher pressure, as it predicts low mass flow rate. For HEM, the vaporisation happens when the local pressure is equal to the saturation pressure (p_s). As the discharge pressure is lower than the saturation pressure, the liquid flashes at the exit of the short tube and flow is choked which causes sudden drop in pressure at the exit of the short tube. For case 3 with p_{dis} = 4.8 bar, all the three models predicts choking at the exit of short tube which causes rapid decrease in pressure at the exit of the short tube. DEM and IDEM predict metastable liquid region (zone II) and two-phase metastable region (zone III) inside the short tube, whereas HEM predicts single phase liquid inside the short tube. HEM predicts highest pressure profile as it predicts lowest mass flow rate. IDEM predicts lowest pressure profiles due to high mass flow rate, whereas the predictions of DEM are between IDEM and HEM and are close to the measured values. It should also be noted that DEM predicts more metastable liquid region (zone II) than IDEM, as it predicts low mass flow rate then IDEM, which causes low pressure drop across the short tube.

Figure 5.20a-c show the comparison of predicted pressure profiles using HEM, DEM and IDEM against the experimental data of Aaron and Domanski (1990) for R22 with different levels of subcooling. All the three models predict choking at the exit of the short tube. The propellant inside the short tube exists in metastable liquid region (zone II) or metastable two-phase region (zone III) depending upon the level of subcooling. The propellant is in two-phase metastable region for case 3 with low level of subcooling. From the figure, it can be observed that DEM predictions are close to the experimental data, where as IDEM predicts lowest pressure profile and HEM predicts highest pressure profile respectively.

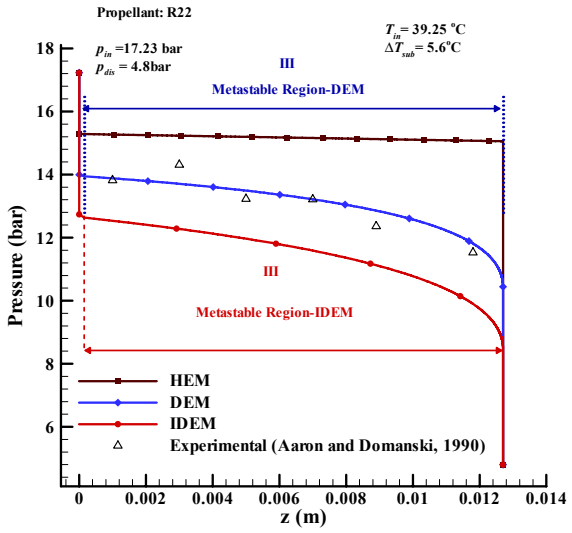

(a) Case 4 : ΔT_{sub} = 5.6 °C

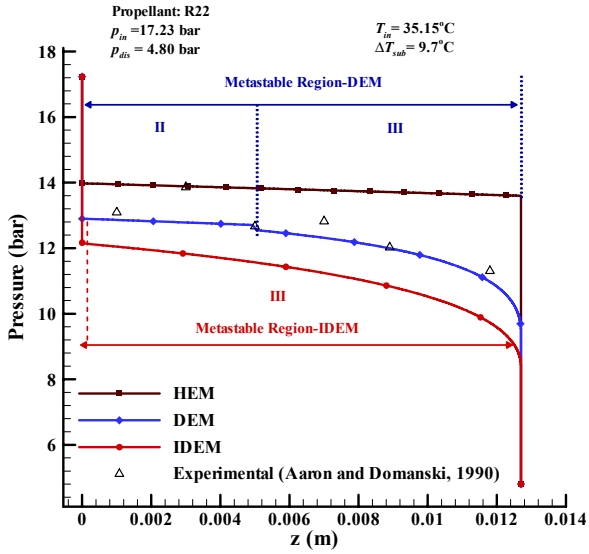

(b) Case 5 : ΔT_{sub} = 9.7 °C

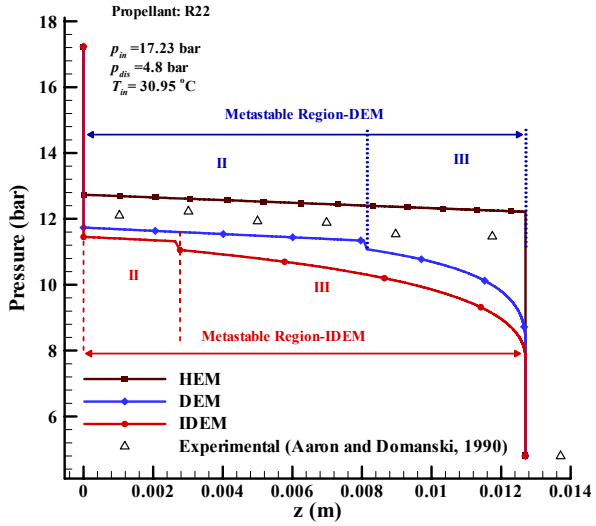

(c) Case 6 : ΔT_{sub} = 13.9 °C

I: Subcooled liquid region

II : Metastable liquid region

III: Metastable two-phase region

Figure 5.20 Comparison of predicted pressure profiles along the short tube against the Aaron and Domanski experimental data for (a) case 4 (b) case 5 and (d) case 6 using HEM, DEM and IDEM at different subcoolings

5.4.3. Summary

In the test cases presented above, it can be seen that HEM seriously underpredicts the mass flow rate with a mean deviation of -17.31%, where as DEM and IDEM predicts the mass flow rate with a mean deviation of -8.37% and -3.83% respectively. The predicted pressure profiles are identical for DEM and IDEM when the propellant inside the short tube is in either single-phase state (zone I) or metastable liquid state (zone II). Significant differences exist in the pressure profiles with decrease in inlet subcooling. DEM predicts the pressure profiles close to the experimental data. On the otherhand, IDEM gives lowest pressure profile and HEM yields highest pressure profiles. This study suggest that DEM predicts the propellant metastability accurately for the flow through short tubes with slight discrepancies in mass flow rate (-8.37%). Whereas IDEM predicts more metastable liquid, consequently underpredicts the pressure distribution inside the short tube. Based on the above study it can be concluded that DEM predictions are better in compare to that of HEM and IDEM for the propellant flow through short tubes. As the twin-orifice systems relevant to pMDIs is a combination of short tubes, DEM will be used to study the characteristics of propellant flow through twin-orifice systems in the next chapters.

5.5. Closure

In this chapter, the flashing propellant flow through short tube orifices and adiabatic capillary tubes have been investigated. The semi-empirical model was successful in predicting the mass flow rate for Kim and O'Neal experimental data, but was unsuccessful in predicting the mass flow rate for Clark's experimental data, suggesting it is good for refrigeration but not for pMDIs. The semi-empirical model is capable of predicting only the mass flow rate but not the flow variables inside the short tube orifice. The other disadvantage of this semi-empirical model is the absence of semi-empirical coefficients that require case-by-case adjustment for different fluids.

Three different models : HEM, DEM and IDEM with pure propellants and propellant mixtures were used to predict the flow variables inside the capillary tube. These three models were successfully validated against a wide range of experimental data

available in the literature. Both the DEM and IDEM predict the mass flow rate along with the flow variables such as pressure, temperature, void fraction, etc along the capillary tube. Unlike the semi-empirical model, they do not need case by case adjustment and predict fairly similar results for long capillary tubes. The differences between DEM and IDEM predictions are due to evaluation of vaporisation index. As mentioned earlier the constant coefficient of DEM relaxation equation and the factor of $(1-y)$ are greater than the corresponding constant and the factor $(1-y)^2$ in IDEM relaxation equation, hence DEM predicts more rapid return to the equilibrium state than IDEM. This is responsible for the kink in the temperature and quality profiles predicted by DEM for subcooled inlet conditions. A much less noticeable kink also occurs in the results for two-phase inlet condition.

These three models : HEM, DEM and IDEM were successfully validated against the experimental data for the propellant flow through short tubes with R22. HEM underpredicted the mass flow rate with a mean deviation of -17.31%, where as DEM and IDEM predicts the mass flow rate with a mean deviation of -8.37% and -3.83% respectively. The comparison of pressure profiles showed that DEM predictions are closer to the experimental data, whereas IDEM predicted lowest pressure profile and HEM predicted highest pressure profile. The results suggested that DEM predicts the propellant metastability accurately for the flow through short tubes with slight discrepancies in mass flow rate (-8.37%). Whereas IDEM predicts more metastable liquid, consequently strictly underpredicts the pressure distribution inside the short tube. Based on the above study it can be concluded that DEM predictions are better in compare to that of HEM and IDEM for the propellant flow through short tubes. Hence, the DEM was chosen to study the continuous discharge and metered discharge flow through twin-orifice system of pMDIs in the following chapters. The original contributions to the knowledge from this chapter are:

- Successful implementation of IDEM for the propellant flow through long adiabatic capillary tubes with pure propellants and propellant mixtures.
- Comparison of HEM, DEM and IDEM for the propellant flow through adiabatic capillary tube.
- Successful implementation of metastability models: DEM and IDEM for the propellant flow through short tubes.

CHAPTER 6

TWIN-ORIFICE SYSTEM OF PMDIS: ANALYSIS OF VARIOUS ASSUMPTIONS

6.1. Introduction

The metered discharge flow through twin-orifice system of pMDI is transient and involves several abrupt changes in the geometry such as abrupt contraction at the entrance of the valve and spray orifice and abrupt expansion at the exit of the valve and spray orifice. In order to predict the flow variables and mass flow rate accurately in these systems, it is important that the assumptions made across these abrupt contractions/expansions are valid and close to the real flow process. The propellant inside these twin-orifice systems is understood to be in two-phase metastable state (Fletcher, 1975; Clark, 1991). The existing literature to model the flow through abrupt area changes (abrupt contraction and abrupt expansion) considers either single-phase flow or equilibrium two-phase flow. An attempt was made to model the two-phase metastable flow across such abrupt area changes by Attou and Seynhaeve (1999a). In chapter 4 (section 3.4.4) a number of new submodels were presented to evaluate metastable flows across these abrupt area changes for the flow through twin-orifice system of pMDIs. Here the results of different submodels are presented a specific combination of assumptions, which offers good agreement with the experimental data is selected for further computations in Chapter 7.

First, the test cases used to carry out the simulations are discussed. Thereafter, two different assumptions made to solve the abrupt expansion at the exit of the valve and spray orifice are applied in conjunction with three different flow regimes : two-phase flow (TPF), liquid only flow (LOF) and metastable only flow (MOF). Then, a grid independence test is carried out for the propellant flow through twin-orifice system of pMDIs. Finally, the chapter is concluded with the combination of the best assumptions that predicts results closest to the experimental data.

6.2. Test Case

As metered discharge is a *transient* phenomenon, the mass of propellant reduces in the course of the propellant discharge event which has the following two consequences:

- Inlet pressure and temperature exhibit a monotonic fall as the metering chamber empties.
- Fluid is a vapour-liquid mixture at the valve orifice inlet.

Clark (1991) carried out an extensive program of measurements on metered discharge flows for a wide range of propellants, orifice, metering chamber and expansion chamber dimensions geometries. Figure 6.1 and Figure 6.2 (after Clark, 1991) shows a typical experimental discharge pressure and temperature profile inside the metering chamber and the expansion chamber. From the figure it can be observed that the metering chamber pressure falls at the beginning of the discharge. Between 25 and 200 ms the conditions in the metering chamber and expansion chamber are almost the same, which indicates that the mass flow rates into and out of the expansion chamber are equal and the flow is quasi-steady. The quasi-steady flow can be simulated as a sequence of instantaneously steady state flows at various time instants.

The test case used for the present study has the following geometry and operating conditions (Clark, 1991: page 182):

- Metering chamber volume: 100 μL = 10^{-7} m^3
- Valve orifice: D_{vo} = 0.26 mm, L_{vo} = 0.5425 mm
- Expansion chamber: D_{ec} = 3.8 mm, L_{ec} = 11 mm
- Spray orifice: D_{so} = 0.26 mm, L_{so} = 1 mm
- Hydraulic roughness of all surfaces: ε = 1.5 μm
- Propellant : R12
- Ambient pressure 1.013 bar, which is the discharge pressure acting as the downstream boundary condition.
- Ambient temperature (T_0) 291 K, which defines the conditions of the metering chamber fluid prior to discharge.
- Other inlet conditions are given in Table 6.1 below.

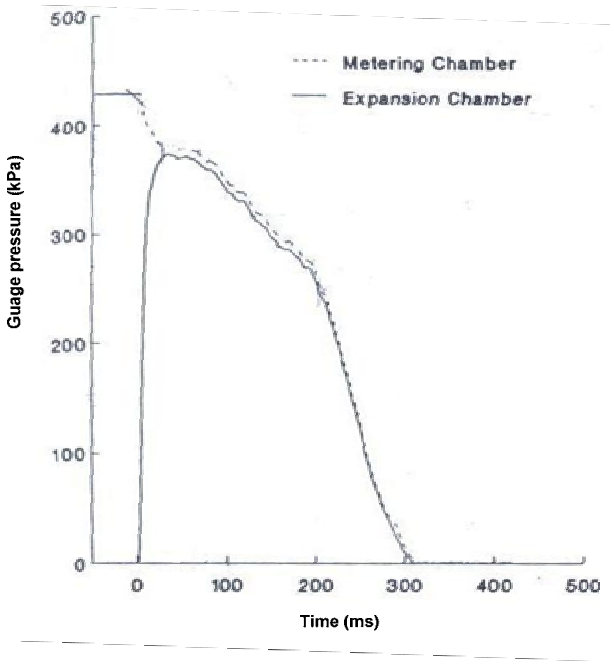

Figure 6.1 Measured pressure inside the metering chamber and expansion chamber (Clark, 1991)

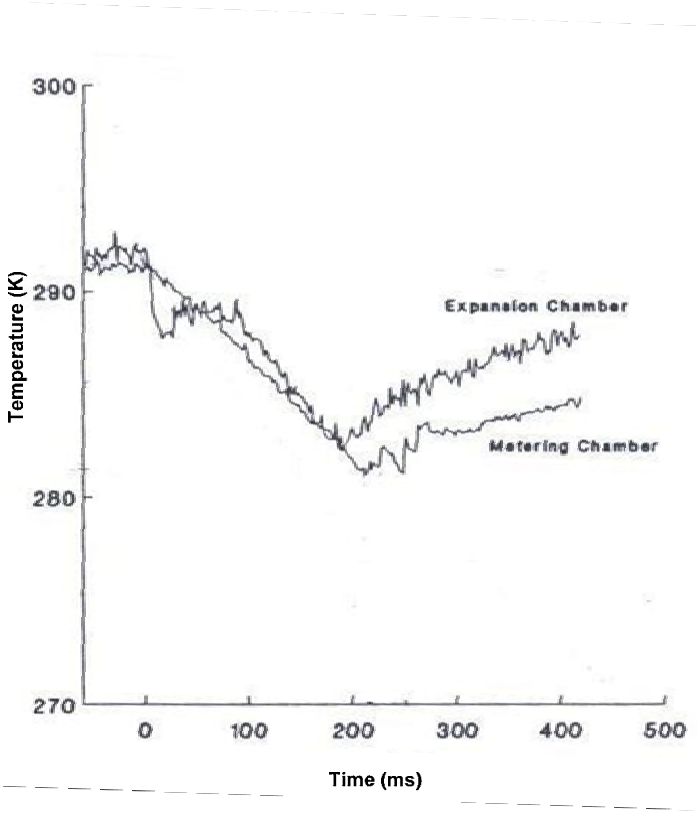

Figure 6.2 Measured temperature inside the metering chamber and expansion chamber (Clark, 1991)

The length of the valve orifice and expansion chamber were not given in Clark's thesis but it stated that the experiments were made with a specific valve design (Bespak BK 356). Dimensions of this design were obtained from the manufacturer. Also, the hydraulic roughness of the pipe was not given. Hence it was assumed for a Copper/Brass pipe.

This data set is chosen because this is the only the data set for which the experimental metering chamber pressures and temperatures were available in the thesis. The inlet conditions can be completely defined with the help of this data set. These were derived using the measured propellant state in the metering chamber. Experimental values of metering chamber pressure and temperature are available between 25 and 200 ms from Clark's (1991) experimental data (Figure 6.1 and Figure 6.2). In order to completely specify the problem, quality x and the vaporisation index y of the mixture in the metering chamber are required. Assuming that measured temperature represents the mean temperature and ambient temperature represents the metastable temperature, the value of 'y' can be evaluated from mean temperature equation (3.18). The value of quality 'x' is evaluated from mean enthalpy equation (3.8). These two equations can be rearranged to yield equations (6.1) and (6.2) for vaporisation index and quality, respectively.

Table 6.1 Inlet conditions for numerical simulations

t (ms)	p_{in} (bar)	T_{in} (°C)	x_{in}		y_{in}		
			TPF	LOF & MOF	TPF	LOF	MOF
25	4.85	16.95	0.007	0.0	0.312	0.312	0.0
50	4.80	16.04	0.013	0.0	0.524	0.524	0.0
75	4.73	14.92	0.021	0.0	0.720	0.720	0.0
100	4.50	13.51	0.030	0.0	0.757	0.757	0.0
150	4.09	11.13	0.045	0.0	0.759	0.759	0.0
200	3.68	8.59	0.06	0.0	0.752	0.752	0.0

$$y = \left(T_0 - T_{\exp}\right) / \left(T_0 - T_{sat,l}(p)\right) \quad 6.1$$

$$x = [h_{l,0} - (1-y)h_{lm} - yh_{l,sat}(p)] / [h_{v,sat}(p) - h_{l,sat}(p)] \quad 6.2$$

where $h_{l,0}$ is the liquid enthalpy at ambient temperature (T_0), h_{lm} is the metastable liquid enthalpy evaluated as a function of pressure and entropy *f(p, s)* from REFPROP. T_{exp} is the experimental metering chamber temperature (Clark, 1991) and subscript 'sat' indicates saturated liquid at the prevailing local pressure.

The propellant flow regime in the metering chamber at the entry to the valve orifice is also unknown. Three extreme scenarios have been explored:

- Two-Phase Flow (TPF): The vapour and liquid are finely dispersed everywhere in the metering chamber (Figure 6.3a). A homogenous mixture of liquid and vapour enters the valve orifice at a quality, *x*, obtained from equation (6.2). Clark (1991) made this assumption to obtain the metering chamber conditions for his theoretical model.
- Liquid-Only Flow (LOF): The propellant is stratified in the metering chamber due to gravity with vapour at the top and a mixture of saturated and metastable liquid at the bottom (Figure 6.3b). During pMDI actuation the valve orifice is located near the bottom of the metering chamber, so the assumed inlet quality of the fluid entering the valve orifice will be zero i.e. $x = 0$ and the vaporisation index '*y*' is evaluated from equation (6.1).
- Metastable-Only Flow (MOF) : In addition to stratification of vapour and liquid due to gravity, the propellant inside the metering chamber is also thermally stratified. Evaporation produces vapour at the top and saturated liquid at the centre and metastable liquid remains closes to the bottom (Figure 6.3c). So, the assumed inlet quality and vaporisation index of the fluid entering the valve orifice will be $x = 0$, $y = 0$.

Propellant properties are obtained from REFPROP v.7.0 (2002). The saturated properties of the propellant in the two-orifice system are estimated as a function of local pressure, *f(p)* and metastable liquid properties are estimated as a function pressure and entropy *f(p, s)*.

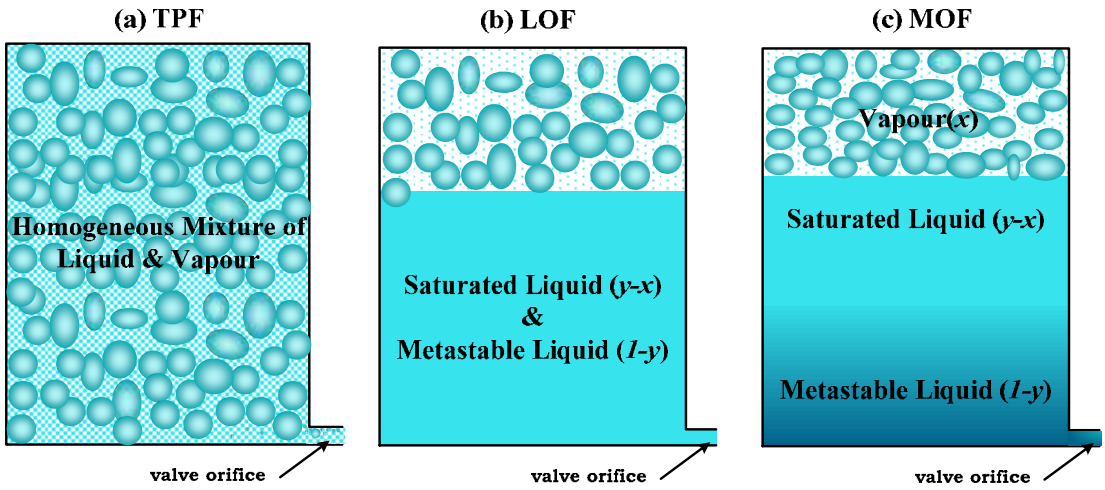

Figure 6.3 Flow regimes in the metering chamber : (a) Two-Phase Flow (TPF) (b) Liquid Only Flow (LOF) and (c) Metastable Only Flow (MOF)

6.3. Analysis of Various Assumptions made across the Sudden Expansion (SE) at the exit of the Valve Orifice

The conceptual model, assumptions, mathematical expressions to model the flow across abrupt expansion of the exit of the valve orifice were detailedly discussed in chapter 4 (section 3.4.4.2). The detailed procedure to solve these mathematical equation were explained in chapter 5 (section 4.4.1.4). In this section, first the two different assumptions made across the abrupt expansion of valve orifice are summarized and thereafter the results obtained using these two different assumptions are discussed.

Assumption 1:

Following Attou and Seynhaeve (1999a) the vaporisation index across the abrupt expansion has been assumed constant. i.e. $y_I = y_O$. The subscript 'I' and 'O' corresponds to inlet and outlet of abrupt expansion respectively.

Assumption 2:

The vaporisation index at the outlet of abrupt expansion (y_O) is evaluated integrating the modified DEM relaxation equation over a distance of 5h (Figure 3.10).as the flow is fully recovered at this point. The modified relaxation equation (3.46) is expressed as:

$$\frac{dy}{dz} = k_y \frac{4}{D(z)}(1-y)\left[\frac{p_s - p}{p_c - p_s}\right]^{0.25} \qquad 6.3$$

The coefficient of relaxation equation used for assumption 2b is equal to 0.02, which originates from experiments on steam-water systems (Feburie et al., 1993).

Three different values of k_y are considered.

Case 2(a) k_y = 0.002 (reduced by a factor 10)

Case 2(b) k_y = 0.02 (the basic case)

Case 2(c) k_y = 0.2 (increased by a factor of 10)

The value of k_y are chosen in a such a way that the effect of coefficient k_y on the flow variables and mass flow rate is clearly visible. The best assumption is selected based on prediction of the mass flow rate and the expansion chamber pressure but not on the expansion chamber temperature. This is because, the exact meaning of the temperature measurement in a transient two-phase flow is less clear so the level of confidence is lower with the measured temperature values.

Results and Discussion

Figure 6.4 to Figure 6.6 show the comparison of predicted expansion chamber pressure at various instants during the metered discharge of R12 with Clark's (1991) experimental data using different assumptions for three different inlet conditions (TPF, LOF and MOF). All these inlet conditions, underpredict the expansion chamber pressure. Assumption 2c predicts the higher expansion pressure, closer to the experimental data. Assumptions 1 and 2a, which give almost identical results, predict the lowest expansion chamber pressure and the predictions of the expansion chamber pressure using the assumption 2b lies in between the assumptions 2a and 2c.

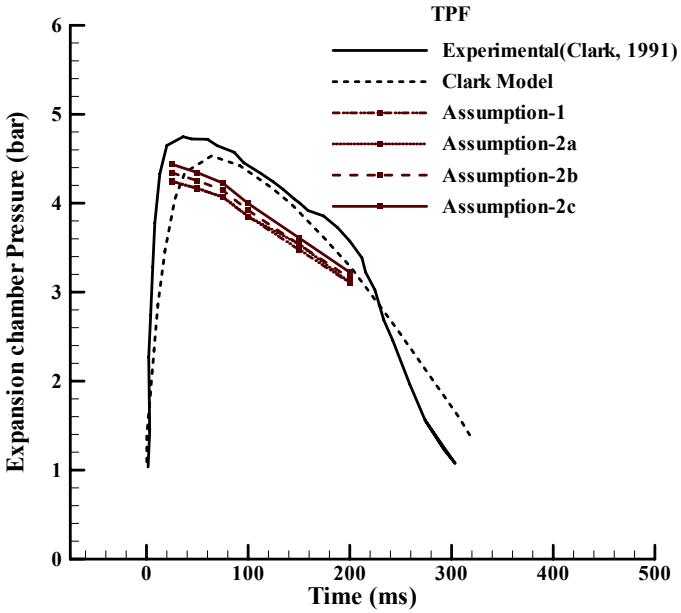

Figure 6.4 Comparison of expansion chamber pressure against Clark's (1991) experimental and numerical results with TPF inlet flow regime

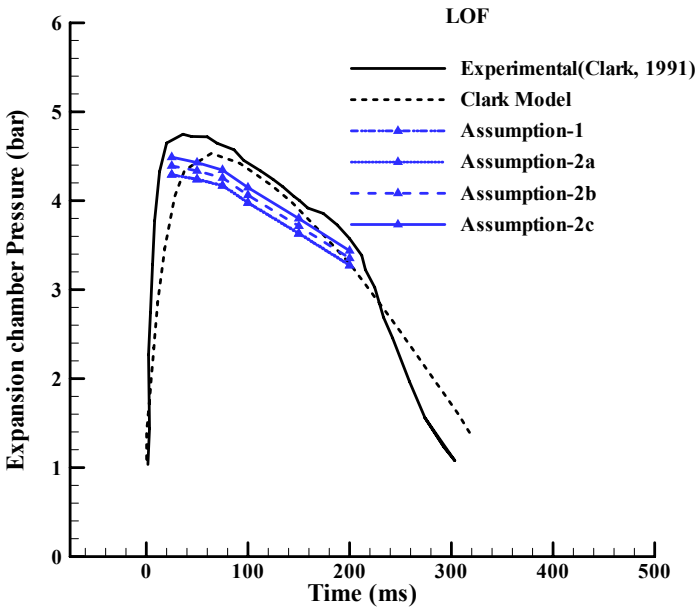

Figure 6.5 Comparison of expansion chamber pressure against Clark's (1991) experimental and numerical results with LOF inlet flow regime

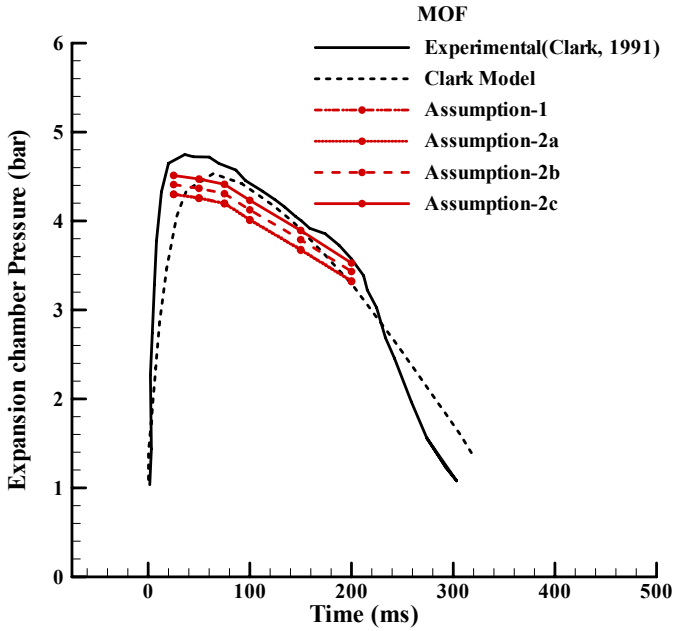

Figure 6.6 Comparison of expansion chamber pressure against Clark's (1991) experimental and numerical results with MOF inlet flow regime

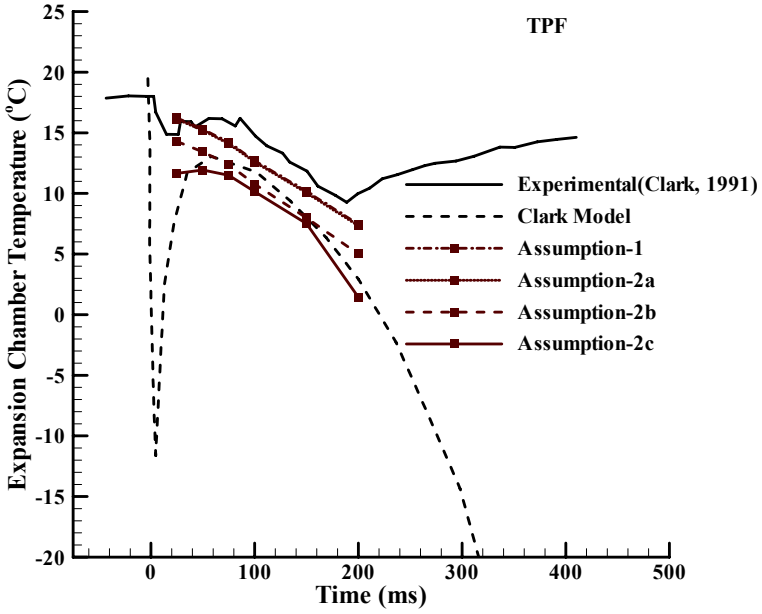

Figure 6.7 Comparison of expansion chamber temperature against Clark's (1991) experimental and numerical results with TPF inlet flow regime

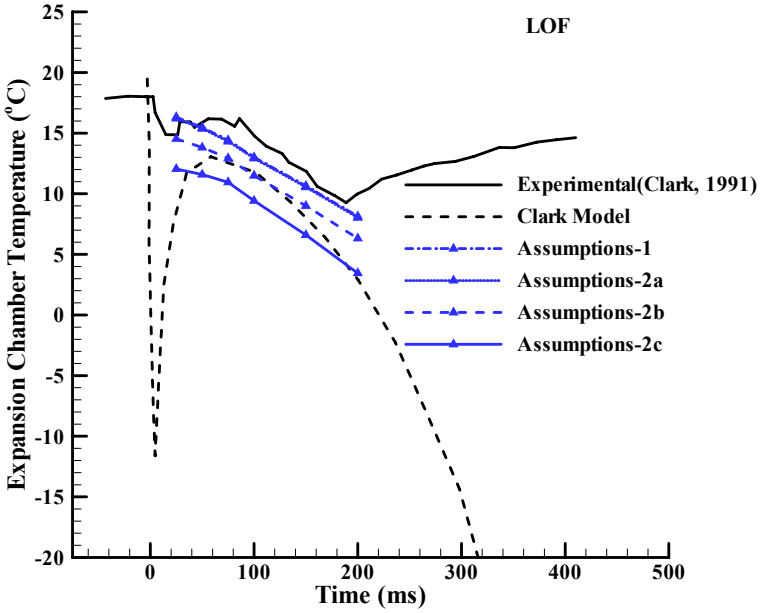

Figure 6.8 Comparison of expansion chamber temperature against Clark's (1991) experimental and numerical results with LOF inlet flow regime

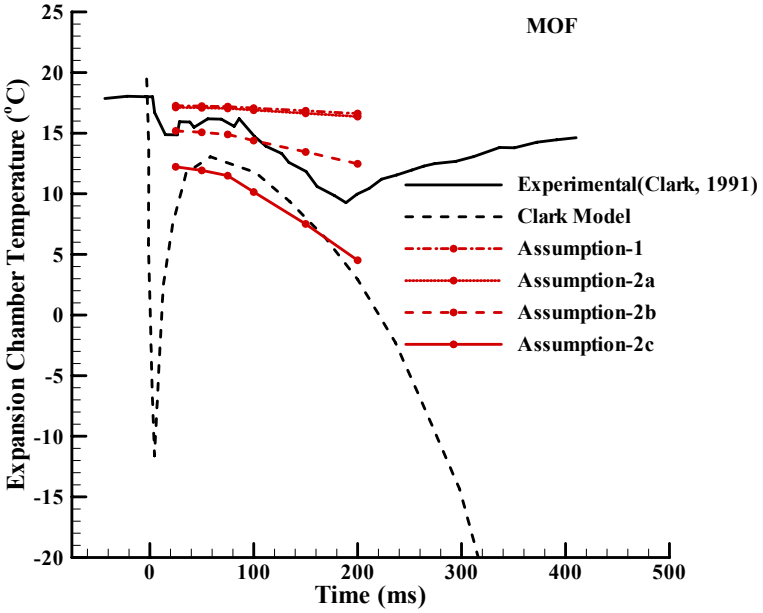

Figure 6.9 Comparison of expansion chamber temperature against Clark's (1991) experimental and numerical results with MOF inlet flow regime

Table 6.2 Predicted mass flow rates with various assumptions for different inlet flow regimes

Assumptions	**t (ms)**	***ṁ* (kg/h)**		
		TPF	**LOF**	**MOF**
1	25	1.605	1.790	1.756
	50	1.489	1.797	1.733
	75	1.369	1.801	1.700
	100	1.208	1.742	1.604
	150	0.991	1.621	1.438
	200	0.8176	1.486	1.274
Average *ṁ* (Assumption 1)		**1.247**	**1.706**	**1.584**
Error (%)		**-20.35**	**9.02**	**1.22**
2a	25	1.61	1.797	1.764
	50	1.493	1.803	1.741
	75	1.301	1.808	1.708
	100	1.211	1.749	1.613
	150	0.993	1.628	1.448
	200	0.8167	1.493	1.2838
Average ***ṁ*** (Assumption 2a)		**1.237**	**1.713**	**1.593**
Error (%)		**-20.94**	**9.45**	**1.78**

(Table 6.2 continued…)

Assumptions	t (ms)	$\dot{m}$ (kg/h)		
		TPF	**LOF**	**MOF**
2b	25	1.493	1.647	1.601
	50	1.400	1.661	1.575
	75	1.372	1.674	1.538
	100	1.154	1.614	1.432
	150	0.950	1.489	1.256
	200	0.784	1.350	1.089
Average $\dot{m}$ (Assumption 2b)		**1.192**	**1.572**	**1.415**
Error (%)		**-23.82**	**0.47**	**-9.57**
2c	25	1.362	1.481	1.422
		1.294	1.503	1.392
		1.218	1.526	1.350
		1.085	1.463	1.232
		0.897	1.329	1.042
	200	0.7410	1.181	0.8734
Average $\dot{m}$ (Assumption 2c)		**1.10**	**1.414**	**1.219**
Error (%)		**-29.75**	**-9.67**	**-22.13**

$$\% \text{ error} = \left(\frac{\dot{m}_{avg} - m_{meausred}}{m_{measured}} \right) \times 100$$

Negative sign (-) indicates under prediction

Positive sign indicates over prediction

Figure 6.7 to Figure 6.9 shows the comparison of expansion chamber temperature against Clark's (1991) experimental and numerical data using various assumptions for the three different inlet conditions (TPF, LOF and MOF). The expansion chamber temperature predicted by assumption 1 and assumption 2a are identical and they yield higher temperatures. The assumption 2c on the otherhand predicts the lowest temperatures and the predictions of assumption 2b lies in between.

Table 6.2 shows the numerically predicted quasi-steady mass flow rate at different time instants and their average for three different assumed inlet regimes with various assumptions. From the table it can be seen that the LOF inlet flow regime predicts the largest mass flow rate, whereas the TPF inlet flow regime predicts lowest mass flow rate. The mass flow rate predicted by MOF lies between LOF and TPF. The average mass flow rate is calculated by adding the mass flow rates at different instants and dividing it by total number of cases i.e.

$$\dot{m}_{avg} = \frac{\sum \dot{m}}{n}$$

where,

$\dot{m}_{avg}$ = average mass flow rate (kg/h) and

n = total number of cases (=6)

The average mass flow rate predicted by assumption 1 and assumption 2a which involve the most metastable flows are almost equal and always are the largest ones. Assumption 2c yields the lowest average mass flow rate, and the predictions made by assumption 2b are intermediate.

Using the metering chamber volume of 100 μL, liquid density of 1304 kg/m^3 and a discharge event duration of 300 ms, we can make an approximate estimate of the average mass flow rate of 4.35×10^{-4} kg/s = 1.565 kg/h. The error in Table 6.2 is evaluated using this mass flow rate as reference point and shows that the predictions with the LOF-2b scenario is very close to this estimate with an error of 0.47%. From the above table it can be observed that all the TPF scenarios poorly predicts the mass flow rate.

Assumption 2c predicts the lowest mass flow rate in comparison to that of assumptions 2a and 2b, since more vapour is formed inside the expansion chamber as a consequence of the higher value of the coefficient of the relaxation equation, k_y. A larger value of this coefficient increases the evaporation, whereas smaller coefficient inhibits the evaporation and encourages metastability due to which more vapour is formed. Because of the low mass flow rate associated with assumption 2c, the expansion chamber pressures in Figure 6.4 to Figure 6.6 are highest. The expansion chamber temperatures are evaluated using equation 3.18. According to this equation an increase of the vaporisation index '*y*' will cause the mean temperature to be dominated by the saturated liquid temperature. If '*y*' becomes small then the mean temperature is dominated by the metastable temperature. As more evaporation takes place with assumption 2c, the vaporisation index '*y*' increases more rapidly, so the mixture temperature is close to the saturated liquid temperature yielding the lowest expansion chamber temperatures in Figure 6.7 to Figure 6.9.

In assumption 2a, the coefficient of the relaxation equation is smaller which inhibits the evaporation in the expansion chamber and encourages metastability. This causes increase in the mass flow rate due to which assumption 2a predicts the lowest expansion chamber pressures in Figure 6.4 to Figure 6.6 and high temperatures in Figure 6.7 to Figure 6.9. With assumption 2a the vaporisation index '*y*' evaluated at the exit of the abrupt expansion is almost equal to the value of assumption 1 at the inlet of the abrupt expansion. Therefore, the predictions of flow variables with assumptions 2a are almost identical to those of constant '*y*' assumption 1.

Figure 6.4 - Figure 6.6 and Table 6.2 show that the TPF consistently under predicts the mass flow rate and expansion chamber pressure drastically. This suggest that the TPF inlet flow regime is not valid as an assumption for modeling the flashing flow through twin-orifice system of pMDIs. Assumptions 2a and 1 combine good predictions of the mass flow rate (Table 6.2) with MOF inlet flow regime, but give the lowest expansion chamber pressures (Figure 6.4 to Figure 6.6) with an average error of -8% for MOF-1 and MOF-2a. So, these two assumptions are also eliminated from consideration. Now, the remaining options are assumptions 2b and 2c for LOF and MOF inlet conditions. Although MOF-2b and MOF-2c predict the expansion chamber

pressure approximately with an average error of 6% and 3.7% respectively, they underpredicts the mass flow rate with an average error of -9.57% and -22.13% respectively. This suggest that MOF-2b and MOF-2c are also not valid assumptions. From the Table 6.2 it can be observed that LOF-2b gives the best prediction of mass flow rate with an error of 0.47%, while predicting the expansion chamber pressure with an average error of 7%. This suggest that LOF-2b is the best in predicting both the mass flow rate and expansion chamber pressure close to the experimental data. Hence, LOF inlet flow regime with assumption 2b will be used to model the flow through twin-orifice system. As mentioned earlier, the judgment of best assumption is based on mass flow rate and expansion chamber pressure but not on expansion chamber temperature due to low level of confidence with the measured expansion chamber temperatures.

6.4. Abrupt Expansion at the exit of Spray Orifice: Discharge Shock Wave (DSW)

When the flow is choked at the exit of the spray orifice, the spray of a pMDI discharges to ambient pressure and the spray accelerates into the atmosphere as $p_{choke} > p_{dis}$. As the geometry of the emerging jet is undefined by the exit conditions, two extreme scenarios are considered: case (1) straight jet : see Figure 3.11 and case (2) conical jet : see Figure 3.12.

Case 1 : Straight jet

As mentioned previously (section 3.4.4.3), it is unclear how the evaluation of vaporisation index (y) and quality (x) should be calculated at the exit of control volume (CV) (Figure 3.11). Two different ways are adopted to evaluate 'x' and 'y' at the outlet of CV.

Case 1a : equations of mean specific volume and mean enthalpy are solved simultaneously which yield equations (3.52) and (3.53) to calculate y and x respectively at the outlet of the CV.

Case 1b: following Attou and Seynhaeve (1999a), the vaporisation index, y, is assumed constant across the expansion and the quality, x, is calculated using mean enthalpy equation 3.8.

Case 2 : Conical jet

For conical expansion, it is assumed that the spray has completed adiabatic evaporation, so y=1, at the outlet of CV (Figure 3.12) and the quality, x, is evaluated from mean enthalpy equation (3.56). As described in section (3.4.4.3), two different cone angles have been considered to investigate the effect of spray angle on exit velocity.

Case 2a: $\theta = 45°$

Case 2b: $\theta = 0°$

The conceptual model, governing equations and procedure to solve the shock wave at the exit of the spray orifice for the above two scenarios have been briefly discussed in chapter 4 (section 3.4.4.3) and chapter 5 (section 4.4.1.4). Again, the case at t=25 ms with LOF regime has been used as a test case to verify the above assumptions for the DSW at the exit of the spray orifice.

Table 6.3 shows the evaluated flow variables (quality, x, vaporisation index, y and velocity, U) at the choked conditions and at the discharge after the shock. From the table it can be observed that the values of these variables are same at the choking point. For straight jet (case 1a and case 1b), the velocity is evaluated considering the acceleration effect associated due to difference in the choking pressure and the discharge pressure using equation (3.50). Hence the exit velocity is same for these cases. The differences in the exit quality and vaporisation index are due to different way of evaluating these variables. For case 1a, the increase in the discharge velocity after shock decreases the mean enthalpy and mean density evaluated using the energy equation (3.51) and continuity equation (3.48) respectively, which causes the quality (x) and vaporisation index (y) to decrease at the discharge. For case 1b on the other hand, following to Attou and Seynhaeve (1999a) the vaporisation index (y) is kept

constant across the shock. The decrease in mean enthalpy after the shock increases the numerator of equation (3.54) which causes increase in the quality.

For conical jet (case 2a and case 2b), the exit velocity is evaluated using equation (3.55) and hence depends on the cone angle. The evaluated exit is velocity is high for case 2a, which is due to cone angle θ=45°. For 45° (case 2a), 1/F(θ) = 1.20, in equation (3.55), so the exit cone causes increase in the exit velocity. And for $\theta \rightarrow 0$ (case 2b), 1/F(θ)=1 in equation (3.55) as $\theta \rightarrow 0$, the limit of θ/θ=1, which reduces equation (3.55) to (3.50) which is a straight jet equation for the exit velocity. Hence, the evaluated exit velocity for case 2b is same as that of straight jet (case 1a and case 1b).

The evaluated qualities are higher for conical jet (case 2a and case 2b) compare to those of straight jet (case 1a and case 1b). This is due to our assumption that spray has completed adiabatic evaporation at the discharge. So, the vaporisation index, y=1 at the discharge and high qualities are evaluated.

Table 6.3 Flow variables at the choked conditions and after the shock

	Flow variables at choked conditions (I)			Flow variables at the discharge after the shock(O)		
	x_{choke}	y_{choke}	$U_{choke\ (m/s)}$	x_{dis}	y_{dis}	$U_{dis\ (m/s)}$
Case 1a	0.032	0.143	25.22	0.026	0.065	42.07
Case 1b	0.032	0.143	25.22	0.045	0.143	42.07
Case 2a	0.032	0.143	25.22	0.253	1.000	50.29
Case 2b	0.032	0.143	25.22	0.255	1.000	42.07

As it can be observed from the table that the straight jet (case 1a and case 1b) predicts low qualities at the exit of spray orifice, whereas the conical jet (case 2a and case 2b) predicts high qualities at the exit. Also, considering the cone angle shows modest increase in the exit velocity. Flow visualizations show that choked flows give rise to

conical jet, whereas subcritical flows give rise to straight jet. As the flow is always choked at the exit of the spray orifice (Fletcher, 1975; Clark, 1991 and Versteeg et al, 2002), the conical jet assumption (case 2a) is more appropriate to solve the shock at the spray orifice exit of pMDIs. In order to account for the maximum cone angle θ=45° is selected. Hence, the conical jet assumption (case 2a) with θ=45° will be used to solve the discharge shock wave at the exit of spray orifice for all further simulations.

6.5. Grid Independence Test

A grid independence test was carried out to make sure that the grid size does not affect the computational results. As high gradient persist at the exit of the valve and spray orifice, a non-uniform grid (Figure 4.3) concentrated at the exit of the valve orifice and spray orifice was used. Computations were carried out using three different grids: grid 1 = 550 nodes, grid 2 = 700 nodes and grid 3 = 850 nodes (Table 6.4). Again, the test case, at t=25 ms (Table 6.1) with LOF regime is used for the grid independence test as the pressure changes are largest at t=25 ms, so gradients will most severe for this case.

Table 6.4 Details of three different grids

Grid	Valve Orifice (N_{vo}) Nodes	Expansion Chamber (N_{ec}) Nodes	Spray Orifice (N_{so}) Nodes	Total Number of Nodes (N)
1	250	50	250	550
2	300	100	300	700
3	350	150	350	850

Figure 6.10 shows the predicted pressure, quality and velocity distribution along the twin-orifice system of pMDIs using three different grids. As can be seen that these predicted profiles are almost identical on the normal scale. A close-up view (dotted box) at the exit of valve orifice and spray orifice highlights the minor differences between the results obtained using these grids. From the close-up view, it can be observed that there is no significant difference between the profiles using grid 2 and

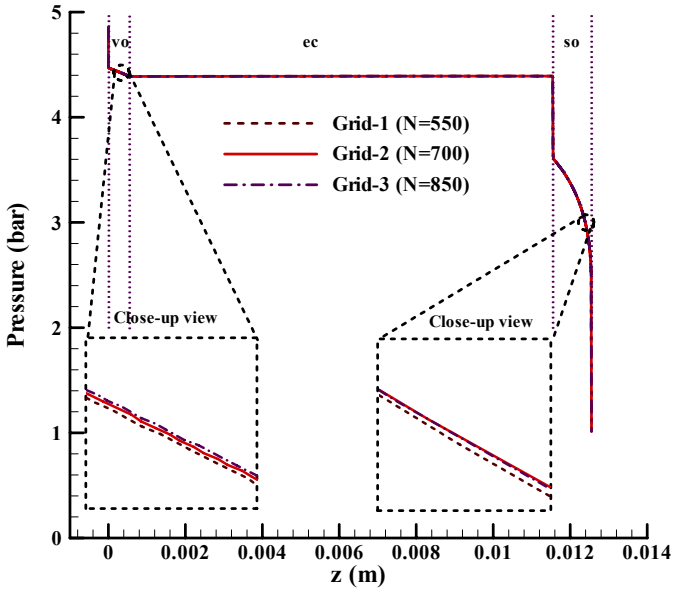

Figure 6.10 Predicted pressure profiles along the twin-orifice system of pMDIs using three different grids

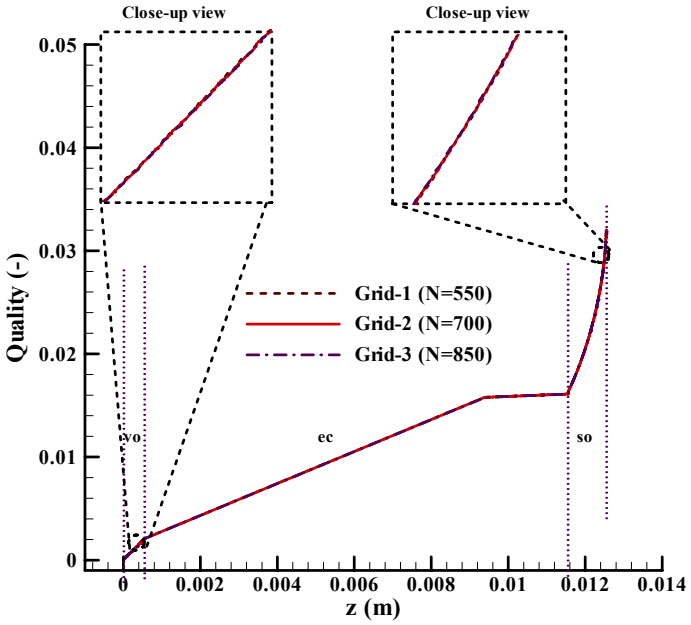

Figure 6.11 Predicted quality profiles along the twin-orifice system of pMDIs using three different grids

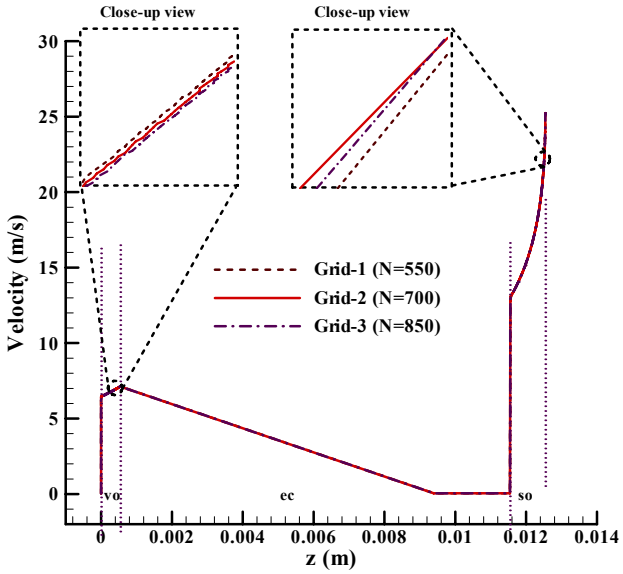

Figure 6.12 Predicted quality profiles along the twin-orifice system of pMDIs using three different grids

grid 3, whereas there is a slight difference between grid 1 and grid 2 in pressure and velocity profiles. The predicted mass flow rate using grid 1, grid 2 and grid 3 are 1.647 kg/h, 1.6466 kg/h and 1.6462 kg/h respectively, which corresponds to discrepancies of 0.026% between grid 1 and grid 2 and 0.022% between grid 2 and grid 3. These are very small and hence, the grid 2 with 700 nodes has been selected as optimum grid for all further simulations.

6.6. Closure

In this chapter, two different assumptions made to evaluated the quality and vaporisation index across the abrupt expansion at the exit of the valve orifice were studied in conjunction with three different metering chamber flow regimes (TPF, LOF and MOF). The results showed that the LOF flow regime with evaluating the vaporisation index using the relaxation equation with coefficient, $k_y = 0.02$ and quality by mean enthalpy equation across the abrupt expansion gives best match with the experimental data. Thereafter, the assumptions made to solve the expansion shock when the flow is choked at the exit of the spray orifice were analyzed. Two different types of expansions were considered : straight jet and conical jet. As the flow is

choked at the exit of the spray orifice, the conical jet assumption is more appropriate to solve the discharge shock at the exit of the spray orifice for pMDIs. Grid independence tests were carried out and it was found that the grid independency was achieved with N=700 (N_{vo} = N_{so} = 300 and N_{ec} = 100). The above combination of modeling assumptions and the grid will be used for the further simulations to validate DEM against experimental results for continuous discharge flows and metered discharge flows in the next chapter.

CHAPTER 7

TWIN-ORIFICE SYSTEM OF PMDIS

7.1. Introduction

From chapter 6, it can be seen that all the three models: HEM, DEM and IDEM can be used to predict the flow variables and mass flow rate for single orifice systems. However, HEM underpredicts the mass flow rate and gives poor predictions of pressure and temperature distribution along the single orifice systems especially in metastable region as it does not account to propellant metastability. IDEM, on the other hand, apparently predicts more metastability than the actual flow, which gives slightly high mass flow rate and shows small deviations in pressure and temperature distribution with respect to the experimental data. The DEM predicts the mass flow rate, pressure and temperature distribution close to the experimental data, hence DEM with the assumptions mentioned in the previous chapter 6 for evaluating the flow variables across the abrupt expansion of valve orifice and spray orifice will be used to predict the mass flow rate and flow variables along twin-orifice system of pMDIs for the continuous discharge of propellant flows.

The purpose of this chapter is to validate the DEM against experimental results for continuous discharge and metered discharge propellant flow through twin-orifice system of pMDIs. For continuous discharge both Fletcher (1975) and Clark (1991) experimental data are used for the validation purpose. Whereas for metered discharge only Clark's (1991) experimental data is used as it is the only data set for which sufficient information is available to estimate the inlet conditions accurately. As the atomization process in a twin-orifice system is quite different from that of a single orifice system, it might be expected that the single value of coefficient, k_y, in the relaxation equation is not enough as it dictates the rate of evaporation along the orifice. Therefore, two different approaches have been used for the coefficient k_y in the relaxation equation (3.9). First, the existing coefficient, k_y = 0.02, proposed by

Feburie et al. (1993) is used. Thereafter a new correlation is developed for this coefficient k_y. The results obtained using this new correlation are compared against the Fletcher's (1975) and Clark's (1991) experimental data for the continuous discharge flows.

The conceptual model, assumptions, mathematical expressions to model the flow through twin-orifice system of pMDIs were presented in detail in chapter 3 (section 3.4). The numerical procedure to solve these mathematical equations was explained in chapter 4 (section 4.4). In this chapter, first, the test cases and results obtained for these test cases for Fletcher (1975) experimental data are discussed. Thereafter, the test cases and results of Clark's (1991) experimental data are presented. Then a new correlation for the coefficient k_y is developed and the results obtained using this new correlation for both Fletcher and Clark's test cases are presented.

7.2. DEM with $k_y = 0.02$

In this section, DEM with $k_y = 0.02$ is used to validate against the experimental results of Fletcher (1975) and Clark (1991) for continuous discharge flow through twin-orifice system of pMDIs.

7.2.1. Comparison against Fletcher (1975) experimental data with k_y=0.02

In this section, the test cases and the results obtained using DEM for these test cases are presented.

7.2.1.1. Test Cases

Fletcher (1975) carried out experimental work on the continuous discharge of propellant R12 /R11 (60%/40%) in a twin-orifice system of a pMDI with various valve and spray orifice configurations. The propellant consisted of 60% R12 (Dichlorodifluoromethane, $C_2Cl_2F_4$) and 40% R11 (Trichloromonofluoromethane,

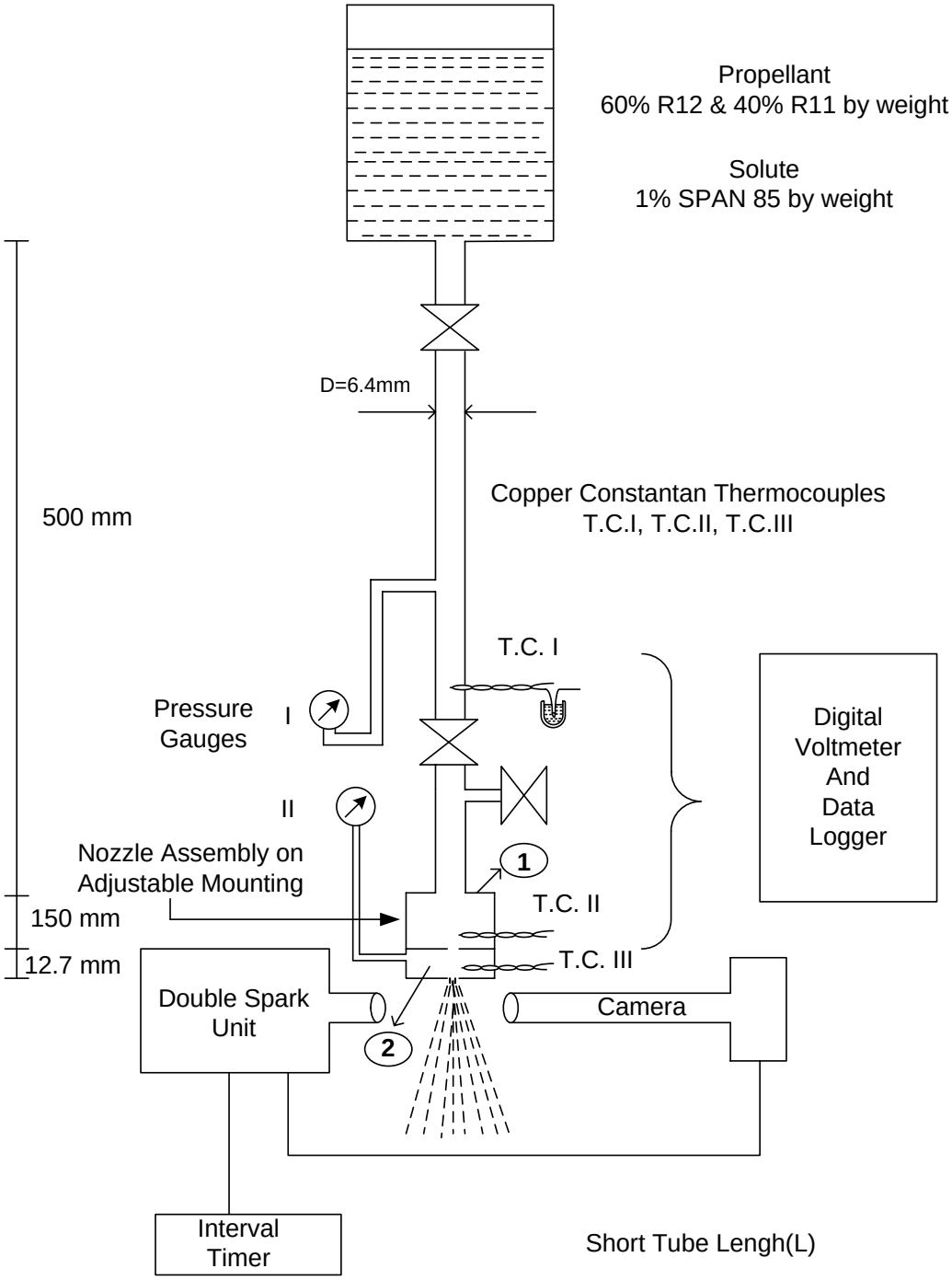

(1) Nozzle Assembly: Assembled with a 150 mm long and diameter of 3.2 mm perspex tube in a brass cylinder

(2) Expansion Chamber : D_{ec} = 3.2 mm & L_{ec}=12.7 mm

Figure 7.1 Schematic diagram of the Fletcher's (1975) experimental setup (Not to scale)

CCl_3F) by weight. Figure 7.1 shows a schematic view of the experimental set up for continuous discharge. A brass bottle supplied saturated liquid propellant via a flexible feed-pipe to a nozzle assembly mounted on a support capable of movement in two dimensions. The emerging spray was photographed by a double-exposure photo micrographic unit at the nozzle exit. Pressures and temperature were measured at the various positions indicated in the Figure 7.1. The nozzle assembly consisted of two-orifices separated by an expansion chamber. These were assembled together with a 150 mm long Perspex tube, in a brass cylinder. The Perspex nozzles were transparent and dismountable.

Fletcher experimental data had the following geometry and operating conditions:

- Expansion chamber (ec): D_{ec} = 3.2 mm, L_{ec} = 12.7 mm.
- Hydraulic roughness of all surfaces: ε = 1.5 μm.
- Ambient pressure 1.013 bar, which is the discharge pressure acting as the downstream boundary condition.
- The dimensions of valve orifice (vo) and spray orifice (so) and the inlet conditions are shown in Table 7.1.
- The propellant assumed to be in saturated state at the entrance of the valve orifice.

Table 7.1 Geometry details and inlet conditions

Nozzle	D_{vo} (μm)	L_{vo} (μm)	D_{so} (μm)	L_{so} (μm)	T_{in} (°C)	D_{so}/D_{vo}
250 x 350	250	390	350	400	19.55	1.400
320 x 350	320	420	350	400	19.7	1.094
320 x 450	320	420	450	370	20.1	1.406
320 x 700	320	420	700	765	20.6	2.188
450 x 350	450	660	350	400	20	0.778
450 x 450	450	660	450	370	20	1.000
450 x 700	450	660	700	765	20.3	1.556
640 x 350	640	675	350	400	20.4	0.547
640 x 450	640	675	450	370	20.1	0.703
680 x 700	680	730	700	765	20.15	1.029

7.2.1.2. Results and Discussion

Distribution of flow variables along the twin-orifice system

The predicted distributions of pressure, temperature, void fraction and velocity for the continuous discharge of propellant R12/R11 (60%/40%) for the case D_{vo} = 450 μm and D_{so} = 350 are shown in Figure 7.2 to Figure 7.4. These give the profiles of flow variables along the length of the two-orifice system. The solid line in Figure 7.2 shows the distribution of pressure starting just upstream of the valve orifice (z<0). The dashed vertical lines at z=0 and z=0.00066 m indicate the valve orifice (vo). The range z = 0.00066 – 0.01336 m to next dashed vertical line covers the expansion chamber (ec) and finally the range z = 0.01336 – 0.01376 m represents the spray orifice (so) at the exit of which the condition are ambient. The sudden pressure drop at the inlet (z=0) is due to flow acceleration at the abrupt entry to the valve orifice. The pressure drops linearly due to the effects of evaporation and acceleration inside the valve orifice. Thereafter the pressure remains almost constant inside the expansion chamber which has a much larger diameter and hence low flow velocities. The next large pressure drop at the entrance of the spray orifice (z = 0.01336 m) is due to rapid fluid acceleration in the abrupt entry to the spray orifice. The propellant pressure drops along the spray orifice due to the acceleration and frictional effects. The large pressure drop at the exit plane of the spray orifice indicates that the flow is choked.

As the fluid inside the twin-orifice system is in two-phase metastable state, following Zhou and Zhang (2006) the average propellant temperature is computed using equation (3.18). The dashed line in Figure 7.2 show the temperature distribution for nozzle D_{vo} = 450 μm and D_{so} = 350. These profiles are similar to that of pressure profile. In adiabatic flow, the temperature of the mixture is closely related to evaporation, which extracts latent heat from the mixture. Rapid evaporation takes place near the exit of the spray orifice, so the temperature decreases abruptly by about 50°C in this region. This rapid evaporation is highlighted by Figure 7.3 which shows the distribution of quality and vaporisation index for nozzle D_{vo} = 450 μm and D_{so} = 350 along the twin-orifice system. The quality increases in regions where the temperature decreases. This starts inside the valve orifice where the quality increases very slightly due to the start of vapour formation. Next, it increases gradually as the fluid enters the spray orifice and metastable liquid gets converted into saturated

mixture. The rapid increase in the quality at the exit of the spray orifice is due to choked conditions. For choked conditions, the discharge shock is solved at the exit of spray orifice assuming the propellant completes adiabatic evaporation from metastable choked conditions to atmospheric pressure, due to which high quality is obtained evaluated at the spray orifice exit. From the Figure 7.3 it can be seen that the vaporisation index (y) is zero at the inlet which indicates that the entire liquid is in metastable state due to the abrupt drop in pressure at the inlet of the valve orifice. The vaporisation index increases inside the valve orifice, expansion chamber and spray orifice. The sudden decrease in y at the entrance of the spray orifice (z = 0.0134m) indicates that the more saturated liquid gets converted into metastable state due to sudden pressure drop across the abrupt contraction.

The sudden change in the flow variables (temperature, quality, vaporisation index, void fraction and velocity) from the exit of the valve orifice to middle of the expansion chamber (z = 0.00754 m) in Figure 7.2 to Figure 7.4 is due to the use of single CV at the exit of valve orifice (z = 0.0006 m) to integrate the relaxation equation (equation 3.46) across the gradual conical expansion over a length z = 0.00754 m. This increases the vaporisation index across the conical expansion, indicating metastable liquid is converted into saturated mixture, which causes temperature to decrease and quality to increase across the expansion. This shows kink in these profiles across the abrupt expansion.

Figure 7.4 shows the predicted distribution of void fraction and velocity along the two-orifice system. The void fraction increases as pressure decreases – rapidly where the pressure reduction is abrupt. The void fraction profiles are similar to that of quality profiles, but it should be noted that the exit quality of the system is around 20%, whereas the void fraction is just below 100% due to the large density difference between liquid and vapour.

The velocity is found to increase due to (i) area reduction, e.g. in abrupt contractions and (ii) void fraction increases. The sonic velocity prevails at the spray orifice exit and is around 20m/s.

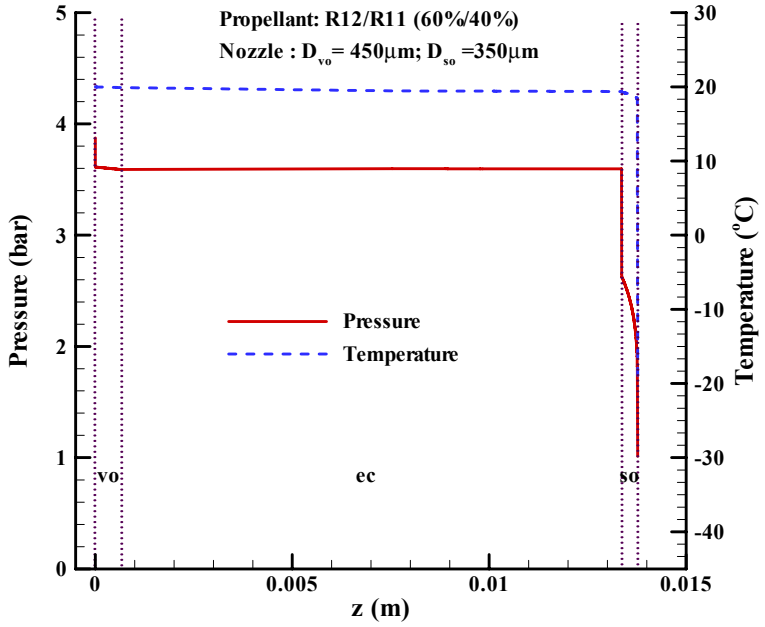

Figure 7.2 Predicted pressure and temperature profiles for nozzle D_{vo} = 450 μm and D_{so} = 350 μm

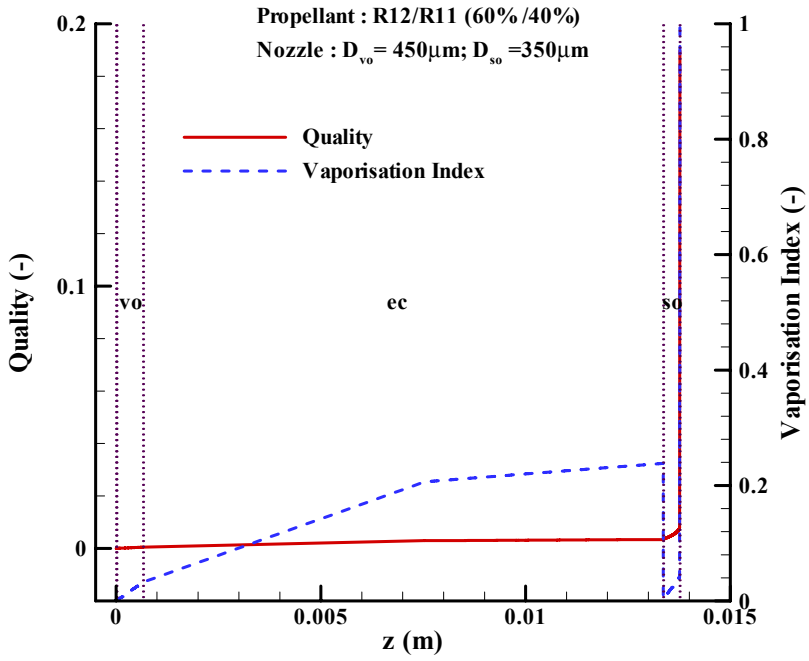

Figure 7.3 Predicted quality and vaporisation index for nozzle D_{vo} = 450 μm and D_{so} = 350 μm

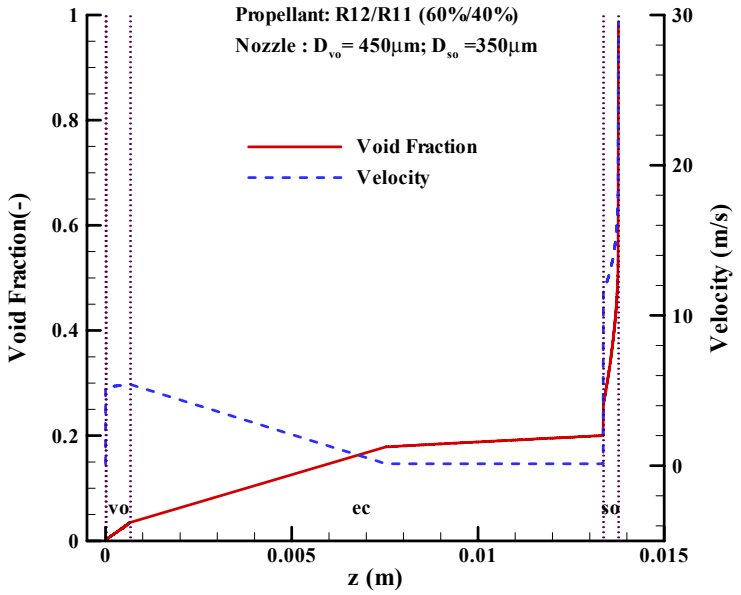

Figure 7.4 Predicted void fraction and velocity for nozzle D_{vo} = 450 μm and D_{so} = 350 μm

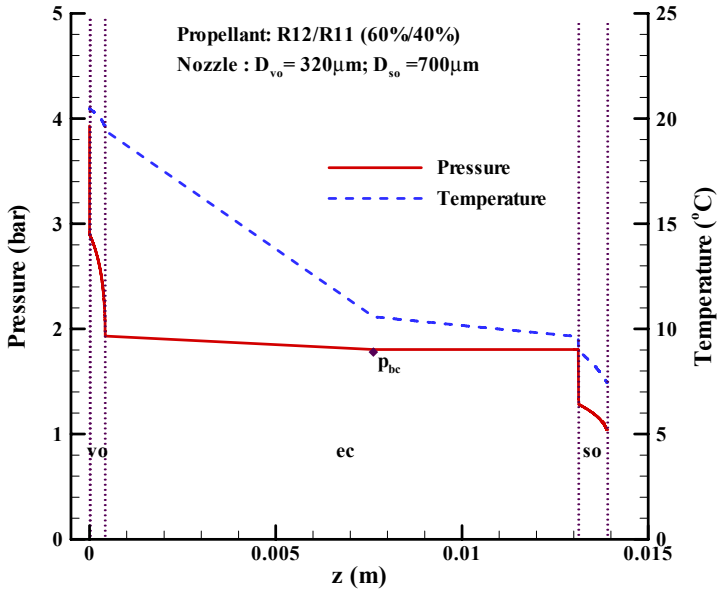

Figure 7.5 Predicted pressure and temperature profiles for nozzle D_{vo} = 320 μm and D_{so} = 700 μm

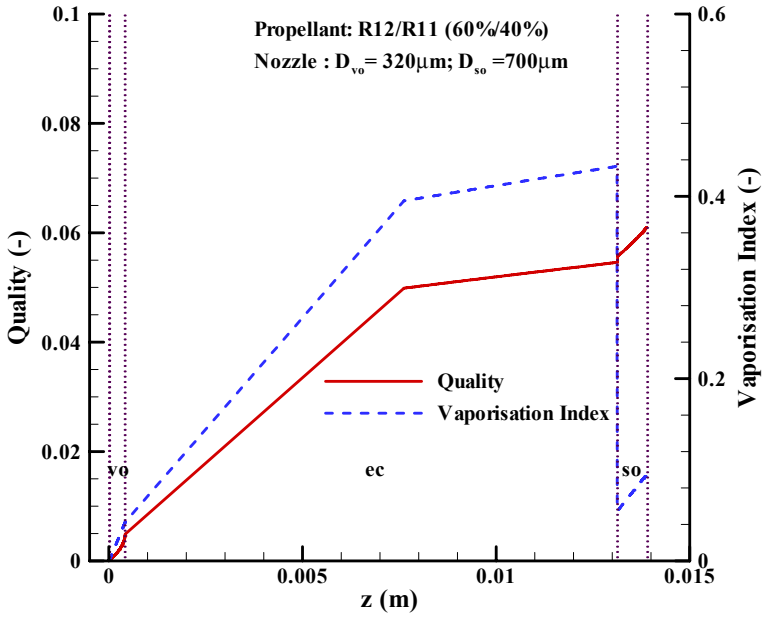

Figure 7.6 Predicted quality and vaporisation index for nozzle D_{vo} = 320 μm and D_{so} = 700 μm

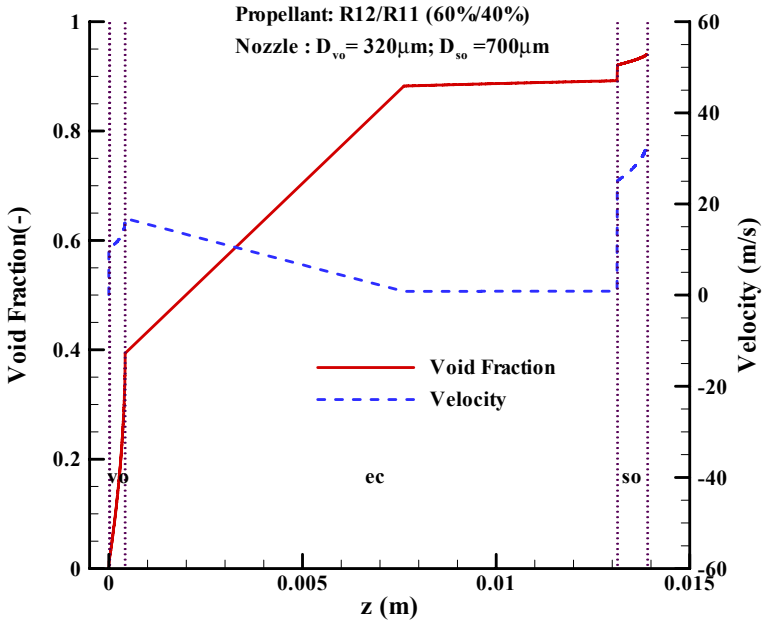

Figure 7.7 Predicted void fraction and velocity for nozzle D_{vo} = 320 μm and D_{so} = 700 μm

These trends are representative of those predicted by the other nozzle combinations except nozzle D_{vo} = 320 μm and D_{so} = 700. For this case, where the downstream orifice is large, the predicted profiles of the flow variables are considerably different from that mentioned above. The present DEM with k_y = 0.02 predicts more evaporation inside the valve orifice due to which it predicts choking at the exit of the valve orifice instead of spray orifice exit.

Figure 7.5 shows the pressure and temperature distribution along the two-orifice system for D_{vo} = 320 μm and D_{so} = 700. The sudden pressure drop at the inlet (z = 0) is due to flow acceleration. The pressure drops non-linearly inside the valve orifice mainly due to acceleration effects associated with rapid evaporation. The large pressure drop at the exit plane of the valve orifice indicates that the flow is choked. Thereafter, the pressure remains constant inside the expansion chamber. The next large pressure drop at the entrance of the spray orifice (z = 0.01315m) is due to rapid fluid acceleration in the abrupt entry to the spray orifice. The propellant pressure drops along the spray orifice due to the acceleration and frictional effects. The diamond symbol in the Figure 7.5 highlights the evaluated back pressure, p_{bc}, using the base pressure algorithm (4.4.1.4). Figure 7.5 also shows the temperature distribution for D_{vo} = 320 μm and D_{so} = 700. These profiles are similar to that of pressure profile.

Figure 7.6 shows the distribution of quality and vaporisation index for D_{vo} = 320 μm and D_{so} = 700 along the twin-orifice system. The quality increases rapidly inside the valve orifice due to vapour formation and rapid pressure drop inside the valve orifice which decreases the temperature. It increases gradually inside the expansion chamber and increases further inside the spray orifice as more metastable liquid gets converted into saturated mixture. From the Figure 7.6 it can be seen that the vaporisation index (y) is zero at the inlet which indicates that the entire liquid is in a metastable state. The vaporisation index increases inside the valve orifice, expansion chamber and spray orifice. The sudden decrease in 'y' at the entrance of the spray orifice (z = 0.01315 m) indicates that the more saturated liquid gets converted into the metastable state due to the sudden pressure drop across the abrupt contraction.

Figure 7.7 shows the distribution of void fraction and velocity along the two-orifice system for D_{vo} = 320 μm and D_{so} = 700. The void fraction increases as pressure decreases – rapidly where the pressure reduction is abrupt. The void fraction profile is similar to that of quality. The rapid increase in the void fraction at the exit of the valve orifice indicates choking flow at the exit plane. The velocity is found to increase due to (i) area reduction, e.g. in abrupt contractions and (ii) void fraction increases. The velocity reaches to sonic velocity at the exit plane of the valve orifice, indicating the flow is choked at the exit plane.

The main difference between this case (D_{vo} = 320 μm and D_{so} = 700) and the previous case (D_{vo} = 450 μm and D_{so} = 350) is the location of choking. In the latter case the flow is choked at the exit of the spray orifice whereas in the former case, choking occurs at the exit of the valve orifice and the flow is subsonic at the exit of spray orifice.

Comparison of Mass Flow Rate

Figure 7.8 presents a comparison of the predicted mass flow rate against the experimental mass flow rate. The ordinate represents the mass flow rate in kg/s, the abscissa is expressed as the ratio of the diameter of the spray orifice (D_{so}) to the diameter of the valve orifice (D_{vo}), which is given in Table 7.1 for all nozzle combination. The particular choice of abscissa was made by Clark (1991) for two reasons: (i) in a continuous equilibrium discharge system the expansion chamber conditions would be expected to be the same for a given ratio regardless of the absolute diameters of orifices themselves. (ii) the ratio of the diameters has the property that it tends to zero when the valve orifice is large and only the spray orifice is present and that it tends to infinity when the spray orifice is large and only valve orifice is present. In general, it can be seen that the present DEM predicts the mass flow rate quite well with an average error of 11.6% and a maximum error of 38% for nozzle D_{vo} = 680 μm and D_{so} = 700 with D_{so}/D_{vo}=1.029. This result implies that, for large valve and spray orifice diameters, the DEM with k_y = 0.02 predicts more metastability then the actual flow causing overprediction of the mass flow rate.

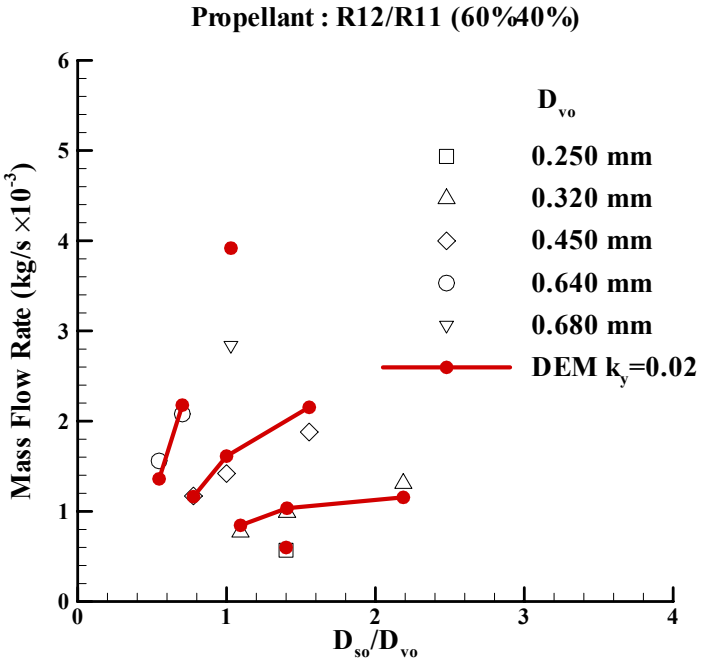

Figure 7.8 Comparison of mass flow rate against Fletcher's (1975) experimental mass flow rate

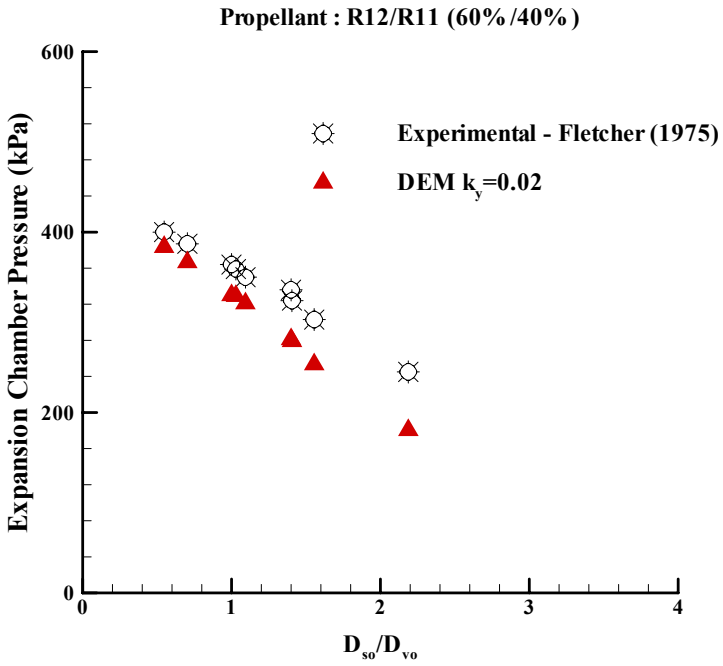

Figure 7.9 Comparison of expansion chamber pressure against Fletcher's (1975) measured expansion chamber pressure

Comparison of expansion chamber pressure (p_{ec})

The comparison between the numerically predicted and measured expansion chamber pressure is presented in Figure 7.9. It can be observed that the present DEM predicts the expansion chamber quite close to the experimental data with an average error of 12%. From the graph it can be observed that for low diameter ratios, $D_{so}/D_{vo,}$ the predicted expansion chamber pressure are very close to the experimental. The discrepancies are large for nozzle D_{vo} = 320 μm and D_{so} = 700. As noted previously the present DEM with k_y = 0.02 predict more evaporation then the actual flow, which causes high pressure drop due to fluid acceleration inside the valve orifice and hence the low expansion chamber pressure.

Comparison of expansion chamber temperature (T_{ec})

The average propellant temperature is computed using equation (3.18). Figure 7.10 shows the comparison of predicted expansion chamber temperature against the measure temperature. From the figure it can be seen that the expansion chamber temperatures are predicted well by the present DEM with an average error of 7.3%. In line with the expansion chamber pressure results of Figure 7.9, the expansion chamber temperature decreases with increase in D_{so}/D_{vo} ratio.

Comparison of exit velocity

Figure 7.11 shows the comparison of predicted exit velocity against the experimental exit velocities of Fletcher (1975). The predicted exit velocities are evaluated after the shock using equation (3.55). From the figure it can be observed that the present numerical predictions generally overpredict the exit velocity slightly, but estimates of the exit velocity are close to the experiment with an average error of 15%. For orifice diameter ratio, D_{so}/D_{vo} =2.18 (corresponding to nozzles 320 x 700), the overprediction is highest because the present DEM predicts sonic velocity at the exit of the valve orifice and not at the exit of the spray orifice. Also, it should be noted that the experimental errors associated with the exit velocities may be substantial as they were calculated indirectly from the photographs. In spite of this, model predictions are quite accurate.

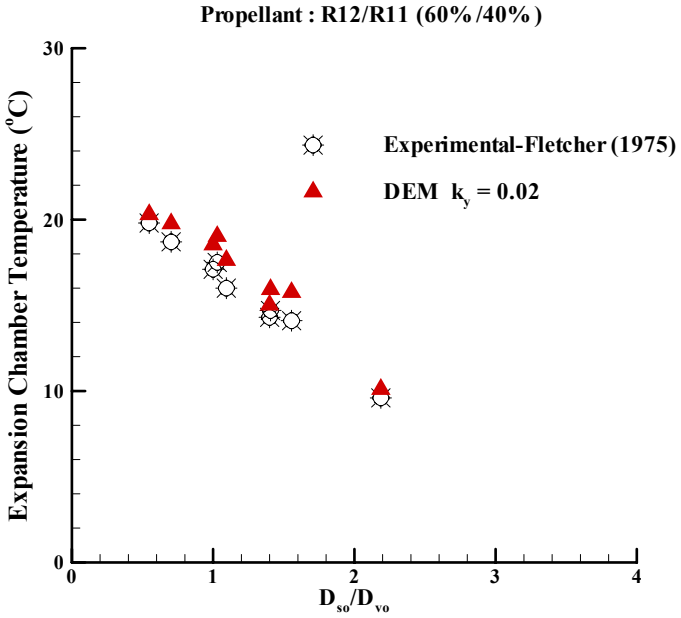

Figure 7.10 Comparison of expansion chamber temperature against Fletcher's (1975) measured expansion chamber temperature

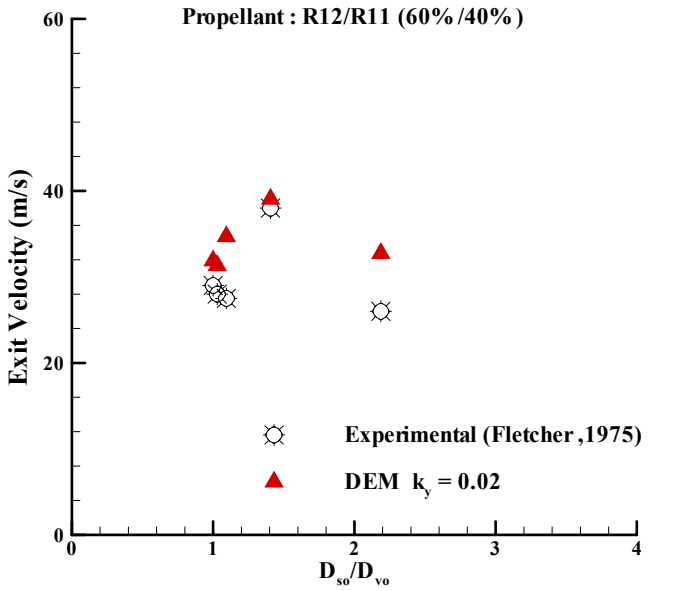

Figure 7.11 Comparison of exit velocity against Fletcher's (1975) measured exit velocity

7.2.2. Comparison against Clark's (1991) experimental data with k_y = 0.02

In this section, the results obtained using the DEM with coefficient k_y=0.02, in the relaxation equation (3.9) are compared against Clark's (1991) experimental work.

7.2.2.1. Test Case

Clark (1991) carried out an extensive program of measurements on continuous discharges for a wide range of combinations of valve and spray orifice diameter and a variety of propellants (R12, R134A, R227 and a mixture of R12/R114). Combination of five valve orifices and nine spray orifices of which four instrumented and five plastic non-instrumented were used. Instrumented orifices were used to measure the expansion chamber pressure and temperature along with the mass flow rate, whereas the non-instrumented (plastic) orifices were used only to measure the mass flow rate. The main difference in the experimental setup between the Clark (1991) and Fletcher (1975) are:

- The base of the propellant reservoir was directly connected to the inlet ports of valve assembly via a brass manifold to ensure negligible propellant pressure head.
- The spray orifice was at right angles to the flow in the valve stem.

Both these modifications make the experimental setup resemble the actual pMDI more closely and therefore bring the test results closer to the final application. From the point of view of the model, the former reduces the (unknown) amount of subcooling that was present in Fletcher's test due to reservoir head. The latter modification improves the spray forming performance of certain combinations of valve and spray orifice by preventing the impact of a jet of propellant liquid on to the spray orifice. From a modeling standpoint, the regime of flow is assumed to be homogeneous and the velocities in the expansion chamber are comparatively low. If these modelling assumptions are correct, the contribution of the right angle bend to the flow development and evaporation is likely to be modest.

The test cases used for the present study are taken from Clark's (1991) experimental work which has the following geometry and operating conditions:

- The length of the valve orifice and spray orifices were kept constant: L_{vo} = 0.5425 mm and L_{so} = 1 mm.
- The diameters of valve and spray orifices and the diameter ratios are given in Table 7.2
- Expansion chamber: D_{ec} = 3.8 mm, L_{ec} = 11 mm
- Hydraulic roughness of all surfaces: ε = 1.5 µm
- Ambient pressure 1.013 bar, which is the discharge pressure acting as the downstream boundary condition
- The liquid at the inlet of valve orifice is assumed to be in saturated state. So, ambient temperature (T_{in}) 291 K, defines the inlet conditions of the valve orifice.

Table 7.2 Orifice diameter ratios for continuous discharge flows

Valve Orifice Diameter (D_{vo}) (µm) →	259	420	589	823	1005
Spray Orifice Diameter (Instrumented) (D_{so}) (µm) ↓	Diameter Ratio (D_{so}/D_{vo})				
294	1.135	0.700	0.499	0.357	0.293
479	1.849	1.140	0.813	0.582	0.477
598	2.309	1.424	1.015	0.727	0.595
1023	3.950	2.436	1.737	1.243	1.018
Plastic Spray Orifices	Diameter Ratio (D_{so}/D_{vo})				
425	1.641	1.012	0.722	0.516	0.423
565	2.181	1.345	0.959	0.687	0.562
725	2.799	1.726	1.231	0.881	0.721
975	3.764	2.321	1.655	1.185	0.970
1147	4.429	2.731	1.947	1.394	1.141

7.2.2.2. Results and Discussion

Distribution of flow variables along the twin-orifice system

Figure 7.12 to Figure 7.17 show the predicted distributions of flow variables (pressure, temperature, quality, vaporisation index, void fraction and velocity) for the continuous discharge of propellant R134A for a valve orifice D_{vo} = 420μm in conjunction with two different spray orifices (D_{so} = 479μm and D_{so} = 1023μm). These give the profiles of flow variables along the length of the twin-orifice system. These trends are representative of those predicted with other nozzles.

Figure 7.12 shows the distribution of pressure and temperature along the twin-orifice system. The abrupt pressure drop at the inlet (z = 0) is due to abrupt contraction. Then the pressure decreases linearly inside the valve orifice mainly due to acceleration effects. The pressure is almost constant inside the expansion chamber due to the large diameter. The next large pressure drop at the entrance of the spray orifice (z = 0.01336 m) is due to abrupt contraction. Thereafter, the pressure decreases rapidly inside the spray orifice due to acceleration effects and more evaporation. The temperature profiles are similar to that of pressure profiles. In spite of the different propellant (R134A), these trends are very similar to those of Fletcher's case (D_{vo} = 450 μm and D_{so} = 350 μm shown in Figure 7.2 - Figure 7.4). The main difference between this case and Fletcher's case is that significant pressure drop is observed across the valve orifice for the current case, whereas for Fletcher's case the pressure drop across the valve orifice is almost constant. This is caused by the substantial differences in the orifice diameter ratio D_{so}/D_{vo} (0.78 for Fletcher's case and 1.14 for Clark's case.

Figure 7.13 shows the distribution of quality and vaporisation index along the twin-orifice system. These trends are similar to those of Figure 7.3 (Fletcher's case: D_{so} = 450 μm and D_{so} = 350 μm). The predicted exit quality for the Fletcher case is nearly 20% whereas for the current case is nearly 28% as a consequence of the higher volatility of R134A. Figure 7.14 show the distribution of void fraction and velocity along the twin-orifice system. Again, these trends are similar to that of Figure 7.4

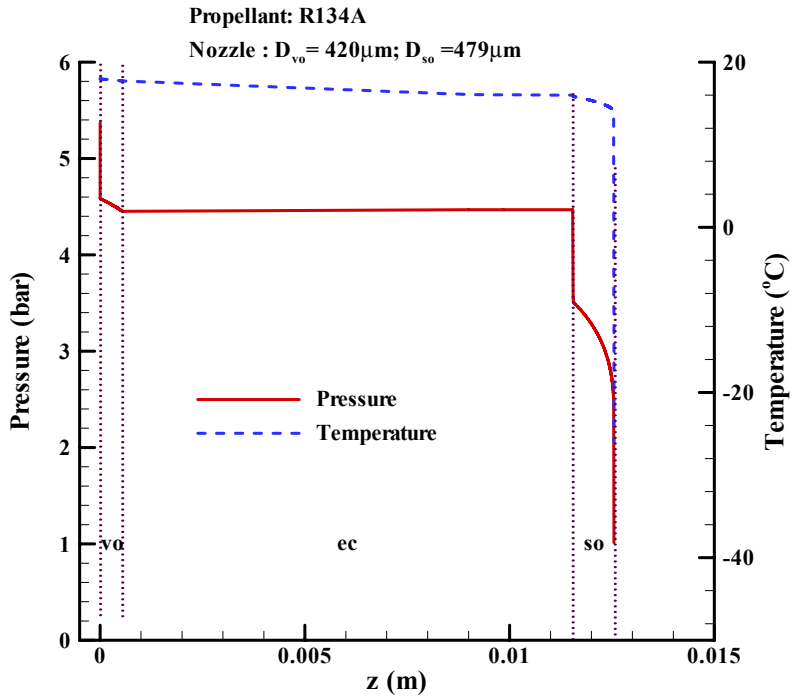

Figure 7.12 Predicted pressure and temperature profiles for nozzle D_{vo} = 420μm and D_{so} = 479 μm

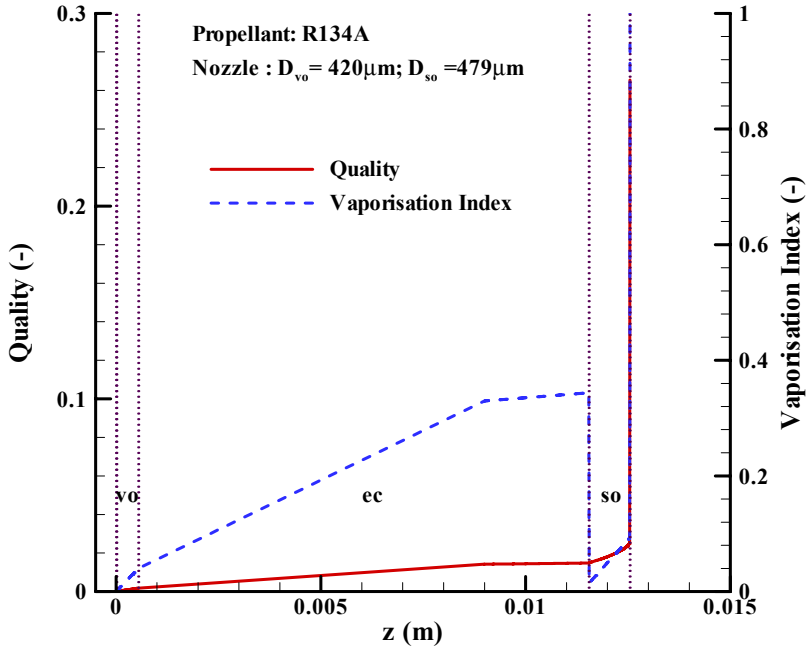

Figure 7.13 Predicted quality and vaporisation index for nozzle D_{vo} = 420μm and D_{so} = 479 μm

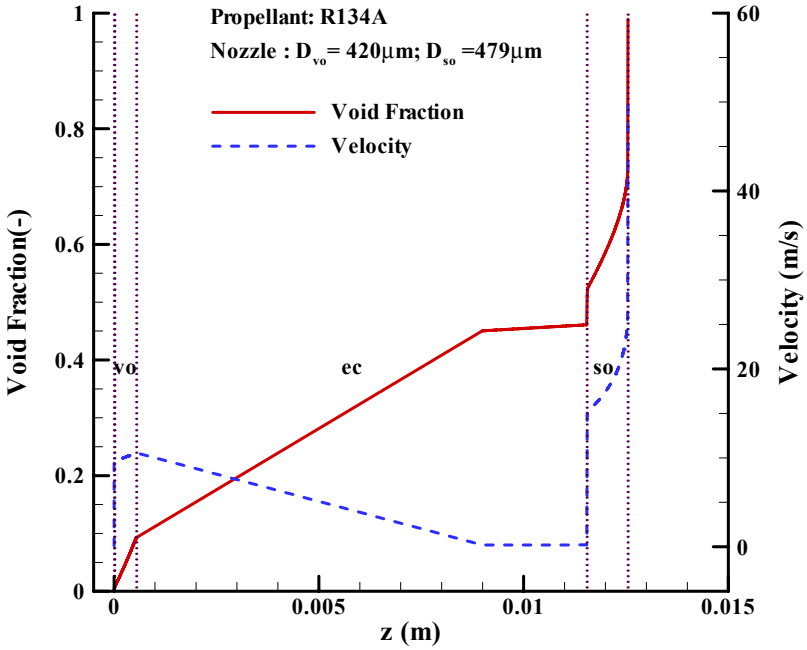

Figure 7.14 Predicted void fraction and velocity for nozzle D_{vo} = 420µm and D_{so} = 479 µm

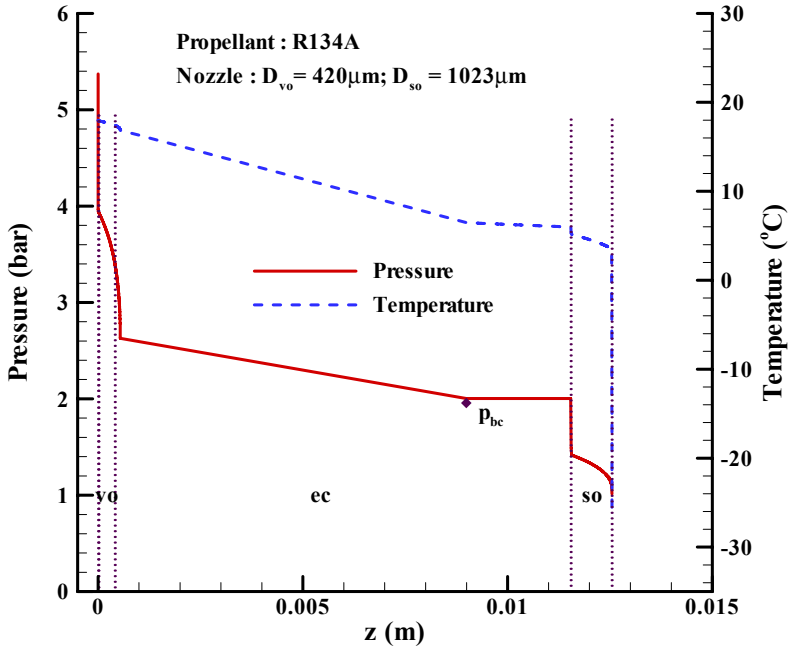

Figure 7.15 Predicted pressure and temperature profiles for nozzle D_{vo} = 420µm and D_{so} = 1023 µm

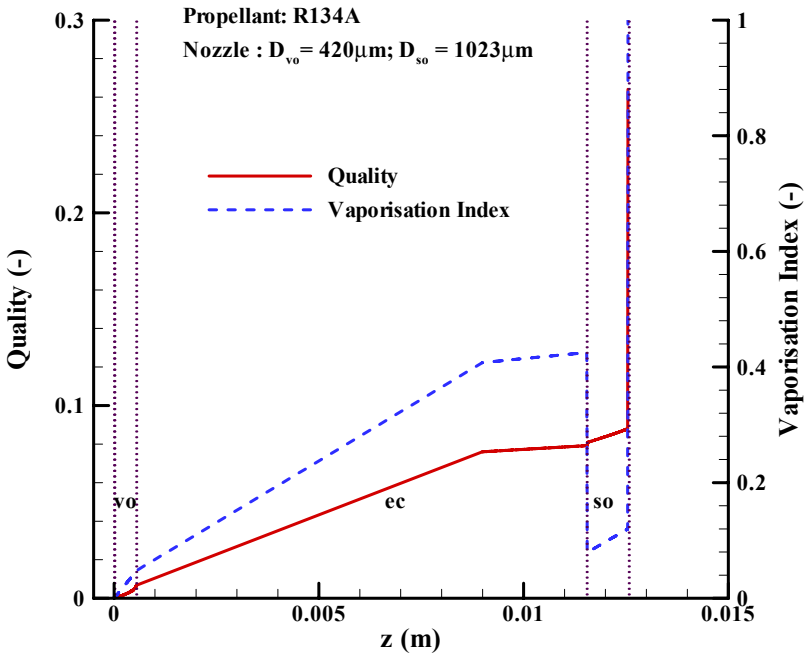

Figure 7.16 Predicted quality and vaporisation index for nozzle D_{vo} = 420µm and D_{so} = 1023 µm

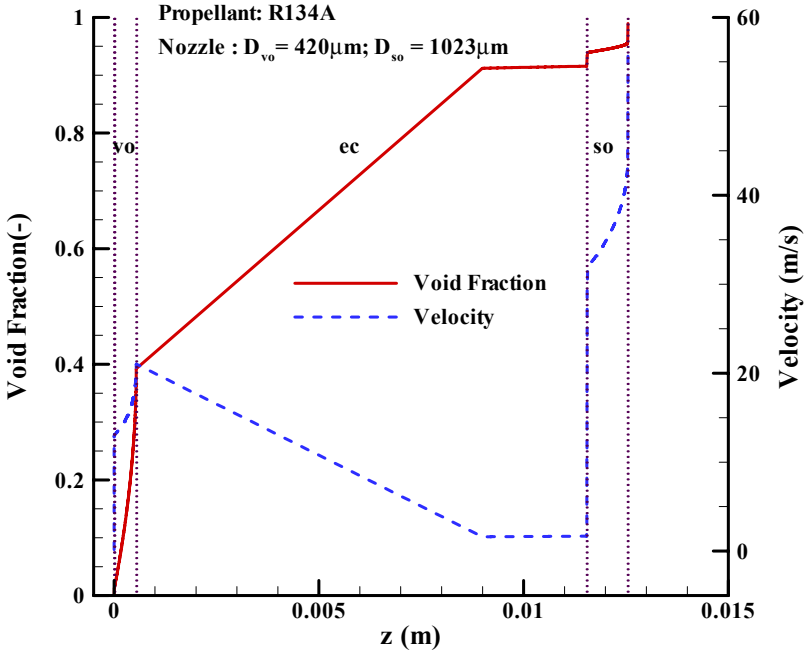

Figure 7.17 Predicted void fraction and velocity for nozzle D_{vo} = 420µm and D_{so} = 1023 µm

(Fletcher's case: D_{so} = 450 μm and D_{so} = 350 μm). The exit velocities for Fletcher's case are nearly 30 m/s, whereas the velocities for the current case is nearly 60 m/s.

Similarly, Figure 7.15 to Figure 7.17 show the distribution of the flow variables (pressure, temperature, quality, vaporisation index, void fraction and velocity profiles) for the nozzle combination D_{vo} = 420μm and D_{so} = 1023 μm. These profiles are similar to those of Fletcher's nozzle combination D_{vo} = 320μm and D_{so} = 700μm discussed in the section (7.2.1.2), which predicts the choking at the exit of the valve orifice. An interesting difference between these two cases is that Fletcher's case (D_{vo} = 320μm and D_{so} = 700μm) predicts choking only at the exit of valve orifice, whereas for the current case double choking is observed. DEM predicts choking both at the exit of the valve orifice and as well as at the exit of spray orifice. The rapid decrease in the pressure and temperature at the valve orifice exit and the spray orifice exit indicate that the flow is choked at the end both orifices. Sonic velocities prevail at the end of valve and spray orifice with values equal to 20 m/s and 55 m/s, respectively.

Comparison of Mass Flow Rate

Figure 7.18 shows the comparison of the computed mass flow rate against the Clark's (1991) experimental mass flow rate for four different propellants : (a) R12, (b) R134A (c). R12/R114 (60%40%) and (d) R227. Overall, the evaluated mass flow rates are in good agreement with the experimental mass flow rates with some discrepancies. The DEM with k_y = 0.02, predicts the mass flow rate with some discrepancies. The percentage of error is defined as:

$$\% \text{ error} = \left(\frac{\left| \dot{m}_{num} - \dot{m}_{\exp} \right|}{\dot{m}_{\exp}} \right) \times 100$$

where

$\dot{m}_{num}$ = numerically predicted mass flow rate (kg/s)

$\dot{m}_{\exp}$ = experimentally measured mass flow rate (kg/s)

The average error is calculated as sum of absolute percentage of errors divided by number of cases. The DEM predicts the mass flow rate with an average error of 26.8% and a maximum error of 88.9% for nozzle D_{vo} = 1005μm and D_{so} = 975μm.

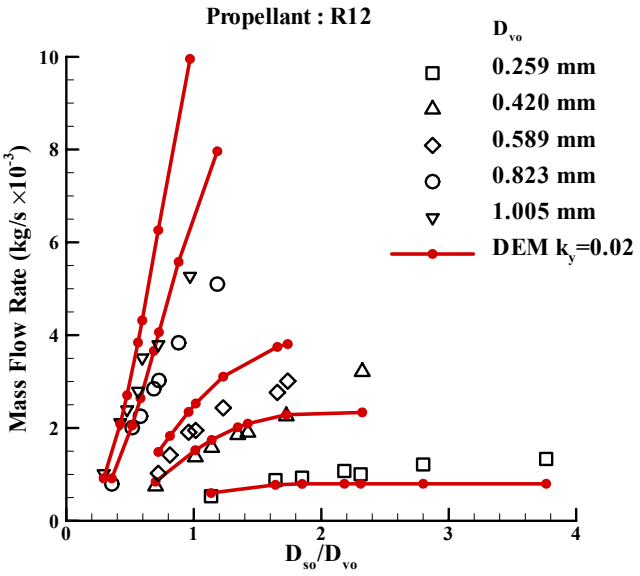

(a) R12

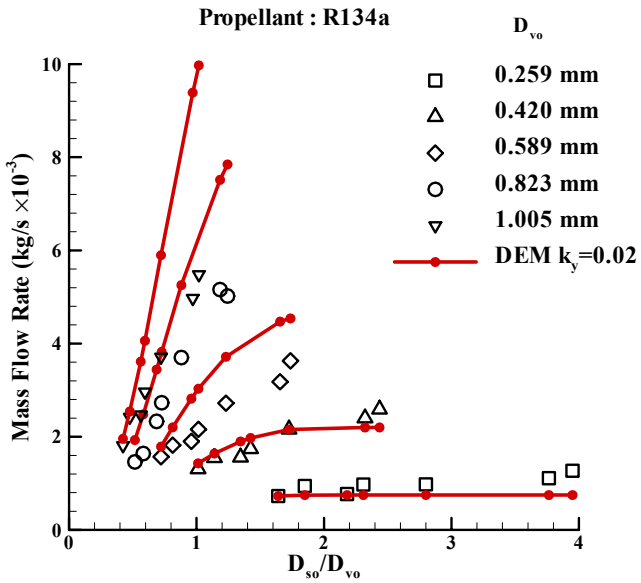

(b) R134A

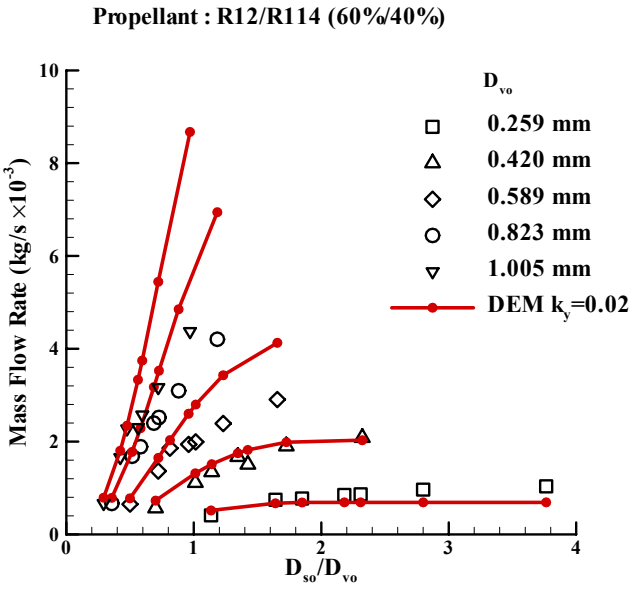

(c) R12/R114 (60%/40%)

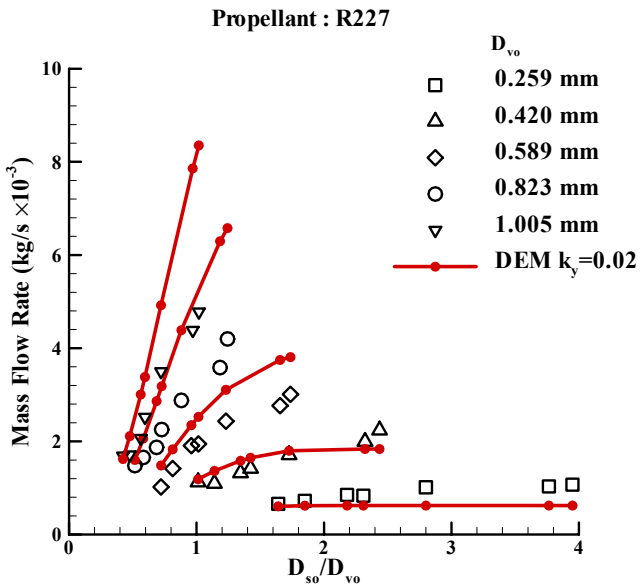

(d) R227

Figure 7.18 Comparison of mass flow rate against Clark's (1991) experimental data for four different propellants: (a) R 12 (b) R134A (c) R12/R114 (60%/40%) and (d) R227 with k_y = 0.02

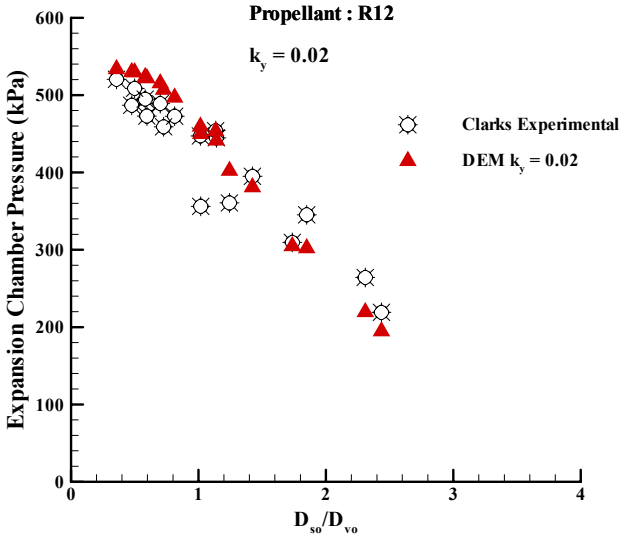

(a) R 12

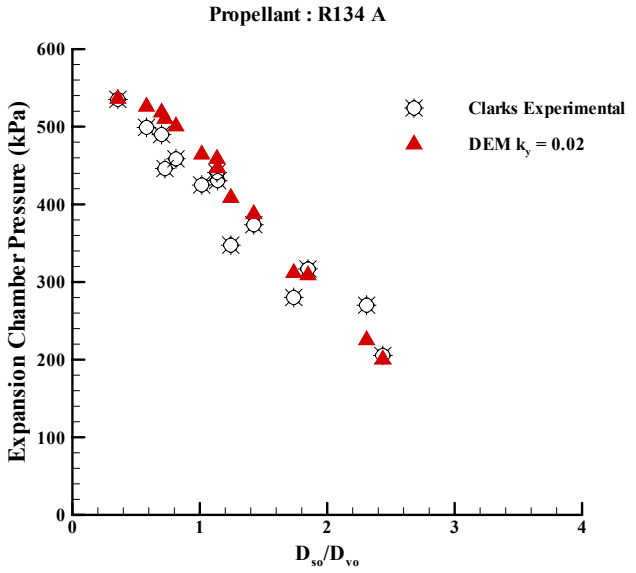

(b) R134A

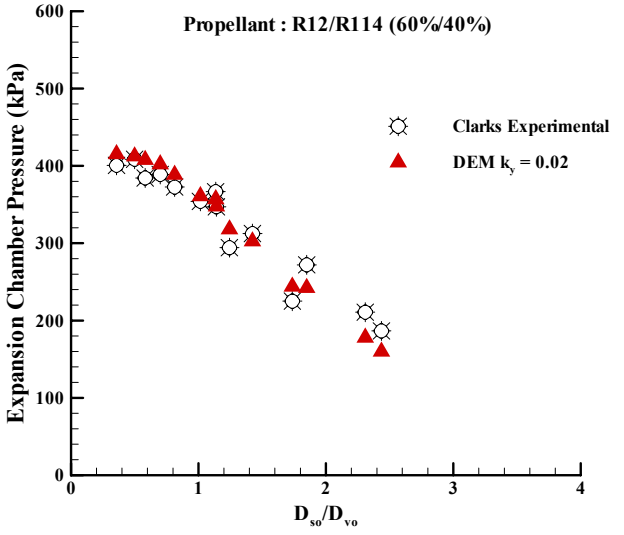

(c)R12/R114 (60%/40%)

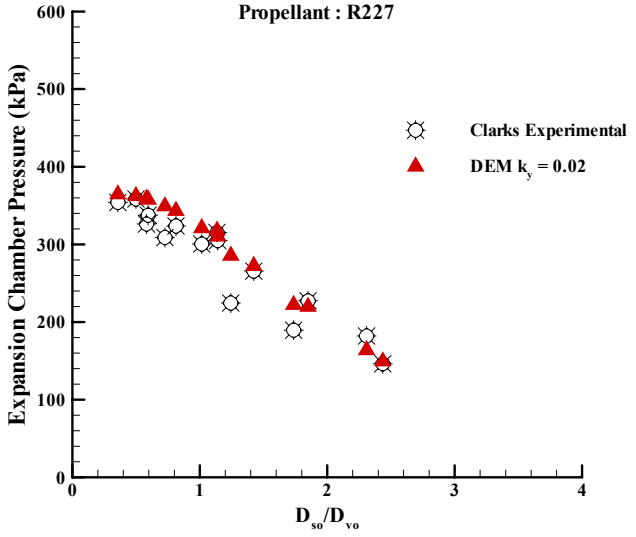

(d) R227

Figure 7.19 Comparison of expansion chamber pressure against Clark's (1991) experimental data with four different propellants: (a) R 12 (b) R134A (c) R12/R114 (60%/40%) and (d) R227 with $k_y = 0.02$

For the small valve orifices (D_{vo} = 259 μm and D_{vo} = 420 μm), the present DEM under predicts the mass flow rate as the diameter of the spray orifice becomes large in comparison to that of the valve orifice (i.e. at large D_{so}/D_{vo} ratios). This is because, DEM with k_y = 0.02 predicts more evaporation inside the valve orifice than the actual flow, due to which sonic velocities are obtained at the exit of the valve orifice for $D_{so}/D_{vo} > 2$. Whereas for large valve orifices (D_{vo} = 589 μm, D_{vo} = 823 μm and 1005 μm) as the spray orifice diameter increases DEM with k_y = 0.02 predicts more metastable flow then the actual flow, due to which it overpredicts the mass flow rate.

Comparison of expansion chamber pressure (p_{ec})

Figure 7.19 shows the comparison of predicted expansion chamber pressure with Clark's (1991) measured values for four propellants and various orifice combinations. The evaluated expansion chamber pressure generally shows good agreement with the experimental results. The DEM with k_y = 0.02 predicts the expansion chamber pressures with an average error of 7.2% and a maximum error of 21.7%. From the figure it can be seen that the present DEM slightly overpredicts the expansion chamber pressure for low D_{so}/D_{vo} ratios and tends to underpredict for high D_{so}/D_{vo} ratios.

Comparison of temperature drop across the valve orifice (ΔT_{vo})

Figure 7.20 shows the comparison of predicted temperature drop across the valve orifice with the measured temperature drop by Clark (1991) for four propellants and various orifice combinations. The DEM with k_y = 0.02 predicts the temperature drop across the valve orifice with an average error of 65.4% and a maximum error of -98.7%. The errors are large for low D_{so}/D_{vo} ratios i.e. for large valve orifice diameter. Whereas for large D_{so}/D_{vo}, the predicted temperature drop across the valve orifice is closer to the experimental data. The large discrepancies between the predicted and experimental values may be attributed to the uncertainties associated with the experiments as well as the definition of the predicted temperature (equation 3.18). It should be noted that, ΔT_{vo} is hard to predict accurately than expansion chamber temperature (T_{ec}). On a percentage basis the error looks much larger for ΔT_{vo} then T_{ec}, since the valve of ΔT_{vo} tend to zero as D_{so}/D_{vo} tend to zero. Though the errors are large the DEM with k_y = 0.02 follows the experimental trend nicely.

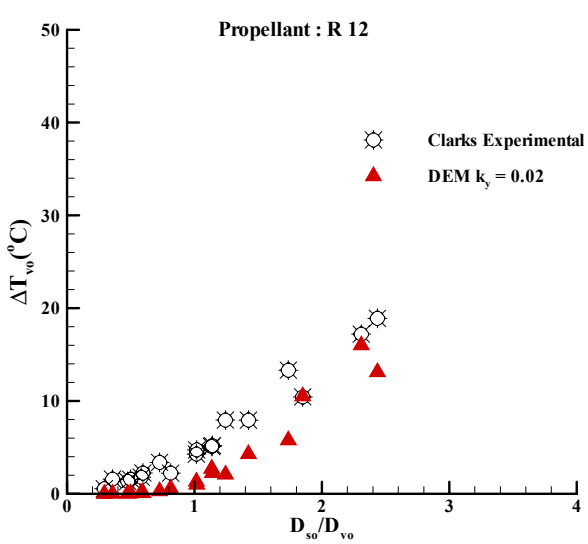

(a) R 12

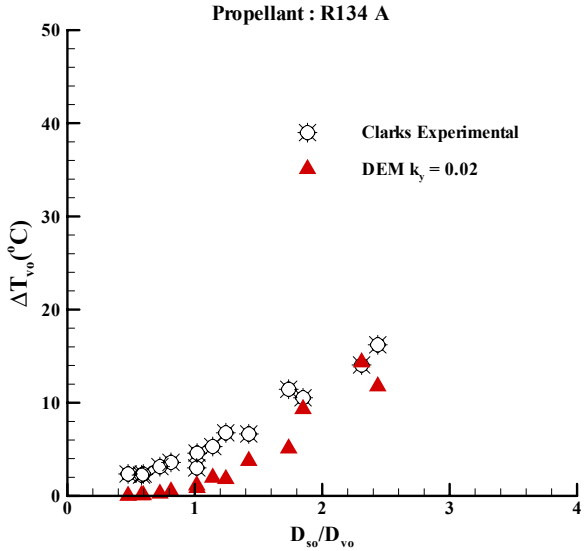

(b) R134A

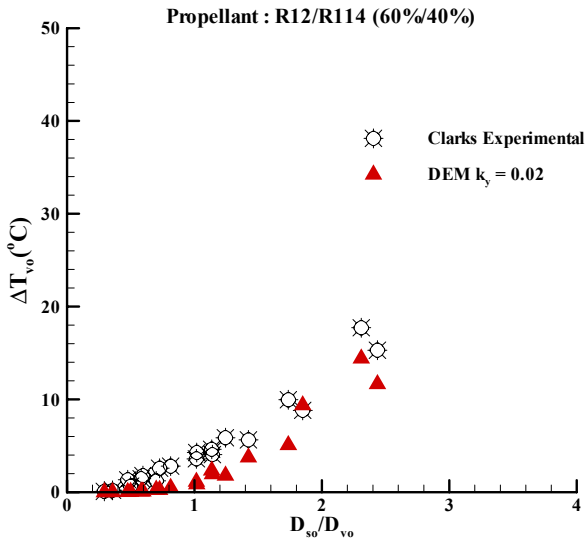

(c)R12/R114 (60%/40%)

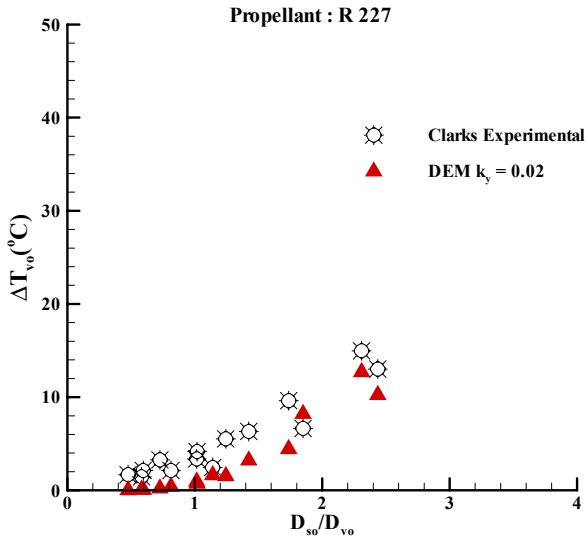

(d) R227

Figure 7.20 Comparison of temperature drop across the valve orifice against Clark's (1991) experimental data for four different propellants: (a) R 12 (b) R134A (c) R12/R114 (60%/40%) and (d) R227 with k_y = 0.02

Comparison of spray orifice discharge velocity

Figure 7.21 - Figure 7.24 show the comparison of evaluated discharge velocities (spray velocities) against the Clark's measured exit velocities, when the flow is choked at the exit of valve orifice and spray orifice for four different propellants. These velocities are evaluated using equation (3.55) after the shock. The discharge velocity includes the acceleration effect caused by the pressure difference between the choking pressure and ambient pressure. For the cases, where the flow is choked only at the valve orifice and not at the spray orifice, the discharge velocity is same as exit velocity before the shock. Overall, the evaluated discharge velocities show good agreement against the measured values with an average error of 19.7% and a maximum error of 53.4%. Generally a good agreement is observed between the evaluated discharge velocities and measured data for propellants R12/R114 (60%/40%) (Figure 7.23a-b) and R227 (Figure 7.24a-b), where as the discrepancies are slightly higher for propellants R134A (Figure 7.21a-c) and R12 (Figure 7.22a-b). The DEM with k_y = 0.02, predicts choking at the valve orifice exit for small valve orifices D_{vo} = 259 μm and D_{vo} = 420 μm (D_{vo} = 259 μm, D_{so} = 598 μm ; D_{vo} = 259 μm, D_{so} = 1023 μm; D_{vo} = 420 μm, D_{so} = 1023 μm). This is because, the DEM with k_y = 0.02 predicts more evaporation inside the valve orifice then the actual flow for these orifices and hence predicts choking at the exit of the valve orifice. Also, a double choking is observed for the nozzle combinations D_{vo} = 259 μm, D_{so} = 598 μm and D_{vo} = 420 μm, D_{so} = 1023 μm with propellant R134A and hence high velocities are evaluated at the exit of spray orifice for these nozzle configuration (Figure 7.21c).

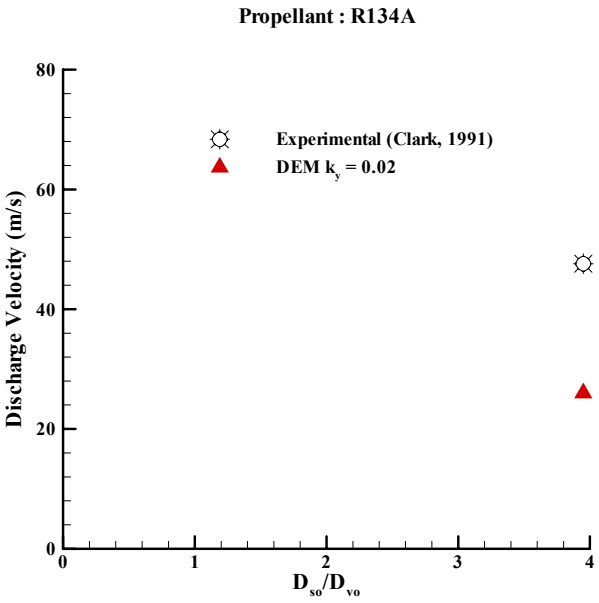

(a) Valve orifice choked

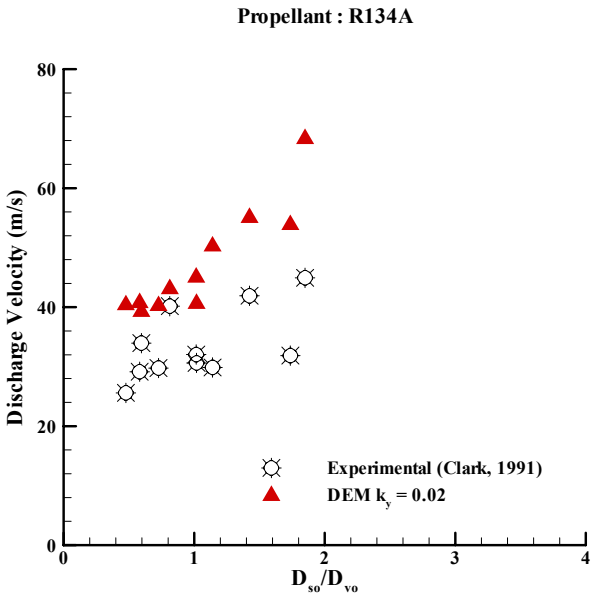

(b) Spray orifice choked

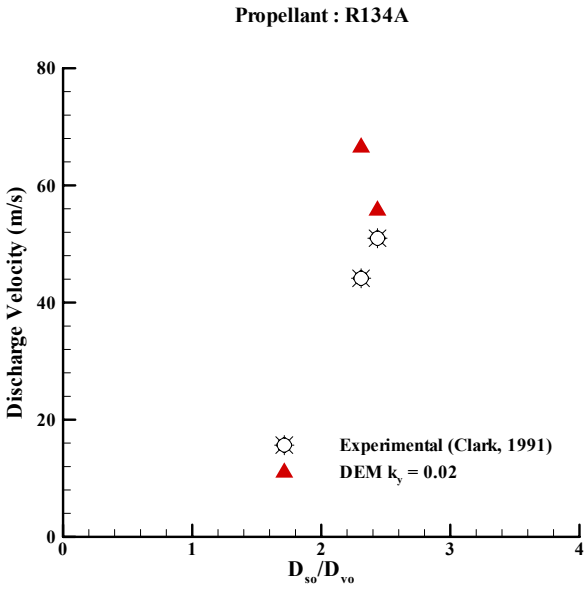

(c) Both valve and spray orifices are choked

Figure 7.21 Comparison of discharge velocities against against Clark's (1991) experimental data at the spray orifice exit for propellant R134A when the flow is choked at the exit of (a) valve orifice, (b) spray orifice and (c) both valve and spray orifices with k_y = 0.02

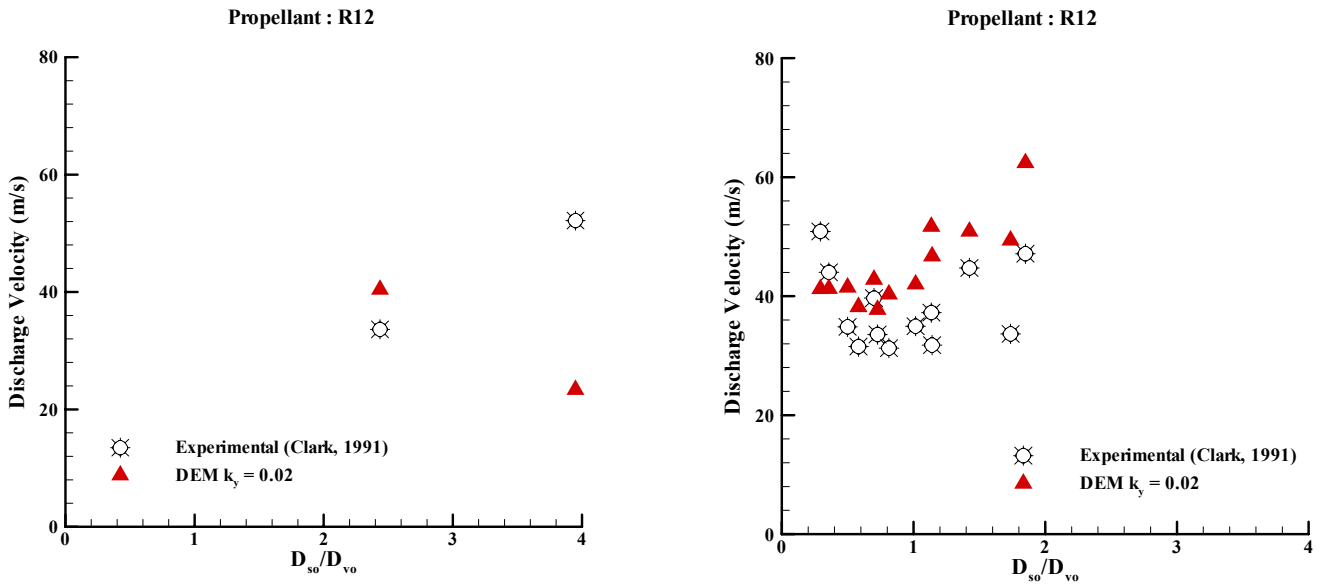

(a) Valve orifice choked (b) Spray orifice choked

Figure 7.22 Comparison of discharge velocities against against Clark's (1991) experimental data at the spray orifice exit for propellant R12 when the flow is choked at the exit of (a) valve orifice and (b) spray orifice with k_y = 0.02

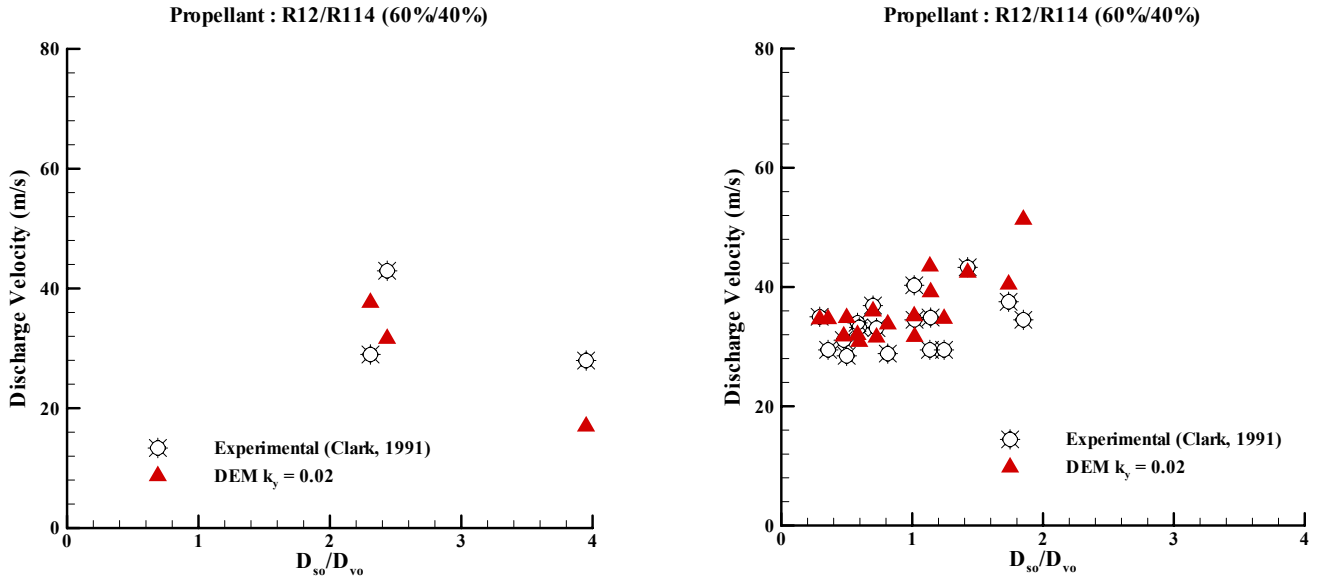

(a) Valve orifice choked (b) Spray orifice choked

Figure 7.23 Comparison of discharge velocities against against Clark's (1991) experimental data at the spray orifice exit for propellant R12/R114(60%/40%) when the flow is choked at the exit of (a) valve orifice and (b) spray orifice with k_y = 0.02

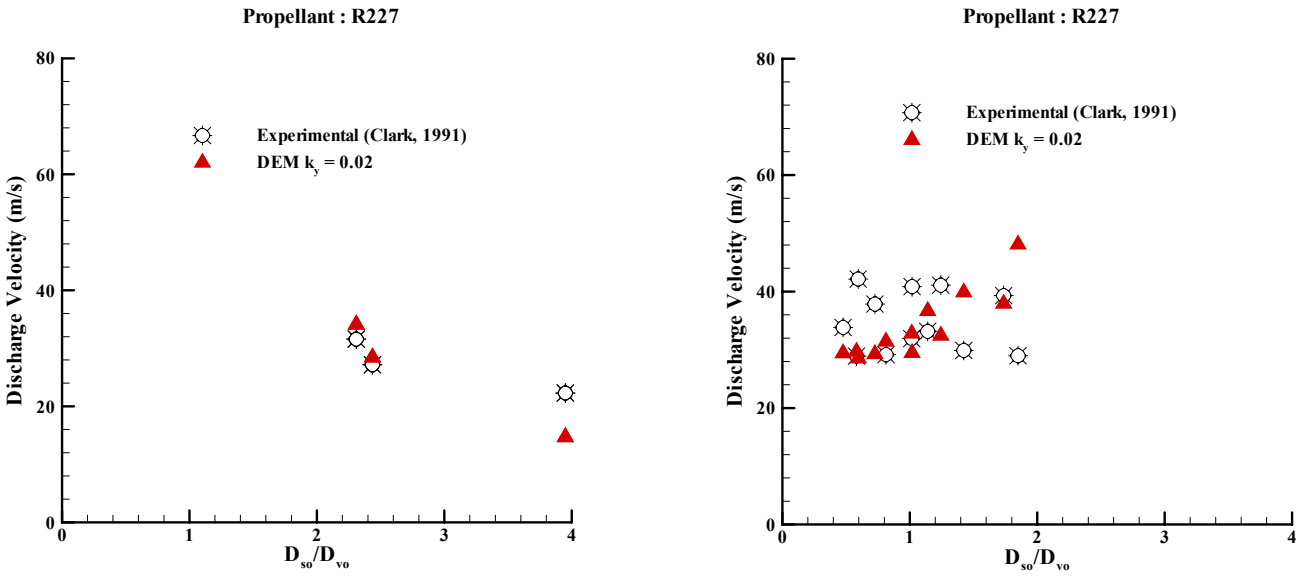

(a) Valve orifice choked (b) Spray orifice choked

Figure 7.24 Comparison of discharge velocities against against Clark's (1991) experimental data at the spray orifice exit for propellant R227 when the flow is choked at the exit of (a) valve orifice and (b) spray orifice with $k_y = 0.02$

7.2.3. Summary

The continuous discharge of the two-phase propellant flow through a twin-orifice system has been successfully modeled using the Delayed Equilibrium Model (DEM) with coefficient $k_y = 0.02$, accounting for the propellant metastability. The model has been validated against the Fletcher's (1975) and Clark's (1991) continuous discharge flows with some discrepancies. The discrepancies are less for Fletcher's cases which have a range of diameter ratios (D_{so}/D_{vo}) between 0.5 and 2.2. And for these orifice configurations, the DEM with $k_y = 0.02$ showed reasonably good agreement with the experimental data. The discrepancies are larger for Clark's test cases which cover a much wider range of diameter ratios, D_{so}/D_{vo} varied from 0.4 to 4 and the DEM with $k_y = 0.02$ struggled somewhat. The reason for the discrepancies is the evaluation of vaporisation index using the relaxation equation (3.9). From, the relaxation equation (3.9), it can be seen that the rate of vaporisation index along the orifice is inversely proportion to the diameter of the orifice i.e.

$$\frac{dy}{dz} \propto k_y \frac{P}{A} \propto \frac{k_y}{D} \qquad 7.1$$

For small diameter ratios (D_{so}/D_{vo}) i.e. for large valve orifices, the present DEM with k_y = 0.02 overpredicts the mass flow rate and slightly overpredicts the expansion chamber pressure and it underpredicts the temperature drop across the valve orifice. As the valve orifice diameter increases, it decreases the overall coefficient (k_y/D) in the relaxation equation. A smaller coefficient encourages metastability and inhibits evaporation. This causes a reduction of pressure drop across the valve orifice and hence, higher mass flow rates and high expansion chamber pressures along with lower temperature drop across the valve orifice. The error in the mass flow rate increases as the spray orifice diameter increases because this further inhibits the evaporation inside the spray orifice and increases mass flow rates.

For small valve orifice (D_{vo} = 259 μm and 420μm) in conjunction with $1<D_{so}/D_{vo}<3$, the DEM with k_y = 0.02 predicts the mass flow rate and the expansion chamber conditions close to the experimental data. However, it slightly underpredicts expansion chamber pressure. The reason for this is that a decrease of the valve orifice diameter increases the overall coefficient (k_y/D) in the relaxation equation, which increases the evaporation inside the valve orifice. This causes slightly higher pressure drop inside the valve orifice then the actual flow. Hence, predicts slightly lower expansion chamber pressures. The error in the mass flow rate increases as the spray orifice diameter increases because the increase in the spray orifice diameter decreases the coefficient (k_y/D), which encourages metastability and inhibits evaporation inside the spray orifice. As more evaporation occurs inside the valve orifice, large pressure drop occurs inside the valve orifice, due to which sonic velocities are evaluated at the exit of the valve orifice, which restricts the mass flow rate. This is also the reason for predicting the low expansion chamber pressures, as the diameter ratio increases with Fletcher's cases.

7.3. Development of new correlation for the coefficient of relaxation equation k_y

As seen from the above discussion that a single coefficient, $k_y = 0.02$ is not enough to predict the mass flow rate and expansion chamber variables along the twin-orifice system of pMDIs. There is a need to optimize this coefficient in order to accommodate all orifice configurations. The mass flow rate is the main variable which is important to optimize, as the orifices of pMDI are designed for a particular mass flow rate. Therefore, the purpose of this sections is to develop a new correlation for the coefficient k_y, optimizing against the experimental mass flow rates.

Following Fletcher's (1975) and Clark's (1991) frozen assumption inside the valve orifice, it is assumed that no vaporisation occurs inside the valve orifice and the propellant remains in metastable state and the evaporation occurs inside the expansion chamber and spray orifice. i.e. the vaporisation index, y=0 and the quality, x=0 inside the valve orifice. As seen from the previous section, the discrepancies in the mass flow rate largely varied with change in valve orifice and spray orifice diameters. So, it is expected that a new correlation function of these orifice diameters would give better predictions.

7.3.1. Test Cases

The test cases used to study develop the correlation for the coefficient k_y are Clark's (1991) experimental data. The valve and spray orifices described in section 7.2.2.1 with propellant R134A are used to develop a new correlation for the coefficient k_y. Then this correlation is tested on other propellants. Five valve and seven spray orifice combinations were used. The procedure used to develop the correlation for the coefficient k_y is described in the following section.

7.3.2. Procedure for developing the correlation for the coefficient k_y

Figure 7.25 shows the effect of mass flow rate on varying the coefficient k_y in the relaxation equation for D_{vo} = 420 µm and D_{so} = 565 µm. The trends are representative of those predicted with different valve and spray orifice. The mass flow rate increases as k_y decreases. From the figure it can be observed that the effect of k_y, on the mass flow rate reduces as $k_y > 0.1$. The following steps are used to obtain the correlation:

Step 1 : For each valve and spray orifice configuration seven different values for k_y were selected. These values are selected in such a way that the evaluated mass flow rate falls on both sides of the experimental mass flow rate (i.e. some values overpredict the mass flow rate and the others underpredict the mass flow rate).

Step 2 : The results are plotted in graphs and the point is located where experimental mass flow rate equals the predicted mass flow rate. For example, the optimum value of k_y = 0.0812 in Figure 7.25 for D_{vo} = 420µm and D_{so} = 565µm.

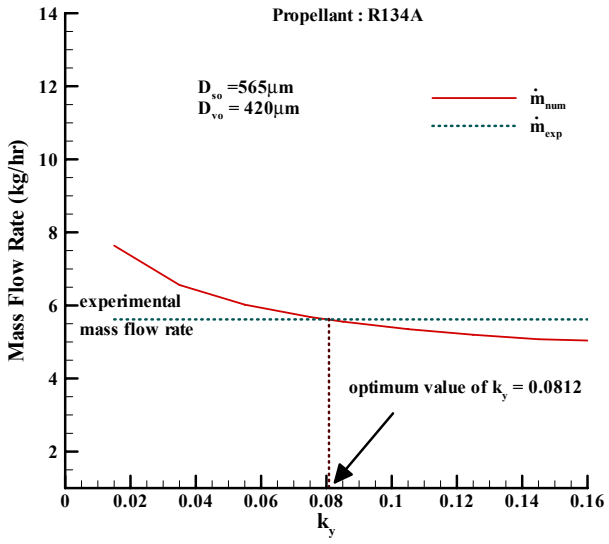

Figure 7.25 Effect of coefficient k_y on mass flow rate

Step 3 : In a similar manner, the optimum values of k_y are evaluated for all the valve and spray orifices. The results are given in Table 7.3.

Step 4 : The spray orifice diameter (D_{so}) and the valve orifice diameter (D_{vo}) and the optimum k_y values are used to obtain two different correlations:

Correlation (*a*):

The first correlation is in the form of

$$k_y = a\left(D_{so}/D_{vo}\right)^b \qquad 7.2$$

where a = 0.082, b = 1.07.

Correlation (*b*):

And the second correlation is in a form of

$$k_y = a \times D_{so}^b \times D_{vo}^c \qquad 7.3$$

where a = 0.20143, b = 2.7238 and c = -0.468. Rounding these coefficients to first decimal place, a = 0.20, b = 2.7 and c = -0.5. DataFit 9.0 software was used to obtain these coefficients.

The equation (7.2) and (7.3) together with the optimum k_y values are presented in Figure 7.26 and Figure 7.27, respectively. The coefficient of correlation (a) for the data was 0.54 with a maximum deviation of ±60%, whereas the coefficient for correlation (b) was 0.943 with a maximum deviation of ±30%. As correlation (b) showed better agreement with a maximum deviation of ±30%, the correlation (b) with $k_y = a \times D_{so}^b \times D_{vo}^c$ has been considered for further simulations.

Table 7.3 Optimum k_y values for various orifice configurations

D_{vo} = 259 μm	
D_{so} (μm)	Optimum value of k_y
425	0.0772
479	0.0553
565	0.5372
598	0.5800
725	0.6824
975	0.9176
1023	0.0820

D_{vo} = 420 μm	
D_{so} (μm)	Optimum value of k_y
425	0.0257
479	0.0262
565	0.0812
598	0.0658
725	0.0637
975	0.2928
1023	0.1642

D_{vo} = 589 μm	
D_{so} (μm)	Optimum value of k_y
425	0.0205
479	0.0365
565	0.0812
598	0.0692
725	0.0927
1023	0.2610

D_{vo} = 823 μm	
D_{so} (μm)	Optimum value of k_y
425	0.0368
479	0.0615
565	0.0543
598	0.0436
725	0.0509
975	0.0946
1023	0.1583

D_{vo} = 1005 μm	
D_{so} (μm)	Optimum value of k_y
425	0.0162
479	0.0131
565	0.0500
598	0.0378
725	0.0670
975	0.1946
1023	0.1769

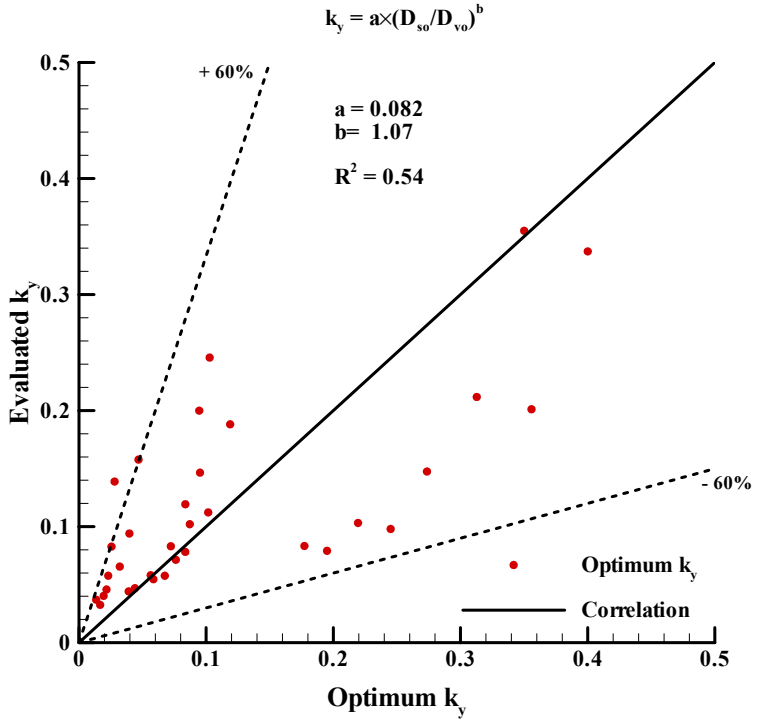

Figure 7.26 Correlation (a) for the coefficient k_y equation using propellant R134A

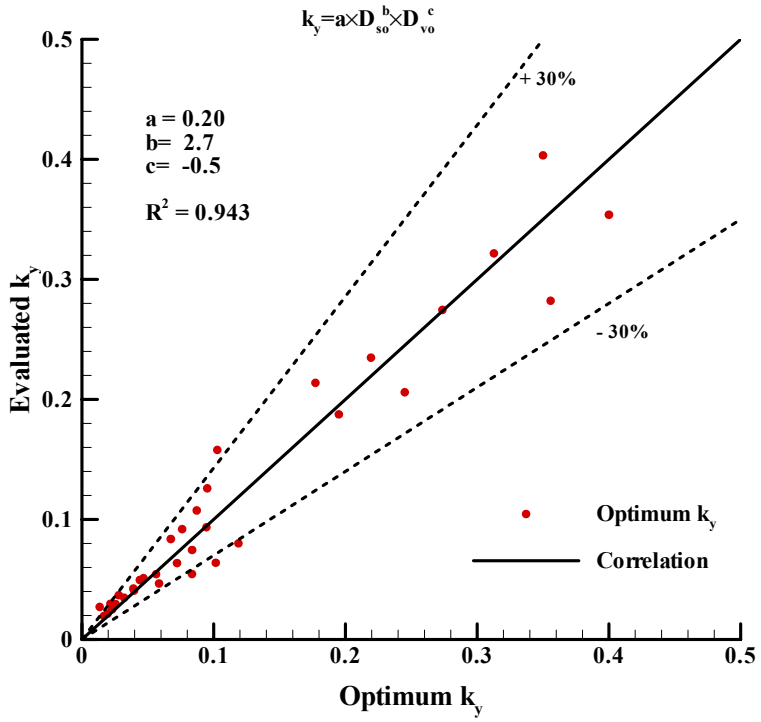

Figure 7.27 Correlation (b) for the coefficient k_y equation using propellant R134A

7.4. DEM with new coefficient ($k_y = 0.2 D_{so}^{2.7} D_{vo}^{-0.5}$)

In this section, DEM with new correlation $k_y = 0.2 D_{so}^{2.7} D_{vo}^{-0.5}$ is used to validate against the experimental results of Fletcher (1975) and Clark (1991) for continuous discharge flows through twin-orifice system. It should be noted that the correlation was developed on a different data set and for a different propellant, so the comparisons that follow are tests of the broader validity of the proposed correlation.

7.4.1. Comparison of Fletcher (1975) experimental data with the predictions of DEM using new coefficient (k_y)

In this section, the results obtained using the present DEM with the new correlation $k_y = 0.2 D_{so}^{2.7} D_{vo}^{-0.5}$ are presented. The test cases are same as those described in section 7.2.1.1.

7.4.1.1. Results and Discussion

Comparison of mass flow rate

Figure 7.28 shows the comparison of predicted mass flow rate with the experimental mass flow rate using the DEM with new coefficient, $k_y = 0.2 D_{so}^{2.7} D_{vo}^{-0.5}$ in the relaxation equation. From the figure it can seen that the predicted mass flow rates are in very good agreement against the experimental mass flow rates with an average error of 7.2%. For the nozzle, D_{vo} = 680 μm and D_{so} = 700 μm with D_{so}/D_{vo}=1.029; the DEM with coefficient k_y = 0.02 overpredicted the mass flow rate by 38%, whereas with the new coefficient predicts the mass flow rate with an error of 8.8%, close to the experimental value.

Comparison of expansion chamber pressure (p_{ec})

The comparison between the computed expansion chamber pressures using DEM with new coefficient, $k_y = 0.2 D_{so}^{2.7} D_{vo}^{-0.5}$ in the relaxation equation with the measured

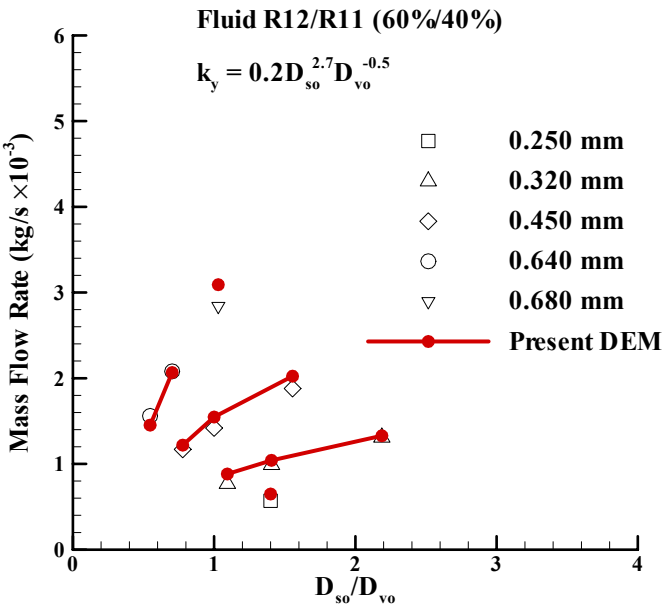

Figure 7.28 Comparison of mass flow rate against Fletcher's (1975) experimental mass flow rate

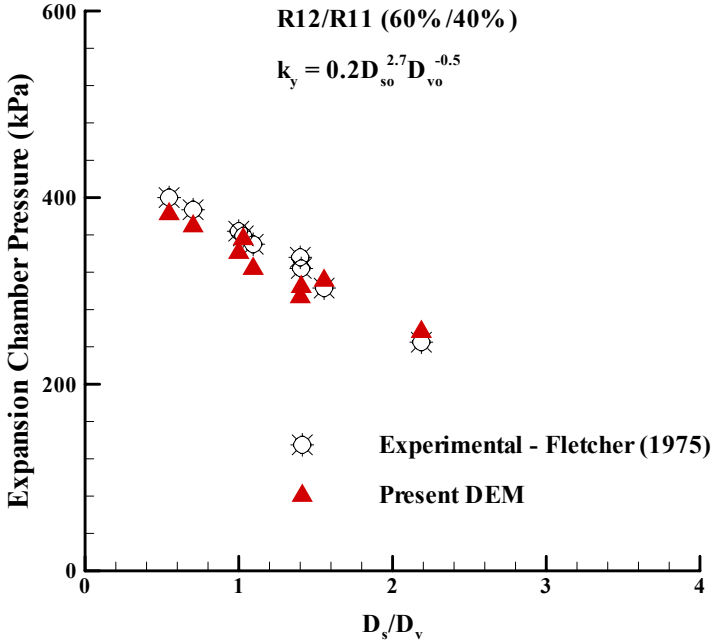

Figure 7.29 Comparison of expansion chamber pressure against Fletcher's (1975) measured expansion chamber pressure

expansion chamber pressures is shown in Figure 7.29. The evaluated expansion chamber shows good agreement against the experimental values with an average error of 5.52% and a maximum error of -12.7% when D_{so}/D_{vo} = 1.4. These predictions are better than those with constant k_y = 0.02, which underpredicted the expansion chamber pressure with an average error of 12% and a maximum error of -26% when D_{so}/D_{vo} = 2.2. The close agreement between the predictions of the DEM with the new k_y correlation and experimental values indicate that the metastability has been accounted accurately.

Comparison of expansion chamber temperature (T_{ec})

Figure 7.30 shows the comparison of predicted expansion chamber temperature using present DEM with new coefficient $k_y = 0.2D_{so}^{2.7}D_{vo}^{-0.5}$ with the Fletcher's (1975) measured expansion chamber temperature. The predicted expansion chamber temperatures show good agreement against the measured expansion chamber temperatures with an average error of 8.61% and a maximum error of -27.5% when D_{so}/D_{vo} = 2.2. The increase in the spray orifice diameter increases the new coefficient, k_y, which in turn increases the vaporisation index (y) inside the expansion chamber. This causes the average temperature to decrease as the average temperature is dominated by the saturated liquid temperature and hence underpredict the expansion chamber temperatures.

Comparison of exit velocity

Figure 7.31 shows the comparison of predicted exit velocity against the experimental exit velocities. The exit velocities are evaluated after the shock using the equation (3.55). From the figure it can be observed that the predictions made by the present DEM with new coefficient are reasonably good with an average error of 25.7% excluding the nozzle with diameter ratio, D_{so}/D_{vo} = 2.2. For this nozzle, the present DEM with new correlation over predicts the exit velocity with a maximum error of 140%. The large spray orifice diameter and the small valve orifice diameter increases overall coefficient ($k_y = 0.2D_{so}^{2.7}D_{vo}^{-0.5}$) in the relaxation equation, which causes rapid evaporation inside the expansion chamber and the spray orifice, due to which large velocities are evaluated at the exit. The predictions of constant k_y = 0.02 are better in

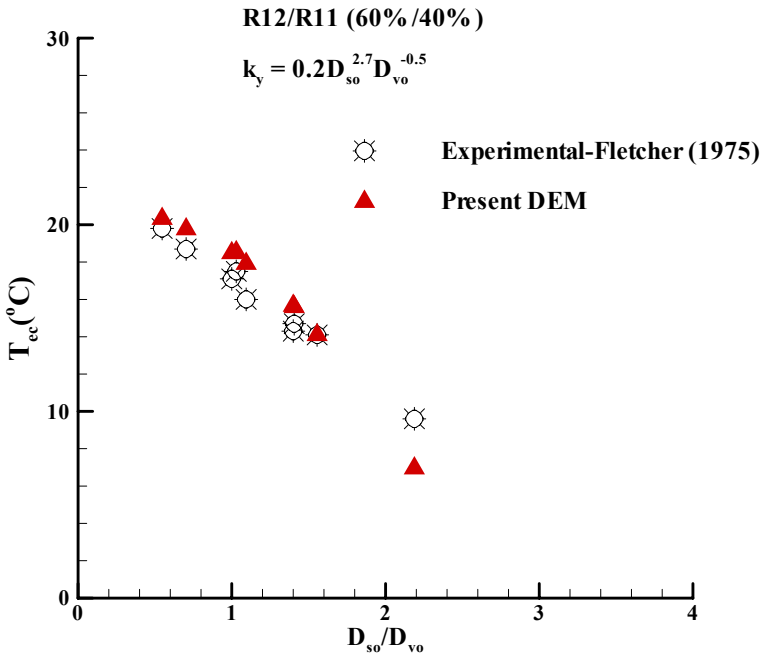

Figure 7.30 Comparison of expansion chamber temperature against Fletcher's (1975) measured expansion chamber temperature

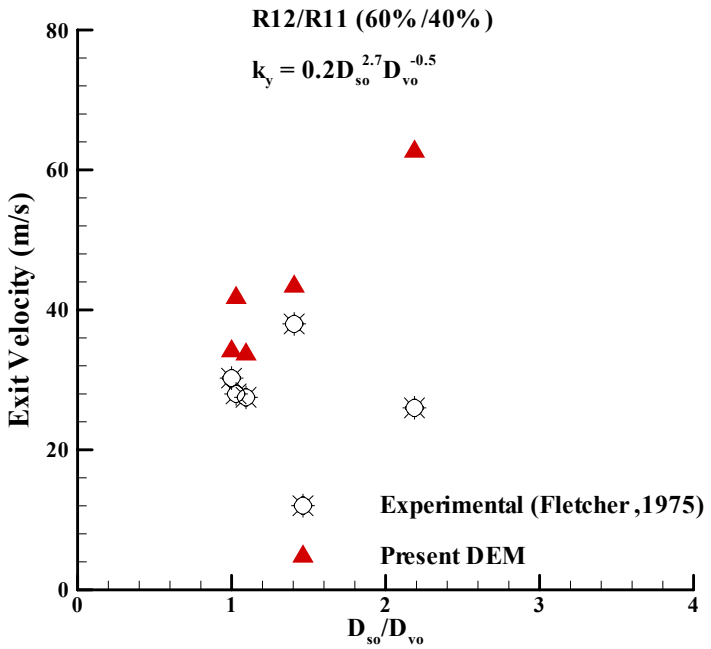

Figure 7.31 Comparison of exit velocity against Fletcher's (1975) measured exit velocity

compared to those of $k_y = 0.2 D_{so}^{2.7} D_{vo}^{-0.5}$.

7.4.2. Comparison of Clark (1991) experimental data with the predictions of DEM using new coefficient (k_y)

In this section, the results obtained using the present DEM with the new correlation for the coefficient of the relaxation equation, $k_y = 0.2 D_{so}^{2.7} D_{vo}^{-0.5}$ are compared against Clark's (1991) experimental data. The test cases have been defined previously in the section 7.2.2.1

7.4.2.1. Results and Discussion

Comparison of mass flow rate

Figure 7.32 shows the comparison of predicted mass flow rate using the present DEM with new coefficient $k_y = 0.2 D_{so}^{2.7} D_{vo}^{-0.5}$ with Clark's (1991) experimental mass flow rates for four different propellants and various orifice combinations. The present DEM with new coefficient predicts the mass flow rates well against the experimental values with an average error of 12% and a maximum error of 41% for D_{vo} = 1005 μm and D_{so} = 294 μm. This maximum error occurs as the coefficient evaluated in the relaxation equation using the new correlation is lowest for D_{vo} = 1005 μm and D_{so} = 294 μm, encourages metastability inside the expansion chamber and spray orifice and hence predicts highest mass flow rate. These predictions with new coefficient are better compared to that of k_y=0.02 which predicted the mass flow rate with an average error of 26.8% and a maximum error of 88.9%.

Comparison of expansion chamber pressure (p_{ec})

The predicted expansion chamber pressures using DEM with new coefficient $k_y = 0.2 D_{so}^{2.7} D_{vo}^{-0.5}$ are compared against Clark's (1991) measured expansion chamber pressure in Figure 7.33. The predicted expansion chamber pressures show reasonably good agreement against the experimental values with an average error of 16.5% and a maximum error of 50% for nozzle D_{vo} = 420 μm and D_{so} = 1023 μm.

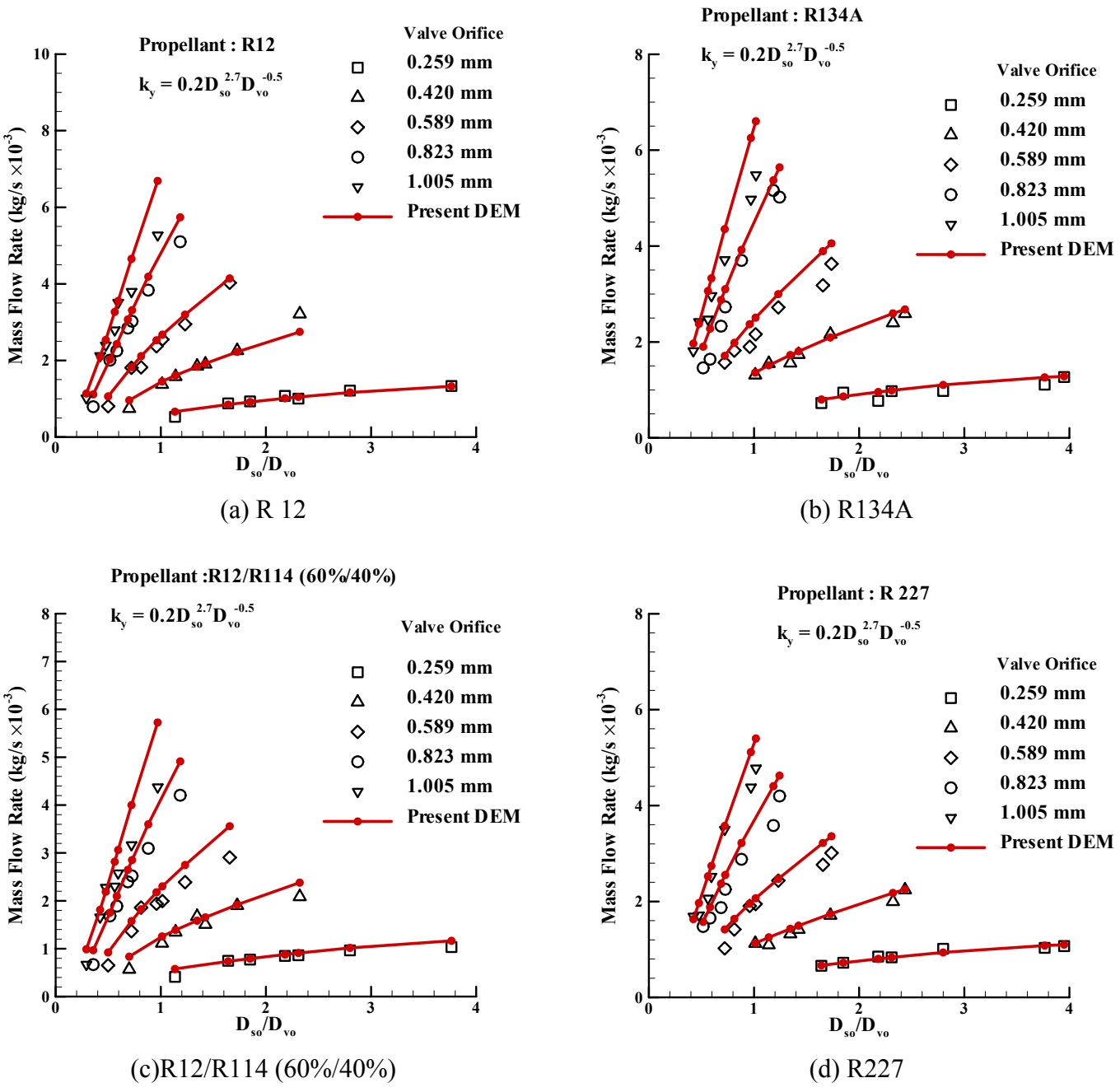

Figure 7.32 Comparison of mass flow rate against Clark's (1991) experimental data with four different propellants: (a) R 12 (b) R134A (c) R12/R114 (60%/40%) and (d) R227 with $k_y = 0.2D_{so}^{2.7}D_{vo}^{-0.5}$

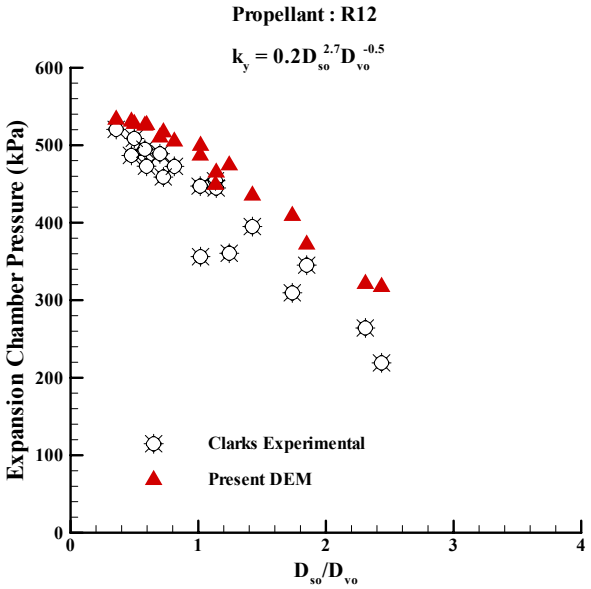

(a) R 12

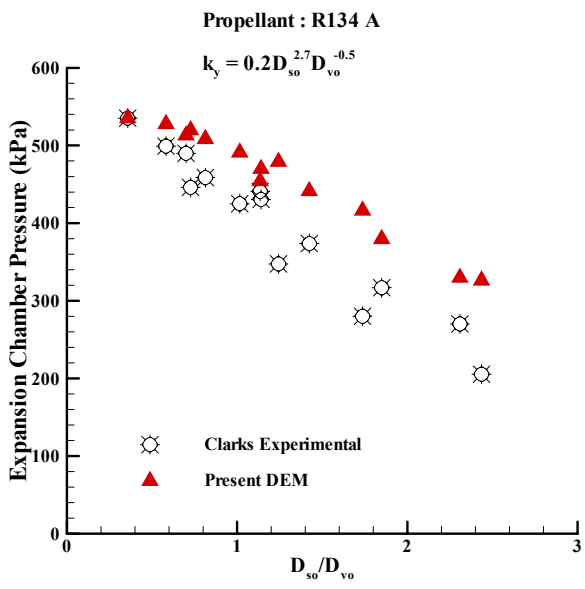

(b) R134A

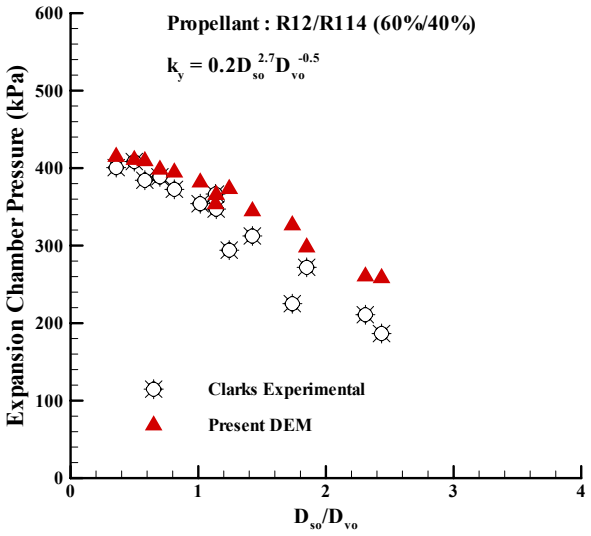

(c)R12/R114 (60%/40%)

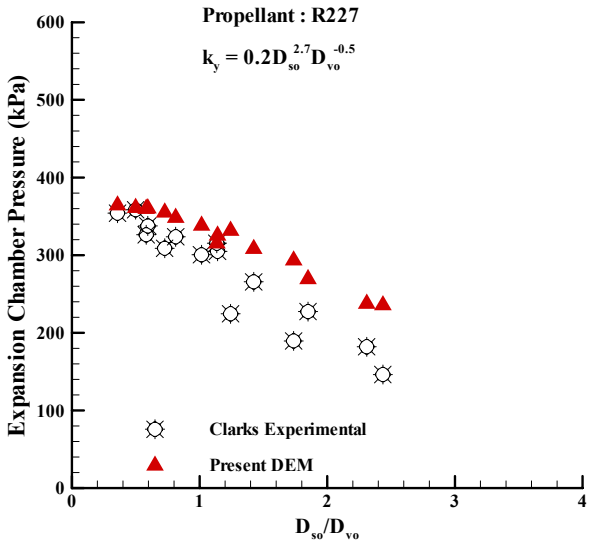

(d) R227

Figure 7.33 Comparison of expansion chamber pressure against Clark's (1991) experimental data with four different propellants: (a) R 12 (b) R134A (c) R12/R114 (60%/40%) and (d) R227 with $k_y = 0.2D_{so}^{2.7}D_{vo}^{-0.5}$

These discrepancies are may be attributed to our modeling assumption in developing the correlation that no evaporation occurs inside the valve orifice, which causes low pressure drop inside the valve orifice and hence the model predicts high expansion chamber pressures. This suggest that evaporation occurs inside the valve orifice in the actual flow. The expansion chamber pressures predicted with k_y=0.02 are better in compared to that of new correlation because it predicts evaporation inside the valve orifice.

Comparison of temperature drop across the valve orifice (ΔT_{vo})

Figure 7.34 shows the comparison of predicted expansion chamber temperature using the DEM with new coefficient $k_y = 0.2 D_{so}^{2.7} D_{vo}^{-0.5}$ against the measured expansion chamber temperature by Clark (1991) for four propellants and various orifice combinations. The predicted expansion chamber temperature show reasonably good agreement against the experimental values with an average error of 58% and a maximum error of -98%. These predictions are better in compared to that of with k_y = 0.02 in terms of average error. However the maximum error remains same for both the models. These large differences can be attributed to the uncertainties in measuring the expansion chamber temperature and also to our modeling assumption that no evaporation occurs inside the valve orifice.

Comparison of spray orifice discharge velocity

Figure 7.35 shows the comparison of computed discharge velocities (spray velocities) with the Clark's measured exit velocities. The velocities are evaluated after the shock at the exit of the valve orifice for the choked flow at the exit of the spray orifice using equation (3.55). The DEM with $k_y = 0.2 D_{so}^{2.7} D_{vo}^{-0.5}$ predicts choking only at the exit of the spray orifice for all the nozzle configurations. The computed discharge velocities show reasonable agreement against the experimental data with an average error of 41% and a maximum error of 93%. However, the discharge velocities evaluated with k_y = 0.02 are better than new correlation. The reason for these discrepancies is that the new correlation $k_y = 0.2 D_{so}^{2.7} D_{vo}^{-0.5}$ predicts high choking

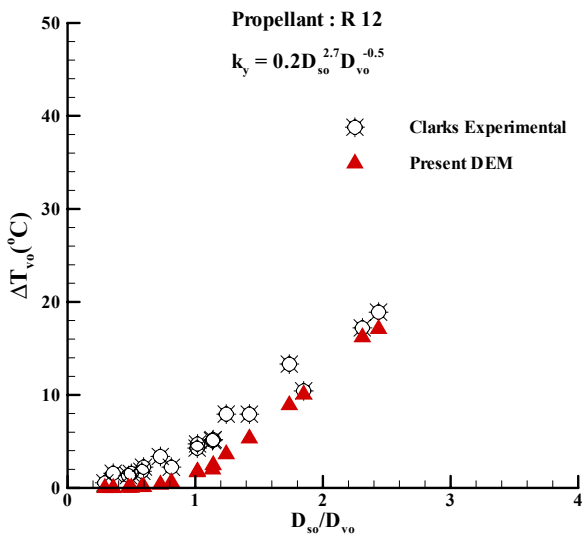

(a) R 12

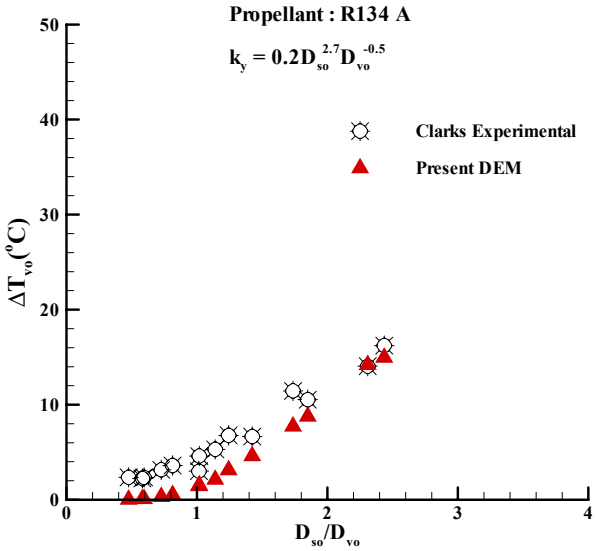

(b) R134A

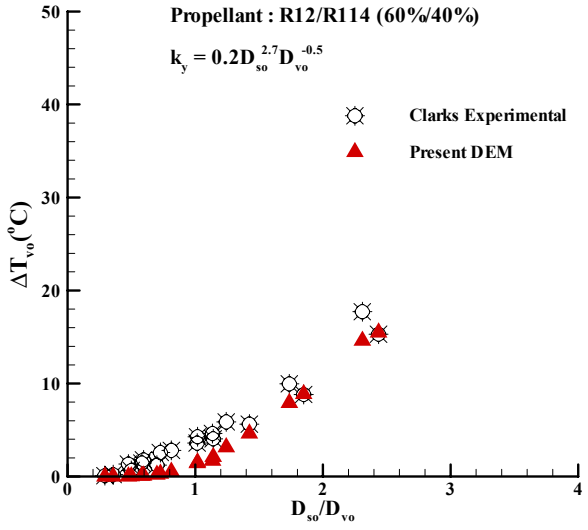

(c)R12/R114 (60%/40%)

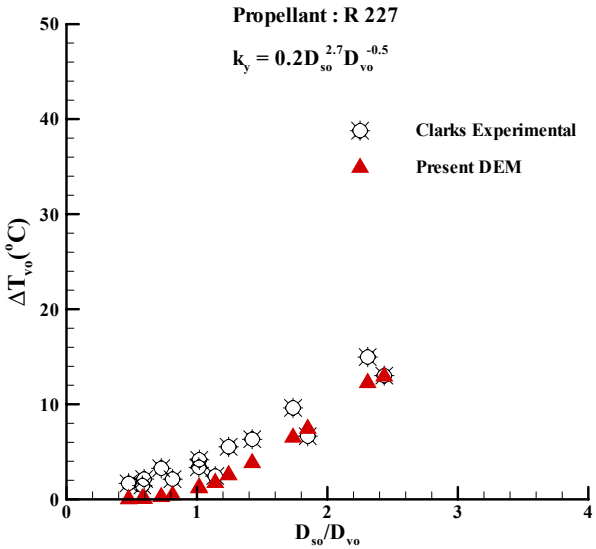

(d) R227

Figure 7.34 Comparison of temperature drop across the valve orifice against Clark's (1991) experimental data with four different propellants: (a) R 12 (b) R134A (c) R12/R114 (60%/40%) and (d) R227 with $k_y = 0.2D_{so}^{2.7}D_{vo}^{-0.5}$

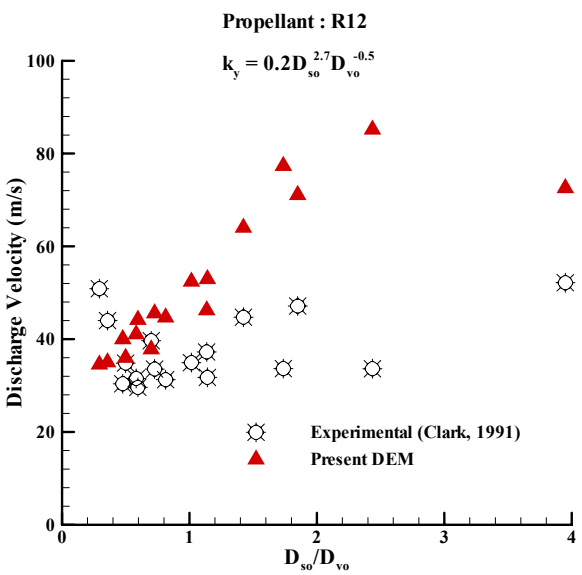

(a) R 12

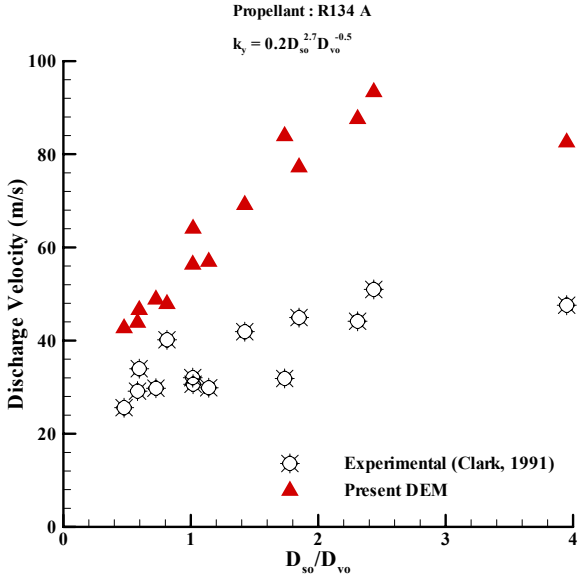

(b) R134A

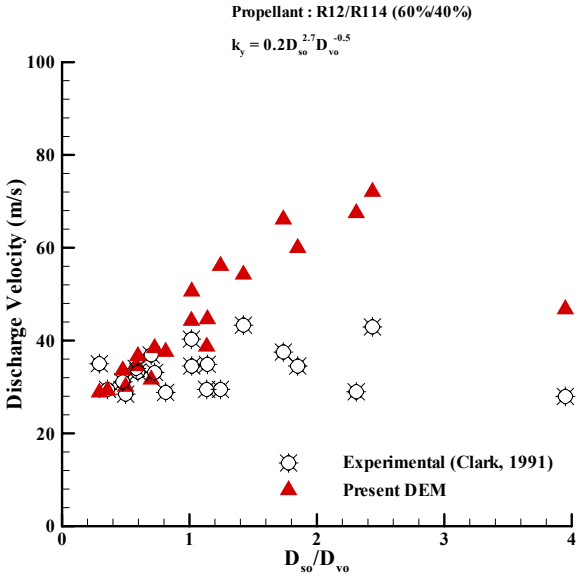

(c)R12/R114 (60%/40%)

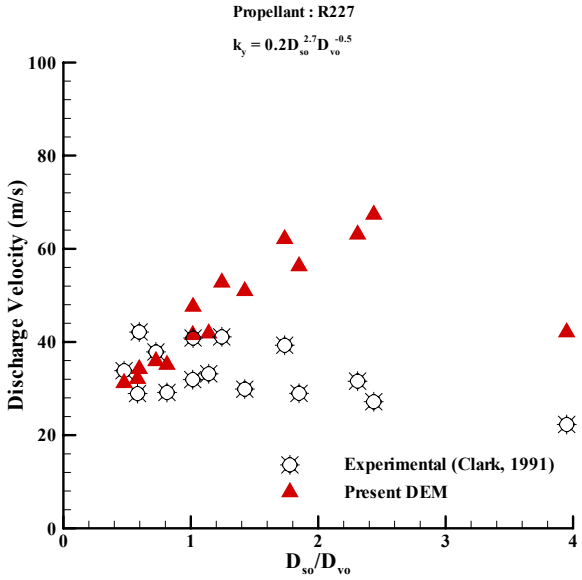

(d) R227

Figure 7.35 Comparison discharge velocity against Clark's (1991) experimental data with four different propellants: (a) R 12 (b) R134A (c) R12/R114 (60%/40%) and (d) R227 with $k_y = 0.2D_{so}^{2.7}D_{vo}^{-0.5}$

pressures at the spray orifice exit, due to which, large discharge velocities are evaluated.

7.4.3. Summary

The continuous discharge of two-phase flashing propellant flow through twin-orifice systems was modeled using the DEM with a new coefficient $k_y = 0.2 D_{so}^{2.7} D_{vo}^{-0.5}$. The results were compared against Fletcher (1975) and Clark (1991) experimental data. The comparison with Fletcher's experimental data showed good agreement in the mass flow rate, expansion chamber pressures, temperatures and exit velocities. The comparison with Clark's experimental data showed good agreement with the mass flow rate but some discrepancies in the expansion chamber pressures, temperature drop across the valve orifice and the exit velocities. The discrepancies in these variables is due to the fact that no evaporation is predicted inside the valve orifice. Consequently, there is less pressure drop across the valve orifice and pressures and temperatures are higher inside the expansion chamber. Also, the new coefficient gives large coefficients for large spray orifices and small valve orifices, which increases the evaporation inside the expansion chamber and spray orifice and hence gives higher exit velocities at spray orifice exit.

In order to show the difference between these two models: k_y = 0.02 and $k_y = 0.2 D_{so}^{2.7} D_{vo}^{-0.5}$, a comparison between the predicted flow variables (pressure, vaporisation index, quality and velocity) is shown in Figure 7.36 for nozzle D_{vo} = 420μm and D_{so} = 1023 μm with propellant R134A. Figure 7.36a, shows that the new correlation predicts lower pressure drop across the valve orifice, as no vaporisation occurs inside the valve orifice and hence predicts high expansion chamber pressures and choking pressures. The effect of spray orifice diameter can be seen in Figure 7.36b and Figure 7.36c. The vaporisation index increases rapidly inside the expansion chamber and spray orifice due to effect of $D_{so}^{2.7}$, in the new coefficient k_y. This causes quality to increase inside the expansion chamber and the spray orifice.

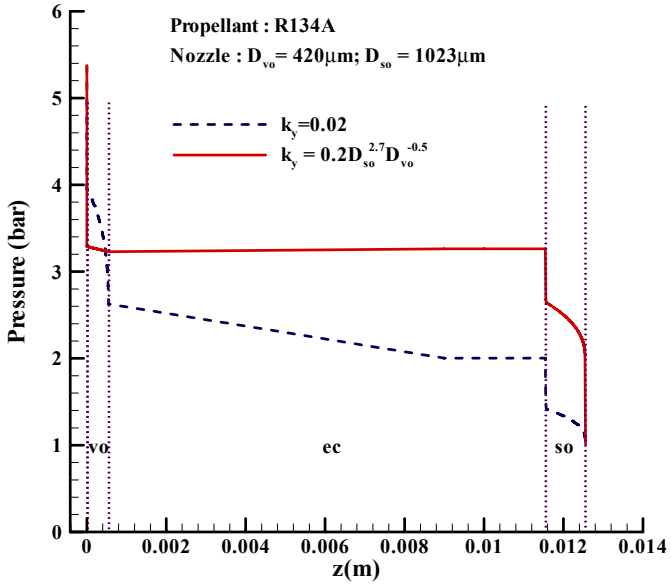

(a) Pressure

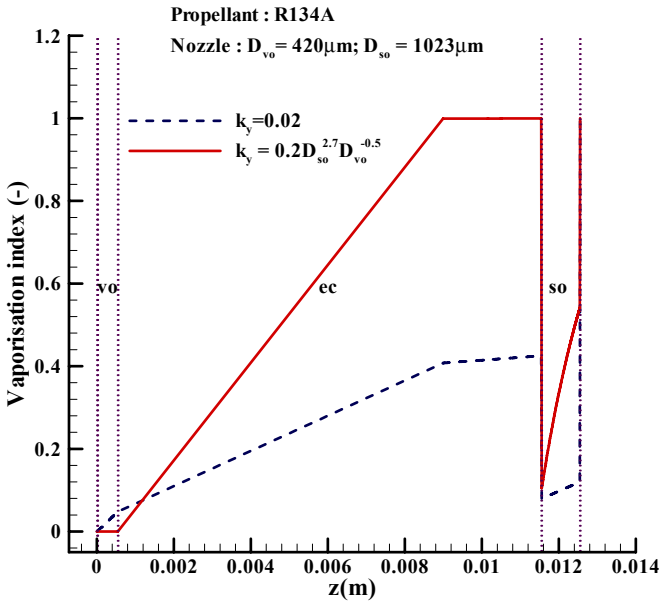

(b) Vaporisation index

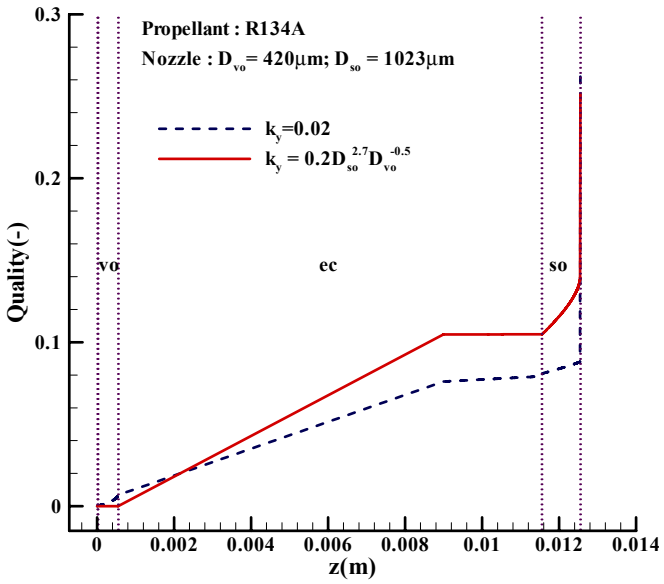

(c) Quality

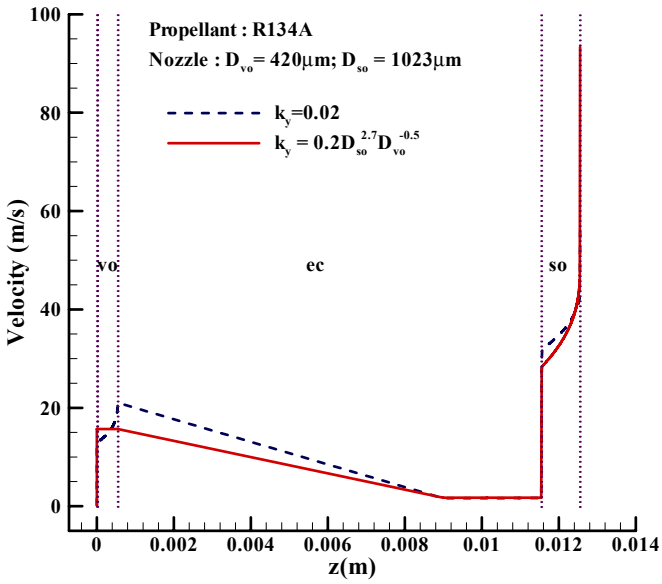

(d) Velocity

Figure 7.36 Comparison of predicted flow variables along the twin-orifice system using both models: k_y = 0.02 and $k_y = 0.2D_{so}^{2.7}D_{vo}^{-0.5}$ for D_{vo} = 420μm and D_{so} = 1023 μm with propellant R134A

Figure 7.36d shows the predicted velocity distribution along the twin-orifice system. The coefficient k_y = 0.02 predicts larger velocities (21 m/s) inside the valve orifice compared to the new correlation (15.6 m/s). After that, both the models predict almost similar velocities. The evaluated discharge velocities are higher with the new correlation because of high choking pressures at the valve orifice exit. This increases the difference between the choking pressure and ambient pressure and hence large discharge velocities are evaluated.

The new coefficient optimizes the prediction of mass flow rate, but this has the consequences for the predictions of pressure, temperatures and exit velocities. Based on the mass flow rate it can be concluded that the new coefficient predicts the mass flow rate better in compare to that of coefficient, k_y = 0.02.

7.5. Metered Discharge Flows

In this section, the DEM with coefficient k_y = 0.02 and $k_y = 0.2 D_{so}^{2.7} D_{vo}^{-0.5}$ developed for continuous discharge flows is used to simulate the metered discharge flow assuming quasi steady state. With the new correlation, $k_y = 0.2 D_{so}^{2.7} D_{vo}^{-0.5}$, it is assumed that no vaporisation occurs inside the valve orifice and the propellant is in metastable state (i.e. y=0 and x=0). The DEM results with both coefficients are compared against Clark's (1991) experimental data and the well-established homogeneous equilibrium model (HEM).

7.5.1. Test Cases

The test cases are as those of described in previous chapter (section 6.2). The main problem data and model scenarios are restated here for completeness:

- Metering chamber volume: 100 µL = 10^{-7} m^3
- Valve orifice: D_{vo} = 0.26 mm, L_{vo} = 0.5425 mm
- Expansion chamber: D_{ec} = 3.8 mm, L_{ec} = 11 mm
- Spray orifice: D_{so} = 0.26 mm, L_{so} = 1 mm

Table 7.4 Inlet conditions for numerical simulations

t (ms)	p_{in} (bar)	T_{in} (°C)	y_{in}
0	5.35	18.00	1
25	4.85	16.95	0.312
50	4.80	16.04	0.524
75	4.73	14.92	0.720
100	4.50	13.51	0.757
150	4.09	11.13	0.759
200	3.68	8.59	0.752

- Hydraulic roughness of all surfaces: ε = 1.5 μm
- Propellant : R12
- Ambient pressure 1.013 bar, which is the discharge pressure acting as the downstream boundary condition
- Ambient temperature (T_0) 291 K, which defines the conditions of the metering chamber fluid prior to discharge
- Other inlet conditions are given in Table 7.4

The Liquid Only Flow (LOF) scenario was found to be most accurate (Chapter 6), so the propellant is assumed to be in liquid only at the inlet. In LOF scenario, the propellant is stratified in the metering chamber due to gravity with vapour at the top and a mixture of saturated and metastable liquid at the bottom (Figure 6.3b). The valve orifice is located near the bottom of the metering chamber, so the assumed inlet quality of the fluid entering the valve orifice will be zero i.e. x = 0 and the vaporisation index 'y' in Table 7.4 evaluated using equation (6.1).

7.5.2. Results and Discussion

Figure 7.37a-b shows a comparison of predicted pressure distribution for all three models (HEM, DEM k_y = 0.02, DEM $k_y = 0.2 D_{so}^{2.7} D_{vo}^{-0.5}$) along the twin-orifice system for the metered discharge flow of propellant R12 at t = 25 ms and t=200 ms. The sudden pressure drop in Figure 7.37a-b at the inlet (z = 0) is due to the abrupt

contraction at the entrance of the valve orifice. Thereafter the pressure remains almost constant inside the expansion chamber. The next large pressure drop at the entrance of the spray orifice (z = 0.0115m) is due to rapid fluid acceleration in the abrupt contraction at the entrance to the spray orifice. The propellant pressure drops along the spray orifice due to the acceleration and frictional effects. The large pressure drop at the exit plane of the spray orifice in Figure 7.37a-b indicates that the flow is choked at both time instants (t=25 ms and t=200 ms). It can also be observed that the pressure profiles are similar for both the time instants, except that at t=200 ms, the pressure profiles are lower since the inlet pressure is lower since the metering chamber pressure has fallen. The predicted pressure profiles are very similar for all the three models : HEM, DEM k_y = 0.02 and DEM with new correlation. The predictions of HEM and DEM k_y = 0.02 are almost identical except in the spray orifice where HEM yields slightly higher pressures. DEM with new correlation predicts the lowest pressure profile.

Figure 7.38a-b shows the comparison of predicted temperature distribution along the twin-orifice system of midis using all the three models for t = 25 ms and t = 200ms. In DEM with both the coefficients, the propellant is represented as a mixture of metastable (superheated) liquid and saturated mixture. So, as the local pressure changes in the flow direction, two temperatures have to be distinguished: the superheated liquid temperature (T_{lm}) and the saturation liquid temperature (T_l). The average temperature is evaluated using the equation (3.18) proposed by Zhou and Zhang (2006). From the figure it can be seen that the temperature distribution is similar to that of pressure, but DEM accounts for metastability of the propellant and hence yields higher temperatures. The HEM involves saturated propellant and hence predicts lowest temperature profiles. As the pressure profiles, the temperature profiles for both the time instants (t = 25 ms and t = 200 ms) are similar, but lower temperatures are obtained at t=200 ms because the inlet temperature is lower since the metering chamber fluid is colder at this time.

Figure 7.39a-b shows the comparison of predicted void fraction distribution. The void fraction increases as the propellant enters the valve orifice for HEM and DEM k_y = 0.02 due to the start of vapour formation as the pressure decreases. The DEM with the

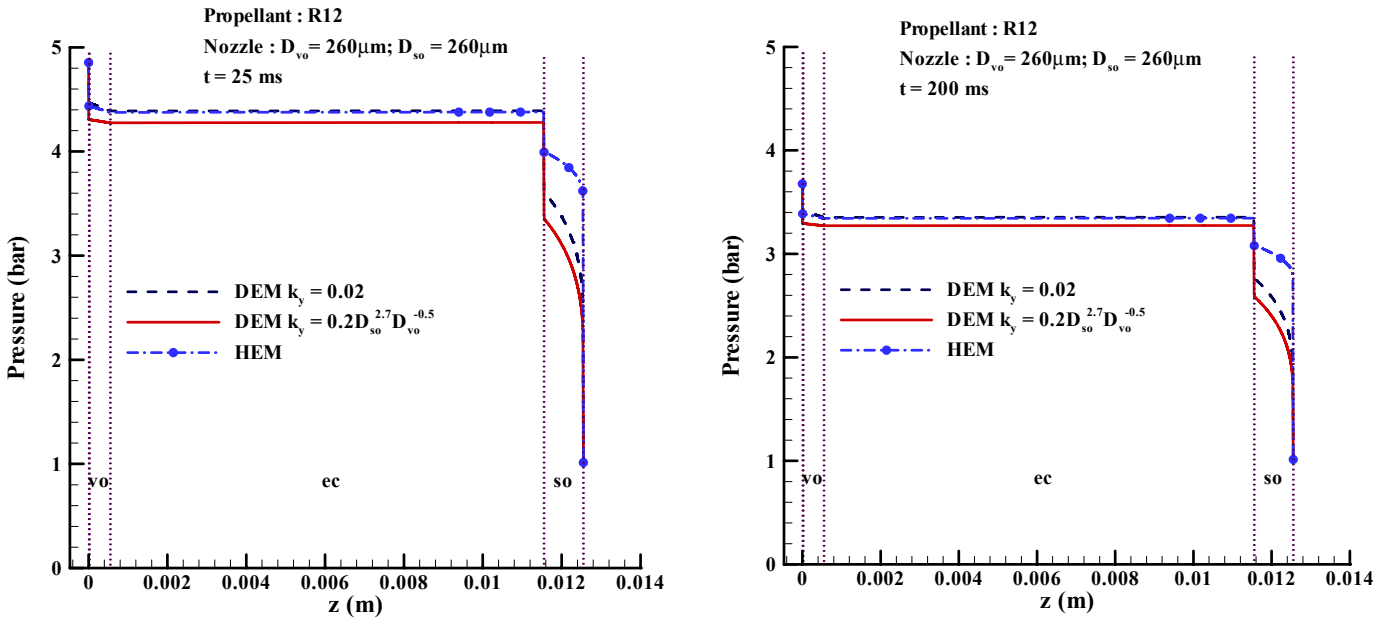

(a) t = 25 ms (b) t=200 ms

Figure 7.37 Comparison of predicted pressure distribution along the twin-orifice system using HEM, DEM k_y = 0.02 and DEM $k_y = 0.2D_{so}^{2.7}D_{vo}^{-0.5}$ for D_{vo} = 260μm and D_{so} = 260 μm

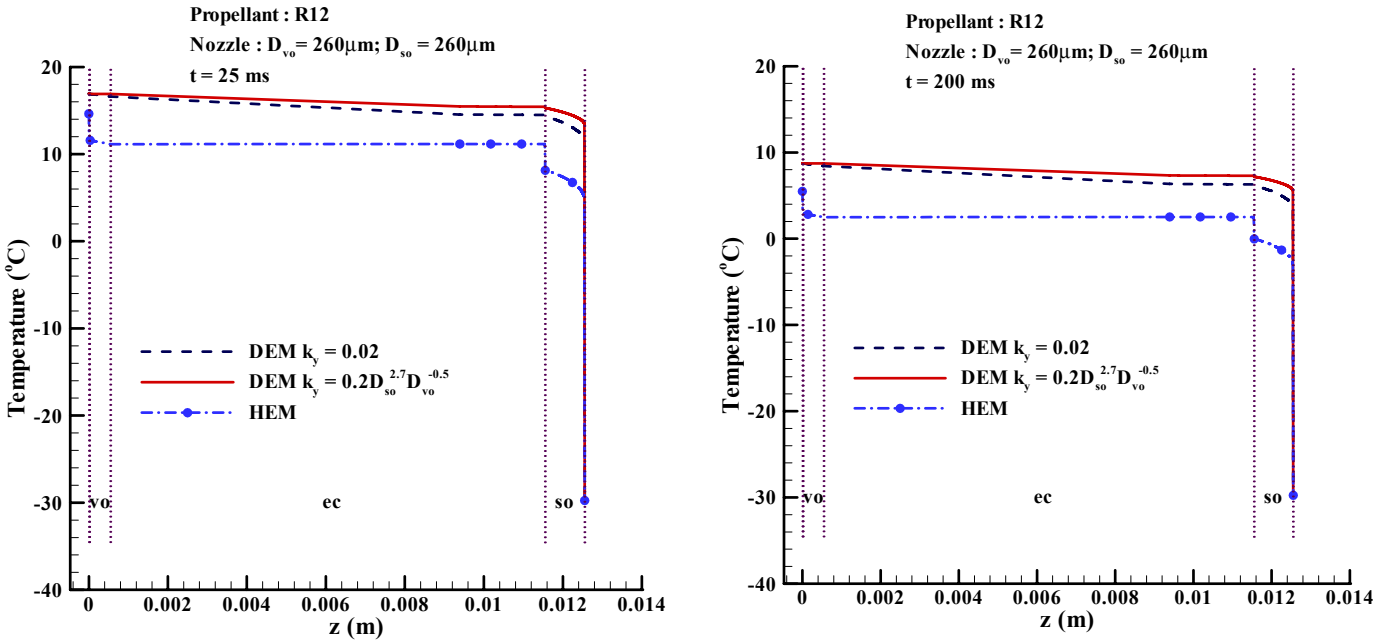

(a) t = 25 ms (b) t=200 ms

Figure 7.38 Comparison of predicted temperature distribution along the twin-orifice system using HEM, DEM k_y = 0.02 and DEM $k_y = 0.2D_{so}^{2.7}D_{vo}^{-0.5}$ for D_{vo} = 260μm and D_{so} = 260 μm

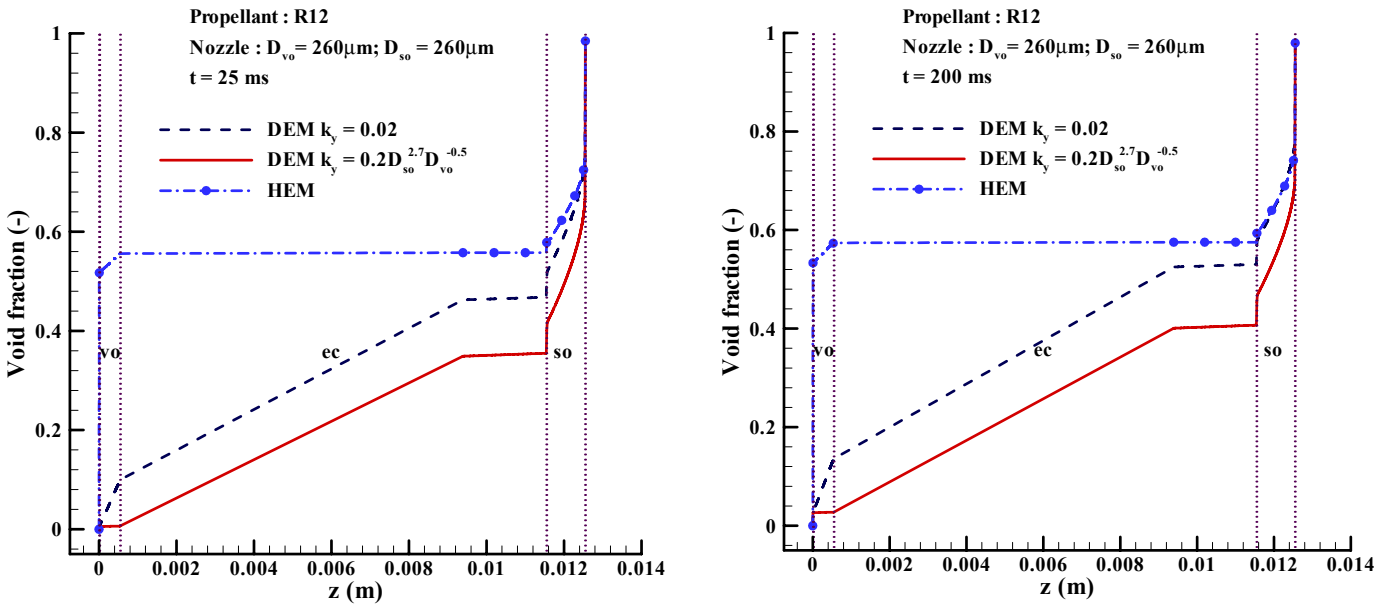

(a) t = 25 ms (b) t=200 ms

Figure 7.39 Comparison of predicted void fraction distribution along the twin-orifice system using HEM, DEM k_y = 0.02 and DEM $k_y = 0.2D_{so}^{2.7}D_{vo}^{-0.5}$ for D_{vo} = 260μm and D_{so} = 260 μm

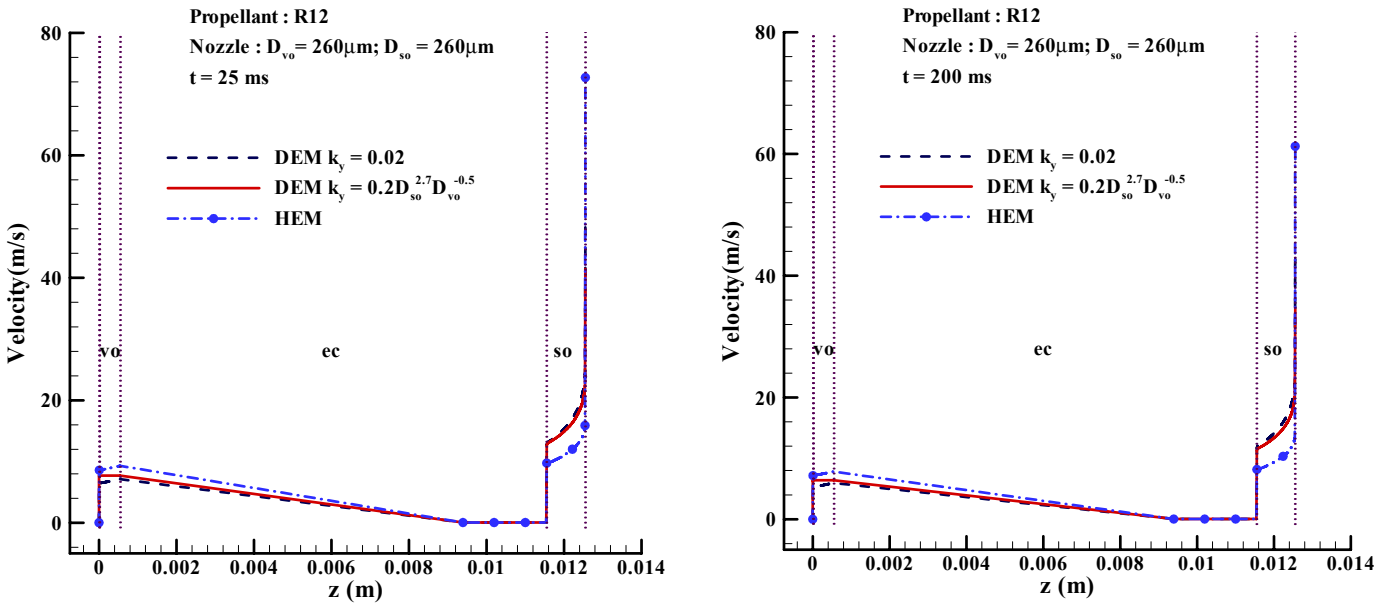

(a) t = 25 ms (b) t=200 ms

Figure 7.40 Comparison of predicted velocity distribution along the twin-orifice system using HEM, DEM k_y = 0.02 and DEM $k_y = 0.2D_{so}^{2.7}D_{vo}^{-0.5}$ for D_{vo} = 260μm and D_{so} = 260 μm

new coefficient, k_y, predicts void fraction zero inside the valve orifice as evaporation is suppressed. The void fraction increases in the expansion chamber. Next, there is a sudden increase at the inlet of the spray orifice is due to the vapour formation associated with the pressure reduction at the abrupt contraction. Then it increases non-linearly inside the spray orifice. HEM predicts the highest void fractions, whereas DEM with new correlation predicts the lowest void fractions. The large differences in the predicted void fraction within the expansion chamber for the three different models are a consequence of differences in evaporation associated with the metastability assumptions. Interestingly, the predicted expansion chamber void fraction is very different for the three models, but this has a little effect on mass flow rate or expansion chamber pressure because these are governed by events in valve orifice and spray orifice. It can also be observed that the evaluated void fractions for t=200 ms are slightly higher then that of t=25 ms with DEM. Whereas with HEM, the evaluated void fraction are almost same for both the time instants.

The comparison of predicted velocity profiles along the twin-orifice system at t=25 ms and t=200 ms is shown in Figure 7.40a-b. As before, mass conservation and evaporation explain the velocity trends. The velocity increases as a consequence of (i) area reduction (at the inlet of valve orifice and spray orifice) and (ii) void fraction increase (in ducts with constant cross-sectional area). The DEM with both the coefficients gives almost identical velocity profile. Whereas the HEM predict slightly higher velocities inside the valve orifice and lowest velocities inside the spray orifice. HEM predicts the high discharge velocity (see Table 7.6) at the spray orifice exit evaluated after the shock because of high choking pressure, which increases the discharge velocity due to acceleration of the flow.

In conclusion the DEM with $k_y = 0.2 D_{so}^{2.7} D_{vo}^{-0.5}$ predicts lowest pressures, highest temperatures and lowest void fractions because the new coefficient evaluates a value of 0.01 for this case which is smaller then the coefficient k_y = 0.02, which encourages metastability and inhibits evaporation. As mentioned previously, the linear increase in the void fraction and the linear decrease in the velocity from the exit of the valve orifice (z = 0.005425 m) to middle of expansion chamber (z = 0.0093) for delayed equilibrium models (DEMs) (in Figure 7.39a-b and Figure 7.40a-b) associated with

the integration of relaxation equation (3.46) across a CV representing a gradual conical expansion from the exit of the valve orifice over a length of 5h (= 0.00885 m).

7.5.2.1. Comparison of mass flow rate

Table 7.5 shows the numerically predicted quasi-steady mass flow rates at the start of the discharge event and at six later instants for the two DEMs and HEM. The DEMs predict substantially larger mass flow rates compared with the HEM. Using the metering chamber volume of 100 μL, liquid density for R12 of 1304 kg/m^3 and approximate discharge event duration of 300 ms, we can make an estimate of the average mass flow rate of 4.35×10^{-4} kg/s = 1.565 kg/h. Table 7.5 shows that the DEM with k_y = 0.02 predictions are very close to this estimate with an error of 3%. The DEM with new correlation overpredicts the mass flow rate.

7.5.2.2. Comparison of expansion chamber pressures

Figure 7.41 shows the comparison of predicted expansion chamber pressure at different instants during the metered discharge of R12 with Clark's (1991)

Table 7.5 Predicted mass flow rates for different models

Case	t (ms)	Numerical Mass Flow Rate $\dot{m}$ (kg/h)		
		HEM	DEM	
			$k_y = 0.02$	$k_y = 0.2 D_{so}^{2.7} D_{vo}^{-0.5}$
1	0	1.175	1.863	2.169
2	25	1.098	1.647	1.961
3	50	1.089	1.661	1.970
4	75	1.077	1.674	1.976
5	100	1.040	1.614	1.912
6	150	0.973	1.489	1.779
7	200	0.902	1.350	1.631
Average $\dot{m}$		1.051	1.614	1.914

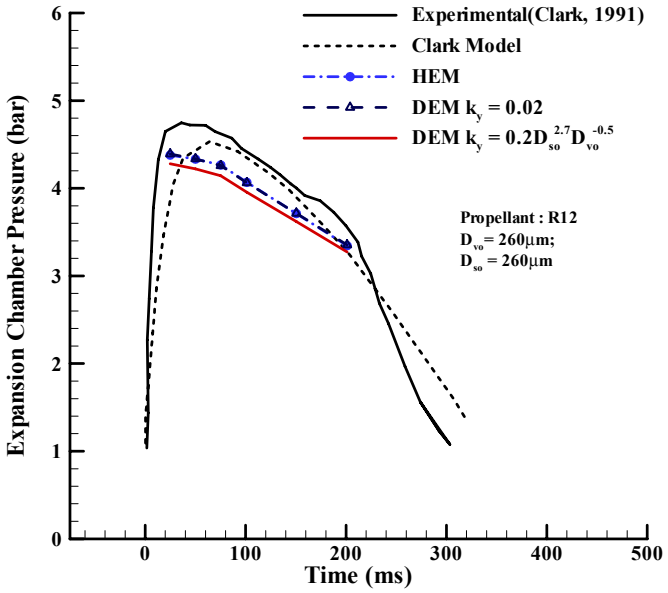

Figure 7.41 Comparison of expansion chamber pressure against Clark's (1991) experimental results

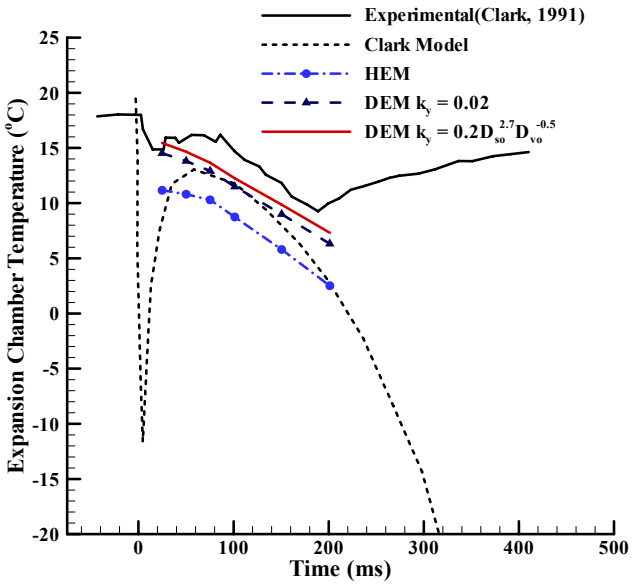

Figure 7.42 Comparison of expansion chamber temperature against Clark's (1991) experimental results

experimental and theoretical results. All three models underpredict the expansion chamber pressures. The HEM and DEM with k_y =0.02 predict identical expansion chamber pressures with an average error of 7.22%, whereas the DEM with the new correlation predicts lowest expansion chamber pressure with an average error of 9.39%, while the Clark's (1991) theoretical model predicts the expansion chamber pressures with an average error of 6.37%.

7.5.2.3. Comparison of expansion chamber temperature

Figure 7.42 shows the comparison of expansion chamber temperatures using all the three models with Clark's (1991) experimental and theoretical results. HEM predicts the lowest expansion chamber temperature with an average error of 43.1%. Clark's theoretical model predicts the expansion chamber temperature with an average error of 34.4%. DEM with k_y = 0.02 and new correlation predicts the expansion chamber temperature with an average error of 24.4% and 13% respectively. The differences in these models is due to different modeling assumptions. HEM assumes homogeneous equilibrium and hence predicts the saturation temperatures inside the expansion chamber, which are the lowest possible values. In both DEMs (with k_y = 0.02 and new correlation) the average temperature is calculated as mean of metastable liquid temperature and saturated temperature using equation (3.18) and hence they predict higher expansion chamber temperatures. The large discrepancies between the predicted and experimental values may be attributed to the uncertainties associated with the experiments in measuring the expansion chamber temperature as well as the uncertainties of prediction formula (3.18).

7.5.2.4. Comparison of spray orifice exit velocities

Figure 7.43 compares the predicted discharge velocity using equation (3.55) at the spray orifice exit for the three models against Clark's (1991) experimental and theoretical results. Unlike the pressure and temperature, the spray discharge velocity appears to be highly sensitive to the modeling assumptions. Both DEMs (with k_y = 0.02 and new correlation) predicts discharge velocities with an average error of 9.51% and 9.69%. The Clark's theoretical model predicts discharge velocities with an

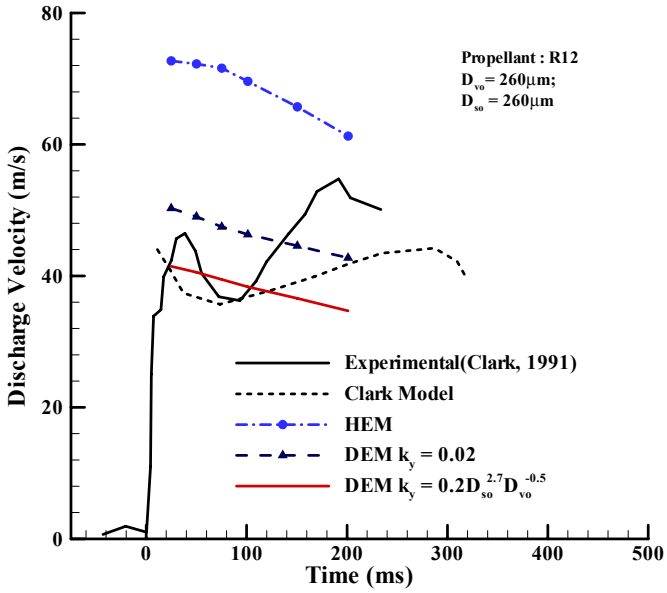

Figure 7.43 Comparison of exit velocity at the spray orifice exit against Clark's (1991) experimental results

average error of 10.82%, which exhibit a rapid velocity decrease between 25 and 100 ms followed by a slow increase after 100 ms. It is interesting to note that the DEMs show a monotonic decrease, whereas Clark's model follows the experimental trend. HEM predicts the highest discharge velocity with an average error of 61.7%, which is due to high choking pressures at the exit of the spray orifice that accelerate the flow in to ambient atmosphere. The DEM with new correlation gives lowest choking pressures at the spray orifice exit, whereas DEM with k_y = 0.02 predicts intermediate choking pressures and hence predicts the discharge velocities in between the HEM and DEM with new correlation.

7.5.3. Summary

The metered propellant discharge from a pMDI has been modeled as a twin-orifice system with different inlet conditions representing different instants during the quasi-steady phase of a pMDI discharge event accounting for propellant metastability. To gain an insight into the role played by metastability, steady-state simulations with

different modeling assumptions – DEM (with k_y = 0.02 and $k_y = 0.2 D_{so}^{2.7} D_{vo}^{-0.5}$) and HEM - are compared with Clark's (1991) experimental and theoretical results. Based on the mass flow rate and expansion chamber pressure, it can be concluded that the predictions of DEM with k_y = 0.02 are close to the experimental data. HEM underpredicts the mass flow rate, whereas DEM with $k_y = 0.2 D_{so}^{2.7} D_{vo}^{-0.5}$ overpredicts the mass flow rate. For this particular case as the diameter of spray orifice is small, it yields small coefficient that encourages metastability and inhibits evaporation. It should also be noted that LOF flow regimes has been considered at the valve orifice inlet, whereas two-phase with low qualities exist in actual metered discharge flows.

The differences in these models is due to different modeling assumptions. Clark's theoretical model assumes that no phase change occurs inside the valve and spray orifice and the vapour expands isentropically as a perfect gas and equilibrium conditions are assumed inside the expansion chamber. The HEM assumes that the two-phases are in equilibrium everywhere inside the twin-orifice system and evaporation happens instantaneously at the saturated pressure. The DEM assumes that the propellant exists in three phases: metastable liquid, saturated liquid and vapour and the evaporation does not happen instantaneously, but only a fraction *y* (the so-called vaporisation index) of the propellant is transformed into saturated mixture, the state of the other fraction *(1-y)* remains metastable liquid and is submitted to an isentropic evolution.

The fact that the expansion chamber pressure is predicted well with Clark's Model, whereas the expansion chamber temperature is predicted most closely with DEM would suggest that the conditions in the expansion chamber are likely to be fairly close to equilibrium with a modest level of metastability. This is in agreement with conclusions drawn by Clark (1991) and Fletcher (1975) and backed up by the profiles of vaporisation index and quality shown Figure 7.44a-b and Figure 7.45a-b respectively at t = 25 ms and t = 200 ms. From the quality profiles, it can be observed that the quality predicted by the DEM with k_y = 0.02 is close to the equilibrium value inside the expansion chamber, which is the reason why HEM and DEM with k_y = 0.02 predict almost equal expansion chamber pressures. The DEM with new correlation, on

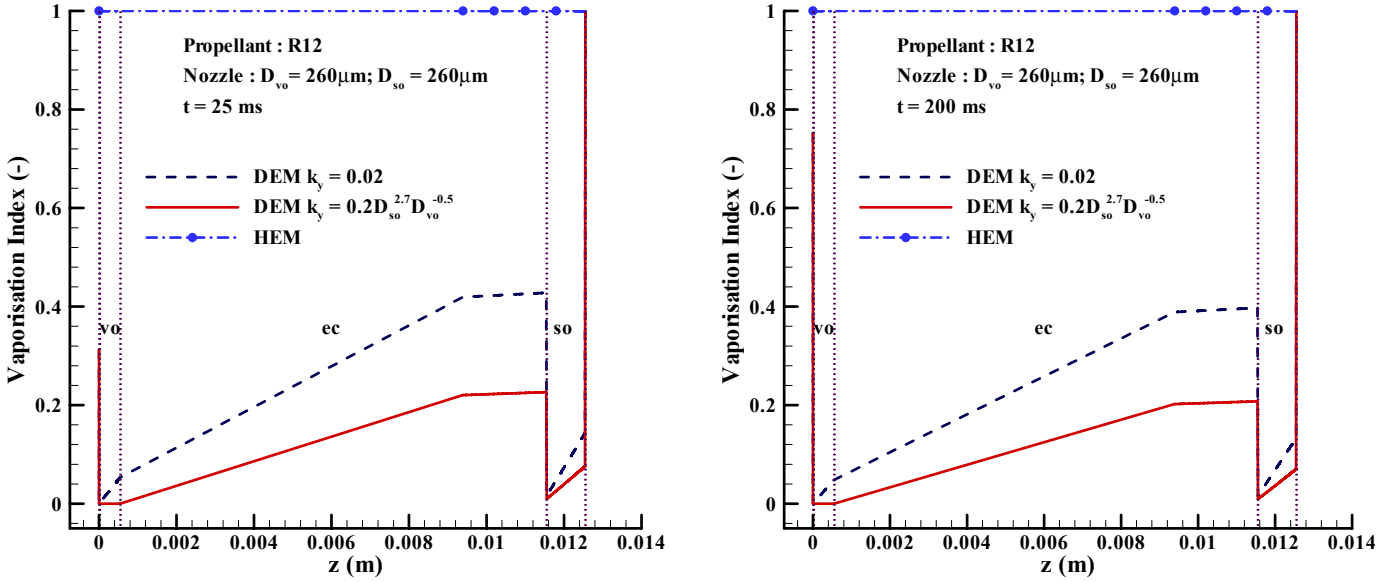

(a) t = 25 ms (b) t=200 ms

Figure 7.44 Comparison of predicted vaporisation index along the twin-orifice system using HEM, DEM $k_y = 0.02$ and DEM $k_y = 0.2D_{so}^{2.7}D_{vo}^{-0.5}$ for D_{vo} = 260μm and D_{so} = 260 μm

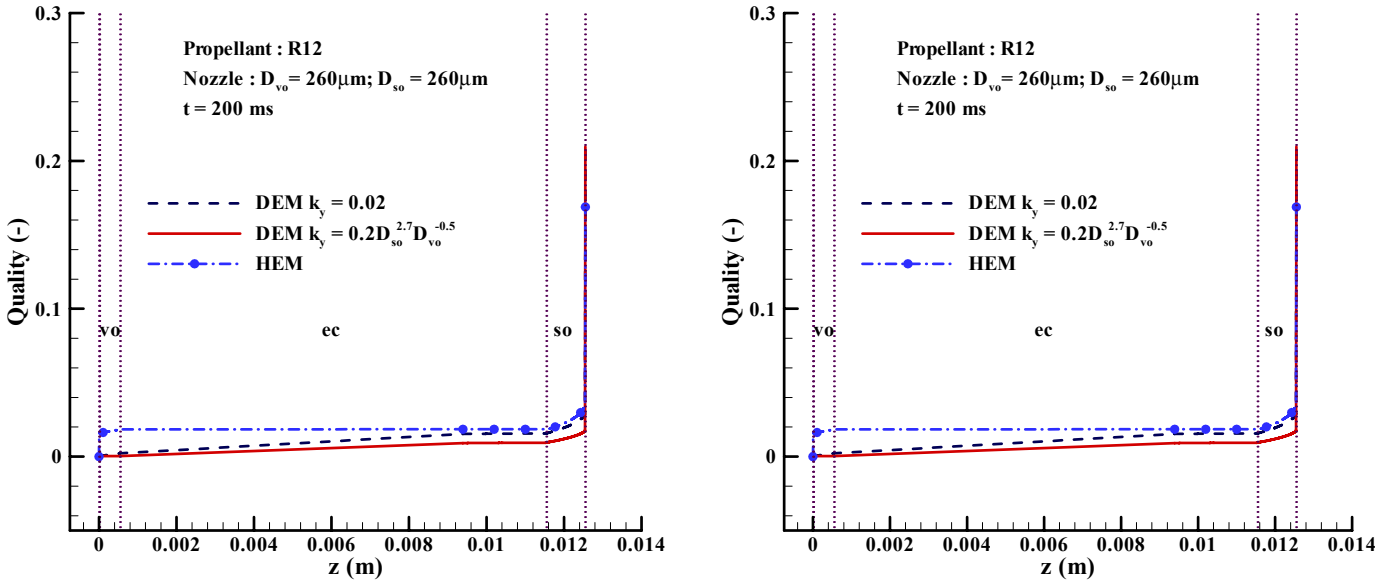

(a) t = 25 ms (b) t=200 ms

Figure 7.45 Comparison of quality distribution along the twin-orifice system using HEM, DEM $k_y = 0.02$ and DEM $k_y = 0.2D_{so}^{2.7}D_{vo}^{-0.5}$ for D_{vo} = 260μm and D_{so} = 260 μm

the other hand predicts slow return to equilibrium as k_y<0.02 for this case and hence predicts low expansion chamber pressures. Observing the vaporisation index (Figure 7.44a-b), one can see that both the DEMs predict metastability inside the expansion chamber at t=25 ms and t=200 ms, and the expansion chamber temperatures are predicted well using these two models. It can also be noticed that DEM with k_y = 0.02 predicts lower level of metastability than DEM with new correlation for both time instants. The DEM with k_y = 0.02 predicts a value of 0.4 for the vaporisation index. Beyond differences in the treatment of metastability, the discrepancies in the mass flow rate and expansion chamber pressure may also be attributable to other modeling assumptions such as no slip between the vapor and liquid phases, as equilibrium kinematic conditions are unlikely to be reached inside the valve and spray orifices. Also, it should be noted that the relaxation equation (3.9) originates from experiments on steam-water system for capillary tubes assuming heterogeneous nucleation, where the frictional forces are dominant (Hardy and Mali, 1983; Feburie et al. 1993; Attou and Seynhaeve, 1999a-b). Whereas, for short tubes, the pressure drop occurs due acceleration and the homogeneous nucleation occurs due to nuclei sitting inside the flow is more likely.

Finally, it should be noted that the geometry of Clark's twin-orifice system contains a 90° turn just ahead of the spray orifice. If the state of the propellant is non-homogeneous in the expansion chamber, the inlet quality of the spray orifice may be different from the predicted values.

The atomization process is strongly influenced by the liquid properties of density, viscosity and surface tension (Lefebvre, 1989). These properties depend on the local pressure and temperature. Also, in order to predict spray formation from pMDIs it is essential to have accurate knowledge of thermodynamic state, void fraction and velocity of the fluid at the spray orifice exit. As highlighted above, metastability will cause large differences in the void fraction of the expansion chamber and strongly influence the subsequent flow development in the spray orifice. Table 7.6 summarizes the flow properties at the spray orifice exit, which represent the starting conditions for the droplet aerosol produced by a pMDI. The differences in discharge velocities

between these models is due to predicted choking pressures. HEM predicts the largest choking pressures and hence predicts high discharge velocity and low void fraction. Thee DEM with new correlation predicts lowest choking pressures and hence the lowest discharge velocities and highest void fraction. Whereas the DEM with k_y = 0.02 predicts intermediate choking pressures and discharge velocities. The below table shows large differences between the predicted velocity and void fractions for our models with widely differing metastability assumptions, suggesting that accurate prediction of metastability is very important for the future development of accurate atomization models.

Table 7.6 Predicted flow conditions at spray orifice exit corresponding to the droplet spray source

		Spray Exit Velocity (m/s)			Exit Void Fraction		
	t (ms)	U_{DEM}		U_{HEM}	α_{DEM}		α_{HEM}
		$k_y = 0.02$	$k_y = 0.2 D_{so}^{2.7} D_{vo}^{-0.5}$		$k_y = 0.02$	$k_y = 0.2 D_{so}^{2.7} D_{vo}^{-0.5}$	
Case 1	0	49.44	41.66	76.70	0.9881	0.9882	0.9861
Case 2	25	50.29	41.45	72.71	0.9877	0.9878	0.9847
Case 3	50	49.01	40.55	72.26	0.9873	0.9875	0.9845
Case 4	75	47.47	39.45	71.61	0.9869	0.9871	0.9843
Case 5	100	46.31	38.34	69.60	0.9864	0.9865	0.9835
Case 6	150	44.58	36.58	65.72	0.9853	0.9855	0.9818
Case 7	200	42.74	34.70	61.27	0.9841	0.9843	0.9796

7.6. Closure

In this chapter, the continuous discharge of propellant flow through twin-orifice of pMDI has been modeled using DEM with two different coefficients (DEM with k_y = 0.02 and $k_y = 0.2D_{so}^{2.7}D_{vo}^{-0.5}$). The results were compared against Fletcher's (1975) and Clark's (1991) experimental data. Both models showed good predictions with Fletcher's experimental data. However, some discrepancies are noticed with Clark's experimental data. The DEM with k_y = 0.02 showed good agreement with Clark's experimental data for small valve orifices (D_{vo} = 259 μm and D_{vo} = 420μm) with $1<D_{so}/D_{vo}<3$. However, for large valve orifices and small valve orifice with $D_{so}/D_{vo}>3$, it showed larger discrepancies. The DEM with $k_y = 0.2D_{so}^{2.7}D_{vo}^{-0.5}$ overall predicted the mass flow rate well compared to that of k_y = 0.02, as this new coefficient was optimized considering the mass flow rate. Thereafter, the quasi-steady metered discharge of propellant was modeled as a twin-orifice system with different inlet conditions. To understand the role played by metastability, steady-state simulations with DEM (k_y = 0.02 and $k_y = 0.2D_{so}^{2.7}D_{vo}^{-0.5}$) and HEM were compared with Clark's experimental data. Detailed examination of the results suggested metastability strongly affects the void fraction in the expansion chamber and subsequent void fraction in the spray orifice and discharge velocity of the spray confirming that metastability has to be accounted for accurately.

CHAPTER 8

CONCLUSIONS AND RECOMMENDATIONS FOR FUTURE WORK

The thermodynamic and fluid mechanics of propellant flow in pressurised metered-dose inhalers (pMDIs) is very complex and poorly understood. To predict spray formation from pMDIs it is essential to have accurate knowledge of thermodynamic state, void fraction and velocity of the fluid at the spray orifice exit. Previous work by Fletcher (1975) and Clark (1991) has done much to reveal the general nature of pMDI propellant flows. They developed semi-empirical models of flashing propellant flows through a pMDI based on assumptions of thermodynamic equilibrium in the metering and expansion chambers and homogeneous frozen flow in the valve and spray orifices. The results of their models were in broad agreement with experimental trends, but a number of detailed issues remained unresolved. One of these was the experimental observation that propellant temperatures in the expansion chambers were higher than the saturation temperature at the prevailing pressures. This conflicted with the assumed modeling conditions of thermodynamic equilibrium within these spaces and above authors suggested metastability may play a role in the flashing propellant flow.

The main objective of this thesis, as outlined in chapter 3, was to develop a new numerical model which would predict the internal flow conditions (pressure, temperature, velocity, void fraction, quality, etc.) and provide deeper insight into the atomization process and fluid mechanics involved in the twin-orifice of pMDIs accounting for propellant metastability. In order to achieve the above objective, first the flashing propellant flow inside single orifices was studied using different theoretical models in Chapter 5. A semi-empirical model was used to model the flow through short tubes. The well established homogeneous equilibrium model (HEM), delayed equilibrium model (DEM) and improved delayed equilibrium model (IDEM) were used to model the flow through long and short capillary tubes.

The geometry of the twin-orifice system of a pMDI is complex and involves several singularities (sudden enlargements and sudden contractions). Various assumptions

were made to evaluate their effect on the vaporisation process and to evaluate the flow variables after the shock at the exit of the spray orifice when the flow is choked. Also, three different propellant flow regimes (LOF, TPF and MOF) were explored at the inlet of the valve orifice. The effect of these assumptions and different flow regimes was investigated in Chapter 6.

Numerical investigations were carried out using the delayed equilibrium model (DEM) with these new assumptions to validate the two-phase metastable flow through twin-orifice systems with continuous flows of various propellants studied previously by Fletcher (1975) and Clark (1991) with various propellants. A new correlation was developed for the coefficient k_y ($k_y = 0.2 D_{so}^{2.7} D_{vo}^{-0.5}$) in the relaxation equation (3.9). Along with this correlation the constant coefficient k_y = 0.02 was used in the relaxation equation to model the metastability. The DEM with coefficients k_y = 0.02 and $k_y = 0.2 D_{so}^{2.7} D_{vo}^{-0.5}$ developed for continuous discharge flows were applied to investigate quasi-steady flashing flow for metered discharge of propellant at various time instants. The DEM results were compared with Clark's metered discharge experimental data and the well established homogeneous equilibrium model (HEM). These investigations were presented in Chapter 7.

8.1. Conclusions

The key conclusions from the flashing propellant flow through single orifice/tube are as follows:

- The semi-empirical model for the short tubes showed good agreement between the predicted mass flow rate and the experimental data of Kim and O'Neal (1994a) for both the inlet conditions : subcooled and two-phase. However, the semi-empirical model overpredicted the mass flow rates in comparison with Clark's (1991) experimental data for short tubes at high expansion chamber pressures. This was not unexpected since Kim and O'Neal experiments were

conducted at conditions representative of refrigeration applications and hence covered much higher discharge pressures than those in pMDIs.

- For the flow through long adiabatic capillary tubes with pure propellants, the predicted mass flow rate, pressure and temperature profiles using three models-HEM, DEM and IDEM-showed reasonably good agreement against the experimental data. However, the mass flow rate and temperature profiles predicted by DEM were closer to the experimental results compare to those of HEM and IDEM. HEM underpredicted the mass flow rate, whereas IDEM over predicted the mass flow rate.

- For the flow through long adiabatic capillary tubes with propellant mixtures (R410A and R407C), all the three models, HEM, DEM and IDEM, predicted similar pressure and temperature profiles. The mass flow rates predicted by IDEM were close to the experimental data. Both HEM and DEM underpredicted the mass flow rate.

- For the flow through short capillary tubes, DEM predicted the mass flow rate and pressure distribution along the short tube well. IDEM predicted well the mass flow rate, but underpredicted the pressure distribution inside the short tube, where as HEM underpredicted both the mass flow rate and pressure distribution.

The key conclusions from the flashing propellant flow through twin-orifice system of pMDIs are as follows:

- The predicted mass flow rate, expansion chamber pressure, expansion chamber temperature and the exit velocity using both DEMs (k_y = 0. 02 and $k_y = 0.2 D_{so}^{2.7} D_{vo}^{-0.5}$) showed good agreement against Fletcher's (1975) experimental data with slight discrepancies. The DEM with coefficient $k_y = 0.2 D_{so}^{2.7} D_{vo}^{-0.5}$ predicted the mass flow rate and expansion chamber pressure well compared to

constant coefficient k_y = 0.02. And the coefficient k_y = 0.02 predicted the expansion chamber temperature and exit velocities better than $k_y = 0.2 D_{so}^{2.7} D_{vo}^{-0.5}$.

- The comparison of DEM with coefficient k_y = 0.02 and $k_y = 0.2 D_{so}^{2.7} D_{vo}^{-0.5}$ against Clark's (1991) experimental data showed that $k_y = 0.2 D_{so}^{2.7} D_{vo}^{-0.5}$ predicts the mass flow rate and the expansion chamber temperature well in compare to that of k_y = 0.02, but slightly overpredicts the expansion chamber pressures. Whereas the constant coefficient k_y = 0.02 predicts the expansion chamber pressures and discharge velocities better than $k_y = 0.2 D_{so}^{2.7} D_{vo}^{-0.5}$.

- The present study suggests that single coefficient is not enough to model the metastability inside twin-orifice of pMDIs and different coefficients are required to model the metastability for different range of orifice configurations.

- The comparison between the HEM and DEM with k_y = 0.02 and $k_y = 0.2 D_{so}^{2.7} D_{vo}^{-0.5}$ against the Clark's (1991) experimental data showed that the DEM with k_y = 0.02 predicted the mass flow well in compare to that of HEM and DEM with $k_y = 0.2 D_{so}^{2.7} D_{vo}^{-0.5}$.

- For metered discharge the analysis of different possible flow regimes, showed that predictions based on the LOF give the better agreement with measured mass flow rate compared to TPF and MOF. TPF underestimates the mass flow rate and the expansion chamber pressure, whereas MOF underestimates the mass flow rate. This would suggest that the fluid regime in the metering chamber is predominantly stratified.

8.2. Recommendations for future work

The following suggestion are made for the further study:

- **Modification of the coefficient (k_y) in the relaxation equation**

  The new coefficient ($k_y = 0.2 D_{so}^{2.7} D_{vo}^{-0.5}$) developed for the relaxation equation assumes no vaporisation inside the valve orifice. It predicts the mass flow rate well, but slightly over predicts the expansion chamber pressures. Also, as the diameter of the spray orifice decreases it overpredicts the mass flow rate as it evaluates small coefficient due to $D_{so}^{2.7}$. A new correlation assuming vaporisation inside the valve orifice and assuming homogeneous nucleation would improve the model for a wide range of valve and spray orifices.

- **Separated Flow model**

  The present model assumed the two-phases (liquid and vapour) are in equilibrium and do not account for slip between the phases. It would be beneficial if the further investigations can be made considering the slip between the phases. This would improve the predictions of expansion chamber pressures and the velocities at the spray orifice exit.

- **Metered Discharge Flows**

  Although the present code, could be used to simulate the metered discharge flows assuming quasi steady state at various time instants, it would more desirable to make the current code unsteady to simulate the actual flow through metered discharge flows.

- **Suspended Solids**

  The present work assumes that the drug is present in very small quantities and dissolved in propellant and homogeneously mixed and does not affect the propellant flow or its evaporation. But, in many pharmaceutical formulations the drug is suspended in the propellant. The effect of suspended drug particles was

not taken into account in the present study as it was felt that the propellant metastability needed to be understood on fundamental basis. Further studies are needed on the effects of suspended drug particle which will require extension of the model to three-phase flow an inclusion of the effect of suspended drug particles on nucleation and vapour phase formation.

- **Experimental Work**

  The existing experimental work (Fletcher, 1975 and Clark, 1991) show results the pressure, temperature distribution along twin-orifice system of pMDIs. Detailed experimental work, measuring the pressure and temperature at different locations inside the expansion chamber along the axis would be useful to further validate the present numerical code.

8.3. Present Contribution

The key contributions from the current work are:

- A 1D code to simulate the flashing propellant flow through long adiabatic capillary tubes using both pure propellants (R12, R22, R134A) and propellant mixtures (R410A and R407C). The code was written in Microsoft Visual C++ 6.0.

- Validation of the above code against experimental results available in the literature for the propellant flow through short and long adiabatic capillary tubes.

- A set of modeling assumptions to describe the two-phase metastable flow (i) across the abrupt contractions at the inlet of the valve orifice and spray orifice for twin-orifice systems, (ii) across the abrupt expansion at the exit of the valve orifice and (iii) to solve the shock at the exit of the spray orifice when the flow is choked.

- Using the above assumptions a Microsoft Visual C++ 6.0 based 1D code to simulate the flashing flow through twin-orifice systems of pMDIs of propellants

and propellant mixtures with account of metastability. The current code is capable of handling the critical conditions both at the exit of the valve orifice and the exit of the spray orifice. The present code predicts internal flow conditions (such as pressure, temperature, quality, void fraction, etc.).

- Comprehensive validation of the present code with various propellants against the experimental results of Fletcher (1975) and Clark (1991) for the flashing propellant flow through twin-orifice systems.

- The findings of the present thesis have given a better understanding of the role played by the propellant metastability inside twin-orifice systems of pMDIs. Also, they have provided detailed knowledge of thermodynamic state, void fraction and critical velocity of the propellant at the spray orifice exit, which are essential step towards the development of improved atomization models.

Publications

- Henk Versteeg and Abdul Qaiyum Shaik [2010]. "Design of pressurised metered dose inhalers (pMDI) – Modelling of interal flow". DMD2010-3904, Proceedings of the 2010 Design of Medical Devices Conference, DMD2010, April 13-15, Minneapolis, MN, USA.

- Abdul Qaiyum Shaik and Henk Versteeg [2009]. "Numerical simulation of refrigerant flow through adiabatic capillary tube: A comparison between Homogeneous Equilibrium Model (HEM), Delayed Equilibrium Model (DEM) and Improved Delayed Equilibrium Model (IDEM)", 7th Industrial Simulation Conference, 2009,June 1-3, Loughborough, UK.

- Henk Versteeg and Abdul Qaiyum Shaik [2009]. "Modeling of Flashing propellant flow in Pressurised Metered Dose Inhalers". 7th Industrial Simulation Conference, 2009, June 1-3, Loughborough, UK.

- Abdul.Q.Shaik & Henk K. Versteeg (2008), "Model for the prediction of Internal Flow Conditions in Pressurised Metered Dose Inhalers(pMDIs)", Drug Delivery to Lungs 19, December 10-12, Edinburgh, UK.

Papers manuscript in preparation:

- Abdul Qaiyum Shaik and Henk Versteeg. Numerical Simulation of Refrigerant Flow Through Adiabatic Capillary Tube: A Comparison between Homogeneous Equilibrium Model (HEM), Delayed Equilibrium Model (DEM) and Improved Delayed Equilibrium Model (IDEM). *International Journal of Refrigeration and Air conditioning.*
- Abdul Qaiyum Shaik and Henk Versteeg. Numerical Model for the prediction of internal flow conditions accounting to propellant metastability. *Atomization and Sprays.*

APPENDIX A

DERIVATION FOR CONICAL JET AT THE EXIT OF SPRAY ORIFICE

In this section, an expression derived by Versteeg (2009) for a conical choking propellant jet at the exit of the spray orifice has been presented.

Descriptive Elements and Concept Sketch

- A turbulent propellant jet discharging from a nozzle into the atmosphere is shown diagrammatically in Figure A-1. The jet spray plume development is sub-divided into two regions: (i) far-field jet region and (ii) near-field wide-spray region (see concept sketch below). In the far field (z/D_{so}) the flow behaves like a particle-laden jet: conical region with half angle around 10° (Fletcher, 1975 and Versteeg and Hargrave, 2002).
- For choked conditions the near-field spray exits as a conical spray with an angle θ that can be larger than 10^o. The actual angle is difficult to identify and visualizations show that it appears to be quite dependent on the exit geometry and pressure ratio p_I/p_O. Typically when the flow is checked at the spray orifice exit,

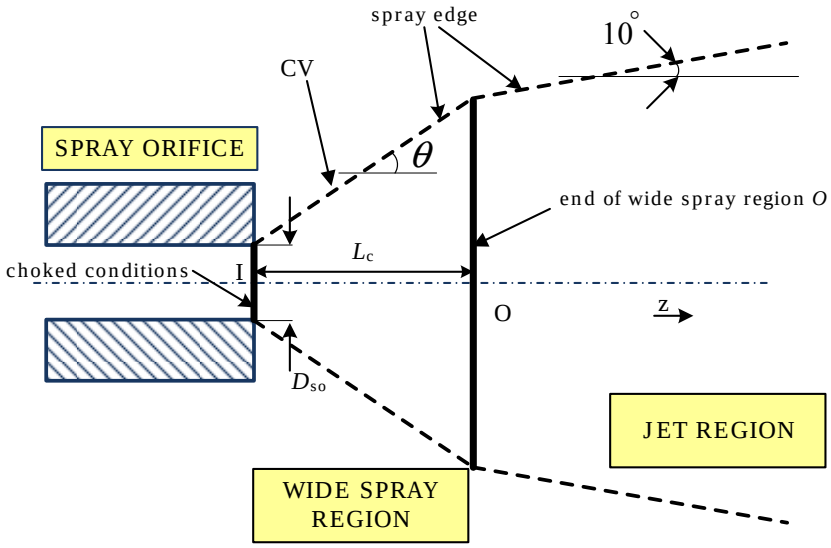

Figure A-1 Control Volume for DSW for conical expansion at the spray orifice exit

the effective angle may be around θ=20° - 45°. When the flow ceases to be choked towards the end of the metered spray event the angle θ decreases to zero. The length L_c of the wide-spray region is also difficult to judge from visualizations, since the two-conical regions merge smoothly, the best guess would be $L_c/D_c \approx$ 2-5.

Process Description

- Near filed (z/D_{so} = 2-5): (i) the cone is surrounded by fluid at atmospheric pressure, (ii) there is no exchange of mass with surrounding air, (iii) the spray undergoes adiabatic evaporation from metastable choked conditions to atmospheric pressure
- In the far field (z/D_{so} >>1) mass transfer is governed by heat transfer due to turbulent mixing between spray and surrounding ambient air.

Mathematical Formulation

Flow is governed by one-dimensional conservation of mass, momentum and energy

Governing Equations:

Under the given assumptions, the flow equations are as follows:

Mass conservation

$$\dot{m} = \frac{U_I A_I}{v_{m,I}} = \int_A \frac{U_{O,z} dA}{v_{m,O}} \qquad \text{A-1}$$

where $A_I = A_{so}$ and $U_{O,Z}$ is z-component of the mean velocity U_O at the outlet of the CV (see)

z-Momentum conservation

Pressure forces:

Under the given assumptions the spray is surrounded by atmospheric air at p_O and the pressure p_I is only acting on A_{so}, so the net pressure force is the same as in straight jet: $(p_I-p_O)A_{so}$

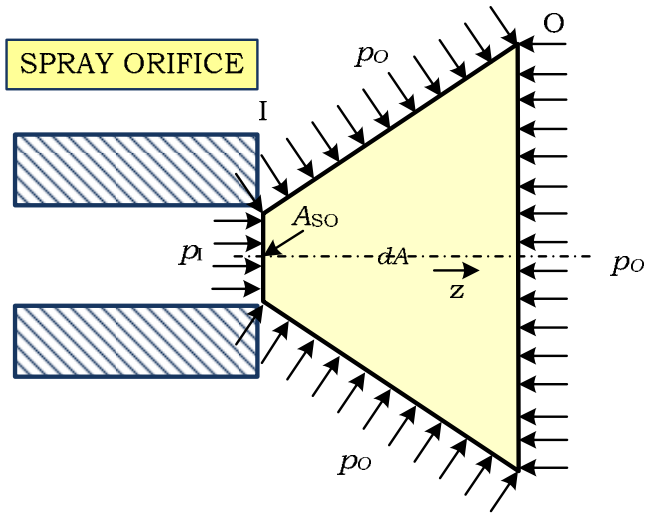

Figure A-2 Pressure forces on CV

$$(p_I - p_O)A_{so} = \dot{m}\left(\overline{U}_{O,z} - U_I\right) \qquad \text{A-2}$$

where $\overline{U}_{O,z}$ is the area-averaged z-velocity component, which is evaluated as the ratio of the z-momentum flux and the mass flux through the outlet area.

(i) *mass flux:*

$$\dot{m} = \frac{2\pi s^2 U_O}{v_{m,O}} \int_{\varphi=0}^{\varphi=\theta} \frac{\sin\varphi \, d\varphi}{\cos^2\varphi} = -\frac{2\pi s^2 U_O}{v_{m,O}} \int_{\varphi=0}^{\varphi=\theta} \frac{d(\cos\varphi)}{\cos^2\varphi} = \frac{2\pi s^2 U_O}{v_{m,O}} \frac{1}{\cos\varphi}\Bigg|_{\varphi=0}^{\varphi=\theta}$$

$$\dot{m} = \int d\dot{m} = \frac{2\pi s^2 U_O}{v_{m,O}} \left(\frac{1}{\cos\theta} - 1\right) \qquad \text{A-3}$$

(ii) z-momentum flux:

$$\int U_{O,z} d\dot{m} = = \int U_{O,z} \frac{U_{O,z}}{v_{m,O}} dA = \int_{r=0}^{r=R_o} \frac{U_{O,z}^2}{v_{m,O}} 2\pi r dr = \frac{2\pi}{v_{m,O}} \int_{\varphi=0}^{\varphi=\theta} \left(U_O^2 \cos^2\varphi\right)(s\tan\varphi)\frac{s d\varphi}{\cos^2\varphi}$$

$$= \frac{2\pi s^2 U_O^2}{v_{m,O}} \int_{\varphi=0}^{\varphi=\theta} \tan\varphi \, d\varphi = -\frac{2\pi s^2 U_O^2}{v_{m,O}} \ln(\cos\varphi)\Big|_{\varphi=0}^{\varphi=\theta} = -\frac{2\pi s^2 U_O^2}{v_{m,O}} [\ln(\cos\theta) - 0]$$

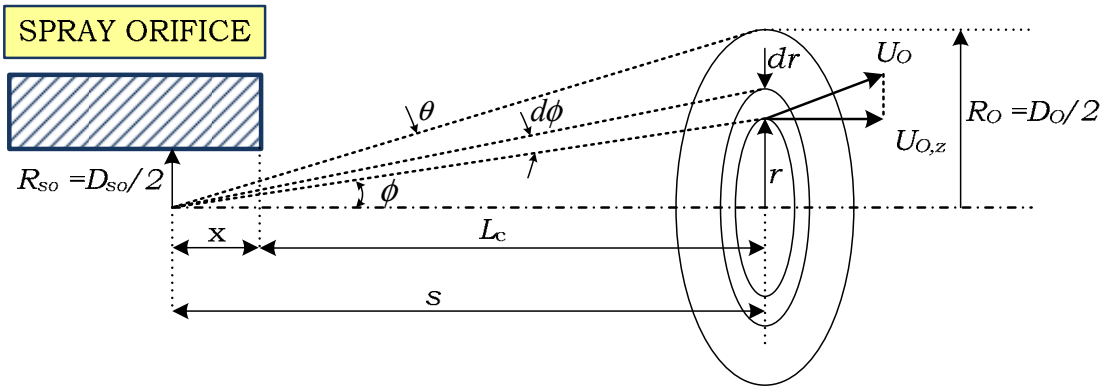

Figure A-3 Definition sketch for mass flux and momentum flux integrals

See Figure A-3: $\tan\varphi = r/s$ and $d(\tan\varphi) = d\varphi/\cos^2\varphi = dr/s$

$$\int U_{O,z}\,d\dot{m} = \frac{2\pi s^2 U_O^2}{v_{m,O}} \ln\left(\frac{1}{\cos\theta}\right) \qquad \text{A-4}$$

(iii) Average z-velocity component $\overline{U}_{O,z}$:

$$\overline{U}_{O,z} = \frac{\int U_{O,z}\,d\dot{m}}{\int d\dot{m}} = U_O \frac{\ln(1/\cos\theta)}{(1/\cos\theta - 1)} = U_O\,F(\theta) \qquad \text{A-5}$$

The values are θ = 20° F(θ) = 0.97 and θ = 45° F(θ) = 0.84. The results are based on the assumption of a flat exit surface perpendicular to the z-direction. The diagram also shows function $G(\theta) = \sin^2\theta/2(1-\cos\theta)$, which involves integration over an exit surface with the shape of a spherical cap, which may be a slightly better representation of the outlet surface O. The differences are quite small in the target region between 20° and 45°, so this derivation is omitted. Note that the function F goes to zero as θ → 90° whereas the limiting value of G is 0.5 highlighting differences between these two exit surface geometries at large angle

Now we re-arrange z-momentum equation (A-2) to obtain the outlet velocity:

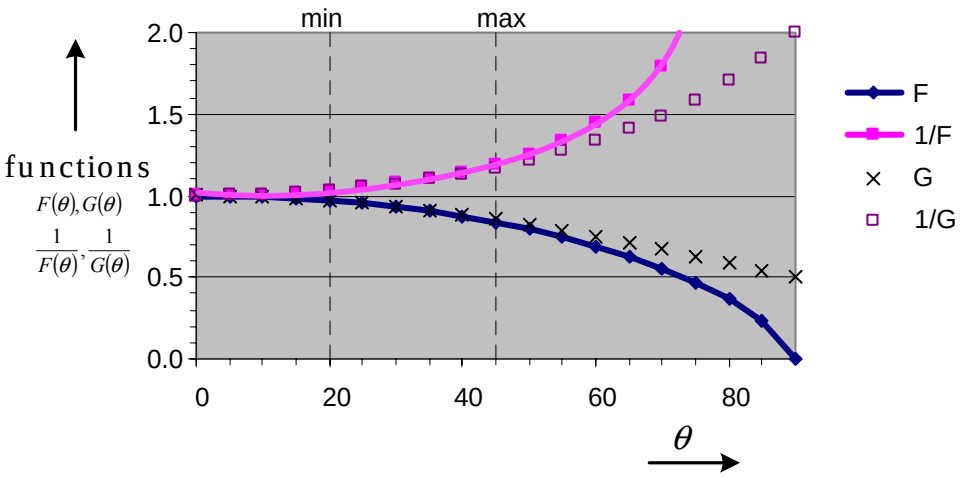

Figure A-4 Average z-velocity function F(θ) as a function of the angle θ

$$(p_I - p_O)A_{so} = \dot{m}(\overline{U}_{O,z} - U_I) = \dot{m}U_I\left(\frac{\overline{U}_{O,z}}{U_I} - 1\right) = \dot{m}U_I\left(\frac{U_O F(\theta)}{U_I} - 1\right)$$

$$\frac{U_O}{U_I} = \frac{1}{F(\theta)}\left[1 + \frac{(p_I - p_O)A_{so}}{\dot{m}U_I}\right], \text{ so } U_O = \frac{U_I}{F(\theta)}\left[1 + \frac{(p_I - p_O)A_{so}}{\dot{m}U_I}\right] \qquad \text{A-6}$$

Note that when θ = 0° F(θ) = 1.0, so the above expression naturally has the correct limiting behaviour for a discharge shock without area enlargement (equation for straight jet). For θ = 20° the value of 1/F(θ) = 1.03 and θ = 45° 1/F(θ) = 1.20, so the area enlargement causes small changes to the z-momentum balance: a modest increase in the z-velocity is associated with the spray widening.

Energy conservation

$$h_{m,O} + \frac{1}{2}U_O^2 = h_{m,I} + \frac{1}{2}U_I^2 \qquad \text{A-7}$$

At the inlet the liquid is metastable, therefore the mixture enthalpy is given by

$$h_{m,I} = (1 - y_I)h_{lm,I} + (y_I - x_I)h_{l,I} + x_I h_{v,I} \qquad \text{A-8}$$

At the outlet it is assumed that the fluid has completed adiabatic evaporation, so y_O = 1 and the mixture enthalpy reduces to

$$h_{m,O} = (1 - x_O)h_{l,O} + x_O h_{v,O} \qquad \text{A-9}$$

Re-arranging the above equation to evaluate x_O at the exit

$$x_O = \frac{h_{m,O} - h_{l,O}}{h_{v,sat,O} - h_{l,O}} \qquad \text{A-10}$$

The ratio of exit and inlet specific enthalpy can be computed from the energy equation (A-7) as follows:

$$\frac{h_{m,O}}{h_{m,I}} = 1 - \frac{\frac{1}{2}\left(U_O^2 - U_I^2\right)}{h_{m,I}} = 1 - \frac{\frac{1}{2}U_I^2}{h_{m,I}}\left[\left(\frac{U_O}{U_I}\right)^2 - 1\right] \qquad \text{A-11}$$

where the velocity ratio can be evaluated using expression (A-6)

Under the given assumptions the exit quality can be obtained from equation (A-10).

The specific volume at the inlet I is obtained using:

$$\nu_{m,I} = 1/\rho_{m,I} = (1 - y)\nu_{lm,I} + (y - x)\nu_{l,I} + x\nu_{v,I} \qquad \text{A-12}$$

Using the $y_O = 1$, the specific volume at outlet O can be obtained from:

$$\nu_{m,O} = 1/\rho_{m,O} = (1 - x_O)\nu_{l,O} + x_O\nu_{v,O} \qquad \text{A-13}$$

The ratio of outlet and inlet specific volume can be obtained by dividing the results (A-12) and (A-13).

APPENDIX B

FLOW CHARTS

Flow Charts for an Adiabatic Capillary Tube

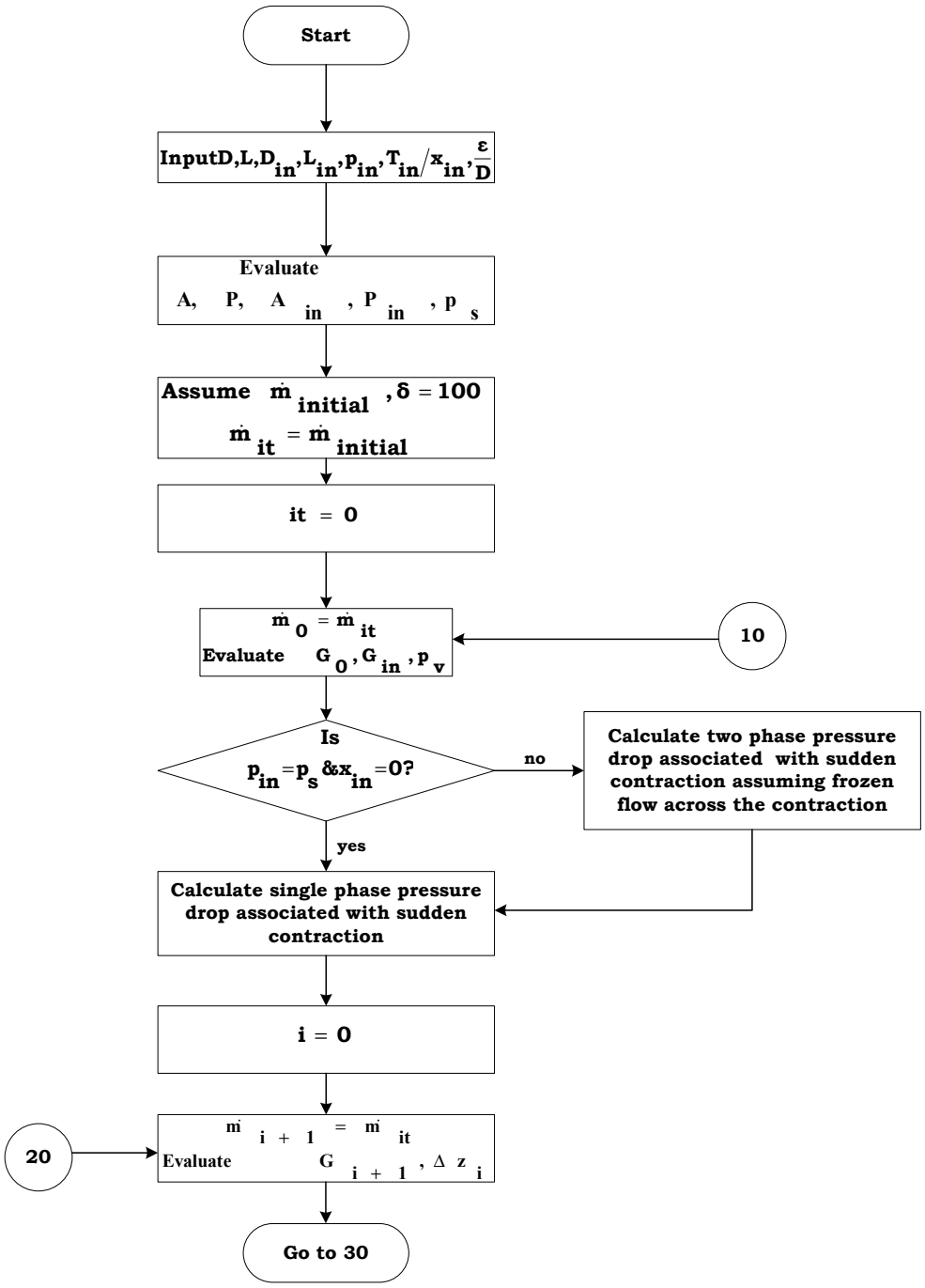

Figure B-1 Flow chart of PIF algorithm using DEM for an adiabatic capillary tube (continued…)

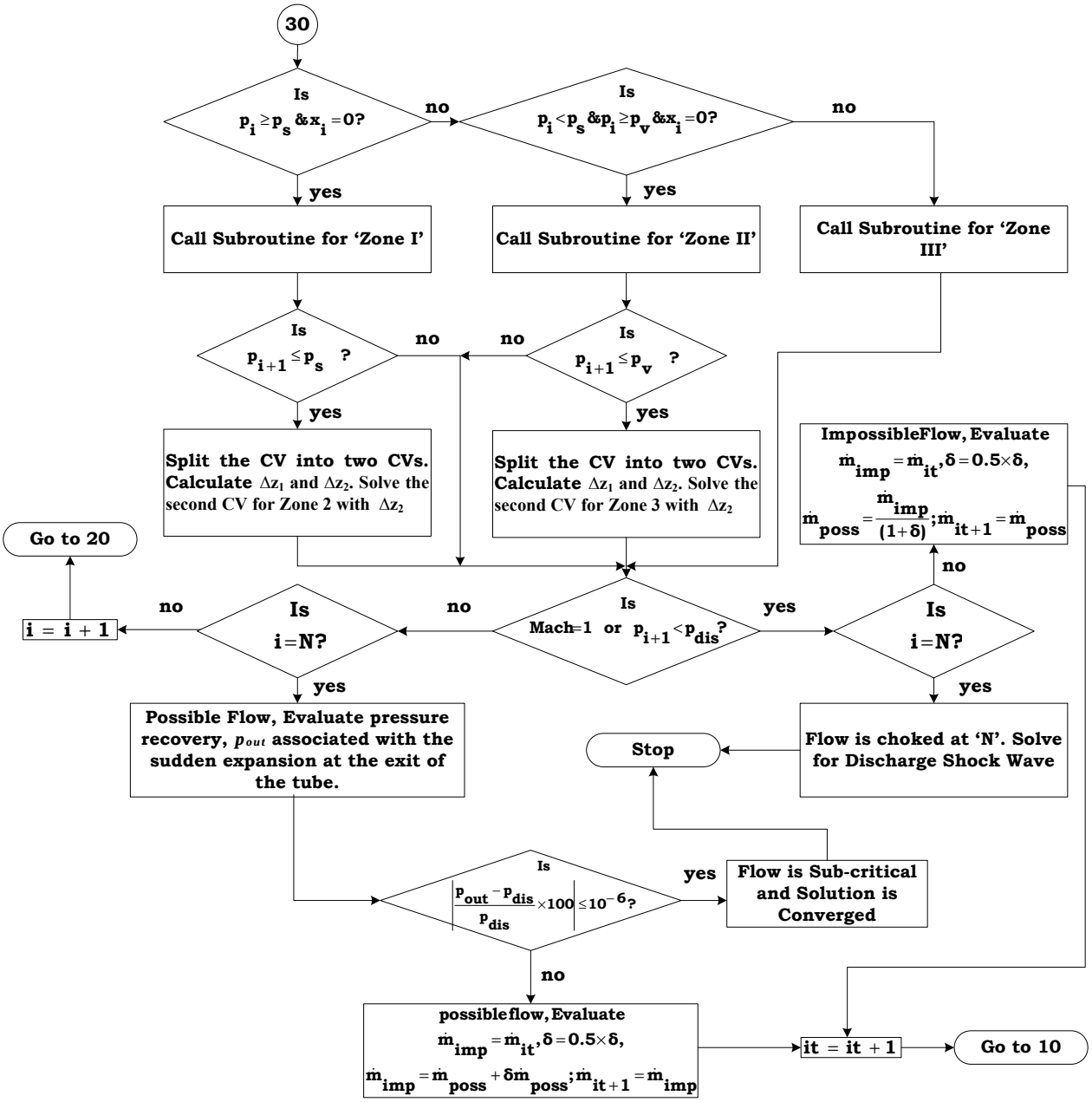

Figure B-1 Flow chart of PIF algorithm using DEM for an adiabatic capillary tube

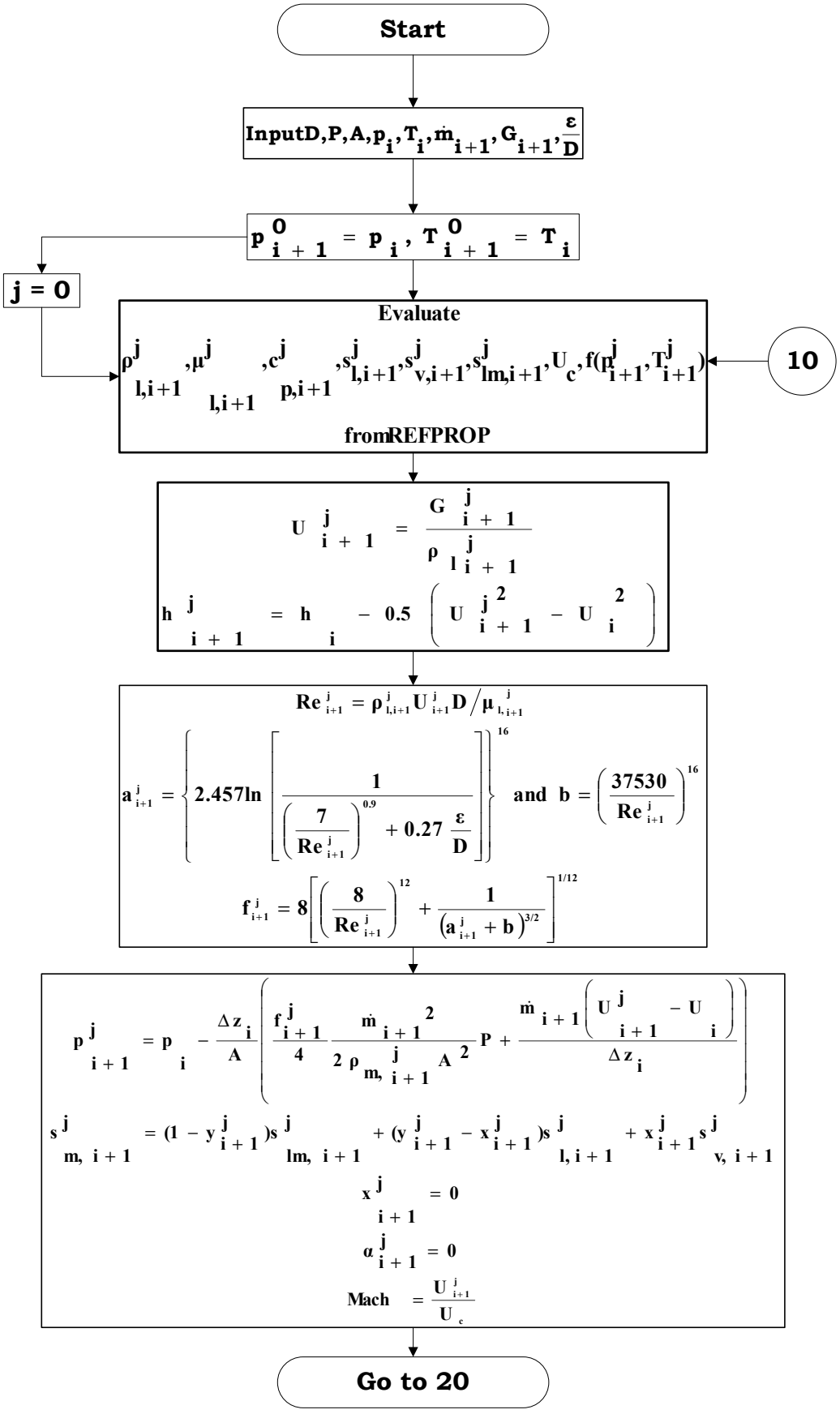

Figure B-2 Flow chart to calculate flow variables for zone I/zone II (continued…)

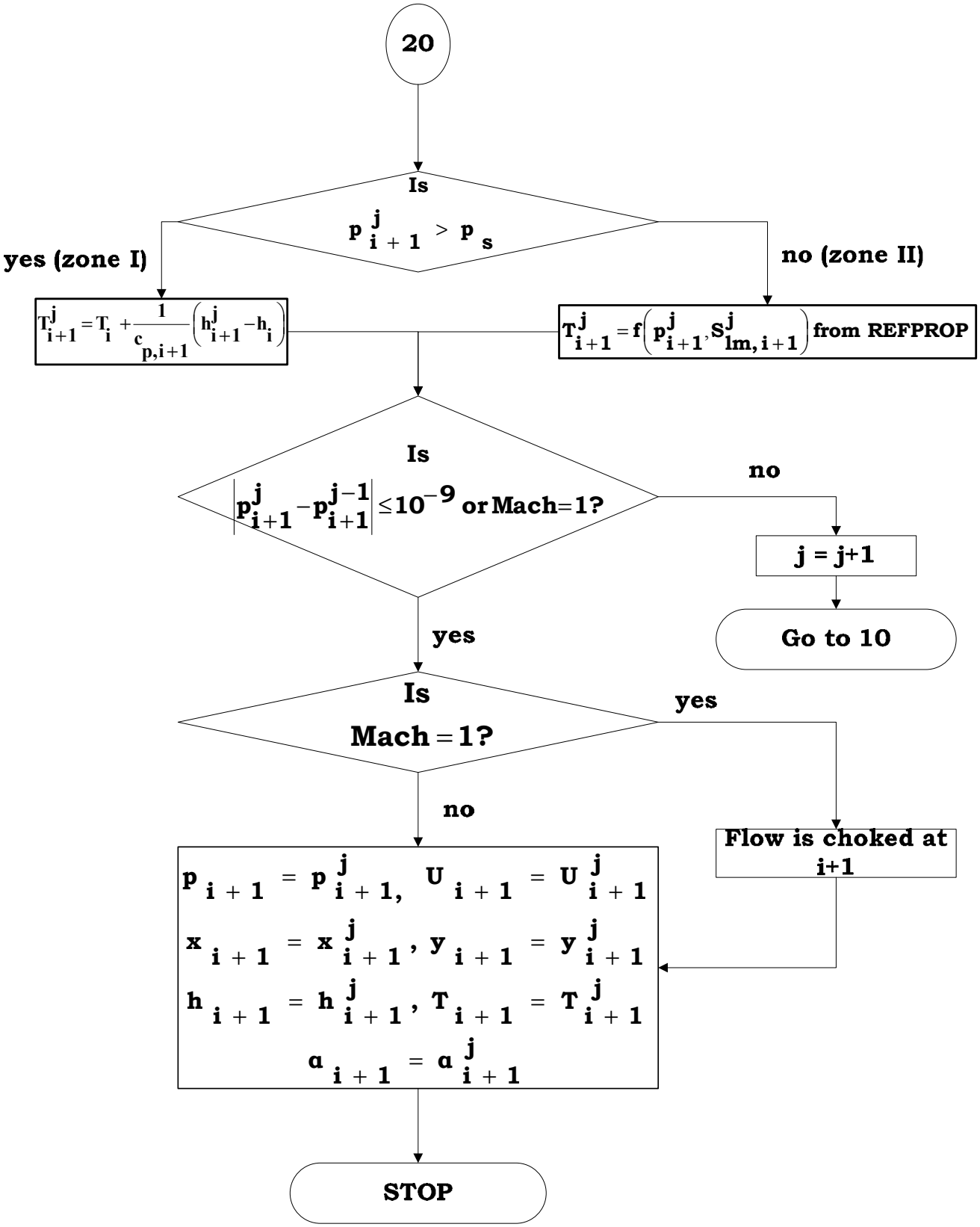

Figure B-2 Flow chart to calculate flow variables for zone I/zone II

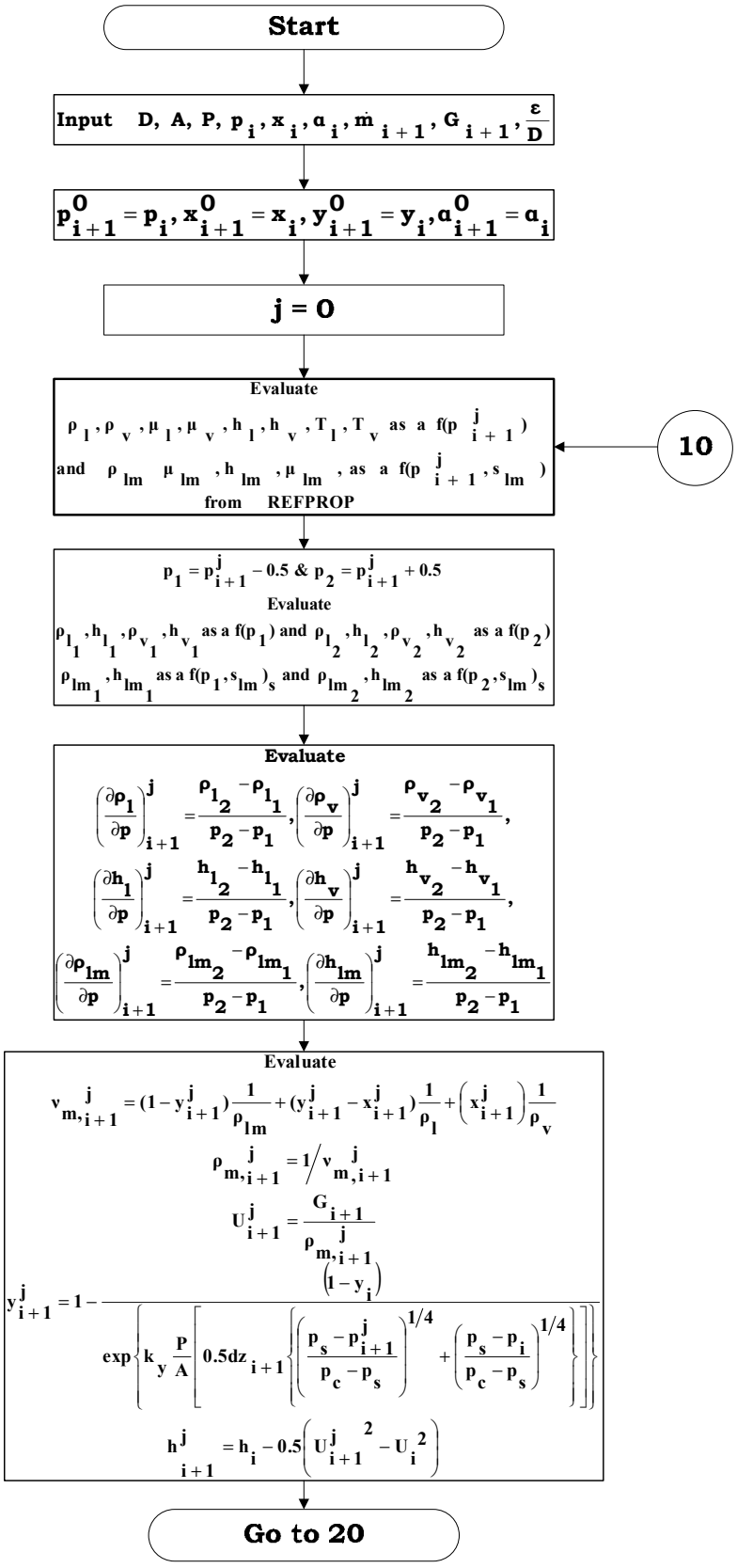

Figure B-3 Flow chart to calculate flow variables for zone III (continued…)

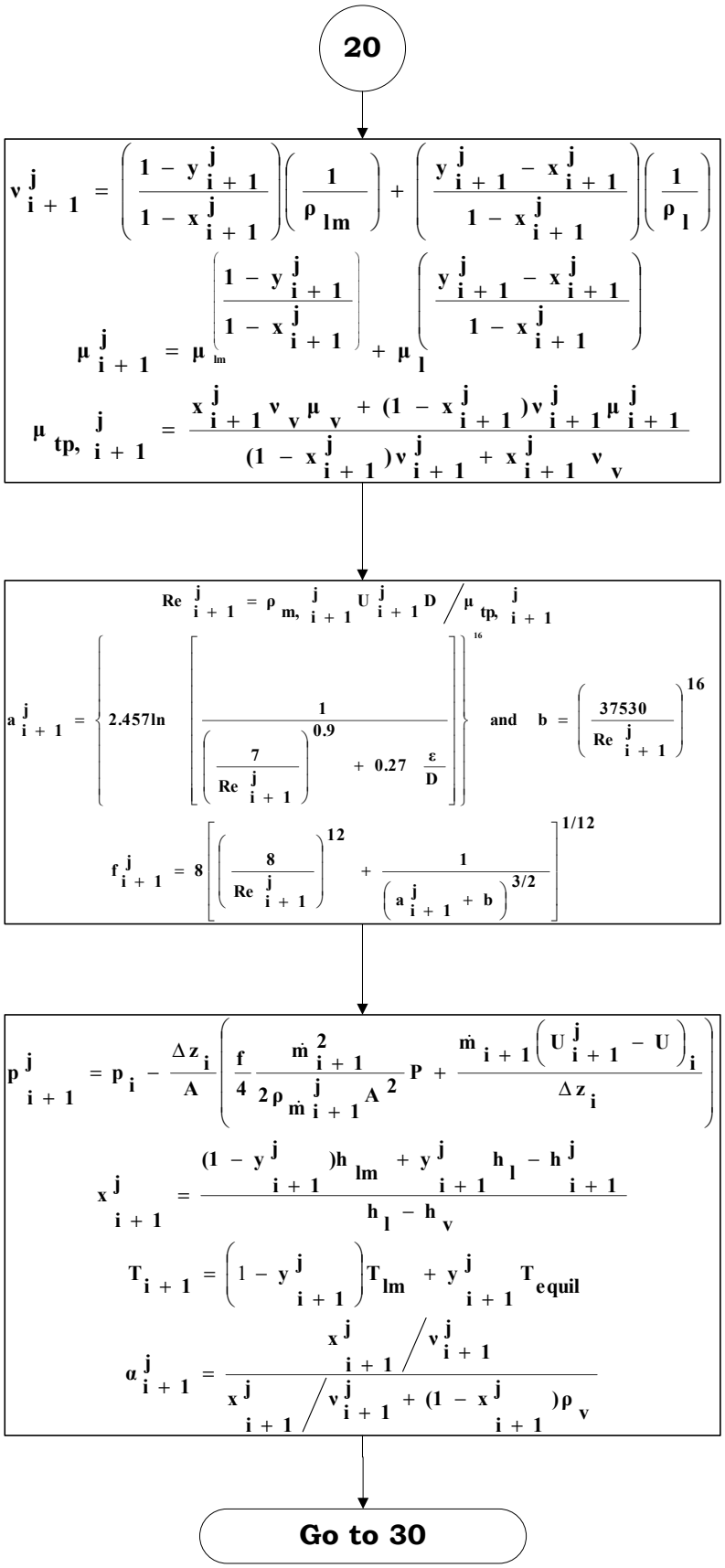

Figure B-3 Flow chart to calculate flow variables for zone III (continued…)

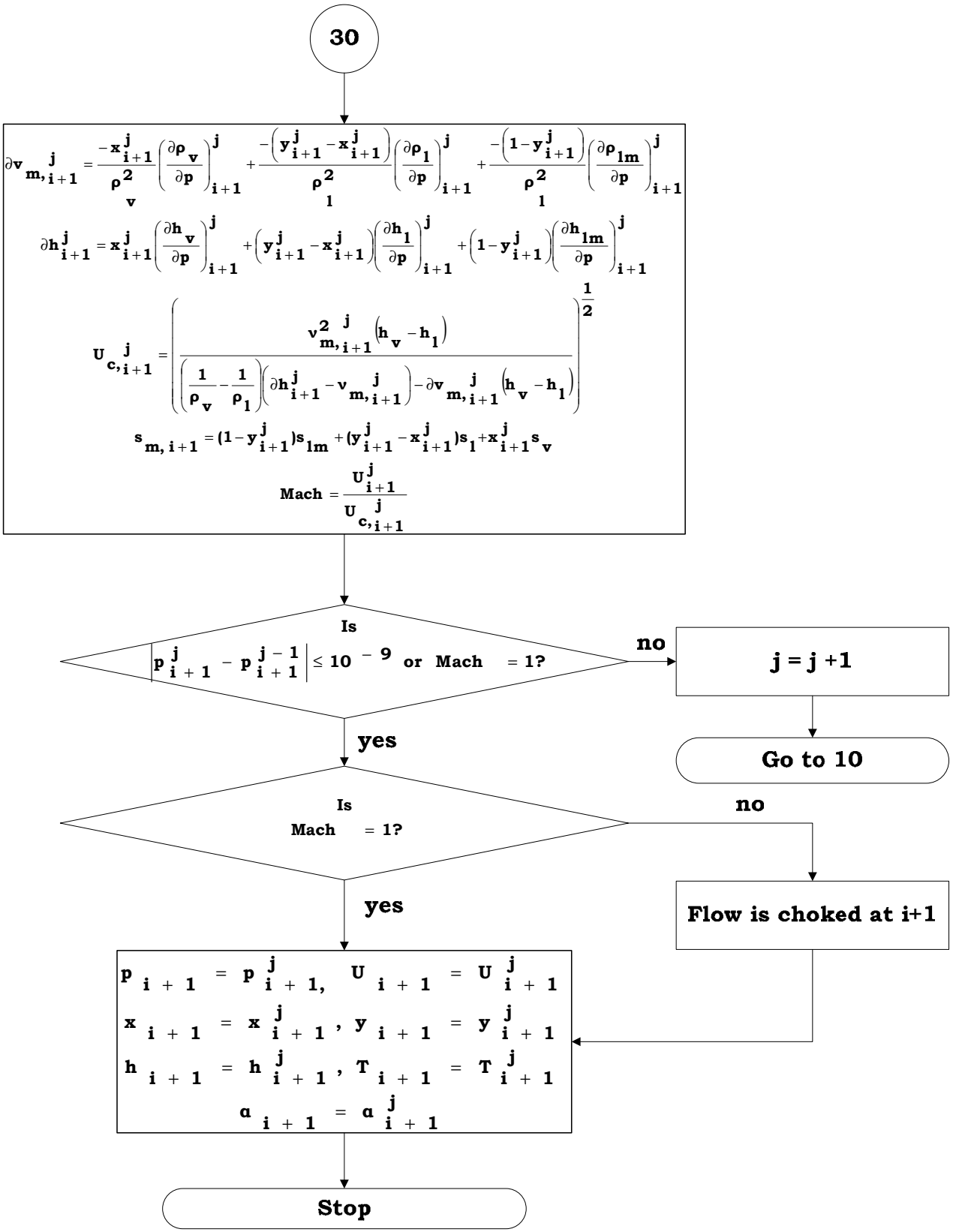

Figure B-3 Flow chart to calculate flow variables for zone III

Flow Charts For Twin-Orifice System of pMDIs

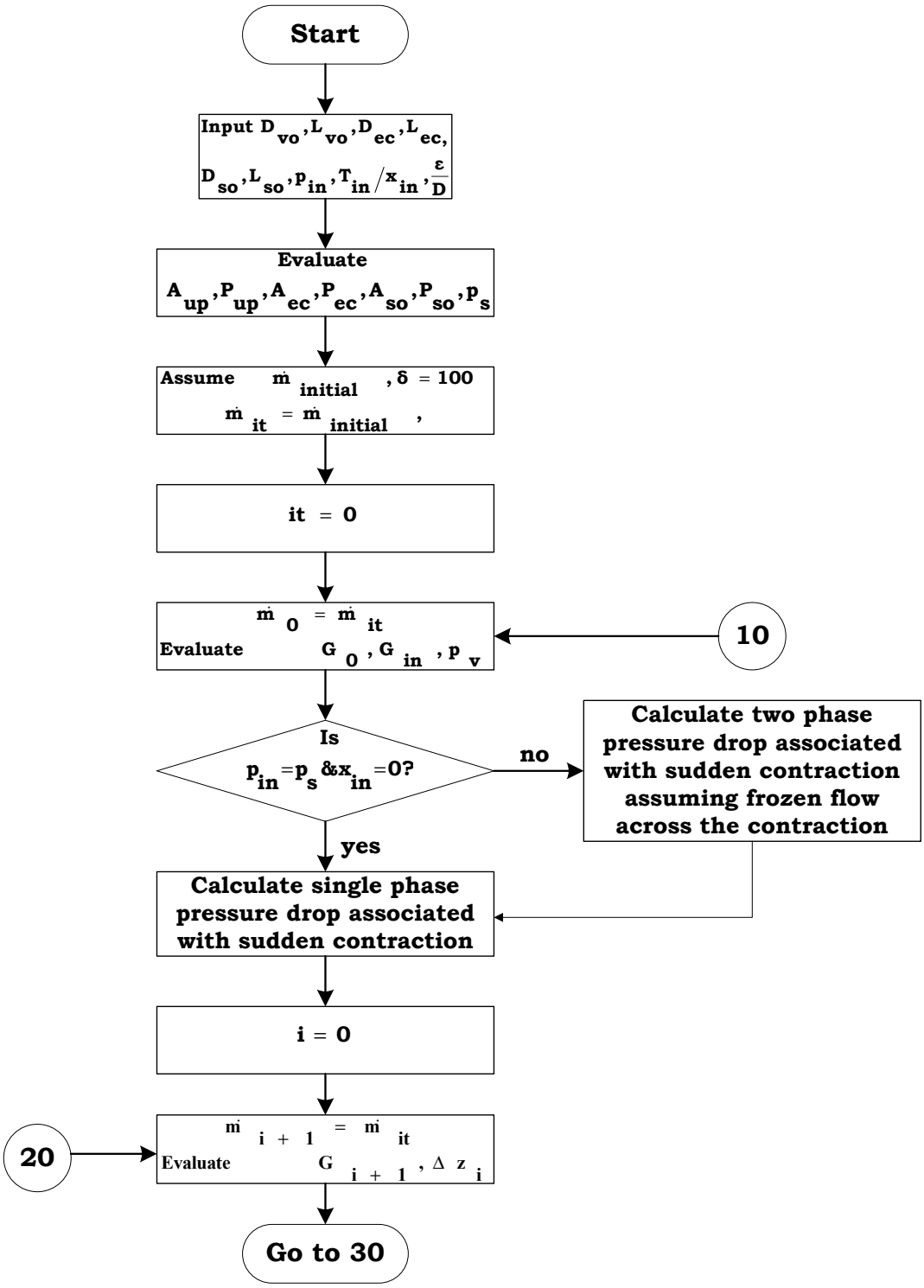

Figure B-4 Flow chart for the twin –orifice system of pMDIs (continued…)

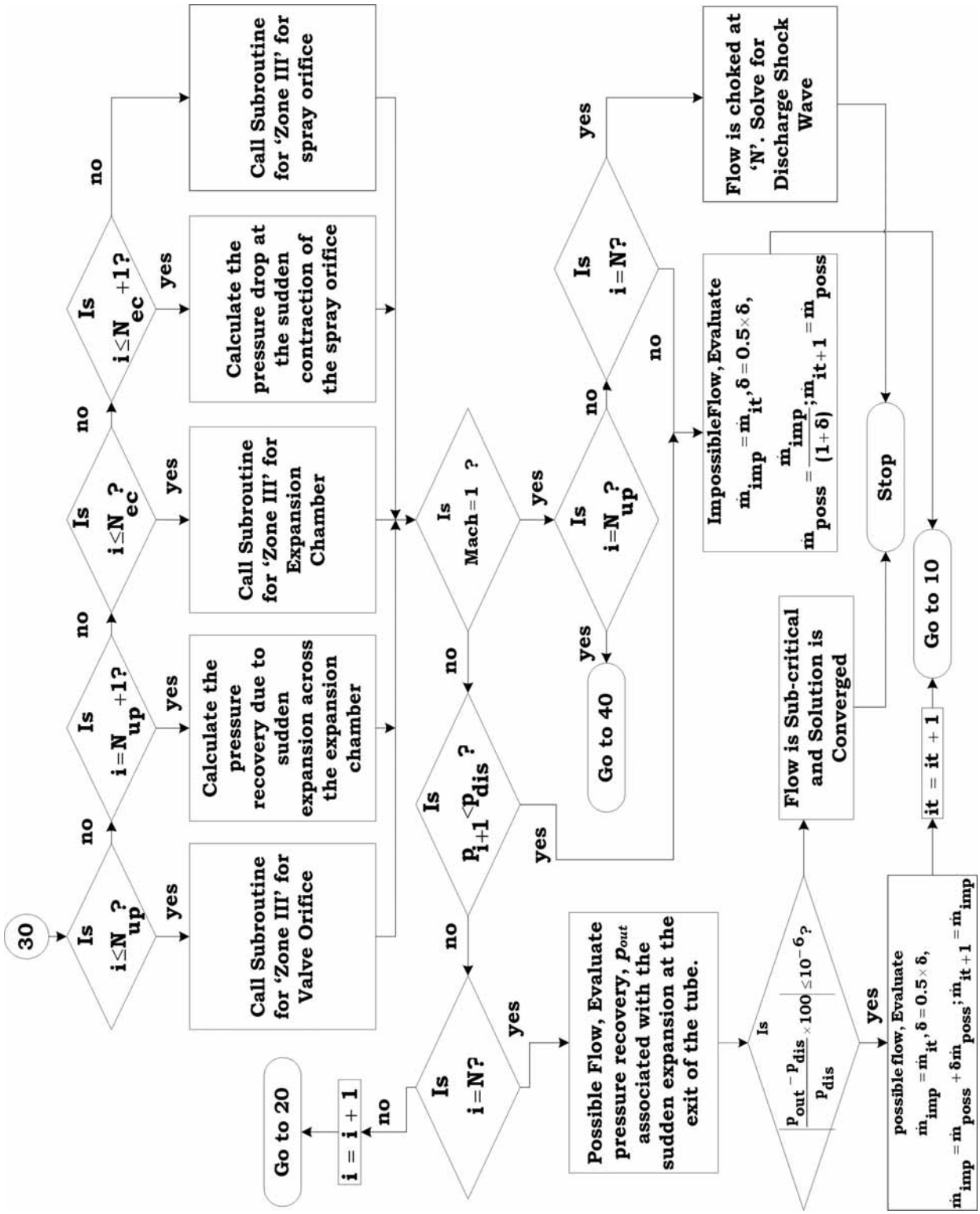

Figure B-5 Flow chart for the twin –orifice system of pMDIs

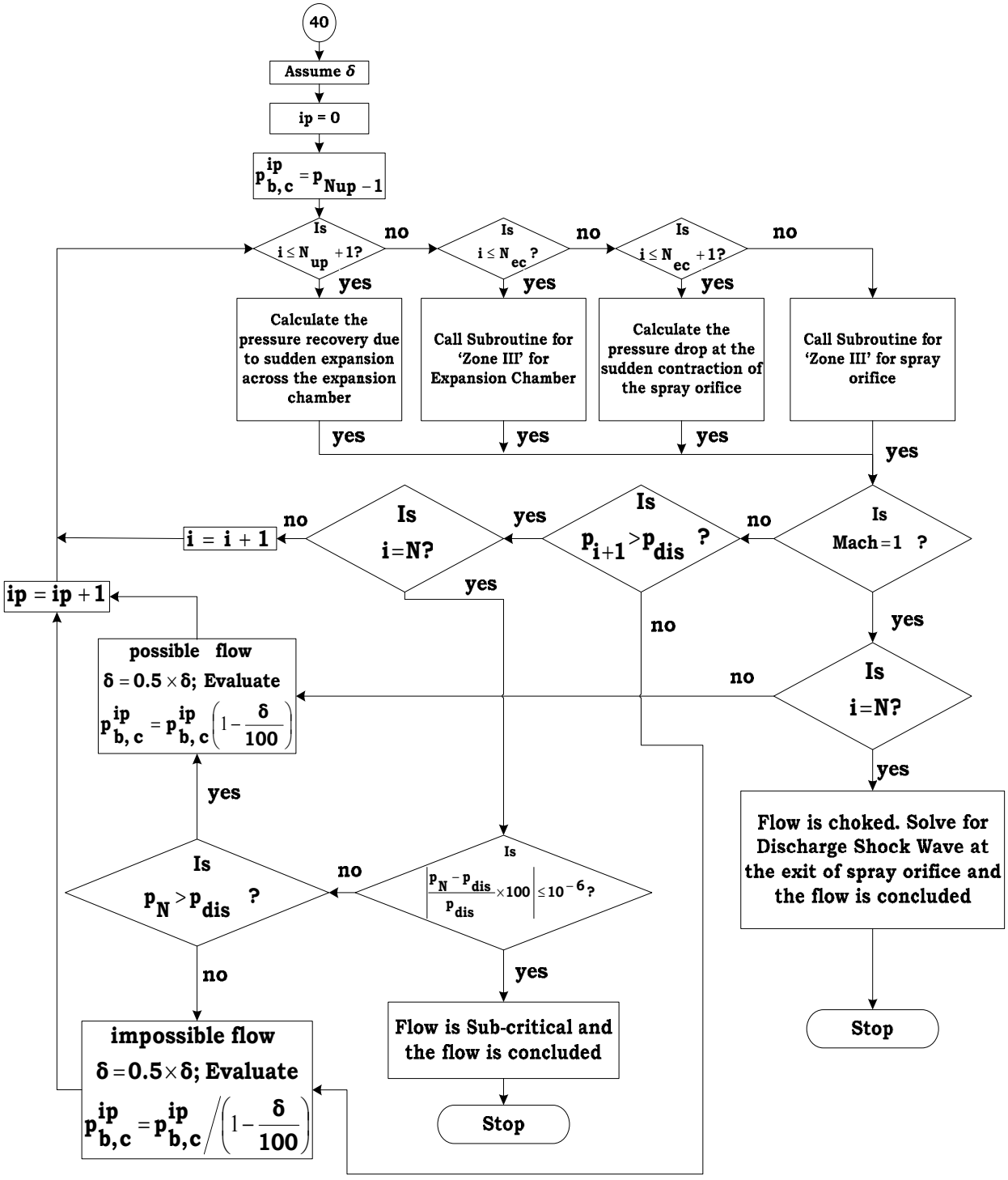

Figure B-6 Flow chart for base pressure algorithm

REFERENCES

AARON, A.A., & DOMANSKI, P.A. 1990. Experimentation, Analysis, and Correlation of Refrigerant-22 flow through short tube restrictors, *ASHRAE Transactions* Vol. 96, No. 1, pp 729-742.

ARDRON, K. H., & ACKERMAN, M.C., 1978 . Studies of the critical flow of subcooled water in a pipe, CEGB Report RD/B/N4299.

ATTOU, A. & SEYNHAEVE J.M. 1999a. Steady-state critical two-phase flashing flow with possible multiple choking phenomenon Part 1: Physical modeling and numerical procedure. *Journal of Loss Prevention in the Process Industries,* Vol. 12, pp 335-345.

ATTOU, A. & SEYNHAEVE J.M. 1999b. Steady-state critical two-phase flashing flow with possible multiple choking phenomenon Part 2: comparison with experimental results and physical interpretations. *Journal of Loss Prevention in the Process Industries,* Vol. 12, pp 347-359.

BANSAL, P.K., & RUPASINGHE, A.S. 1998, An homogeneous model for adiabatic capillary tubes. *Applied Thermal Engineering* Vol. 18, Nos 3-4, pp 207-219

BANSAL, P.K., & WANG, G. 2004. Numerical analysis of choked Refrigerant flow in adiabatic capillary tubes. *Applied Thermal Engineering,* Vol. 24, pp 851-863.

BEATTIE, D.R.H. 1973. A note on the calculation of two-phase pressure losses. *Nuclear Engineering and Design*, Vol. 25, pp 395-402.

BHUPESH CHANDRA & PRABHU, S.V. 2004. Two-phase refrigerant flow through adiabatic capillary tubes: evaluation of two-phase viscosity correlations and friction factor correlations on homogeneous model prediction for R22 and R134A. *42nd AIAA Aerospace Sciences meeting and Exhibit, 5-8 January 2004, Reno, Nevada*, *AIAA 2004-168.*

BITTLE, R.R. & PATE, M.B.,1996. A theoretical model for predicting adiabatic capillary tube performance with alternative refrigerants, *ASHRAE Transactions.* Vol. 102, No.2 pp 52–64.

BITTLE, R.R., CARTER, J.A. & OLIVER, J.V. 2006. Extended insight into the metastable liquid region behavior in an adiabatic capillary tube. *HVAC&R Research*, Vol. 7, No. 2, pp 107-123.

BOLSTAD, M.M., & JORDAN, R.C., 1949, Theory and use of the capillary tube expansion device. Part II, *Nonadiabatic flow, Refrigerating Engineering,* Vol. 57, pp 572-583

BRAMBILLA, G., GANDERTON, D., GARZIA, R., LEWIS, D., MEAKIN, B. & VENTURA, P. 1999. Modulation of aerosol clouds produced by pressurised inhalation aerosols. International Journal of Pharmaceutics. Vol. 186, pp 53-61.

BROWN, R., & YORK J.L, 1962. Sprays formed by flashing jets, *AIChE*, Vol.8, No.*2*, pp 149-153.

CHANG, S.D. & RO, S.T. 1996, Pressure drop of pure HFC refrigerants and their mixtures flowing in capillary tubes. *Int. J. Multiphase Flow,* Vol. 22 No. 3, pp 551-561.

CHAVES, H., KOWALEWSKI, T.A., KURSCHAT, T., MEIER, G.E.A. & MULLER, E.A. 1988. Similarity in the behaviour of initially saturated or subcooled liquid jets discharging through a nozzle. *Chemical Physics*, Vol. 126. pp 137-143.

CHEN, Z.H., LI, R.Y., LIN, S.& CHEN, Z.Y., 1990 A correlation for metastable flow of refrigerant 12 through capillary tubes, *ASHRAE Transactions.* Vol. 96, No. 1, pp 550–554.

CHOI, J. CHUNG, J.T. & KIM, Y. 2004 A generalized correlation for two-phase flow of alternative refrigerants through short tube orifices. *Int. J. Refrig.,* Vol. 27, pp 393-400.

CICCHITTI, A.,LOMBARDI, C., SILVESTRI, M. SOLDAINI, G. & ZAVALLUILLI, R., 1960, Two-phase cooling experiments-pressure drop, heat transfer and burnout measurements. *Energia Nucleare*, Vol. 7, pp 407-425.

CLARK, A.R.1991 Metered atomization for respiratory drug delivery, PhD Thesis, Loughborough University of Technology, Loughborough, UK.

COOPER L, CHU, C.K. & BRISKEN W.R., 1957, Simple selection method for capillaries derived from physical flow conditions, *Refrigerating Engineering,* Vol. 65, pp 37-41.

DataFit Software v.9.0.59 .2008. Oakdale Engineering.

DIRIK, E., INAN, C, TANES, M.Y & ARCELIK, A.S. 1994. Numerical and experimental studies on adiabatic and non-adiabatic capillary tubes with HFC-134A. *International Refrigeration Conference* at Purdue, Purdue University, USA.

DOMNICK, J. & DURST, F., 1995. Measurement of bubble size, velocity and concentration in flashing flow behind a sudden constriction. Int. J. Multiphase Flow, Vol. 21, No. 6, pp 1047-1062.

DUKLER, A.E., WICKS, M. & CLEVELAND, R.G., 1964. Frictional pressure drop in two-phaseflow: a comparison of existing correlations from pressure loss and holdup. *AICHE J.* Vol. 10 No. 1, pp 38-51.

DUNBAR, C. A. 1996. An experimental and theoretical investigation of the spray issued from a pMDI, PhD Thesis, UMIST, Manchester, UK.

DUNBAR, C.A., 1997a. Atomization mechanisms of the pressurized metered dose inhaler. *Particulate Science and Technology*, Vol. 15, pp 253-271.

DUNBAR, C.A., WATKINS, A.P. & MILLER, J.F. 1997b Theoretical investigation of the spray issued from a pressurized metered-dose inhaler. *Atomization and Sprays* Vol. 7, pp 417-436.

EL-FIQI, A.K., ALI, N.H., EL-DESSOUKY, H.T., FAITH, H.S. & EL-HEFNI, M.A. 2007. Flash evaporation in a superheated water and liquid jet. Desalination, Vol. 206, pp 311-321.

ELIAS, E. & LELLOUCHE, G.S. 1994 Two-phase critical flow. *International Journal of Multiphase Flow,* Vol. 20, pp 91-168.

ENGINEERING SCIENCES DATA UNIT (ESDU) Data Item 05024. Flow through sudden contractions of duct area: pressure losses and flow characteristics.

ENGINEERING SCIENCES DATA UNIT (ESDU) Data Item 89012. Two-phase flow pressure losses in pipeline fittings.

ESCANES, F., PEREZ-SEGARRA, D., & OLIVA, A. 1995 Numerical simulation of capillary-tube expansion devices, *International Journal of Refrigeration* Vol. 18, No. 2, pp 113-122.

FAUSKE, H.K., 1962 Contribution to the theory of two-phase, one component critical flow. PhD Thesis.

FAUSKE, H.K., 1963 Two-phase critical flow with application to liquid metal system. *ANL-6633, Argonne National Laboratory, Argonne, IL.*

FAUSKE, H.K. & MIN, A.C. 1963. A study of the flow of saturated freon-11 through apertures and short tubes. *ANL Report No*. 6667.

FEBURIE, V., GIOT, M., GRANGER, S. & SEYNHAEVE, J.M. 1993 A model for choked flow through cracks with inlet subcooling. *Int. J. Multiphase Flow,* Vol. 19, No. 4, pp 541-562.

FINLAY, W.H, 2001. The mechanics of inhaled pharmaceutical aerosols. *Academic Press*, London, pp 277-284.

FLETCHER G.E. 1975. Factors affecting the atomisation of saturated liquids, PhD Thesis, Loughborough University of Technology, Loughborough, UK.

FRASER, D.W.H. & ABDELMESSIH, A.H. 2002a A study of the effects of the location of flashing inception on maximum and minimum critical two-phase flow rates: Part I-experimental. *Nuclear Engineering and Design,* Vol. 211, pp 1-11.

FRASER, D.W.H. &ABDELMESSIH, A.H. 2002b A study of the effects of the location of flashing inception on maximum and minimum critical two-phase flow rates: Part II: analysis and modeling. *Nuclear Engineering and Design,* Vol. 213, pp 11-30.

FULTON R., YEOMANS, A. & ROGERS, E. 1950. C.S.M.A. Proc, pp 51.

GARCIA-VALLADARES, O., 2006. Numerical simulation of trans-critical carbon dioxide (R744) flow through short tube orifices. *Applied Thermal Engineering*, Vol. 26, pp 144-151.

GARCIA-VALLADARES, O., 2007. Numerical simulation of non-adaibatic capillary tube considering metastable region. Part 1 : mathematical formulation and numerical model. *International Journal of Refrigeration*, Vol. 30, pp 642-653.

GARCIA-VALLADARES, O., PEREZ-SEGARRA, C. D., & OLIVA, A. 2002a, Numerical simulation of capillary tube expansion devices behaviour with pure and mixed refrigerants considering metastable region. Part I: mathermatical formulation and numerical model. *Applied Thermal Engineering*, Vol. 22, pp 173-182.

GARCIA-VALLADARES, O., PEREZ-SEGARRA, C. D., & OLIVA, A. 2002b, Numerical simulation of capillary tube expansion devices behaviour with pure and mixed refrigerants considering metastable region. Part II: experimental validation and parametric studies. *Applied Thermal Engineering*, Vol. 22, pp 379-391.

GEMCI, T., YAKUT, K., CHIGIER, N. & HO, T.C. 2001. Cavitation and flash boiling atomization of water/acetone binary mixtures. *ILASS-America* 2001, Dearborn, MI, 20–23 May 2001, pp. 241–246

GEMCI, T., YAKUT, K., CHIGIER, N. & HO, T.C. 2004. Experimental study of flash atomization of binary hydrocarbon liquids. *International Journal of multiphase flow*, Vol. 30, pp 395-417.

GIOT, M., GRANGER, S., PAGES, D. & SEYNHAEVE, J.M. 1994 A model of single and two-phase flow (critical or not) through cracks. 31st meeting of the European Two-phase flow group, Piacenza, 6-8 June 1994.

GOLDSTEIN, P.E., S.D. 1981 A computer simulation method for describing two-phase flashing flow in small diameter tubes. *ASHRAE Transactions* Vol. 87 (2) pp 51-58.

HARDY, PH A& MALI, P. 1983. Validation and development of a model describing subcooled critical flow through long tubes. *Revue Energie Primaire*. Vol. 18, pp 5-16.

HENRY, R.E., 1968. A Study of one and two-Component, two-phase critical flow at low qualities. *Tech. Report ANL-7430.*

HENRY, R.E., 1970. The two-phase critical discharge of initially saturated or subcooled liquid. *Nucl. Sci. Eng*. Vol. 41, pp 336-342.

HENRY, R.E., & FAUSKE, H.K., 1971. The two-phase critical flow of one-component mixtures in Nozzles, Orifices, and Short tubes. *Trans. ASME Journal of Heat Transfer,* Vol. 93*,* pp 179-187.

HEWITT, G.F. & HALL-TAYLOR, N.S. 1970. Annular two-phase flow. Pergamon press.

HICKEY, A.J. & EVANS, R.M. 1996. Aerosol generation from propellant driven metered dose inhalers, in A.J. Hickey (Ed.). *Inhalation Aerosols: Physical and Biological basis for therapy*, Marcer Dekker, Inc., New York, NY, pp 417-439.

KAKADE, P, VERSTEEG, H.K. DEATON, D. & HARGRAVE, G. 2007. Design Optimization of a Novel MDI Actuator. *Proceedings of RDD* 2006. vol. 3. pp 663-666.

KIM Y. & O'NEAL 1994 A semi-empirical model of two-phase flow of refrigerant-134 a through short tube orifices *Experimental Thermal and Fluid Science* Vol. 9, pp 426-435.

KIM Y. & O'NEAL 1995 A comparison of critical flow models for estimating two-phase flow of HCFC22 and HFC134a through short tube orifices. *Int. J. Refrig.,* Vol. 18, No. 7, pp 447-455.

KOIZUMI, H. & YOKOHAMA, 1980, Characteristics of refrigerant flow in a capillary tube, *ASHRAE Transactions, Part 2*, Vol. 86, 19-27

KRAKOW, K.I. & LIN, S. 1988. Refrigerant flow through orifices. ASHRAE Transactions, Vol. 94, pp 484 – 506.

LACKME, C. 1979 Incompleteness of the flashing of a supersaturated liquid and sonic ejection of the produced phases. *Int. J. Multiphase Flow*, Vol. 5, pp 131-41.

LEFEBVRE, A.H. 1989. Atomization and sprays. Combustion: An international series.

LEFEBVRE, M. & TREGAN, T. 1964. *Parfum Cosmet Savons*, Vol. 7 pp 276.

LI, R.Y., LIN, S, CHEN, Z.Y., & CHEN, Z.H., 1990a Metastable flow of R12 through capillary tubes. *International Journal of Refrigeration* Vol. 13 No. 3, pp 181-186.

LI, R.Y., LIN, S., & CHEN, Z.H. 1990b Numerical modeling of the thermodynamic non-equilibrium flow of refrigerant through capillary tubes *ASHRAE Transactions* Vol. 96 No. 1, pp 542-549.

LIANG, S.M. & WONG, T.N. 2001 Numerical modeling of two-phase refrigerant flow through adiabatic capillary tubes. *Applied Thermal Engineering,* Vol. 21, pp 1035-1048.

LIENHARD, J. H.1966. An Influence of superheat upon the spray configurations of superheated Liquid Jets. *Transactions of ASME,* Vol. 88, pp 685-687.

LIENHARD, J. H., & DAY, J. B. 1970. The break up of superheated liquid jets. *Transactions of ASME: Journal of Basic Engineering*, Vol. 92, pp 515-521.

LIN, S., KWOK, C.C.K., LI, R.Y., CHEN, Z.H., & CHEN Z.Y. 1991 Local frictional pressure drop during vaporisation of R12 through capillary tubes. *Int. J. Multiphase Flow,* Vol. 17, No. 1, pp 95-102.

LIU, J.P., NIU, Y.M., CHEN, J.P., CHEN, Z.J. & FENG, X. 2004. Experimental and correlation of R744 two-phaseflow through short tubes. *Experimental Thermal and Fluid Science*, Vol. 28, pp 565-573.

MARCY, G. P., 1949, Pressure drop with change of phase in a capillary tube, *Refrigerating Engineering,* Vol. 57(1), pp 53-57.

MEI, V.C. 1982. Short tube refrigerant flow restrictors. *ASHRAE Transactions*, Vol. 88, part 2, pp 157-169.

MELO, C., FERREIRA, R.T.S., BOABAID NETO, GONCALVES, J.M. & MEZAVILA. 1999. An experimental analysis of adibatic capillary tubes. *Applied Thermal Engineering,* Vol. 19, pp 669-684.

MEYER, J.J., & DUNN, W.E. 1998. New insights into the behaviour of the metastable region of an operating capillary tube. *HVAC&R Research*, Vol. 4, No. 1, pp 105-115.

MIKOL, E. P., 1963 Adiabatic single and two-phase flow in small bore tubes. *ASHRAE J* Vol. 5, pp 75-86.

MIKOL, E.P. & DUDLEY, J.C. 1964 A visual and photographic study of the inception of vaporisation in adiabatic flow. *ASME Transactions* June pp 257-264

MIROPOLSKIY, Z.L., SHNEYEROVA, R.I & KARAMYSHEVA, A.I. 1970. Vapour void fraction in steam fluid mixing flowing in heated and unheated channels paper B4.7. *Int. Heat Trasn. Conf*., Vol.5, Paris.

MIYATAKE, O., TOMIMURA, T., IDE, Y., & FUJII, T., 1981a. An Experimental Study of Spray Flash Evaporation. *Desalination,* Vol. 36, No. 2, pp 113-128.

MIYATAKE, O., TOMIMURA, T., IDE, Y., YUDA, M. & FUJII, T., 1981b. Effect of liquid temperature on spray flash evaporation. *Desalination,* Vol. 37, No. 3, pp 351-366.

MIYATAKE, O., TOMIMURA, T., & IDE, Y., 1985. Enhancement of spray evaporation by means of the injection of bubble nuclei. *Transactions of ASME, Journal of Solar Engineering,* Vol. 107, pp 176-182.

MONTREAL PROTOCOL. 1987. Treaty Series, 1990, No. 19 HMSO.

MOODY, F.J. 1965 Maximum flow rate of a single component two-phase mixture. *J Heat Transfer, Trans ASME Series C*, Vol. 87, No. 1 pp 134-142.

MUTAIR, S. & IKEGAMI, Y. 2009. Experimental study on flash evaporation from superheated water jets: Influencing factors and formulation of correlation. *International Journal of Heat and Mass transfer*, Vol. 52, pp 5643-5651.

NILPUENG, K, & WONGWISES, S. 2009. Experimental investigation of two-phase flow characteristics of HFC-134a through short tube orifices. *International Journal of Refrigeration,* Vol. 32, pp 854-864.

PASQUA, P.F. 1953. Metastable flow of Freon-12. *Refrigeration Engineering*, Vol. 61, pp 1084-1088.

PREMOLI, A., FRANCESCO, D.& PRINA, A. 1971. An empirical correlation for evaluating two-phase mixture density under adiabatic conditions. *European Two-Phase Flow Group Meeting*, Milan, Italy.

REZK, A.M.A. & AWN, A.G. 1979 Investigation of flow of R12 through capillary tubes. *XII International Congress of Refrigeration* pp 443.

RICHTER, H.J. 1983. Separated two-phase flow model: application to critical two-phase flow. *International Journal of Multiphase flow*, Vol. 9, No. 5, pp 511-530.

RUBIN, B.K. & FINK, J.B. 2005. Optimising aerosol delivery by pressurized metered-dose inhalers. *Respiratory Care*. Vol. 50, No. 9, pp 1191-1200.

SAMI, S.M., & TRIBES, C. 1998 Numerical prediction of capillary tube behaviour with pure and binary alternative refrigerants. *Applied Thermal Engineering*, Vol. 18, No. 6, pp 491-502.

SAMI, S, M & MALTAIS, H. 2001. Experimental analysis of capillary tubes behaviour with some HCFC-22 alternative refrigerants. *International Journal of Energy and Research*, vol. 25. pp 1233-1247.

SANZOVO FIORELLI, F.A., SILVA HUERTA, A.A. & MATTOS SILVARES, O.D. 2002. Experimental analysis of refrigerant mixtures flow through adiabatic capillary tubes. *Experimental Thermal and Fluid Science*. Vol. 26. pp 499-512.

SANZOVO FIORELLI, F.A & MATTOS SILVARES, O.D. 2003. Refrigerant mixtures flow through capillary tubes: a comparison between homogeneous and separated flow models. *HVAC & R Research*. Vol. 9. No. 1 pp 33-54.

SANZOVO FIORELLI, F.A. & MATTOS SILVARES, O.D. 2004. Experimental validation of a capillary tube simulation model with refrigerant mixtures flow. *Thermal Engineering*. No.5, pp 15-23.

SEIXLACK, A.L., PRATA, A.T. & MELO, C. 1996. Modeling the HFC-R134A flow through capillary tubes using the two-fluid model. *Proceeding of the 1996 International Refrigeration Conference at Purdue*, West Lafayaette, Indiana, USA, vol.1, pp 89-94.

SEIXLACK, A.L. & BARBAZELLI, M.R. 2009. Numerical analysis of refrigerant flow along non-adiabatic capillary tubes using a two-fluid model. *Applied Thermal Engineering,* Vol. 29, pp 523-531.

SHER, E., & ELATA, C., 1977 Spray formation from pressure cans by flashing. *Industrial and Engineering Chemistry Process Design and Development*. Vol.16, No. 2, pp 237-242.

SILVA HUERTA, A.A., SANZOVO FIORELLI, F.A. & MATTO SILVARES, O., 2007, Metastable flow in capillary tubes: An experimental evaluation, *Experimental Thermal and Fluid Sciences,* Vol. 31, pp 957-966.

SIMOES-MOREIRA, J.R. & BULLARD, C.W. 2003. Pressure drop and flashing mechanism in refrigerant expansion devices. *International Journal of Refrigeration*. Vol. 26. pp 840-848.

SINGH, G.M., HRNJAK, P.S. & BULLARD, C.W. 2001. Flow of refrigerant 134a through orifice tubes. *HVAC&R Research*, Vol. 7, No. 3, pp 245-262.

SMYTH, H., BRACE, G., BARBOUR, T., GALLION, J., GROVE, J. & HICKEY, A.J. 2006. Spray pattern analysis for metered dose inhalers: effect of actuator design. *Pharmaceutical Research*, Vol. 23, No. 7, pp 1591-1596.

SOLOMON, A.S.P., RUPPRECHT, S.D., CHEN, L.D. & FAETH, G. M., 1985. Flow and atomozation in flashing injectors. *Atom. and Spray Tech.* Vol. 1, pp 53-76.

SOZZI, G.L., & SUTHERLAND, W.A., 1975. Critical fow of saturated and subcooled water at high pressures, *General Electric Company, NEDO-13418.*

STARKMAN E.S., SCHROCK, V.E., NEUSEN, K.F. & MANEELY, D.J. 1964. Expansion of a very low quality two-phase fluid through a convergent-divergent nozzle. *Journal of Basic Engineering, Transactions of ASME, Series D*, Vol. 86, No. 2, pp 247-256.

SUZUKI, M.; YAMAMOTO, T.; FUTAGAMI, N. 1978. Atomization of Superheated Liquid Jet. *First International Conference on Liquid Atomization and Spray Systems*, Tokyo, Japan, 1978.

TU, X., HRNJAK, P.S. & BULLARD, C.W. 2006. Refrigerant 134a liquid flow through micro-scale short tube orifices with/without phase change. *Experimental Thermal and Fluid Science*, Vol. 30, pp 253-262.

TESLIN, V.M. 1969. The Soviet Chemical Soc., Vol. 8. pp 70-72

THIEL, C. G. 1996. From Susie's question to CFC free: an inventor's perspective on forty years of MDI development and regulation. Proc. Respiratory Drug Delivery V, Interpharm Press, Buffalo Grove IL, pp 115-123.

VERSTEEG H.K & HARGRAVE G.K, 2001. Inhaled Air and Aerosol Particle Flow characteristics in a model of the Human Upper airway, 4*th International Symposium on Particle Image Velocimetry*.

VERSTEEG, H.K. & HARGRAVE, G.K, 2002. Near orifice spray and valve flow regime of a pharmaceutical pressurized metered dose inhaler. *Institute for Liquid Atomisation and Spray Systems*, Zaragoza.

VERSTEEG, H.K. 2009. Conical spray in spray orifice exit region. Departimental Working Paper, Wolson School of Mechanical Engineering, Loughborough University.

WALLIS, G.B., 1969, One-dimensional two-phase flow. McGraw-Hill, New York.

WALLIS, G.B. 1980 Critical two-phase flow. *Int. J. Multiphase Flow,* Vol. 6, pp 97-112.

WIGLEY, G., VERSTEEG, H.K. & HODSON, D. 2002. Near-orifice PDA measurements and atomisation mechanism of a pharmaceutical pressurised metered dose Inhaler. *Institute for Liquid Atomisation and Spray Systems*, Zaragoza.

WONG, T.N., & OOI, K.T. 1995. Refrigerant flow in capillary tube: An assessment of the two-phase viscosity correlation on model prediction. *Int. Comm. Heat Mass Transfer*, Vol. 22, No.4, pp 595-604.

WONG, T.N., & OOI, K.T. 1996a. Evaluation of capillary tube performance for CFC-12 and HFC-134a. *Int. Comm. Heat Mass Transfer*, Vol. 23, No.7, pp 993-1001.

WONG, T.N.& OOI, K.T. 1996b Adiabatic capillary tube expansion devices: A comparison of the homogeneous flow and the separated flow models. *Applied Thermal Engineering,* Vol. 16, No. 7, pp 625-634.

WONGWISES, S., CHAN, P., LUESUWANATAT, N. & PURATTANARAK, T., W. 2000a Two-phase separated flow model of refrigerants flowing through capillary tubes. *Int. Comm. Heat and Mass Transfer,* Vol. 27, No. 3, pp 343-356.

WONGWISES, S., SONGNETICHAOVALIT, T., LOKATHADA, N., KRITSADATHIKARN, P., SUCHATAWAT, M., & PIROMPAK, W. 2000b. A Comparison of the flow characteristics of refrigerants flowing through adiabatic capillary tubes. *Int. Comm. Heat and Mass Transfer,* Vol. 27, No. 5, pp 611-621.

WONGWISES, S & PIROMPAK, W., 2001 Flow characteristics of pure refrigerants and refrigerant mixtures in adiabatic capillary tubes. *Applied Thermal Engineering*, Vol. 21, pp 845-861.

WONGWISES, S & SUCHATAWUTT, M., 2003, A simulation for predicting the refrigerant flow characteristics including metastable region in adiabatic capillary tubes, *Int. Jou. of Energy Research*, Vol. 27, pp 93-109.

YANG, L & ZHANG, C.L. 2005. Two-fluid model of refrigerant two-phase flow through short tube orifice. *International Journal of Refrigeration*, Vol. 28, pp 419-427.

YOON, S.H., CHO, E.S., HWANG, Y.W., KIM, M.S. MIN, K. & KIM, Y. 2003. Characteristics of evaporative heat transfer and pressure drop of carbon dioxide and correlation development. *International Journal of Refrigeration,* Vol. 27, No. 2, pp 111-119.

YORK, J.L. 1956. *J. Soc. Cosmetic Chemists*, Vol. 7, pp 204.

ZHOU, G AND Y. ZHANG. 2006. "Numerical and experimental investigations on the performance of coiled adiabatic capillary tubes." Applied Thermal Engineering. Vol. 26, No. 11-12, 1106-1114.